Universität Hamburg
DER FORSCHUNG | DER LEHRE | DER BILDUNG

Fachbereich Chemie
Tor zur Welt der Moleküle

Valorisation of Lignin towards Monoaromatics by Selective Oxidative Depolymerisation with Polyoxometalate Catalysts and just-in-time Product Separation

Dissertation with the objective of achieving the doctoral degree *Doctor rerum naturalium* (Dr. rer. nat.)

Submitted to the Department of Chemistry
Faculty of Mathematics, Informatics, and Natural Sciences
Institute of Macromolecular and Technical Chemistry
University of Hamburg

Submitted by

Max Papajewski

Hamburg 2025

1. Evaluator	Prof. Dr.-Ing. habil. Jakob Albert Department of Chemistry Institute of Technical and Macromolecular Chemistry University of Hamburg
2. Evaluator	Jun.-Prof. Dr. rer. nat. Anna Katharina Beine Department of Mechanical Engineering Institute of Energy Process Engineering University of Siegen
1. Examiner	Prof. Dr.-Ing. habil. Jakob Albert Department of Chemistry Institute of Technical and Macromolecular Chemistry University of Hamburg
2. Examiner	Prof. Dr. rer. nat. Lisa Vondung Department of Chemistry Institute of Inorganic and Applied Chemistry University of Hamburg
3. Examiner	Prof. Dr.-Ing. Martin Kaltschmitt Department of Process Engineering Institute of Environmental Technology and Energy Economics Hamburg University of Technology

Date of disputation: 23.01.2026

This work was conducted between April 2021 and March 2024 at the Institute of Technical and Macromolecular Chemistry at University of Hamburg under the supervision of Prof. Dr.-Ing. habil. Jakob Albert.

I. List of publications

Parts of this work and other studies have been published in the following journals or presented on conferences.

Journals

- Max P Papajewski, Jan-Christian Raabe, Hamid Anwari, Dorothea Voß, Jakob Albert, Maximilian J. Poller, *The Synthesis and Characterisation of Ru(III)-Substituted Keggin-Type Phosphomolybdates*, Inorganics 2025, 13(6), 176.

- Max P. Papajewski, Suhaib Nisar, Chaoyue Zhang, Jason P. Hallett, Jakob Albert, *Boosting furfural production by combining polyoxometalates and ionic liquids for effective fractionation of lignocellulosic biomass*, RSC Adv., 2025, 15, 14259-14263.

- Anne Wesner, Max P. Papajewski, Leon Schidowski, Charlotte Ruhmlieb, Maximilian J. Poller, Jakob Albert, *Supported $H_8PV_5Mo_7O_{40}$ on activated carbon: Synthesis and Investigation of influencing factors for catalytic performance*, Dalton Trans., 2024, 53, 14065-14076.

Conferences

- Max P. Papajewski, Stefanie Wesinger, Jakob Albert, *CO_2-neutral production of Vanillin from Lignin by homogeneous oxidative depolymerization (POMLig)*, Poster, 56. Jahrestreffen Deutscher Katalytiker, 2023, Weimar.

- Stefanie Wesinger, Max P. Papajewski, Jakob Albert, *Life Cycle Assessment of the production of Vanillin from Lignin by homogeneous oxidative polymerization (POMLig)*, Poster, Annual meeting on Reaction Engineering, 2023, Frankfurt.

- Max P. Papajewski, Stefanie Wesinger, Jakob Albert, *Continuous selective oxidative depolymerization of lignin to monoaromatics*, Poster, Annual Meeting on Reaction Engineering and ProcessNet Subject Division Heat & Mass Transfer, 2022, Würzburg.

II. Table of contents

III. Abbreviations and Symbols

In-text abbreviations

Acronym	Meaning
AA	Acetic acid
AIL	Acid-insoluble lignin
ANOVA	Analysis of variance
ASL	Acid-soluble lignin
BBD	Box-Behknen-Design
BTX	Benzene, Toluene, Xylene
CAPEX	Capital expenditures
CHNSO	Elemental analysis for carbon, hydrogen, nitrogen, sulphur, oxygen
Cf.	Compare
CSTR	Continuously-stirred-tank-reactors
DoE	Design-of-Experiment
EtOH	Ethanol
FA	Formic acid
F-AAS	Flame atomic absorption spectrometry
FKM (FFKM)	Fluorocarbon-based fluoro-elastomer
FT-IR	Fourier-transform infrared spectroscopy
G	Guaiacyl unit
GC	Gas chromatography
GC-MS	Gas chromatography coupled with mass spectroscopy
GPC	Gel-permeation chromatography
H	p-hydroxyphenyl unit
HAZOP	Hazardous and operability study
HDPE	High-density polyethylene
HPA	Heteropolyanion
HPLC	High-pressure liquid chromatography
ICP-AES	Inductively coupled plasma atomic emission spectroscopy
IPA	Isopolyanion
KFT	Karl-Fischer titration

LLE	Liquid-liquid-extraction
MeOH	Methanol
MeSy	Methyl syringate
MeVa	Methyl vanillate
MWD	Multiple wavelength detector
MWL	Milled wood lignin
NaOH	Sodium hydroxide
NREL	National renewable energy laboratory
OFAT	One-factor-at-a-time
OPEX	Operating expenditures
pH	*potentia hydrogenii* (pH value)
PID	Piping and instrumentation diagram
PET	Polyethylene terephthalate
POM	Polyoxometalate
PTFE	Polytetrafluoroethylene
RID	Refractive index detector
RedOx	Reduction-oxidation-reaction
S	Syringyl unit
S_X	Substrate X
Sy	Syringaldehyde
TCD	Thermal conductivity detector
TGA	Thermogravimetric analysis
THF	Tetrahydrofuran
UV	Ultraviolet
Va	Vanillin

Polyoxometalate abbreviations

Category	**Abbreviation**	**Chemical formula**
Commercial	HPMo-0	$H_3PMo_{12}O_{40}$
	HPW-0	$H_3PW_{12}O_{40}$
	HSiW-0	$H_3SiW_{12}O_{40}$

Vanadium	HPMo-V_1	$H_4PV_1Mo_{11}O_{40}$
	HPMo-V_2	$H_5PV_2Mo_{10}O_{40}$
	HPMo-V_3	$H_6PV_3Mo_9O_{40}$
	HPMo-V_4	$H_7PV_4Mo_8O_{40}$
	HPMo-V_5	$H_8PV_5Mo_7O_{40}$
Cobalt	HPMo-Co_1	$H_7PCo_1Mo_{11}O_{40}$
	HPMo-Co_2	$H_{11}PCo_2Mo_{10}O_{40}$
	HPMo-Co_3	$H_{15}PCo_3Mo_9O_{40}$
	NaPMo-Co_1	$Na_7PCo_1Mo_{11}O_{40}$
	NaPW-Co_3	$Na_{15}PCo_3W_9O_{40}$
	WD-Co_1	$K_{10}P_2Co_1W_{17}O_{62}$
Manganese	HPMo-Mn_1	$H_7PMn_1Mo_{11}O_{40}$
	HPMo-Mn_2	$H_{11}PMn_2Mo_{10}O_{40}$
	WD-Mn_1	$K_{10}P_2Mn_1W_{17}O_{62}$
Nickel	HPMo-Ni_1	$H_7PNi_1Mo_{11}O_{40}$
	HPMo-Ni_2	$H_{11}PNi_2Mo_{10}O_{40}$
	HPMo-Ni_3	$H_{15}PNi_3Mo_9O_{40}$
Niobium	NaPMo-Nb_3	$Na_6PNb_3Mo_9O_{40}$
Indium	HPMo-In_4	$H_{15}PIn_4Mo_8O_{40}$
Bisubstituted	HPMo-V_1Mn_1	$H_8PV_1Mn_1Mo_{10}O_{40}$
	HPMo-V_1Mn_2	$H_{12}PV_1Mn_2Mo_9O_{40}$
	HPMo-V_3Mn_2	$H_{14}PV_3Mn_2Mo_7O_{40}$
	HPMo-V_5Mn_1	$H_{12}PV_5Mn_1Mo_6O_{40}$
	HPMo-Ni_1Mn_1	$H_{11}PNi_1Mn_1Mo_{10}O_{40}$
	HPMo-Ni_1Co_1	$H_{11}PNi_1Co_1Mo_{10}O_{40}$

Flow-diagram abbreviations

Abbreviation	**Meaning**
C	Controller
CV	Check valve
F	Filter
I	Information (data is displayed)

L	Level
M	Motor
MFC	Mass flow controller
P	Pressure
P_X	Pump X
R	Registration (data is stored)
RD	Rupture disk
R_X	Reactor number X
T	Temperature
T_X	Container/Tank X
V	Valve

Formula symbols

Symbol	**Meaning**	**Unit**
A	Area	cm^2
c	Concentration	$mol\ L^{-1}$
D	Polydispersity	-
d	Diameter	m
E_A	Activation energy	$J\ mol^{-1}$
f	Darcy friction factor	-
J	Specific permeate volume flow rate	$mL\ cm^{-2}\ h^{-1}$
k	Reaction rate constant	s^{-1}, min^{-1}, h^{-1}
l	Length	m
M_w	Weight-average molecular weight	Da
M_n	Number-average molecular weight	Da
m	Mass	g
Δp	Pressure drop	Pa
R	Rejection factor	%
R	Universal gas constant	$J\ mol^{-1}\ K^{-1}$
r	Reaction rate	$mol\ L^{-1}\ h^{-1}$
Re	Reynolds number	-

STY	Space-Time-Yield	mg mL^{-1} h^{-1}
T	Temperature	°C
t	Time	h
V	Volume	mL
$\dot{V}$	Volume flow rate	mL h^{-1}
v	Velocity	m s^{-1}
w	Mass fraction	wt.-%
Y	Yield	wt.-%
α	Separation factor	%
β	Mass concentration	mg mL^{-1}
ϑ	Kinetic viscosity	m s^{-2}
ρ	Density	kg m^{-3}
τ	Residence time	h

Formula indices

Index	**Meaning**
0	At time 0
eff	Effective
i	Component i
j	Product j
lam	laminar
m	Partial reaction order of respective component
R	Reaction

1. Abstract (English)

The overarching goal of this work was the process development of an oxidative and homogeneously catalysed depolymerisation method in continuous mode for technical lignins to obtain the monoaromatic compounds vanillin (Va), methyl vanillate (MeVa), syringaldehyde (Sy), and methyl syringate (MeSy), utilizing polyoxometalates (POMs) as catalysts. The project encompassed multiple work packages including lignin characterization, screening of lignin substrates, catalysts, and solvent systems, process parameter optimization, selection and evaluation of downstream separation techniques, and ultimately the construction and operation of a continuous mini-plant.

Lignin characterization revealed that elemental compositions were moderately consistent among different lignin types, except for samples with substantial water content distorting especially the carbon composition to lower values. Compositional analysis confirmed water content variation and revealed considerable differences in macromolecular composition, including carbohydrate content and the proportions of acid-soluble and acid-insoluble lignin. Molecular weight distribution analysis further confirmed that, while differences at the elemental level were limited, lignins displayed significant macromolecular variability, accounting for their differing depolymerisation behaviours. These variations reflect the influence of both biomass origin and pulping process.

During initial **sensitivity studies**, the lignin yielding the highest concentration of monoaromatics in the liquid phase – an organosolv hardwood lignin – was selected as the benchmark substrate. A novel nickel-modified POM, previously unreported in the literature, was synthesized and exhibited superior catalytic activity. Due to the ionic nature of polyoxometalates, a solvent system of methanol and water in an 8:2 (v/v) ratio was determined to be optimal to ensure solubility of both the catalyst and lignin-derived products. Under these conditions (temperature: 140 °C, oxygen partial pressure: 20 bar, reaction time: 24 h, substrate loading: 50 g/L, catalyst loading: 20 g/L), with the organosolv hardwood lignin a monoaromatic yield of ~11 wt.-% was achieved. By contrast, with an organosolv softwood lignin only ~5 wt.-% were achieved, illustrating that process performance is highly substrate dependent. Due to the limited supply of hardwood lignin, all further process optimization was conducted with the softwood lignin.

Optimization studies revealed that oxygen partial pressure has a notable influence on product composition, with elevated pressures promoting formation of esterified products MeVa and MeSy, likely via oxidation of Va and Sy followed by methanol esterification. Below a minimum oxygen threshold, overall monoaromatic yields declined, suggesting oxygen limitation. Reaction time studies indicated rapid solubilization of lignin, while the slower formation of monoaromatics pointed to the depolymerisation of dissolved oligomers as the rate-limiting step. Additionally, the formation pathways of MeVa and MeSy were inferred to follow oxidation of their aldehyde counterparts, while interconversion of Sy and MeSy to Va and MeVa via methoxy group oxidation is plausible. After 16 hours reaction time, the concentration of short-chained aliphatic methyl esters such as methyl formate surpassed that of the monoaromatics, guiding the choice of 16 hours as the standard reaction time for a design of experiments (DoE) study. This study further optimized reaction temperature, stirring rate, and substrate-to-catalyst ratio. While stirring rate had negligible influence, temperature and catalyst loading were critical. A minimum stirring rate of 50 rpm (for homogenization), a reaction temperature of 160 °C, and a substrate-to-catalyst ratio of 10:1 (m/m) increased the monoaromatic yield for the organosolv softwood lignin from ~5 wt.-% to ~11 wt.-%, matching the yield of the hardwood lignin.

Subsequent **kinetic analysis** revealed a partial reaction order of 1.8 with respect to lignin, suggesting a complex reaction network. An activation energy of ~13 kJ mol^{-1} was determined, significantly lower than literature values, underscoring the efficiency of the developed catalytic system and the importance of substrate selection.
Further **substrate screening** at optimized reaction conditions confirmed improved monoaromatic yields for all lignins tested, although none exceeded the performance of the lignin used during optimization, reinforcing the need for individual optimization for each lignin type.

For **product separation** and isolation, both liquid-liquid extraction (LLE) and membrane separation were investigated. Initial LLE screening with ethyl acetate, toluene, n–hexane, octylamine, and 1-heptanol showed moderate success in extracting monoaromatics from stock solutions. Among them, ethyl acetate, toluene, and octylamine were selected for further studies. However, the presence of the catalyst adversely affected extraction due to polarity changes, and in the case of octylamine, no phase separation occurred, potentially due to surfactant behaviour. When applied to real reaction solutions, toluene led to precipitation, likely of oligomeric

compounds, while only ethyl acetate enabled successful separation – achieving a 47 % separation factor for monoaromatics and 99 % catalyst rejection (based on nickel concentration). For the membrane separation, eight different commercial membranes were tested. *Evonik* membranes were impermeable to methanol and thus unsuitable. Of the remaining options, the NADIR membrane from *Mann+Hummel*, with a ~600 Da pore size, provided the best results achieving 99 % catalyst rejection and an exceptional 85 % separation factor for monoaromatics. This membrane system was thus selected for integration into the continuous plant.

To prepare for **continuous processing**, initial tests on lignin solvolysis under inert conditions (100 °C, 8:2 methanol:water, 2 h) were performed. When only the solvolysis filtrate was subjected to subsequent standard depolymerisation conditions, monoaromatic yields were equivalent to those obtained from untreated lignin, validating solvolysis as a pretreatment step to reduce reactor solids. A batch reactor plant was then retrofitted with upstream and downstream sections for continuous operation and commissioned including pump calibration, pressure control adjustment, membrane module controller setup, water trial runs, and residence time determination. Three lignins were tested under continuous flow: kraft, sulphite, and organosolv lignin.

The **kraft lignin** run had to be terminated after 8 hours due to precipitation-induced clogging in the effluent collection line, despite initially solid-free feed. This precipitation, likely from *in–situ* repolymerisation, led to blockage of the particle filter. Nevertheless, a permeate monoaromatic yield of 1.3 wt.-% was obtained after 8 hours residence time which is reasonable compared to the batch yield of 2.6 wt.-% after 16 hours.

For **sulphite lignin**, precipitation occurred unexpectedly in the reactor feed line, halting feed flow after 12 hours. No monoaromatics were detected in permeate samples, indicating either excessive degradation due to harsh conditions or insufficient depolymerisation of the lignin. However, short-chained aliphatic methyl esters like methyl formate and methyl acetate were detected, indicating some oxidative depolymerisation activity.

The **organosolv lignin** run was the most stable, maintaining continuous operation for 24 hours. However, the flow through the membrane module declined over time and eventually ceased due to clogging of the particle filter at the pump inlet. Product analysis revealed monoaromatic

and aliphatic ester yields of 0.8 and 3.0 wt.-%, respectively – substantially lower than in batch mode (7.5 and 10.8 wt.-%, respectively). The decline is likely also attributable to reduced membrane flow affecting separation efficiency.

Overall, the continuous experiments fell short of the desired performance. Only partial monoaromatic yields were obtained, with precipitation emerging as a consistent and critical issue, ultimately terminating all runs. Addressing this limitation is essential. Potential mitigation strategies include modifying the chemical system to enhance solubility, implementing heating of pipes and vessels to reduce temperature-induced precipitation, and decreasing residence times in up- and downstream processing via smaller container volumes.

In conclusion, a viable chemical and catalytic system for the homogeneous, oxidative depolymerisation of lignin to monoaromatics was successfully developed, optimized, and validated in batch operation, achieving yields of up to 11 wt.-% for organosolv hardwood and softwood lignin, respectively. The study demonstrated the importance of lignin substrate selection and confirmed the high potential of transition-metal-substituted polyoxometalates for the oxidative depolymerisation of biogenic polymers. Membrane separation offered a promising method for catalyst and product isolation, although further refinement is needed to prevent fouling. Future work must focus on overcoming precipitation challenges in continuous mode to enable industrial application of the process.

2. Zusammenfassung (German)

Ziel dieser Arbeit war die Entwicklung eines kontinuierlichen, homogen katalysierten Verfahrens zur oxidativen Depolymerisation technischer Lignine, um die monoaromatischen Verbindungen Vanillin (Va), Methylvanillat (MeVa), Syringaldehyd (Sy) und Methylsyringat (MeSy) zu gewinnen. Als Katalysatoren kamen Polyoxometallate (POMs) zum Einsatz. Das Projekt umfasste mehrere Arbeitspakete: Charakterisierung der technischen Lignine, experimentelle Vorauswahl aller Lignine, Variation von Katalysatoren und Lösungsmittelsystemen, Optimierung der Prozessparameter, Auswahl und Evaluation von Downstream-Prozessen sowie den Aufbau und Betrieb einer kontinuierlichen Mini-plant.

Die **Lignincharakterisierung** ergab, dass die elementare Zusammensetzung zwischen den Lignintypen nur moderate Unterschiede aufwies – mit Ausnahme von Substraten mit erhöhten Wassergehalten, welche den Gehalt der gemessenen Elemente signifikant reduzierte. Die Zusammensetzungsanalyse nach NREL bestätigte eine signifikante Variabilität im Wassergehalt und offenbarte deutliche Unterschiede in der makromolekularen Zusammensetzung, insbesondere im Kohlenhydratanteil, sowie in den Anteilen säurelöslichen und -unlöslichen Lignins. Die Analyse der Molekulargewichtsverteilung bestätigte diese makromolekulare Heterogenität, welche maßgeblich das Depolymerisationsverhalten beeinflusst. Diese Unterschiede sind sowohl auf die Biomasseherkunft als auch auf das verwendete Aufschlussverfahren zurückzuführen.

In den initialen **Sensitivitätsstudien** wurde ein Organosolv-Hartholzlignin als Referenzsubstrat identifiziert, da dieses die höchste Ausbeute an Monoaromaten in der Flüssigphase lieferte. Ein neuartiges, bislang nicht in der Literatur beschriebenes, nickelmodifiziertes POM zeigte signifikant verbesserte katalytische Aktivität. Aufgrund der ionischen Natur der POMs wurde ein Methanol-Wasser-Gemisch im Volumenverhältnis 8:2 als optimales Lösungsmittelsystem zur Sicherstellung der Löslichkeit von Katalysator und Produkten identifiziert. Unter diesen Bedingungen (Temperatur: 140 °C, Sauerstoff-Partialdruck: 20 bar, Reaktionszeit: 24 h, Substratbeladung: 50 g/L, Katalysatorbeladung: 20 g/L) konnte aus einem Organosolv-Hartholzlignin eine Monoaromatenausbeute von ~11 Gew.-% erreicht werden, während ein Organosolv-Weichholzlignin lediglich zu einer Ausbeute von ~5 Gew.-% führte, wodurch die substratspezifische Abhängigkeit der Prozessleistung verdeutlicht werden konnte. Aufgrund

begrenzter Verfügbarkeit des Hartholzlignins wurden alle weiteren Optimierungen mit einem Weichholzlignin durchgeführt.

Die **Optimierungsstudien** zeigten, dass der Sauerstoffpartialdruck einen signifikanten Einfluss auf die Produktzusammensetzung hatte: Höhere Drücke förderten die Bildung der Esterprodukte MeVa und MeSy, vermutlich über Oxidation von Va und Sy mit anschließender Veresterung mit Methanol. Unterhalb einer kritischen Sauerstoffkonzentration nahm die Monoaromatenausbeute ab – dies deutet auf eine Sauerstofflimitierung hin. Zeitstudien zeigten ein schnelles Lösen des Lignins, während die Bildung von Monoaromaten deutlich langsamer verlief – ein Hinweis darauf, dass die Depolymerisation gelöster Oligomere der geschwindigkeitsbestimmende Schritt ist. Es wurde postuliert, dass MeVa und MeSy durch Oxidation der jeweilgen Aldehyd-Vorstufen entstehen, während auch eine Umwandlung von Sy und MeSy zu Va und MeVa über Oxidation der Methoxygruppen plausibel ist. Nach 16 Stunden überstiegen die Konzentrationen kurzkettiger, aliphatischer Methylester (z. B. Methylformiat) die der Monoaromaten. Aus diesem Grund wurden 16 Stunden als Standardreaktionszeit für das anschließende Design-of-Experiments (DoE) festgelegt. Dabei wurden Reaktionstemperatur, Rührgeschwindigkeit und Substrat-zu-Katalysator-Verhältnis optimiert. Während die Rührgeschwindigkeit kaum Einfluss hatte, erwiesen sich Temperatur und Katalysatormenge als signifikant beeinflussende Parameter. Eine Rührerdrehzahl von 50 rpm (zur Homogenisierung), eine Reaktionstemperatur von 160 °C sowie ein Substrat-zu-Katalysator-Verhältnis von 10:1 (m/m) steigerten die Monoaromatenausbeute für das Organosolv-Weichholzlignin von ~5 auf ~11 Gew.-% – durch die Optimierung demnach vergleichbar mit dem ursprünglichen Organosolv-Hartholzlignin.

Die anschließende **kinetische Studie** ergab eine partielle Reaktionsordnung von 1,8 bezogen auf die Ligninkonzentration, was auf ein komplexes Reaktionsnetzwerk hinweist. Eine Aktivierungsenergie von ~13 kJ mol^{-1} wurde bestimmt – *deutlich* niedriger als Literaturwerte – und belegt die Effizienz des entwickelten katalytischen Systems sowie die Bedeutung der Substratwahl. Ein weiteres Substratscreening unter optimierten Bedingungen bestätigte gesteigerte Monoaromatenausbeuten für alle getesteten Lignine. Die erzielte Leistung des Referenzlignins blieb unerreicht. Dies unterstreicht die Notwendigkeit substratspezifischer Prozessanpassungen.

Zur **Produktaufarbeitung** (Downstream-Prozessierung) wurden Flüssig-Flüssig-Extraktion (LLE) und Membrantrennung untersucht. Erste LLE-Screenings mit Ethylacetat, Toluol, n-Hexan, Octylamin und 1-Heptanol zeigten Extraktionserfolge aus Standardlösungen. Ethylacetat, Toluol und Octylamin wurden für vertiefte Studien ausgewählt. Die Anwesenheit des Katalysators wirkte sich jedoch negativ auf die Extraktion aus – durch veränderte Polarität – und verhinderte im Fall von Octylamin die Phasentrennung vollständig, vermutlich aufgrund eines amphiphilen Verhaltens. In realen Reaktionslösungen führte Toluol zur Präzipitation oligomerer Verbindungen, während nur Ethylacetat eine erfolgreiche Abtrennung ermöglichte und dabei einen Trennfaktor von 47 Gew.-% für Monoaromaten und 99 Gew.-% Katalysatorrückhalt (bezogen auf Nickel) erreichte. Für die Membrantrennung wurden acht verschiedene Membranen getestet. Die *Evonik*-Membranen waren für Methanol undurchlässig und daher ungeeignet. Bei Verwendung der NADIR-Membran von *Mann+Hummel* mit einer Porengröße von ~600 Da wurden die besten Resultate erzielt: 99 Gew.-% Katalysatorrückhalt und 85 Gew.-% Trennfaktor für Monoaromaten. Daher wurde diese Membran für die Integration in die kontinuierliche Anlage ausgewählt.

Zur Vorbereitung der **kontinuierlichen Prozessführung** wurden erste Tests zur Ligninsolvolyse unter Inertatmosphäre (100 °C, 8:2 Methanol:Wasser, 2 h) durchgeführt. Die anschließende Depolymerisation des Solvolysefiltrats führte zu vergleichbaren Ausbeuten wie unbehandeltes Lignin, womit sich die Solvolyse als Vorbehandlung zur Feststoffreduktion im Reaktor eignete. Eine bestehende Batch-Anlage wurde um Upstream- und Downstream-Prozessierung zur kontinuierlichen Betriebsweise erweitert. Die anschließende Inbetriebnahme umfasste Pumpenkalibrierung, Druckregelung, Inbetriebnahme des Membranmoduls, Wassertestläufe und Bestimmung der Verweilzeiten. Drei Lignine wurden im kontinuierlichen Betrieb getestet: Kraft-, Sulfit- und Organosolv-Lignin.

Der Versuch mit Kraftlignin musste nach 8 h aufgrund von ausgefallenen Stoffen und Verstopfung der Produktleitung abgebrochen werden, obwohl der Feed zunächst feststofffrei war. Die Ausfällung, vermutlich durch *in-situ*-Repolymerisation verursacht, blockierte den Partikelfilter. Dennoch wurde eine Monoaromatenausbeute von 1,3 Gew.-% im Membranpermeat erzielt – im Vergleich zu 2,6 Gew.-% im Batch (16 h).

Bei Verwendung des Sulfitlignins trat eine unerwartete Ausfällung bereits in der Zuleitung auf, wodurch der Reaktorzufluss nach 12 h zum Erliegen kam. Im Permeat wurden keine

Monoaromaten nachgewiesen, was auf übermäßige Zersetzung oder unzureichende Depolymerisation des Lignins hindeutet. Kurzkettige, aliphatische Ester (z. B. Methylformiat, Methylacetat) wurden jedoch detektiert – ein Hinweis auf allgemeine oxidative Depolymerisation, allerdings kein Beweis einer der beiden Theorien.
Der Versuch mit Organosolv-Lignin verlief am stabilsten und ermöglichte einen 24-stündigen Dauerbetrieb. Der Fluss durch das Membranmodul nahm jedoch kontinuierlich ab und kam schließlich durch eine Filterverstopfung zum Erliegen. Die Produktauswertung ergab Monoaromaten- und Ester-Ausbeuten von 0,8 Gew.-% bzw. 3,0 Gew.-% – deutlich unter den im Batch-Versuch erzielten Werten von 7,5 Gew.-% bzw. 10,8 Gew.-%. Der Rückgang ist vermutlich auch auf die abnehmende Membranleistung und Trennschärfe zurückzuführen.

Insgesamt blieb die Performance der kontinuierlichen Experimente hinter den Erwartungen zurück. Nur partielle Ausbeuten wurden erreicht; Ausfällungen stellten ein wiederkehrendes, kritisches Problem dar und führten letztlich zum Abbruch aller Versuche. Die Lösung dieses Problems ist entscheidend, um einen kontinuierlichen Betrieb zu ermöglichen. Mögliche Ansätze umfassen Modifikation des chemischen Systems zur verbesserten Löslichkeit, Beheizung von Leitungen und Behältern zur Minimierung temperaturinduzierter Ausfällung sowie Reduktion der Verweilzeiten durch kleinere Gefäßvolumina in der Vor- und Nachbehandlung.

Zusammenfassend konnte ein effektives chemisches und katalytisches System zur homogenen, oxidativen Depolymerisation von Lignin zu Monoaromaten im Batchbetrieb erfolgreich entwickelt, optimiert und validiert werden. Es wurden Ausbeuten von bis zu 11 Gew.-% (für jeweils Organosolv-Hartholzlignin und -Weichholzlignin) erzielt. Die Ergebnisse unterstreichen die Bedeutung der Substratauswahl und belegen das Potenzial von Übergangsmetall-substituierten Polyoxometallaten. Die Membrantrennung erwies sich als vielversprechende Methode zur Abtrennung von Katalysator und Produkten, wenngleich Fouling noch adressiert werden muss. Zukünftige Arbeiten sollten sich auf die Überwindung von Ausfällungsproblemen im kontinuierlichen Betrieb konzentrieren, um eine industrielle Umsetzung des Verfahrens zu ermöglichen.

3. Introduction

In recent years, a shift has become apparent in the global economy, political landscape, and overall uncertainty. This has been driven in particular by climate change, COVID-19 pandemic, the resurgence of war within Europe, general instability and unrest in the Middle East, and the foreign policy of the previously stabilizing United States. [1–3] This uncertainty may be significantly intensified by the limited or regionally restricted availability of the world's most important raw material – crude oil. This is especially critical as it is predominantly found in just seven countries. [4] Crude oil is so vital because it is used in every sector of modern society. The transportation sector depends on affordable fuels, which are still largely petroleum based. Most forms of plastic are essentially pure crude oil; electronics, cosmetics, pharmaceutical products, and even clothing contain petroleum-derived components. [5] Therefore, at present, crude oil is indispensable. However, in the long term, this must change. While current (2021) proven reserves of 1,550–1,750 Gb (giga barrels) and an annual production of 75–85 million barrels per day will last for several more decades, they are nonetheless finite. [6,7] Furthermore, continued crude oil extraction leads to additional greenhouse gas emissions, which must be drastically reduced in connection with climate change and the Paris Agreement. [8] In summary, the use of crude oil must be minimized over the coming decades, making it essential to find alternative raw materials or sustainable solutions for the production of similar goods.

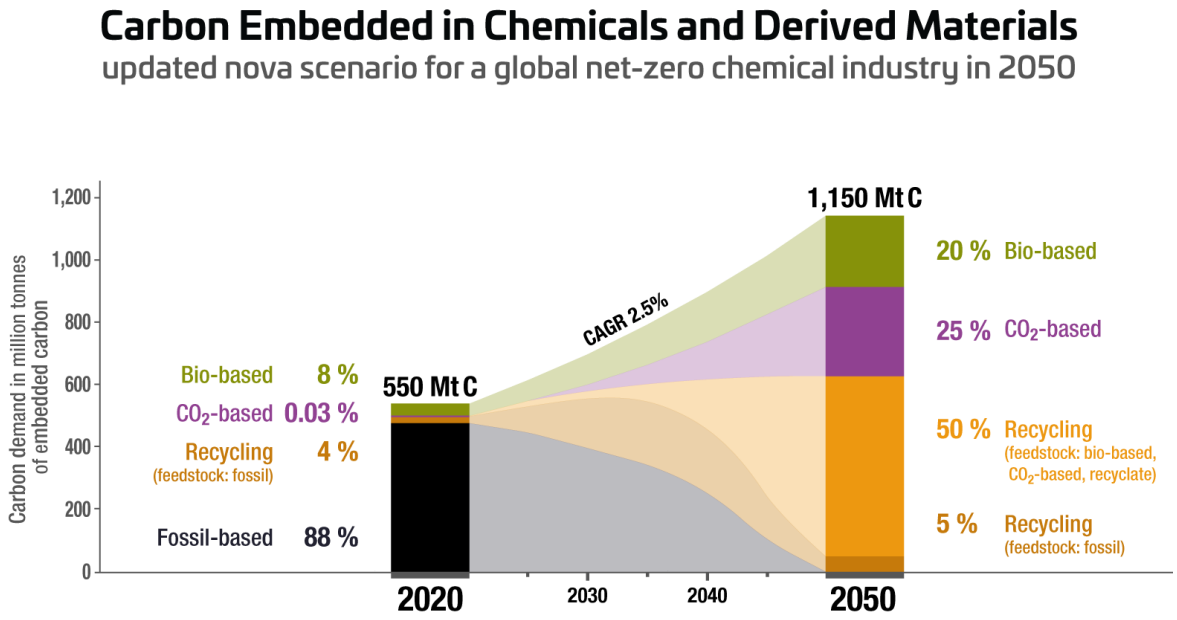

Figure 3-1: Forecast of the carbon demand for global chemical industry grouped by technological origin, i.e. bio-based, CO_2-based, chemical recycling and fossil-based. [9]

This transformation of the chemical industry is projected to rely on three main raw material approaches: Bio-based, CO_2-based, and recycling (initially of fossil-based materials), as suggested in **Figure 3-1**. [9,10] Recycling will play a key role in building a circular economy by mechanically or chemically recycling existing plastic or tire waste, thereby minimizing resource consumption. CCU, or power-to-X, aims to convert captured CO_2 and green hydrogen into petroleum-like hydrocarbon mixtures, although this requires large amounts of electrical energy overall. The third described material source is biomass – renewable, primarily plant-based resources – which offers the advantage of neutral or rather negative CO_2 emissions and global availability. This includes not only the use of fats and oils (e.g., for biodiesel production), but also the use of woody biomass. [11] Trees are composed of this woody, or lignocellulosic, biomass, which is known to grow in all inhabited regions of the world and is therefore globally accessible. [12] Lignocellulose is composed of three main components: cellulose, hemicellulose, and lignin. While cellulose and hemicellulose are sugar-based polymers and already have industrial uses (e.g., in paper production), the majority of lignin generated is currently used only for energy purposes – it is burned. [11,13] Chemically, however, lignin is of particular interest because it is the only renewable source of aromatic structures (i.e., aromatic functionalities) available at such scale. Since annual lignin waste is estimated at 50–100 Mt produced in pulp and paper industry, and nearly all aromatic-based products are currently derived from crude oil, valorising this lignin side stream is essential. [13,14]

This precise material valorisation was the subject of this project which was funded by the Agency for Renewable Resources (FNR), Siemens, and Siemens Energy. Specifically, lignin will be chemically converted into vanillin (vanilla flavour compounds) and its derivatives. Currently, vanillin and all subsequent derivatives considered here are almost exclusively produced from guaiacol, which is of fossil origin. [15,16] Thus, this work aims to substitute crude oil and achieve a material (rather than energetic) utilization of lignin. The focus is primarily on technological development, as the conversion involves several challenges. For example, lignin is still a polymer and therefore requires depolymerization to transform it from a solid to a liquid state. Potential depolymerization methods include acid-catalysed, base-catalysed, solvolytic, reductive, or oxidative technologies. [17] In this work, oxidative depolymerization was applied, as it offers higher atom economy (compared to reductive methods) and the target products inherently contain oxygen already. As catalysts, homogeneous systems – particularly so-called polyoxometalates – have been used, as these are generally more active than heterogeneous catalysts. [18]

To support this topic, a general theoretical background on lignocellulose, lignin, polyoxometalates, and relevant technical aspects will first be provided in the next chapter. Based on this foundation, clear objectives and work packages will be defined. The subsequent methodological section will describe the chemicals used, laboratory equipment and procedures, as well as analytical methods. This is followed by the presentation and discussion of experimental results, which are broadly structured into lignin characterization, chemical system development, product-catalyst separation, and continuous processing. Finally, a brief conclusion and an outlook for future projects will be presented.

4. Theoretical background

In this chapter, a thorough overview of the background and context is provided. This overview covers the definition of renewable resources – breaking down biomass to plant biomass, lignocellulosic biomass and its components. Additionally, the properties and applications of the predominantly utilized chemicals – aromatic compounds and polyoxometalates – are provided. Lastly, all applied process engineering concepts are presented.

4.1 Biogenic resources

Biogenic resources or simply biomass is the entirety of all living phytomass and zoomass (plants and animals), and all their produced residues. This also includes all substances produced by any form of technical conversion of the previously described materials. In total, the global biomass is estimated to be 3,500 Gt (dried weight) and roughly 170 Gt of renewable raw materials regrow annually – for a comparison, the global, finite reserves of crude oil were estimated to be ~220 Gt (2021), which makes the potential of renewable materials clear. In terms of distribution, plants account for approx. 83 % of biomass, followed by approx. 13 % of bacteria and the rest is split between other microorganisms (fungi, archaea, protists and viruses) and animals, as shown in **Figure 4-1**. [11,12,19,20]

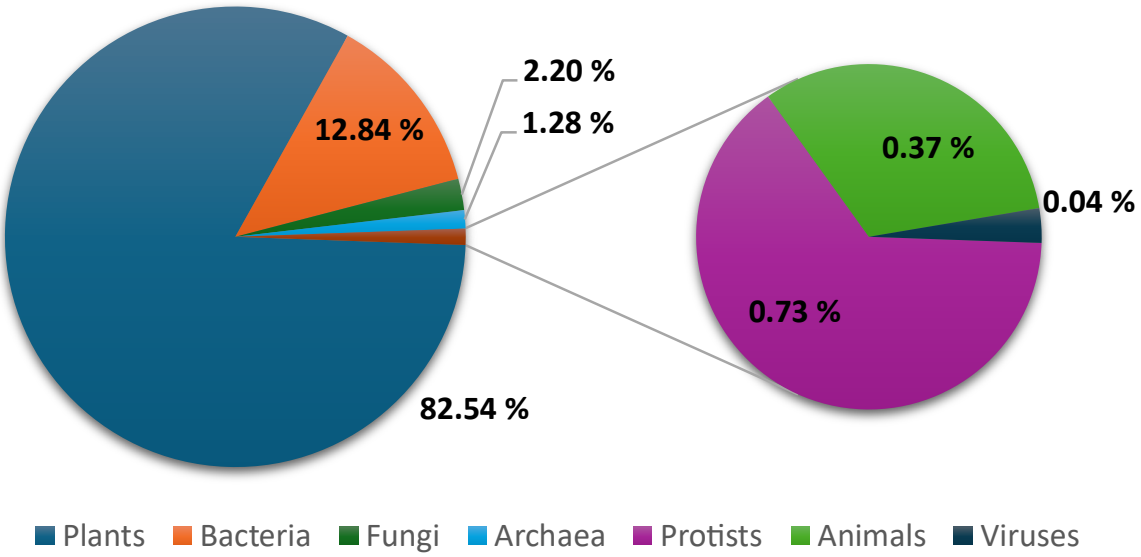

Figure 4-1: Estimated global distribution of biomass by taxa (regarding carbon weight). [19]

Biogenic resources are classified in primary, secondary and tertiary biomass. For the first class, the energy of the sun is directly utilized to form primary biomass directly from photosynthesis. Thus, all the phytomass and its residues contribute to this class. Secondary biomass obtains its energy from the sun indirectly as it is formed by degradation or conversion of primary biomass towards more sophisticated organisms – hence, all zoomass and its residues account for this class. Finally, all substances and materials formed by technical processing of primary or secondary biomasses are tertiary biomass. This includes materials such as paper, wooden furniture or even chocolate. Summarized, both secondary and tertiary biomass depend on primary biomass. Hence, the source of all renewable resources is the sun and its energy enabling photosynthesis of plant biomass. [11,12]

Photosynthesis is the naturally occurring chemical conversion of carbon dioxide (CO_2), water (H_2O) and light to carbohydrates and oxygen (O_2), as depicted in **Scheme 4-1**. The pigment chlorophyll acts as a photoactive catalytic compound and utilizes the energy of the sun light for this conversion storing it inside the produced carbohydrate materials. [21–23]

$$n\ CO_2 + n\ H_2O \xrightarrow{\Delta E_{Light}} C_nH_{2n}O_n + n\ O_2$$

Scheme 4-1: General chemical equation of photosynthesis. [21]

The products of photosynthesis are subsequently converted by secondary biomass (i.e. animals) in cellular respiration into chemical energy. This process produces H_2O and CO_2, thus completing the (CO_2-neutral) cycle and enabling photosynthesis again. [12]

The utilization of renewable resources, particularly plant biomass due to its global abundance, in global industry thus presents an excellent alternative to fossil materials, as well as a solution to climate change. The next section will therefor examine the structure and composition of plant biomass in more detail.

4.1.1 Structure of plant biomass

Plant biomass in its dry state mainly consists of the elements carbon (40-60 wt.-%), oxygen (20-60 wt.-%) and hydrogen (3-10 wt.-%), but also contains other elements such as nitrogen (0-11 wt.-%), sulphur (0-2 wt.-%) and traces of metals and metalloids (i.e. silicon, calcium, potassium, or manganese). Clearly, its elemental composition shows a large variance which is due to its dependence on biomass type, geographical origin and fluctuations of weather and climate. [24–30]

In terms of chemical components, plant biomass mainly consists of carbohydrates, triglycerides, lignocellulose (consisting of cellulose, hemicellulose, lignin), and other neglectable compounds such as proteins or ash. Carbohydrates constitute the majority with approx. 75 % (cellulose, hemicellulose, starch and sugars), followed by lignin with 20 % and triglycerides (including other components, such as proteins) with 5 %, as shown in **Figure 4-2**. In the following sections each of the previously mentioned components will be discussed. [31]

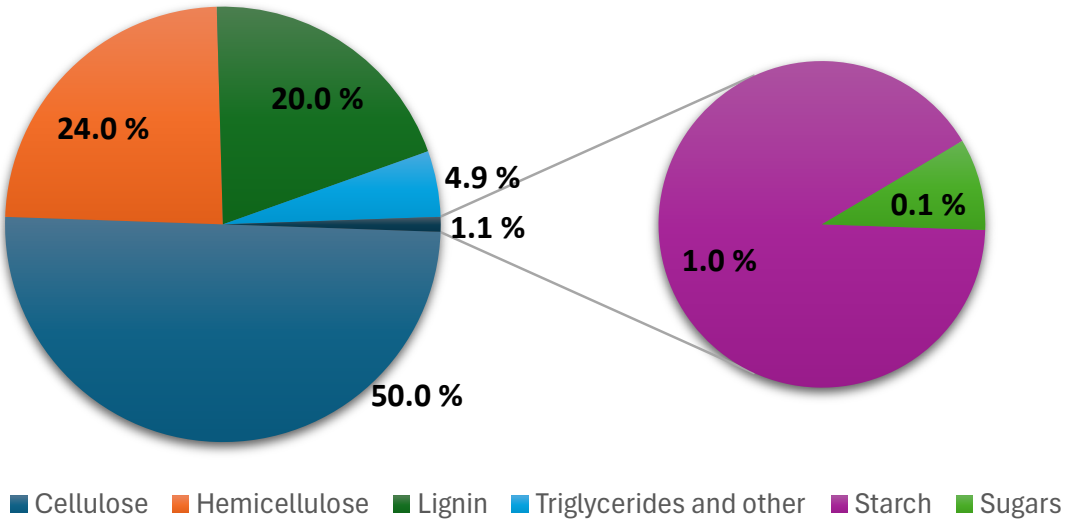

Figure 4-2: Estimated distribution of renewable compounds in plant biomass. [31,32]

4.1.1.1 Structure of carbohydrates

The word *carbohydrate* originates from the molar ratio (1:2:1) of their constituents carbon (C), hydrogen (H) and oxygen (O), respectively, and the chemical formula $C(H_2O)$ suggested in the 19th century. Here, the constituents are carbon (*carbo*) and water (*hydrate*) resulting in the term *carbohydrate*. Nowadays, it is well known that carbon and water are not linked in that way, however, the term remains. [11]

The basic building block of carbohydrates are sugars or saccharides (sugar: *saccharum*, Latin; *saccharon*, Greek) and their general chemical formula is $C_nH_{2n}O_n$ (with n being a natural number) and thus analogous to the chemical equation of photosynthesis (cf. **Scheme 4-1**). The carbon chain length commonly varies between three and six atoms – sugars with three carbons are called trioses, with four tetroses, with five pentoses and with six hexoses. Additionally, saccharides are distinguished by presence of an aldehyde- or ketone-group being called aldoses or ketoses, respectively. A common aldohexose (hexose with an aldehyde group) is glucose and a common ketohexose (hexose with a ketone group) is fructose, as depicted in **Figure 4-3**.

These monosaccharides can be connected to complex carbohydrates, such as the disaccharide sucrose from glucose and fructose, again depicted in **Figure 4-3**. Ultimately, the chemical linkage of saccharides leads to polysaccharides such as starch, cellulose or hemicellulose – the latter two will be described later in this section. [11,33,34]

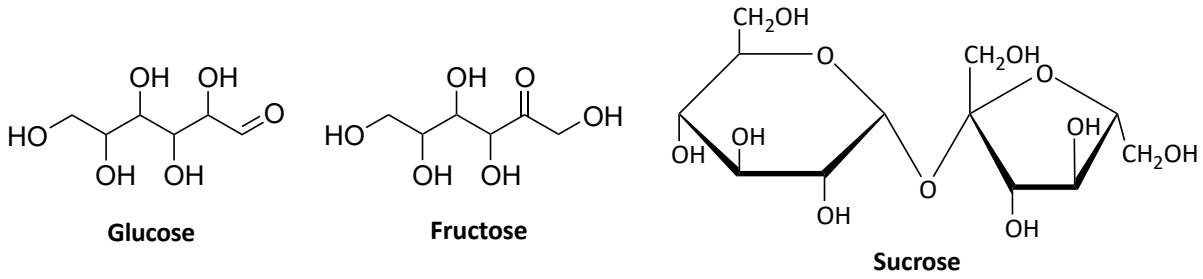

Figure 4-3: Chemical structure of the aldohexose glucose (left), the ketohexose fructose (middle) and the disaccharide sucrose (right). Adapted from [33].

4.1.1.2 Structure of triglycerides

Another component in plant-based biomass are fats and oils which are acting as an energy storage mostly in their seeds. The differentiation of fats and oils is the melting point – fats have a higher melting point than room temperature (making it solid) and oils have a lower (making it highly viscous or liquid). Chemically, fats and oils are triglycerides consisting of the triol glycerol and long-chained carboxylic acids, so-called fatty acids, which are connected by ester bonds, as shown in **Figure 4-4**. [11,32,33]

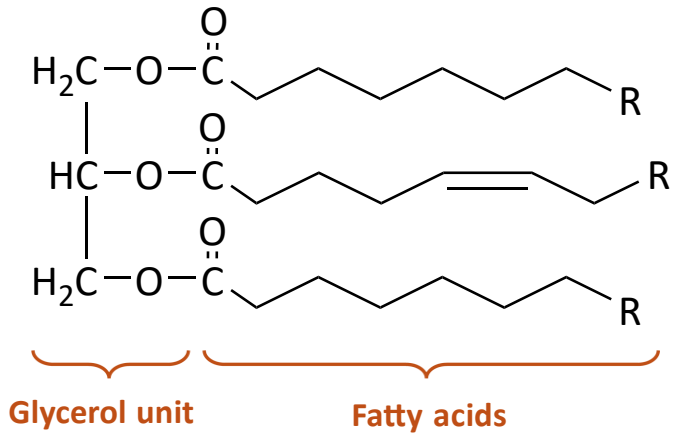

Figure 4-4: Scheme of an exemplary triglyceride showing the glycerol unit and the fatty acids with varying functionalization and R being a saturated or unsaturated alkyl chain. Adapted from [11].

The fatty acids are mostly unbranched, have an even number of carbon atoms and show further functionalization such as alcohol or epoxy groups. They occur both saturated (mostly in *cis*-configuration) and unsaturated and their typical carbon chain length lies between 12-22 atoms, however, specifically 12 and 18 carbon atoms are the predominant chain lengths depending on vegetable oil. The characteristics of the fatty acids determine the ultimate properties of triglycerides. For example, triglycerides with a high content of unsaturated, short-chained fatty acids are usually solid, whereas triglycerides with a high content of branched, long-chained fatty acids are liquid. Thus, for the industrial application the selection of the right vegetable oil is vital. A few industrially relevant vegetable oils are coconut oil, palm oil, rapeseed oil, sunflower oil or soybean oil. [11,32,33]

4.1.1.3 Structure of lignocellulose

Lignocellulosic biomass or lignocellulose makes up approx. 90 % of all terrestrial biomass and, thus, represents the most abundant renewable resource on earth. Lignocellulose is composed of the three biopolymers cellulose, hemicellulose, and lignin. Depending on various factors, such as biomass type, plant maturity or climate effects, these polymers are organized into a complex, heterogeneous structure to different degrees and varying relative composition. **Figure 4-5** shows a scheme of lignocellulose and its three-dimensional structure in which cellulose is the centre component and wrapped by the dense structure formed by hemicellulose and lignin. [35,36]

The tensile fibres of cellulose are combined with lignin and hemicellulose to a bio-based composite material. The three-dimensional polymer lignin consists of aromatic building blocks forming a stiff and rigid matrix, supported by hemicellulose, which protects the cellulose from enzymatic degradation. Due to its non-uniform distribution in plants, the polymer contents vary between 35-50 % for cellulose, 20-35 % for hemicellulose and 10-25 % for lignin. In the following sections a more detailed overview of both cellulose and hemicellulose will be given. [11,32,36–42]

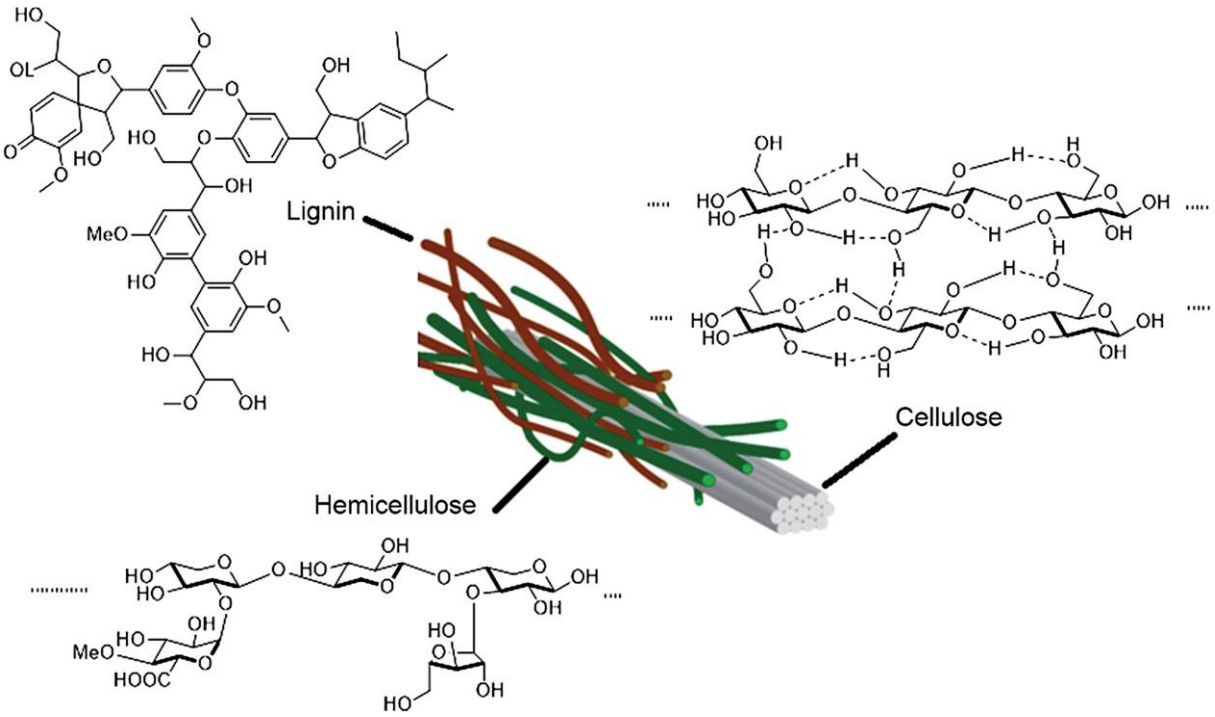

Figure 4-5: Scheme of lignocellulose fibre showing structure and the biopolymers cellulose, hemicellulose, and lignin. [43]

Cellulose

The polysaccharide cellulose is also a carbohydrate, as described in the section **4.1.1.1**, which makes up the majority of wood and woody biomass (such as beech, birch, spruce, or pine) and, thus, cellulose is the most abundant resource on the planet. It consists of a straight chain of 500-5,000 glucose units which are linked by a β-1,4-glycoside bond, as shown in **Figure 4-6**. The average molecular weight lies between 200,000 and 1 Mio. Da. As can be seen in **Figure 4-6**, the linear bonds of cellulose cause a planar structure allowing hydrogen bonding of neighbouring chains. This promotes both stability of the polymer structure and crystallinity, resulting in a heterogeneous polymer with amorphous and crystalline segments. This crystallinity makes cellulose a robust and water insoluble fibre. Biomasses with a high content of cellulose are fibre plants, such as cotton, jute, flax or hemp, showing contents of 70-90 %. [11,32,37,38,42,44,45]

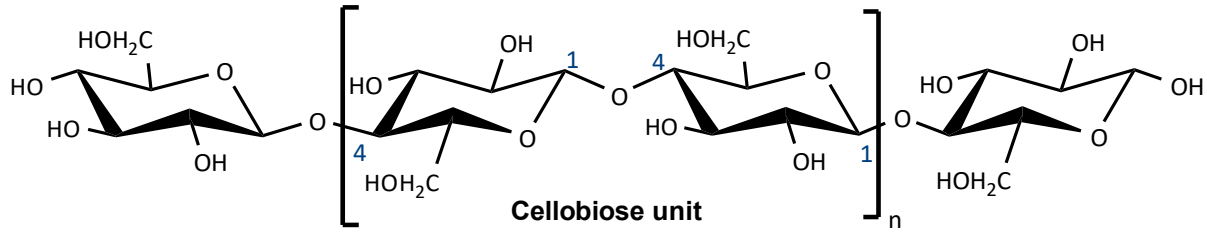

Figure 4-6: Scheme of cellulose polymer chain showing the repeating cellobiose unit. [11]

Hemicellulose

As described earlier, hemicellulose is a part of the matrix protecting the centre component of lignocellulose and is, similarly to cellulose, a polysaccharide. However, hemicellulose is a heteropolymer consisting of the sugars D-xylose, L-arabinose, D-glucose, D-galactose, and D-mannose, as can be seen the top of **Figure 4-7**. The exact composition depends on the type of plant and while for hardwoods (e.g. beech or oak) the predominant hemicellulose is xylan, for softwoods it is glucomannan. These hemicelluloses are depicted in the bottom of **Figure 4-7**. The polymers tend to a branched structure promoting amorphous behaviour. These structural and chemical properties allow for a higher solubility, especially in diluted alkali solution, and hemicellulose can be acidly hydrolysed to its monomer components. This makes hemicellulose more accessible and easier to separate from cellulose. In the matrix of lignocellulose, hemicellulose shows cross-links to either cellulose or lignin strengthening the cell walls. [11,32,36–38,42,46–48]

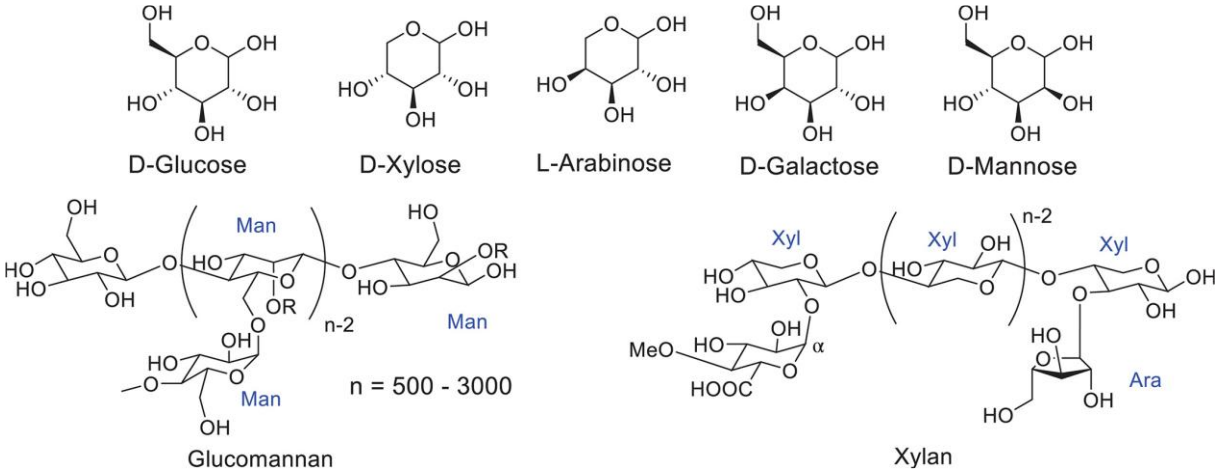

Figure 4-7: Common pentoses and hexoses present in hemicelluloses (top) and structure of glucomannan and xylan (bottom), where *Xyl*, *Ara*, and *Man* stand for xylose, arabinose, and mannose, respectively. Adapted from [43].

Lignin

The third and final compound of lignocellulosic biomass is the three-dimensional, aromatic biopolymer lignin. Due to the importance of this compound for this work, the definition, structure, and application of lignin will be more thoroughly discussed in the next section.

4.2 Lignin

As stated above, lignin is the third and final component of lignocellulosic biomass and is not a carbohydrate in contrast to cellulose and hemicellulose. Its discovery reaches back to 1838, when the French chemist *Anselme Payen* [49] treated wood with concentrated nitric acid and washed it with dilute aqueous sodium hydroxide solution, afterwards. This treatment yielded an insoluble material, which was cellulose, and a partly dissolved, encrusting material he defined as *le material encrustant*. It was the German chemistry professor *Franz Ferdinand Schulze* [49] who designated this material as lignin in 1857. Here, the term lignin originates from the Latin word for wood *lignum*. Later in the 19th and in the beginning of the 20th century, it was the chemist *Peter Johan Klason* [49] who evolved to be a pioneering researcher regarding lignin chemistry. He proposed structural components, the overall composition and developed a chemical procedure for lignin content determination (so-called *Klason* lignin content) which even nowadays is a common parameter for lignin characterization. [11,32,49]

Of course, the characterization techniques and definition of lignin has improved over the decades and in this section a proper definition including properties of lignin will be discussed. This is followed by technical considerations of industrial processes producing lignin and its current industrial applications.

4.2.1 Definition of lignin

Lignin is a three-dimensional, heterogeneous, amorphous, and aromatic biopolymer commonly found in woody biomass. Its global production in trees and forest growth is estimated to be 20 Gt per year and for a comparison the overall global consumption of crude oil is 4-5 Gt per year. This explains why lignin is projected to be a promising renewable feedstock for chemical industry, as it is mostly treated as a waste product, currently. Depending on plant type lignin makes up 15-40 % of lignocellulose, thus, is the third most abundant biomass material on earth and represents the only renewable resource, in these magnitudes, with aromatic functionalities. [11,35,50,51]

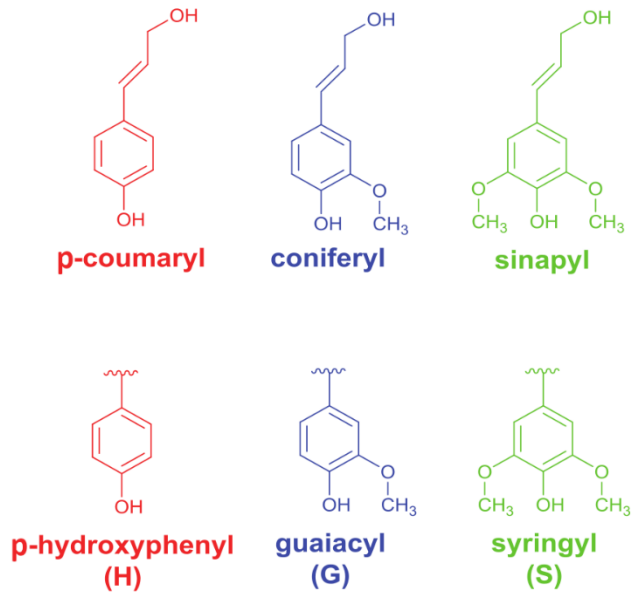

Figure 4-8: Scheme of the three phenylpropanoid lignin monomers, so-called monolignols, and their corresponding unit designations inside the lignin polymer. [52]

In plants lignin has various functions. First and foremost, it is responsible for the compressive structure and stability. However, lignin is also controlling the permeability of water in cell walls, and it provides protection of UV light, mechanical penetration, and microbial degradation. Lignin consists of the three phenylpropanoid units, so-called monolignols (monomers of lignin), p-coumaryl, coniferyl and sinapyl alcohol, as shown in the top of **Figure 4-8**. As can be seen, the only difference of these monomers is the degree of methoxylation in meta position raging from zero to two. The monolignols are formed in plastids, a plant cell organelle, via the phenylalanine metabolic pathway and later incorporated into the polymer structure by radical polymerization. Here, the monomers are designated as p-hydroxyphenyl (*H*), guaiacyl (*G*) and syringyl (*S*) units, as shown in the bottom of **Figure 4-8**. [11,52–55]

Due to the radical-induced polymerization of the monolignols the detailed structure of lignin is highly random, impossible to predict, and, therefore, explains the amorphous and heterogeneous behaviour. In **Figure 4-9** an exemplary, two-dimensional structure of this polymer together with occurring chemical bonds are shown. The actual distribution of the monolignols in lignin heavily depends on the type of plant. Overall, softwoods usually show more *G* units, whereas hardwoods usually have a higher content of *S* units. Grasses, on the other hand, show an even distribution of all three units. Additionally, over the age of a plant the distribution can change. The older the plants get, the more *G* units and eventually *S* units are

formed, which increases cross-linking capabilities and, thus, increasing stiffness of the plant. [52,54]

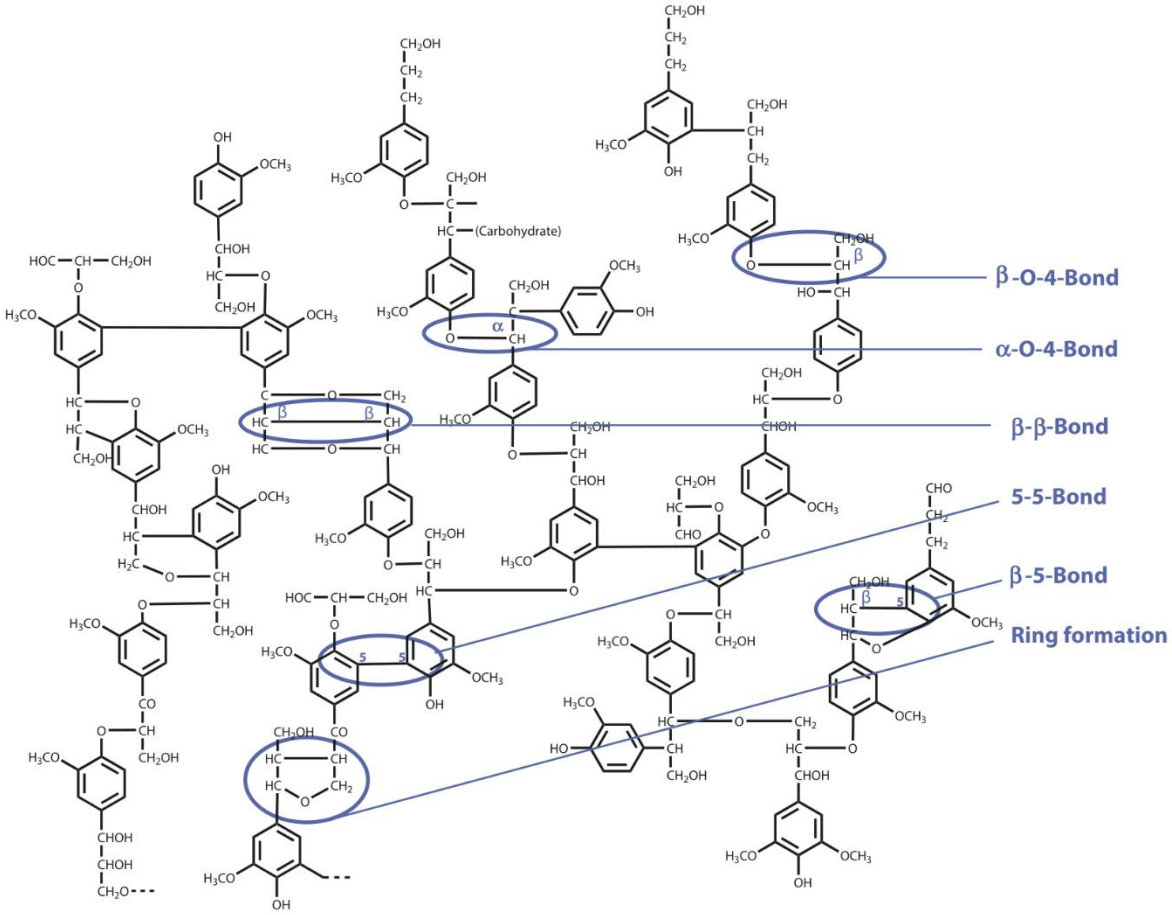

Figure 4-9: Exemplary, two-dimensional structure of lignin and all occurring chemical bonds of monolignol links. [11]

The random structure, the varying distribution of monolignols and the difficulties of lignin separation, due to covalent bonds to cellulose and hemicellulose, are all reasons why a definitive characterization of lignin and its properties is a challenging task. Still, the characterization of lignin has been an active research topic throughout the decades and in the next section both physical and chemical properties of lignin will be discussed. [11,56]

4.2.2 Physical and chemical properties of lignin

The biopolymer lignin is a thermoplastic, polydisperse macromolecule. It is responsible for the aromatic odour of freshly manufactured books. It shows a comparably high calorific heating value with 20-25 GJ/t which is approx. 30 % higher than for other renewable biomass compounds. Due to the aromatic functionality lignin both exhibits the previously mentioned

UV light protection, and it is hydrophobic and, thus, insoluble in water (at least chemically unmodified lignin). The base monolignol (cf. **Figure 4-8**) linkage types are alkyl-alkyl, alkyl-aryl, and aryl-aryl ether bonds. These result in the various linkages depicted in **Figure 4-9** and demonstrate the high randomness of the polymer. The distribution of linkages again depends on plant type and isolation process. Hardwood, for example, shows a higher occurrence of β-O-4 linkages compared to softwood, whereas the 5-5 linkage is more prominent in softwood. [11,39,52–55,57,58]

Since lignin is impossible to isolate from lignocellulose without alteration, most properties described in literature [55] do not refer to native lignin but technical lignins which were extracted by mechanical or chemical modification of lignocellulose. In this context, the applied isolation or extraction procedure is essential when comparing lignin characteristics. It is common practice to describe the lignin with the applied extraction process. So, lignin produced by the so-called kraft process is described as kraft lignin. The details of the most common industrial processes will be described later in section **4.2.3**. The properties discussed below refer to these chemically modified lignins. The industrial processes considered here are kraft process (or sulfate process), sulfite process (producing lignosulfonates), soda process and organosolv process. [55]

Below in **Table 4-1**, various physical and chemical properties of technical lignins are compared. Both the plant type and the isolation significantly influence the properties of the resulting lignin. Particularly, the molecular weight, the sulphur content, and the solubility are subject to change depending on the process type. For lignosulfonate lignins, for example, comparably high molecular weights of up to 50,000 Da and sulphur contents of up to 10 % are present, while exhibiting a solubility in water at all pH values. Organosolv lignins, on the other hand, show small molecular weights at 1,000 Da, no sulphur content at all, and a solubility especially in organic solvents.
Additionally interesting and not part of the table, is the thermal decomposition as this property is not as dependent on the lignin process type as the properties in **Table 4-1**. The thermal decomposition temperature has a broad range from 200-500 °C due to lignin's complex and heterogeneous structure. During the temperature elevation lignin is defragmented into smaller species or the polymer chain is completely rearranged. At lower decomposition temperatures (~200 °C) especially formic acid, formaldehyde, carbon dioxide, sulphur dioxide or water are eliminated causing a weight loss in the remaining polymer. At higher temperatures (>300 °C)

even aromatic compounds are formed and ultimately at temperatures of 500 °C methane and hydrogen can be released. [52,59]

Table 4-1: Comparison of physical and chemical properties of lignins from common technical processes.

Lignin property	Kraft	Sulphite	Soda	Organosolv
M_W / Da	2,000-3,000	20,000-50,000	2,000-5,000	1,000-3,000
Polydispersity	2-3	6-8	1-2	3-6
T_g / °C	120-170	70-90	120-140	90-100
Sulfonates / %	0	1-3	0	0
Organic sulphur / %	1-2	4-8	0	0
Solubility	Soluble in alkali (pH > 10.5), acetone	Soluble in water at all pHs, less soluble in organics	Soluble in alkali, methanol	Soluble in various organic solvents and diluted alkali
Colour	Dark brown	Light brown	Dark brown	Light brown
References	[52,55]	[52,55]	[60–63]	[55,60,64,65]

In summary, both physical and chemical properties of lignins are heavily influenced by the applied process isolation type. For a better understanding, common industrial process types will be described in the next section in detail.

4.2.3 Industrial processes for lignin production

The practically sole producer of lignin is the pulp and paper industry. Here, the cellulose is of particular interest and, thus, is isolated from the lignocellulose and used for paper or cardboard production. While small fractions of lignin can exhibit positive effects on paper, it is mostly an undesired byproduct and generally just burned for energy recovery. The lignin annually produced in this way exceeds 50 Mio. tons and some sources claim to reach up to 100 Mio. tons. [32] During this cellulose isolation lignin is solubilized by chemical procedures which induce process-individual modifications on lignin, as presented in **Table 4-1**. These so-called pulping processes, isolating cellulose and solubilizing lignin, can be distinguished in sulphur-containing and sulphur-free processes. The industrially most relevant and sulphur-

containing methods are the kraft and the sulphite processes which make up the majority (>95 %) of produced lignin stream. Industrially less relevant but still promising regarding valorisation are the sulphur-free soda and organosolv processes for which only small scaled and pilot-plants are in use. In **Table 4-2** an overview and comparison of these four pulping methods are shown and below a more detailed description of each process will be given. [11,13,55,66,67]

Kraft process

The predominant kraft pulping process has been established in 1879 by *Carl Ferdinand Dahl* and in 1890 the first operating factory in Sweden was documented. [11] Generally, and this is similar to all pulping processes, the wood is mechanically debarked and shredded to wood chips with a length of approx. 2 cm and a thickness of approx. 5 mm. This guarantees both that sufficiently long fibres are available for paper production and that the chemicals can penetrate the wood chips to solubilize lignin. This penetration is conducted under alkaline conditions with sodium hydroxide (NaOH) and sodium sulphide (Na_2S) (together known as white liquor) at temperatures usually around 180 °C and at reaction times of 3-5 h. This leads to cleavages of the linkages to cellulose and hemicellulose and to the β-O-4 ether bonds connecting the monolignols which increases the amount of phenolic hydroxyl groups and, thus, the solubility in aqueous environments. During this procedure, sulphur is also added to the lignin polymer (cf. sulphur content in **Table 4-1**) and the process related sulphur losses are compensated by the additive sodium sulphate (Na_2SO_4). This additive has given the process its name (sulphate process) and the more common name kraft is due to the strength of the produced paper and the German word for strength "*kraft"*. The resulting solution has a dark, brownish colour named black liquor. The solid cellulose fraction is separated, and the black liquor is then to be purified and recycled. By burning the concentrated black liquor the Na_2S, necessary for the lignin solubilization, is renewed through the chemical reaction of the additive Na_2SO_4 and the lignin-based carbon. This combustion of black liquor is highly integrated to the process plant and, thus, substantial for the kraft process. The commercial availability of kraft lignin is, therefore, rather low. However, it is possible to isolate the lignin by precipitation adding acidic additives reducing the pH to 5-7 and various precipitation methods have been established over the years, i.e. IndulinLignin, LignoBoost or LignoForce. [11,13,54,67–69]

Table 4-2: Overview of parameters for common pulping processes producing lignin. Production estimations originate from the years 2000 to 2010.

Process property	Kraft	Sulphite	Soda	Organosolv
Est. global production / t a^{-1}	55,000,000	1,800,000	10,000	5,000
Solvents	Water	Water	Water	Mixture of H_2O & MeOH, EtOH, acetone
Additives	NaOH, Na_2S, $NaCO_3$, $NaSO_4$	Na_2/Ca/$MgSO_3$ SO_2	NaOH	HCl, formic acid, acetic acid
pH range	10-13	2-7	13-14	4-7
Temperature / °C	150-180	140-150	140-180	170-200
Lignin purity / % ***(excluding moisture)***	60-90	75-85	Comparable to kraft	>90
References	[11,13,54,67–69]	[11,13,54,67,68,70]	[13,54,67,71]	[11,13,54,65,67,70]

Sulphite process

The sulphite pulping process was invented earlier than the kraft process in 1866 by the American *Benjamin Tilghman* [11] but was not able to achieve the same strength and tear-proof properties as kraft lignin. During this process an acidic aqueous environment, sodium-, calcium- and magnesium-based sulphite salts and, comparably, milder temperatures are utilized. Again β-O-4 but also α-O-4 ether bonds, linkages to cellulose and hemicellulose are cleaved this way and, additionally, sulfonated groups are added to the lignin polymer leading to a higher content of sulphur (cf. **Table 4-2**). The resulting solution is called brown liquor, and it is easily separated from the cellulose pulp. The brown liquor can then be combusted for energy recovery but most importantly lignosulphonates are precipitated, so the remaining chemicals can be recycled for the process. The precipitation is done by ultra-filtration and other membrane separation techniques. The isolated lignosulphonates are the predominant commercially available form of lignin. [11,13,54,67,68,70,72]

Soda process

The soda process was one of the first pulping processes invented around the 1850s and the first mill was operated in 1866 in the US. In contrast to the nowadays commercial processes, soda pulping is sulphur-free but otherwise quite similar to the kraft process. Because of this, most of the soda mills were converted into kraft mills once it was established. The major difference is that sodium hydroxide (sometimes additionally anthraquinone) is the sole additive and higher pH values are usually utilized. This also leads to ether bond cleavages and to an increase of phenolic hydroxyl groups allowing the lignin solubilization. After that the solid pulp is separated and the lignin fraction can be precipitated by acidifying with sulphuric acid to pH 2-3. Typically, the soda process is applied for the treatment of non-woody materials such as grasses, straws and agricultural waste products. [13,54,67,71,73]

Organosolv process

The organosolv process is a relatively new method and was invented and patented in 1971 [11]. Like soda pulping, organosolv is a sulphur-free process and from the discussed processes the only one utilizing organic solvents. Usually a mixture of 40-60 % of organic solvent, such as methanol (MeOH), ethanol (EtOH) or acetone, and water are applied together with acidic additives such as hydrochloric acid (HCl), formic acid (FA) or acetic acid (AA) as a cooking liquor. The treatment is performed mildly acidic at comparably higher temperatures reaching 200 °C. Similar to the other pulping processes the α-O-4, β-O-4 ether bonds and linkages to carbohydrates are cleaved solubilizing the lignin. For organosolv, however, the resulting lignin shows the higher purity and is claimed to be the closest to native lignin which is a promising feature for the valorisation of lignin. The solid pulp is separated, and the lignin can be precipitated by the addition of water as the lignin is only soluble in organic solvents or by the evaporation of the organic solvent. In both cases, most of the solvent can be recycled. However, this recovery is quite energy intensive and, thus, costly. Additional disadvantages are moderate environmental risks due to the solvents and a higher complexity of reactor vessels due to higher partial pressures of the solvent. There are various sub-forms of the organosolv process, such as organocell, alcell or acetosolv. [11,13,54,65,67,70,74]

Other processes

There are of course additional processes for lignin fractionation which all have their advantages. One method yields milled-wood lignin (MWL) which is produced solely by mechanical

procedures and thus is considered native lignin. Another one is steam explosion where a sudden pressure relief leads to the cleavage of carbohydrate linkages. Lastly, hydrolysis of lignocellulosic biomass yields hydrolysis lignin which is majorly produced in so-called biorefineries, or lignin from ionic liquid fractionation where the lignin is dissolved in ionic liquids and later precipitated. Due to small production volumes, these lignins are not relevant industrially, so far. [13,17]

Now that the pulping processes producing lignin as a side-stream have been explained, the next interesting step is to discuss the industrial and other potential applications of lignin which will be done in the next section.

4.2.4 Industrial applications of lignin

Even though the annual production of lignin is estimated to be between 50 and 100 Mio. tons (2004) [66], only a minority is commercially available. This is due to the fact that kraft pulping is the predominant pulping process accounting for >90 % of produced lignin and the here produced lignin is mainly burned for energy recovery and chemical recycling. It is estimated that annually 1.5 Mio. tons of lignin are not burned, currently. Roughly 80 % of this commercially available lignin stems from the sulphite process, only 15 % emerge from the kraft process and, finally, the remaining 5 % stem from processes like soda, organosolv and others. Commercial producers currently are Borregaard LignoTech, which is dominating this business, but also Tembec, Fraser Papers and Nippon Papers supply lignin. The current industrial applications will now be discussed in detail, followed by emerging technologies researched in recent years. [43,55,62,75]

Industrial applications

Industrial applications of lignin are limited to lignosulphonates and kraft lignins as to their production capacity. Due to commercial availability, lignosulphonates find a broad range of uses. The predominant field of application is in civil engineering where the lignosulphonates in concrete and cement act as a water reducer and improve strength and resistance to degradation. They have a similar effect and use in the production of bricks, ceramics and refractions. In fodder industry lignosulphonates are used as a binder in animal feed and pellets to encapsulate the particles providing improved handling but still enabling disaggregation when in contact with water due to its water solubility. They are also used in dyes, pigments or pesticides as a

dispersant agent, and they can also be utilized as a dust controlling agent. When they are applied to the surface of drying particles, the lignosulphonates, absorbing the evaporating water, become viscous and enclose the now dusty particles preventing dust formation. Another application, different to the previous ones, is the chemical depolymerisation to the compound vanillin, which is the main flavouring agent of vanilla and, thus, used in food and fragrance industry. This conversion process is currently only done by Borregaard LignoTech. To summarize, lignosulphonates are mostly utilized as additives without further modification to improve certain material properties. On the other hand, kraft lignins find less application due to their limited commercial availability. Their field of application is similar to that of lignosulphonates. But kraft lignins must be chemically altered by oxidation or sulphonation to mimic the properties of lignosulphonates, however, the resulting properties are inferior to those of lignosulphonates. [54,55,59,66,72,75]

Emerging technologies

Due to the current limited chemical application of lignin and its potential as an alternative to fossil aromatic compounds, the chemical conversion and valorisation of lignin has been a prominent research topic in recent years [17]. These technologies focus on lignin conversion by oxidation, reduction, hydrolysis (including acidic and alkaline), solvo- and thermolysis, pyrolysis or gasification, and a broad product range is achieved by these methods. For pyrolysis, the main products are solid-biochar, bio-oils or gaseous hydrocarbons depending on the process parameters. Similarly, but with the addition of water, gasification of lignin is designed to yield syngas (CO/H_2) which can be used in the already existing syngas economy. However, in both cases a significant portion of lignin's aromaticity is lost. The remaining conversion technologies are, thus, generally designed to preserve these aromatic functionalities producing monolignol derivatives together with aliphatic hydrocarbons containing aldehyde, ketone, carboxylic or hydroxy groups. Reductive depolymerisation usually yields both linear and cyclic aliphatic hydrocarbons with reduced functional groups, besides aromatic compounds. Typical oxidative products at mild process conditions (T: 50-100 °C, p: 5-20 bar) are highly functionalized phenolics and carboxylic acids. At harsher conditions (T: 100-200 °C, p: 20-50 bar) primarily carboxylic acids. Depolymerisation by alkaline/acidic hydrolysis or solvo-/thermolysis majorly produce aliphatic hydrocarbons, including saturated, and minorly phenolics. The aliphatic hydrocarbons represent platform chemicals which can be further processed to applicable

products. Projected application of phenolic products is in polymer industry and as speciality chemicals. [13,17,67]

To conclude, lignin is majorly used for energy recovery and only a small fraction of less than 5 % is utilized otherwise. Here, unmodified lignin is majorly applied as an additive. Yet, as lignin is the only renewable, major source of aromatic functionalities, the depolymerisation of lignin towards phenolic compounds has been a major research topic. In the following, the relevant aromatic compounds within this work will be further discussed.

4.3Relevant aromatic compounds

Regarding the industrial transition towards sustainability, more environmentally friendly aromatic platform chemicals must be found. Two promising compounds that could be a part of the substitution of fossil-based platform chemicals are vanillin and syringaldehyde as both can be produced from lignin and a concise overview of both will be given in the following sections.

4.3.1 Vanillin and its derivatives

Vanillin or 4-hydroxy-3-methoxybenzaldehyde is the name for the chemical compound with the formula $C_8H_8O_3$ and the structure shown in **Figure 4-10**. It exhibits a benzylic ring as its base which is further functionalized with an aldehyde, methoxy and hydroxy group. The first reported isolation was described by *Gobley* in 1858 [76]. This was achieved by alcoholic extraction and subsequent crystallization of vanilla beans of the plant *vanilla plantifolia*. Vanillin is a solid, colourless powder at room temperature exhibiting a characteristic smell of vanilla flavour. The melting point is at 81 °C and it is hardly soluble in water, while extremely soluble in organic alcohols, such as methanol or ethanol. Due to the highly reactive functional groups in vanillin, it exhibits certain instabilities. During atmospheric distillation vanillin undergoes partial decomposition. Dimerization to dehydrodivanillin can occur when exposed to light in alcoholic solvents and even exposure to air can cause oxidation to vanillic acid. The technical reduction of vanillin, on the other hand, results in vanillyl alcohol with high yields. [15,77]

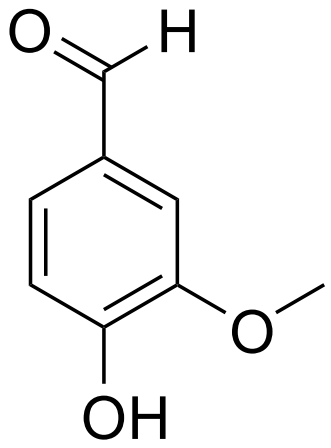

Figure 4-10: Chemical structure of vanillin. [120]

Due to the low contents of vanillin in the vanilla plant, being around 2 %, and due to the complex extraction process, the price of this natural vanillin is extremely high with 1,000 to 4,000 $/kg. This is the reason why the majority (approx. >90 %) of vanillin is produced synthetically resulting in reduced prices. Roughly 15 % of produced vanillin stem from lignin. This process is conducted by the Swedish pulp and paper company Borregaard Industries Limited. The lignin-containing side streams of their sulphite process are oxidized at alkaline conditions to produce vanillin. In recent years, the process development for vanillin production adapted to the other pulp and paper processes has been a prominent topic in literature. By utilizing lignin, the vanillin is still synthetic but could be CO_2-neutral. On the other hand, the remaining 80 – 85 % of vanillin are synthesized from the BTX compounds of crude oil and, thus, emitting CO_2. First, preferably benzene is functionalized to phenol by halogenation followed by hydrolysis. During the second step, phenol is further modified to add the methoxy group, first to catechol, as an intermediate, and then to guaiacol. Lastly, the aldehyde group is added by varying reaction pathways, i.e. by Gatternann reaction, or Reimer-Tiemann reaction plus hydrolysis. In conclusion, the majority of the globally 20,000 t/a produced vanillin originates from anthropogenic sources and, accordingly, promote climate change. [15,17,77–84]

Vanillin is utilized in various fields of application. The first and most obvious field is in food industry as a flavouring compound for baking, chocolate, confections, vanillin sugar and beverages. It is also used as an additive to animal fodder to flavour-mask any off-taste of added minerals. These applications make up approx. 30 % of vanillin use. Another prominent application is in perfume and cosmetic industry. In fragrances vanillin can make up to 10 % of the odour, in deodorant it is, again, utilized to cover any unpleasant smell of additives and in sun-scream both the pleasant smell and the UV-light blocking properties are utilized. Lastly, vanillin is an important base chemical in pharmaceutical industries, as it can be converted to various drugs, such as Methyldopa used against high blood pressure, L-Dopa used for Parkinson's disease treatment, Trimethoprim for treatment of urinary tract infections or venereal diseases, Mebeverine as an antispasmodic, or Verazide as an antitubercular agent. For

the derivates vanillic acid, vanillyl alcohol and 2-methoxyhydroquinone, the field of applications is not as big, however, they show a high potential in polymer industry. Through further modification, i.e. by epoxy, cyclic carbonates, allyl, amine, alcohol or carboxylic units they can be directly used for the production of polymers, such as polyesters, epoxy resins, or composite materials. [15,85–89]

4.3.2 Syringaldehyde and its derivatives

Syringaldehyde, or 4-hydroxy-3,5-dimethoxybenzaldehyde, has the chemical formula $C_9H_{10}O_4$ and its structure is shown in **Figure 4-11**. In literature it was first mentioned in 1897 by *Gadamer* who derived syringaldehyde from sinapinic acid, which can be found in wine, vinegar or black plums. However, further studies reported that it was firstly derived by oxidation and hydrolysis of syringin which also is a natural compound found in lilac plants, such as *syringa vulgaris*. Over the last decade, several synthetic routes have been proposed. The industrially most relevant one is based on *p*-cresol due to its broad availability, being a product from oil refineries, and, thus, low prices. [90–95]

The structural difference of syringaldehyde to vanillin (c.f. section **4.3.1**) is the addition of a methoxy group in *meta*-position. At room temperature it is a white to slightly yellow, often needle-shaped, solid exhibiting a characteristic aromatic odour. The material melts at temperatures around 113 °C and it shows similar solubilities as vanillin. Similarly, due to its moderately reactive functionalization, syringaldehyde shows various derivatives such as syringic acid, syringyl alcohol, or syringol. [93,95]

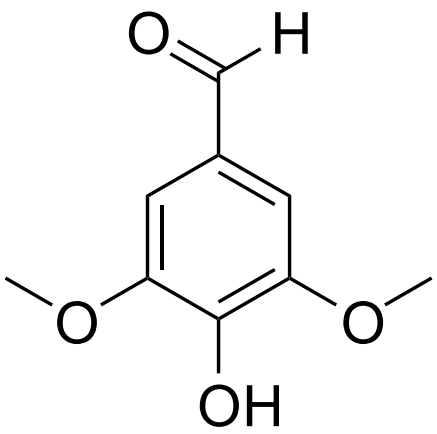

Figure 4-11: Chemical structure of syringaldehyde. [120]

Industrially, syringaldehyde is not as established as vanillin resulting in smaller production capacities and a more comprehensible field of application. Its main application lies in pharmaceutical industry where it is utilized in its pure form as it shows antihyperglycemic, antioxidative, and antiphlogistic behaviour if orally taken. Additionally, syringaldehyde is utilized for the

synthesis of the antibiotics Trimethoprim and Bactrim/Biseptol which promotes the growing interest. Lastly, as both syringaldehyde and vanillin can be formed by lignin treatment and share chemical functionalization, syringaldehyde also shows potential to substitute fossil-based aromatics in polymer industries for products, such as polyesters, polyacrylates, or polycarbonates. [93,96–100]

4.4 Polyoxometalates

Polyoxometalates (POMs) are a compound class representing a diverse family of metal oxide anion clusters. They exhibit a highly symmetric, often cubic structure, consist of $[MO_x]$ units where M represents early transition metals and, lastly, show unique properties regarding topological and electronic diversity. The first report of such a compound, specifically a phosphomolybdate, was in 1826 by *Berzelius* and in the following one hundred years researchers, such as *Marignac*, *Werner* and *Rosenheim*, proposed numerous structural compositions. In 1933 *Keggin* first experimentally determined the structure of the phosphotungstate $[PW_{12}O_{40}]^{3-}$ which is the reason why this POM structure received its name Keggin. Due to technical and analytical limitations further research on POMs has been a challenge, but with advancing sophisticated technology and the publications of *Pope* in the 1990s, the understanding and development of POMs has been massively promoted. This led to an exponentially growing interest of POMs over the last 30 years in various research fields, including chemistry, physics, biology, and materials science. [101–109]

4.4.1 Classification and properties of polyoxometalates

Polyoxometalates are formed by the condensation of the $[MO_4]^{2-}$ units resulting in the general formula $[MO_x]_y$. Here, the number of oxygen atoms (x) traditionally lies between four and seven and determines the geometry of the corresponding oxoanion and, subsequently, the overall structure of the POM. For example, this varying degree of condensation can lead to tetrahedra (for $x = 4$) or heptahedra (for $x = 7$). Overall, each metal atom is located within a $[MO_x]$ coordination polyhedron (usually an octahedron or a quadratic pyramid) which is shifted towards the polyhedral vertices due to M-O-π bonds. These early transition metals, mostly molybdenum (Mo), vanadium (V), niobium (Nb) or tungsten (W), are present in their highest oxidation state (+VI, +V, +V, +VI, respectively). One important structural principle of these clusters lies within maintaining the symmetry of the central polyhedron. However, the arrangement of the surrounding polyhedrons is subject to change enabling vast coordination

possibilities which then can be considered derivatives. The synthesis of POMs is usually conducted at aqueous conditions, however, there are reports of synthesises in non-aqueous solvents. The formation of these clusters is heavily dependent temperature, concentrations and pH value. For example, depending on the pH value various POM species can coexist in equilibrium. Their solubility is one of their key features allowing utilization in various polar mediums and even organometallic chemistry. Additionally, POMs possess excellent thermal stability and exhibit chemical stability against potential oxidants, as the metals are already in their highest oxidation state [110]. Lastly, POMs can be further classified depending on the presence of a heteroatom at the cluster centre. If none is present, the resulting cluster is called an isopolyanion (IPA) and if not, the POM is referred to as a heteropolyanion (HPA). These two subdivisions will be briefly discussed below.[102,106,111–114]

Isopolyanions

Besides the oxygen, there are only transition metals present in IPA clusters and the number of metals inside a framework can reach up to 150. The general chemical formula can be described as $[M_nO_{(4n-m)}]^{(2n-m)-}$, with the degree of condensation (n) being equal or larger than six. The most prominent IPA is the Lindqvist structure type, shown in **Figure 4-12**, with the chemical formula $[M_6O_{19}]^{y-}$ and its formation shown in **Scheme 4-2**. Here, six octahedral oxoanions are arranged to form a larger-scaled octahedral structure and the metal atoms are located within each of the six smaller octahedra. The oxygen atoms are located at the vertices of each octahedron and mostly exhibit bonds to two neighbouring metals. However, at the corners of the larger-scaled octahedral structure, there are six terminal oxygen atoms only showing bonds to one metal and at the inner centre of this cluster, there is one oxygen atom showing bonds to all six metal atoms at once. For further adjustment of chemical properties, the base metal atoms can be substituted during synthesis by various other metals, such as vanadium. This allows IPAs, and POMs overall, to be tailor-made and customized towards desired applications. [102,106,111,114–116]

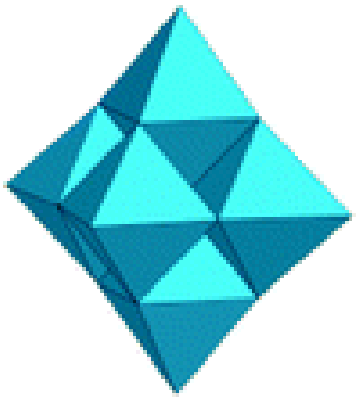

Figure 4-12: Polyhedron depiction of the Lindqvist structure type. [133]

$$6\,MO_4{}^{2-} + 10\,H^+ \leftrightarrow [M_6O_{19}]^{2-} + 5\,H_2O$$

Scheme 4-2: Reaction route for the formation of a Lindqvist-type IPA. [112]

Heteropolyanions

In contrast to the IPAs, the condensation of oxoanions occuring around a centric heteroatom or a different metal atom leads to the formation of HPAs with the general formula $X_sM_nO_m{}^{y-}$, where X traditionally is a main group element, such as silicon (Si), phosphorous (P), arsenic (As) or germanium (Ge). Generally, HPAs are known for their blue colour in their reduced forms, but their oxidized forms can exhibit various colours depending on the framework metals, the heteroatom and even on the counter cations. The corresponding reaction to a HPA is considered kinetically controlled rather than thermodynamically. During the reaction a certain number of water molecules are incorporated into the crystalline structure to ensure cohesion. The water of crystallization can be set free at temperatures around 170 °C and even the constitutional water can be released at temperatures around 360 °C, while the HPA's structure stays intact. However, due to thermodynamic reasons the HPA is rehydrated in presence of moisture (including humid air). The decomposition of these POMs only occurs at temperatures between 400 and 450 °C affirming their exceptional thermal stability. [102,106,110,112,117]

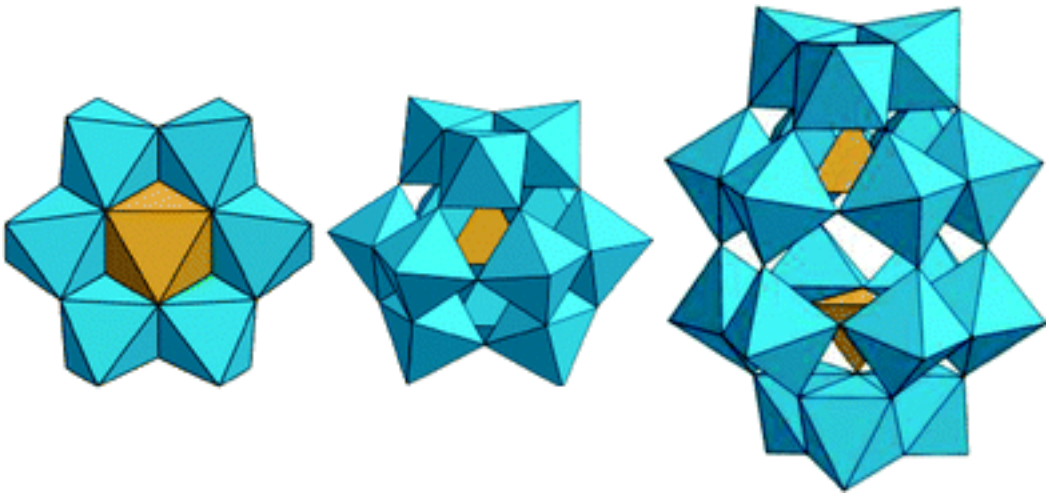

Figure 4-13: Depiction of polyhedral structures of the most prominent heteropolyanion types of Anderson (left), Keggin (middle) and Wells-Dawson (right). [131]

Generally, HPAs are characterized by the ratio X/M as this defines the structure. Due to the presence of heteroatoms, capable of promoting the clusters stability, a vast amount of structurally varying HPA clusters can be formed. The most prominent HPA structure types are

depicted in **Figure 4-13**, which are the Anderson-, Keggin- and Wells-Dawson type with the X/M ratios 1/6, 1/12 and 2/18, respectively. Of these HPAs, the Keggin-type is the best-studied structural type. Its chemical formula is $[XM_{12}O_{40}]^{y-}$, with M traditionally being Mo or W and X being a tetrahedrally coordinated heteroatom, such as Si or P. The heteroatom is bonded to four oxygen atoms forming this tetrahedral structure which is located at the centre of the cluster. Similar to IPAs, the M-O-bonds form octahedrons, but here a combination of three octahedrons yields a trimetallic group M_3O_{13} exhibiting one common site which is connected to one vertex of the centre tetrahedron. Thus, there are four of these trimetallic groups arranged around the tetrahedron resulting in this alternative formula $[XO_4][M_3O_9]_4$. The hereby induced three axes of symmetry allow several rotational possibilities and, thus, isomers. Of the five theoretically possible isomers, only three have been successfully synthesized in literature. Besides this, further modification can be achieved by the treatment of Keggin-POMs in precisely tuned alkaline solutions leading to the loss of one or several metal centres. The resulting isomers are called lacunary species and are especially of interest for the substitution of framework metals with other metals. [112,117,118]

Combining two of the lacunary Keggin species with the formula $XM_9O_{34}^{y-}$ yields a dimer which is called Wells-Dawson. This structure is characterized by the presence of the previously described trimetallic groups M_3O_{13}, but also bimetallic groups M_2O_{10} occurring through the condensation of two octahedra. These form the monomers mentioned above which are then linked towards the Wells-Dawson structure. The third type is the Anderson POM structure characterized by the chemical formula $XM_6O_{24}^{y-}$ and its notable planar structure. This is caused by the arrangement of the typical $[MO_6]$ groups around the central heteroatom which, however, is also coordinated octahedral. [102,106,117]

Especially Keggin-type HPAs containing free protons as counterions, such as phosphotungstic acid with the formula $H_3PW_{12}O_{40}$, show exceptional Brønsted acidic behaviour with a pKa of -13 [119], even stronger than other conventional acids (for comparison, the pKa of hydrochloric acid is at -6 [120]). Additional to the counterion, the acidity is dependent on both the heteroatom and the type of framework metal. It was shown that the acidity for Keggin-type POMs, defined by the dissociation constant, increases as followed: $H_4SiMo_{12}O_{40} < H_3PMo_{12}O_{40} \approx H_4SiW_{12}O_{40} < H_3PW_{12}O_{40}$. Thus, the substitution of framework metals also alters the acidity. As the framework metals occur in their highest state of oxidation, they are capable of acting as an oxidizing agent. It was demonstrated that polyoxometalate structures of Type I (exhibiting

mono-oxo metal centres, such as the Keggin-type) can undergo facile reversible reduction yielding isostructural species. The redox potential is dependent on the cluster's structure, nature of the metal atoms, and the charge which has a significant influence on the resulting potential. Similarly, the substitution of framework metals with elements like Mn, V, or Co not only influences the anion's charge, it can also alter the electron transfer processes. [113,117,121]

In summary, polyoxometalates are suitable for many applications due to their architectural and physicochemical properties, including: [122]

- Brønsted acidity
- High proton mobility
- Fast multi-electron transfer
- High solubility in various solvents
- High resistances to hydrolytic, oxidative, and thermal degradation
- Highly tuneable

Therefore, a concise overview of emerging technologies and research for the application of POMs will be given in the next section.

4.4.2 Utilization for oxidative biomass conversion

Due to their highly versatile properties, polyoxometalates show a large field of research and potential applications. In analytical chemistry, POMs are utilized for spectrophotometric detection of Si and P, referred to as the molybdenum yellow and molybdenum blue method, respectively. As such a detector compound, they are also utilized for the determination of oxidants and biomolecules, in food chemistry, or as a gas sensor. Due to their dielectric behaviour, they show great potential for the application in capacitors and in memory devices. Another promising research field is the application in rechargeable batteries making use of their RedOx potential. [106,112,123–127]

Another large and still growing research field of polyoxometalates utilizing their acidic and oxidative properties is in catalysis. Due to their tunability, POMs can be highly customised regarding their solubility, acid strength, or RedOx potential according to the desired reaction leading to both heterogeneous and homogeneous applications. For heterogeneous application,

POMs can be complexed, i.e. with caesium (Cs), impregnated onto solid materials, such as SiO_2, ZrO_2, or TiO_2, or incorporated into supports like Zeolites, Mobil Composition of Matter (MCMs), or Metal-Organic-Frameworks (MOFs). Especially the incorporation of POMs into MOFs has grown in interest over the last decade for the application in various reactions, such as for the oxidation of alkenes to alcohols, oxidative cyclization , esterification of aldehydes, desulfurization, and for photo- or electrocatalysis. [128–135]

$$[HPA]_{Ox} + n\,H^+ + Substrate \rightleftharpoons H_n[HPA]_{Red} + Substrate_{Ox}$$
$$H_n[HPA]_{Red} + {}^{n}/_{4}\,O_2 \rightleftharpoons [HPA]_{Ox} + {}^{n}/_{2}\,H_2O$$

Scheme 4-3: RedOx reactions for the oxidation of a substrate by reducing a heteropolyanion followed by the reoxidation of the heteropolyanion with molecular oxygen. [106]

On the other hand, the utilization of POMs in homogeneous catalysis provides one key feature compared to heterogeneous catalysts, which is reducing the mass transfer barrier to zero due to the soluble nature of the POM. This is the reason why POMs are exceptionally suitable for the catalytic conversion of biomass, as these usually are not quite soluble in most technically relevant solvents. The POM mostly investigated for this purpose is the Keggin-type heteropolyanion which shows both RedOx potential and, in the multi-proton form of $H_yXM_{12}O_{40}$, strong Brønsted acidity. Utilized for the oxidation, the HPA undergoes a reduction towards the reduced form $[HPA]_{red}$ while oxidizing a substrate, i.e. biomass. Subsequently, the reduced form $[HPA]_{red}$ is reoxidized to $[HPA]_{ox}$ by utilizing oxidizing agents, such as oxygen (O_2) or hydrogen peroxide (H_2O_2). This catalytic cycle is shown in **Scheme 4-3**. Together with their acidity, these HPAs can be applied for the conversion of complex biomasses, such as cellulose, by the combination of hydrolysis and oxidation. [106,136,137]

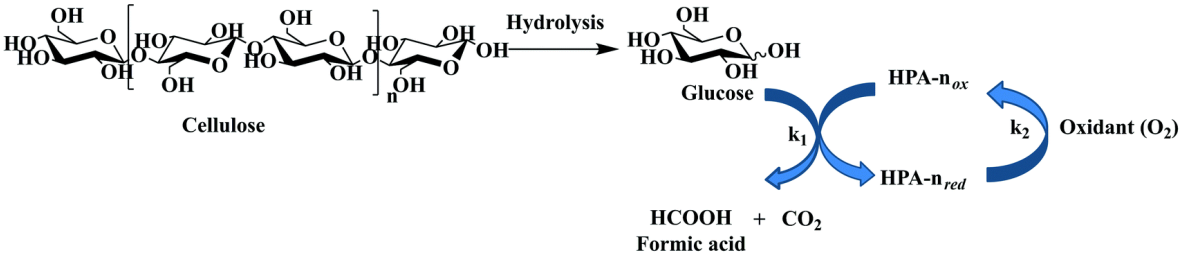

Figure 4-14: Depiction of the two-step conversion of cellulose to formic acid by (first) hydrolysis and (second) oxidation induced by HPA catalysts. [137]

This new method to transform carbohydrate-based biomass to formic acid (FA) was firstly reported by *Wasserscheid* et al. in 2011 [138] and is depicted in **Figure 4-14**, with *n* representing the degree of substitution in the HPA. Here, the Keggin-type transition-metal-substituted POM (TMSPOM) $H_5PV_2Mo_{10}O_{40}$ was utilized for its enhanced RedOx activity. [138] Later, it was shown that for vanadium-substituted Keggin POMs the degree of substitution is stable between 1 – 6 and that they are applicable for a broad scope of complex biogenic feedstocks. Especially the HPMo-5 catalyst ($H_8PV_5Mo_7O_{40}$) shows a large field of application in biomass conversion, including acidic esterification, dehydration, delignification or biomass fractionation, oxidative desulphurization and, of course, oxidation of biomass. [18,139–143] For the oxidation of biomass however, these vanadium-substituted HPAs show a highly oxidative behaviour hampering the oxidation of biomass towards larger molecules than formic acid. For this reason, various other transition metals, such as Nb, tin (Sn), iron (Fe), indium (In), cobalt (Co), or nickel (Ni), have been substituted into Keggin-type POMs in order to fine-tune both the oxidative and acidic behaviour for the oxidative conversion of biomass. [144–146]

4.5 Concepts of process engineering

The development of new processes based on biogenic feedstocks in order to substitute fossil-based processes requires a thorough understanding of substrate and catalyst influences on product routes, process parameter optimization and implementation of up-stream and down-stream concepts. In this chapter, a brief overview of the engineering concepts for the process development will be discussed, first, giving an overview of this process development, second, discussing the reactor concepts, and lastly, examining concepts of product isolation and catalyst recycling.

4.5.1 Production of monoaromatic compounds from lignin

Process development requires several steps of research and engineering before entering any industrially relevant dimensions. These steps are shown in **Scheme 4-4** which start with the lab research. Here, the influence of substrates and catalysts on the range of products is observed and the most promising system is determined. The next three steps belong to the process development and include (1.) the process synthesis, discussing the most suitable process concepts and carrying out feasibility studies, (2.) the process elaboration, verifying the concepts and gaining process-know-how by running an up-scaled mini-plant, and (3.) the basic design,

utilizing the gained knowledge to finalize a potential industrial up-scaling. Lastly, the project planning begins with the basic engineering whereby plant dimensioning, piping and instrumentation diagrams, instrumentation and control engineering are developed. [147]

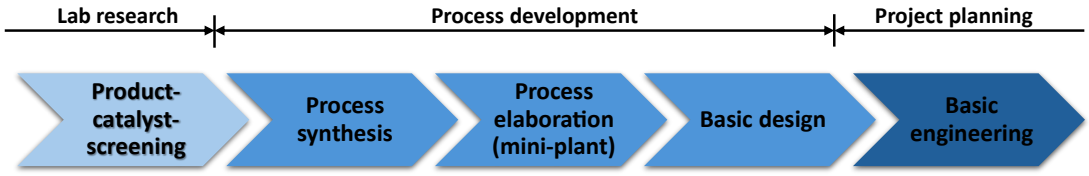

Scheme 4-4: Schematic steps of process development. [147]

One of the most crucial parts in this procedure is the mini-plant. Compared to a pilot-plant, the mini-plant is much smaller reducing costs, commissioning time and plant complexity making it significantly more modifiable. Especially the application of homogeneously catalysed reactions is suitable for mini-plants, as the catalyst recycling and regeneration can be easily studied. The acquired data can be utilized in process simulations potentially skipping the construction of a larger-scaled pilot-plant and directly going to an industrially relevant dimension which cuts the costs and the commission time (usually several years) of the pilot-plant. [147–149]

However, due to the limited amount of process knowledge regarding the chemical valorisation of lignin, the first step of product and catalyst screening is required first. This is traditionally executed in batch-mode reactors with low volume to allow cost-effective screening experiments. [150]

4.5.1.1 Batch mode

In batch mode the chemical reaction is run discontinuously. All reactants, solvents and catalysts are placed inside the reactor prior to the start of the reaction, and no further feed or output is taking place. Accordingly, the concentrations of all reactants change through time, as depicted in the middle graph of **Figure 4-15**, and due to the assumed ideal-mixed behaviour the concentration is not a function of the location (cf. right graph in **Figure 4-15**). As previously mentioned, these batch reactors are particularly suitable for screening experiments due to their low investment costs, minimal start-up or shutdown time, and versatile applications. This makes batch reactors ideal for the determination of the chemical system for the valorisation of lignin.

On the other hand, batch reactors are labour-intensive and show low product volumes, causing their undesirability in industrial applications. [14,151]

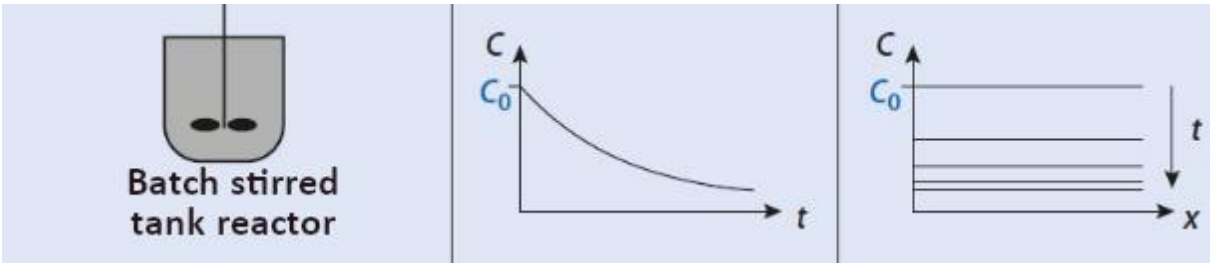

Figure 4-15: Symbol and concentration profiles over time (middle graph) or location (right graph) for batch reactors (left). C stands for concentration, t for time and x for location. The index 0 indicates the reaction time being zero. [14]

4.5.1.2 Continuous mode

To reach large product volumes, continuous-stirred-tank-reactors (CSTRs) are utilized which include both a feed and an output stream, as shown on the left in **Figure 4-16**. By this, the time-intensive periodic emptying of batch reactors is avoided, making CSTRs more attractive for industrial applications. After a transient start-up time with fluctating concentrations, the reactor becomes stationary (steady state). At this point, the reactants' concentration inside the reactor and output stream do not change with time or location, as shown in the graphs in **Figure 4-16**. Besides large product volumes, low personnel-requirements and constant product quality stand out for CSTRs.

Thus, the transition from a batch to a continuous reactor is the desired approach for the process development of lignin valorisation. [14,151]

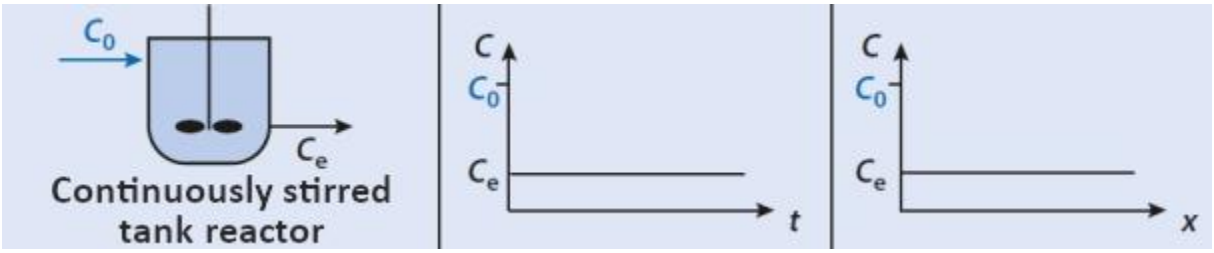

Figure 4-16: Depiction and concentration profiles over time (middle graph) and location (right graph) for continuously-stirred-tank reactors (CSTR on the left). C is the concentration, t the time, x the location. The index "0" stands for the reaction time being zero, and "e" stands for exit. [14]

4.5.2 Product isolation and catalyst recycling

For the development of a continuously running mini-plant, especially the downstream processing represents a key difficulty, as here products must be isolated from the remaining reaction medium. Additionally, due to the soluble nature of polyoxometalates, separation concepts must be chosen which allow the POM to remain in the reaction medium and to be recycled. Two promising concepts are liquid-liquid-extraction (LLE) and membrane separation. For LLE the solubility properties of POMs are utilized, whereas for membrane separation its comparably large size is taken advantage of. [150]

4.5.2.1 Liquid-Liquid-Extraction

Liquid-liquid-extraction (LLE) utilizes limited miscibility of at least two liquid substances resulting in two liquid phases. LLE is suitable for several reasons: One, the products are temperature sensitive and, thus, cannot be distilled. Two, if there are azeotropic mixtures in product streams ruling out high purities through distillation. Three, if large amounts of a third substance must be distilled first in order to acquire small amounts of the desired high-boiling compounds. While in lab-scale discontinuous separating funnels are commonly used (cf. **Figure 4-17** (a)), in industry several continuously running concepts are employed due to higher volume flow rates. The most classical method is the mixer-settler approach (cf. **Figure 4-17**(c)). Here, both product stream and extraction solvent are directed into a mixing unit and, subsequently, into the separator unit where both phases can be separated into two streams, the permeate and retentate. The permeate is the stream including the desired compounds, whereas the retentate usually is recycled and redirected into the reaction system. [14,152,153]

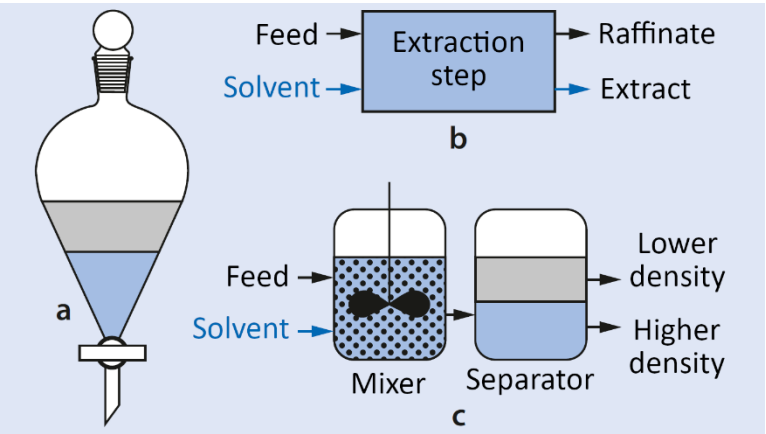

Figure 4-17: Depiction of a discontinuously run separation funnel (a) and a mixer-settler unit in continuous mode (c) to acquire a raffinate and extract phase (b). [14]

In case one extraction procedure is not sufficient, several units can be adaptively added and arranged in a cross-stream or counter-stream method. Each extraction unit receives its own extraction solvent stream for a cross-stream. Alternatively, one extraction solvent stream is introduced at the last extraction unit and it passes each unit for a counter-stream. Another approach is the so-called *in-situ* extraction. Here, a biphasic liquid-liquid system is employed inside the reactor. The reaction preferably takes place in one of the phases including catalyst and substrate and the resulting products show higher solubilities in the second phase and, thus, are removed from this first phase. This approach offers several advantages, including fewer peripheral apparatuses but most importantly a just-in-time extraction. If one of the products is not a final but an intermediate product, it potentially could be further converted into undesired products while in contact with the catalyst. However, if these products are more soluble in the second phase while the catalyst shows higher solubility in the first phase, a subsequent conversion to undesired products can be prevented. On the other side, LLE also shows disadvantages, including energy intensive extraction solvent regeneration and often hazardous or toxic extraction solvents. [14,152,154,155]

To conclude, the method of liquid-liquid-extraction offers a promising solution for the downstream processing in a mini-plant for the valorisation of lignin, as it also has been employed for separation in homogeneous catalysis using polyoxometalates already [155]. Due to the downsides the additional approach of membrane separation will be considered and discussed next.

4.5.2.2 Membrane separation

Membrane separation is based on the selective permeability of a membrane induced by external driving forces, such as concentration or pressure gradients. The applied membranes are a selective thin layer of a semipermeable organic or inorganic material. The organic materials traditionally are polymers and, thus, show numerous possibilities due to the vast scope of polymer industry. For inorganic materials, ceramic, metallic or zeolite membranes are typically employed. Another key factor, besides the material, is the pore size. Membranes can be categorized into microfiltration showing pore sizes between 100 – 10,000 nm, ultrafiltration showing pore sizes between 10 – 100 nm and, lastly, nanofiltration for pore sizes between 1 – 10 nm. Due to the denser membranes in nanofiltration compared to ultrafiltration, higher driving forces are required, usually pressure gradients. For the application two methods have

been established: the crossflow and the dead-end filtration, as depicted in **Figure 4-18**. These differ in the direction of the feed stream in dependency of the membrane and permeate stream. For the crossflow method, the feed stream is tangential to the membrane surface and perpendicular to the permeate stream. This approach promotes the removal of any deposited material on the membrane's surface induced by the shear forces. Consequently, the dead-end method is prone to fouling (depositing material on the membrane's surface) due to the feed stream being perpendicular to the surface. Another key property of membrane separation is the ionic charges inside the membrane affecting the permeability of ionic compounds and, therefore, enabling further fine-tuning capabilities of membranes. [14,156–158]

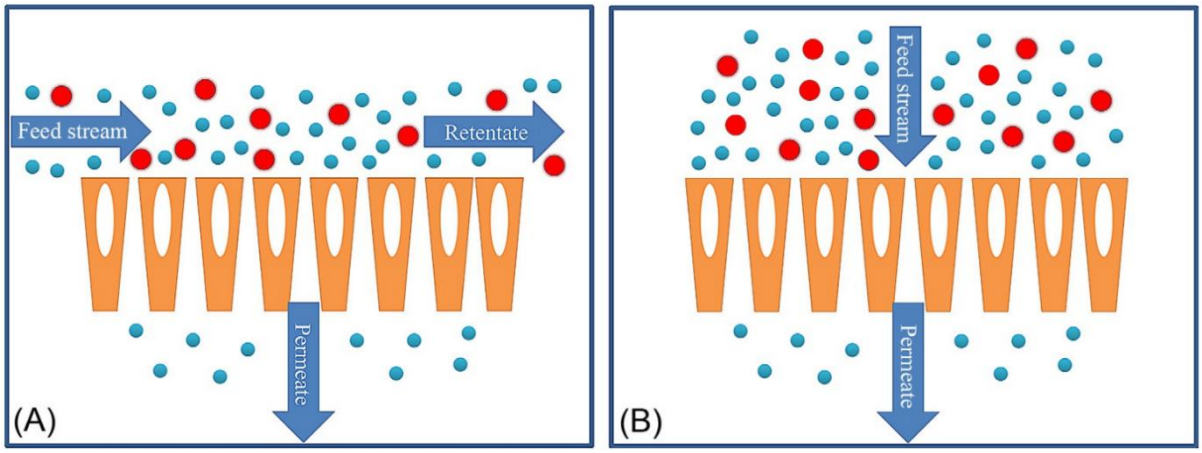

Figure 4-18: Depiction of membrane separation in crossflow (a) and dead-end flow (b) with corresponding directions of feed, retentate and permeate. [156]

Regarding application, membranes can be utilized for the retention of multivalent anions while permeating monovalent anions, for the retention of organic compounds and permeation of monovalent salts, and for the separation of low and high molecular compounds. The points of multivalent anion and high molecular retention are ideal for the approach of lignin valorisation via homogeneous catalysis with polyoxometalates. Keggin POMs show a size of roughly 1 nm making them a high molecular compound, applicable for nanofiltration and they are multivalent anions potentially enabling increased retention. On the other hand, the desired products vanillin, syringaldehyde and their derivative show no ionic charges and are substantially smaller than POMs increasing their permeability. Additionally, it has been shown that the retention of Keggin POMs while permeating smaller organic compounds can reach high selectivities. Altogether, these points support the consideration of membrane separation for the downstream processing in the mini-plant. [159–162]

5. Definition of thesis objectives

The overarching objective of this dissertation is the technical development of a continuous, homogeneously catalyzed process for the oxidative depolymerisation of technical lignins to produce the monoaromatic compounds vanillin (Va), methyl vanillate (MeVa), syringaldehyde (Sy), and methyl syringate (MeSy), by employing polyoxometalates as catalysts.

This work is motivated by the growing necessity for the chemical industry to transition towards environmentally sustainable approaches. Currently, most consumer products rely on fossil-based raw materials, such as crude oil, contributing significantly to greenhouse gas emissions and accelerating climate change. Although the target monoaromatic compounds occur naturally in certain plants, their industrial production is predominantly based on guaiacol derived from the crude oil BTX fraction. By developing a process that utilizes carbon-neutral feedstocks, this research aims to contribute to a more sustainable industrial landscape.

One of the key challenges in this context is the solid and heterogeneous nature of lignin. As a solid, lignin reduces the efficiency of heterogeneous catalysts, while homogeneous catalysts introduce separation challenges. Moreover, the structural heterogeneity of lignin – affected by both biomass origin and pulping process – poses difficulties in maintaining process consistency. To address these issues, different types of technically available lignins will be evaluated to better understand how lignin variability impacts the process. Simultaneously, homogeneous catalysts, specifically polyoxometalates, will be used to improve depolymerisation efficiency. However, this also necessitates the development of an effective separation method for recovering both the dissolved catalyst and the target products.

All research findings will ultimately feed into the design and operation of a continuous reactor system. The work and specifically the project behind it is organized into the following work packages:

1. Characterization of technical lignins
2. Performance screening of different lignins
3. Development of the catalytic system
4. Optimization of the solvent system
5. Optimization of process parameters

6. Development of a product-catalyst separation method
7. Modification, commissioning, and operation of a continuous plant

These investigations are conducted primarily through experimental and empirical methods. Given the applied and technical nature of this work, certain fundamental scientific questions, such as detailed reaction mechanisms, are considered secondary. Additionally, the characterization of the polyoxometalate catalysts and the techno-economic assessment of the developed process are outside the scope of this work, as they are being addressed in parallel by other members of the research group.

Altogether, the outlined work packages aim to provide a comprehensive understanding of the oxidative depolymerisation of lignins and lay the groundwork for the development of a viable continuous process.

6. Materials and methods

This chapter addresses the experimental procedures carried out within this thesis. First, all utilized chemicals, biomasses and catalysts, including their synthesis, are discussed. This is followed by a description of all technical plants, their operation, and the experimental procedures for the catalyst separation by extraction or membrane separation. Lastly, all analytical procedures and experiment evaluation methods are explained.

6.1 Utilized chemicals

In this thesis, various technical lignins were evaluated, including those derived from the most prominent pulp processes (kraft and sulphite), as well as lignin from more experimental sources, such as organosolv, hydrolysis, or soda processes. These were acquired from various commercial suppliers and directly from pulp mills.

Commercial ethanol, methanol and demineralized water from the laboratory tap were utilized as reaction solvent. Additionally, various commercial organic solvents were tested for effectiveness in extracting monoaromatic products from the reaction mixture. Calibration and validation of analytical methods were conducted using pure substances of the reaction components or as internal standard with purities of ≥98 %

For the oxidative reactions, oxygen (grade 5.0) from Westfalen AG or a combination with nitrogen (grade 5.0) from Linde AG were utilized. Additionally, hydrogen (grade 5.0), helium (grade 4.6) both from Linde AG, and argon (grade 4.6) from Heide Gas were employed for analytical purposes (i.e. gas chromatography and gas chromatography coupled with mass spectrometry).

Lastly, for the catalytic experiments, several polyoxometalates were utilized. Both commercially available (all from SigmaAldrich) and synthesized POMs with various substituted framework metals were validated for the depolymerisation of lignin. Here, the counter ion was hydrogen, potassium or sodium, the heteroatom was phosphorous or silicon, the framework metal was molybdenum or tungsten, and the substitution elements were vanadium, cobalt, manganese, nickel, niobium, or indium.

All commercial components have been utilized without further treatment or modification. A comprehensive list of chemicals, gases and catalysts can be found in the appendix in **Table B-1**.

6.2 Catalyst synthesis

Throughout this thesis a total of 28 POM catalysts (including three commercial POMs) were validated for the oxidative depolymerisation of lignin which are shown in **Table 6-1** and **Table 6-2**. All non-commercial POMs were synthesized by *Dr. Jan-Christian Raabe*, an employee in the research group of Prof. Albert at the institute of technical and macromolecular chemistry, department of chemistry, University of Hamburg. The synthesis procedures are based on the publications of *Odyakov* et al. [163–166] and have been modified and described by *Albert* et al. [121,143–145,167] Here, both the so-called Lacunary-method and the Self-Assembly method have been employed.

Table 6-1: Overview of utilized catalysts, part I.

Category	Chemical formula	Abbreviation
Commercial	$H_3PMo_{12}O_{40}$	HPMo-0
	$H_3PW_{12}O_{40}$	HPW-0
	$H_3SiW_{12}O_{40}$	HSiW-0
Vanadium	$H_4PV_1Mo_{11}O_{40}$	HPMo-V_1
	$H_5PV_2Mo_{10}O_{40}$	HPMo-V_2
	$H_6PV_3Mo_9O_{40}$	HPMo-V_3
	$H_7PV_4Mo_8O_{40}$	HPMo-V_4
	$H_8PV_5Mo_7O_{40}$	HPMo-V_5
Cobalt	$H_7PCo_1Mo_{11}O_{40}$	HPMo-Co_1
	$H_{11}PCo_2Mo_{10}O_{40}$	HPMo-Co_2
	$H_{15}PCo_3Mo_9O_{40}$	HPMo-Co_3
	$Na_7PCo_1Mo_{11}O_{40}$	NaPMo-Co_1
	$Na_{15}PCo_3W_9O_{40}$	NaPW-Co_3
	$K_{10}P_2Co_1W_{17}O_{62}$	WD-Co_1

For the vanadium-substituted POMs ($H_{3+x}V_xMo_{12-x}O_{40}$; x=1-5), in a first step molybdenum trioxide was suspended in deionised water, a 25 % phosphoric acid solution was added and heated to reflux forming a clear yellow solution. During the second step, divanadium pentoxide was suspended in water and cooled to 0 °C. This solution was stirred while a 30 % hydrogen peroxide solution was added dropwise. Because of this, the divanadium pentoxide began to

dissolve in the form of a red/brown solution and a release of oxygen gas was observed. A 25 % phosphoric acid solution was added to the batch and stirred at room temperature, after the divanadium pentoxide was completely dissolved. This vanadium solution was then added to the refluxing molybdenum solution dropwise. This mixture was further refluxed for 60 min, then cooled to room temperature and finally filtered and concentrated.

Table 6-2: Overview of utilized catalysts, part II.

Category	Chemical formula	Abbreviation
Manganese	$H_7PMn_1Mo_{11}O_{40}$	HPMo-Mn_1
	$H_{11}PMn_2Mo_{10}O_{40}$	HPMo-Mn_2
	$K_{10}P_2Mn_1W_{17}O_{62}$	WD-Mn_1
Nickel	$H_7PNi_1Mo_{11}O_{40}$	HPMo-Ni_1
	$H_{11}PNi_2Mo_{10}O_{40}$	HPMo-Ni_2
	$H_{15}PNi_3Mo_9O_{40}$	HPMo-Ni_3
Niobium	$Na_6PNb_3Mo_9O_{40}$	NaPMo-Nb_3
Indium	$H_{15}PIn_4Mo_8O_{40}$	HPMo-In_4
Bisubstituted	$H_8PV_1Mn_1Mo_{10}O_{40}$	HPMo-V_1Mn_1
	$H_{12}PV_1Mn_2Mo_9O_{40}$	HPMo-V_1Mn_2
	$H_{14}PV_3Mn_2Mo_7O_{40}$	HPMo-V_3Mn_2
	$H_{12}PV_5Mn_1Mo_6O_{40}$	HPMo-V_5Mn_1
	$H_{11}PNi_1Mn_1Mo_{10}O_{40}$	HPMo-Ni_1Mn_1
	$H_{11}PNi_1Co_1Mo_{10}O_{40}$	HPMo-Ni_1Co_1

For the bisubstituted V-Mn-POMs, divanadium pentoxide was put in water at 5 °C and 30 % hydrogen peroxide was added dropwise resulting in a brown solution while oxygen gas was emitted. Subsequently, the solution was warmed to room temperature, and 25 % phosphoric acid was added and cooled to 5 °C again. In a second solution, molybdenum trioxide was suspended in water, and 25 % sulphuric acid was added which was then heated to reflux for 60 min forming a clear yellow solution. Solution 1 was added to solution 2 dropwise while being heated and refluxed. After 30 min a manganese acetate solution was added to the mixture which was then continued to be heated and refluxed for further 90 min. Lastly, the mixture was concentrated by evaporation.

For the manganese-, nickel-, and cobalt-substituted POMs ($H_{3+4x}Y_xMo_{12-x}O_{40}$; Y: Mn, Ni, Co x=1-3 for Ni, Co and x=1-2 for Mn), their acetate salts were utilized and dissolved in water. This solution was added dropwise to another solution containing molybdenum trioxide or sodium tungstate dihydrate and 25 % phosphoric acid which was heated to reflux for 60 min before. This procedure was also applied analogously for the bisubstituted Ni-Mn- and Ni-Co-POMs. For the purification of sodium containing POMs, a nanofiltration method described by *Raabe* et al was utilized. On the other hand, a sodium-POM can be acquired by neutralizing an acidic POM in solution by sodium hydroxide. [145]

The indium-POM was synthesized utilizing indium(III) hydroxide dissolved in a 37 % hydrochloric acid solution. This solution was then added to a Lacunary solution. The Lacunary solution can be formed by dissolving sodium molybdate dihydrate and disodium hydrogen phosphate in water and adjusting the pH value to ~1 by adding 37 % hydrochloric acid solution. This was then heated and refluxed for 30 min, and the pH was then adjusted to a value of ~2 by adding a sodium carbonate solution.
Similarly, the niobium-POM was formed, by dissolving potassium hexaniobate in a 1.5 % hydrogen peroxide solution and then adding this to the Lacunary solution. This solution was then heated and refluxed for 60 min. Afterwards, the pH was adjusted to 1.6 by adding a hydrochloric acid solution. Both the indium- and niobium-POMs were then filtered and purified using the nanofiltration method.

6.3 Technical plants and experimental procedures

Throughout this thesis, various experimental setups and procedures were built and conducted in order to validate the lignin depolymerisation. Three laboratory-scaled technical plants were utilized for the lignin depolymerisation. Additionally, two downstream processing methods, extraction and membrane separation, were assessed. The experimental setups and procedures of technical plants and downstream processing methods will be elaborated in the following section, starting with the technical plants.

6.3.1 Technical plants

The first plant (Setup 1), the so-called 10-fold plant, was primarily utilized for experimental screening of feedstocks, solvents and catalysts. The second plant (Setup 2), called 3-fold plant, was utilized for the process optimization due to higher reactor volumes. The third plant

(Setup 3) was used to demonstrate the developed process in a continuous environment. Each of the three setups will be discussed in detail, hereinafter.

6.3.1.1 Batch tank reactor 20 mL (Setup 1)

Experimental plant for Setup 1

This plant setup, shown in the piping and instrumentation diagram (P&ID) in **Figure 6-1**, consists of ten 20 mL reactors made of Hastelloy C-276, an alloy consisting of nickel, chromium, molybdenum and tungsten, and was manufactured by *Parr Industries*. The alloy provides a significant corrosion resistance against oxidizing or reducing agents even at high pressures and temperatures. On the other hand, all peripherals (pipes, valves and screwing) consist of conventional stainless steel (1.4571) and all utilized sealings were made of Teflon. All reactors were placed in a heating plate manufactured by *IKA®-Werke GmbH & Co. KG*. The temperature of the plate is measured by two sensors (TIR0.1 and TIC0.2) fixated in the plate and subsequently regulated by a control box (TIR0.3 and TIC0.4) manufactured by *Horst GmbH*. Each reactor is equipped with a rupture disc (RD1 – RD10) that activates at 120 ± 10 % bar, a local (PI1.1 – PI10.1) and a digitally recording pressure gauge (PIR1.2 – PIR10.2) all manufactured by *Keller AG*, as well as a ball valve (V7 – V17). The remaining valves (V1 – V6) are utilized for pressurizing with oxygen or nitrogen or depressurizing the reactors and the corresponding pipes are additionally equipped with a local pressure gauge (PI0.5) to check for any remaining pressure in the pipes.

Experimental procedure for Setup 1

First, all necessary reactors were filled with all solid or liquid reactants (usually solvent, substrate and catalyst). Before closing the reactors by a hook wrench, all sealings as well as the lubricating paste were checked and if necessary, changed or added. After all reactors were closed, they were placed in the heating plate and connected to the piping system. Their position inside the heating plate was noted to evaluate any occurring irregularities. For purging, the valves V6 – V17 were opened, while valves V1 – V5 were closed. To purge with oxygen, V2 was opened, V3 was set for oxygen stream and V4 was set to pressurize the reactors. Lastly, V5 (a needle valve) was slowly opened and after reaching a pressure of 20 bar, V2, V3 and V5 were closed. To depressurize, V4 was set to the exhaust and V5 was again slowly opened. This process was repeated two more times, however the third time, the pressure was increased to 50 bar to perform a leak test, usually with a leak detection spray.

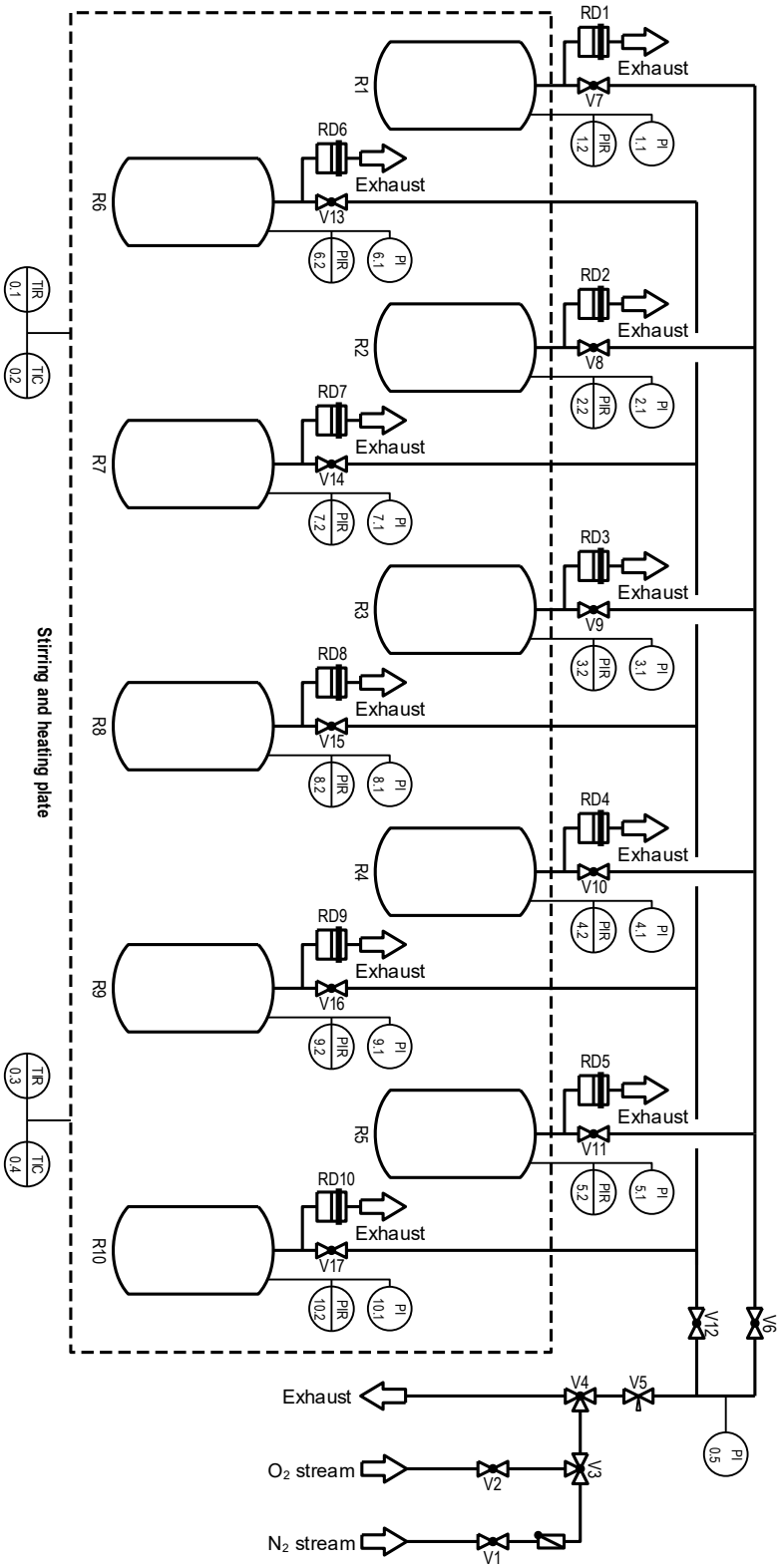

Figure 6-1: P&ID of the 10-fold plant (Setup 1).

Then, the desired pressure was employed by the same procedure. Exemplarily, for a reaction pressure of 20 bar at 140 °C, a pressure of 14 bar was employed at room temperature. The

desired reaction temperature was then set at the control box (TIR0.3). To reach 140 °C, it usually took 10-15 min. Upon reaching the reaction temperature, the time was noted as reaction start. The same procedure can be applied for nitrogen utilizing the nitrogen valve (V1). All experiments concluded on the 10-fold plant were not stirred.

To terminate the reaction, all reactors were disconnected from the piping system and placed inside a fume hood to cool down. Upon reaching room temperature, the remaining pressure and the current exact temperature were noted. Subsequently, the reactor's gas phase was evacuated into a sample gas bag which was then utilized for a measurement on the gas-chromatography device (see section **6.4.8** for more details). For the evacuation, a connector was linked to the reactor head and an attached silicon tube was put on the valve of the sample gas bag. The valve of the sample gas bag was then opened and the corresponding reactor valve (V7 – V17) was slowly opened to fill the gas bag. If any excess pressure was left inside the reactor, it was connected to the plant's piping system for depressurizing, as explained above. After evacuation, the reactors were opened to collect the liquid and any remaining solid sample. For this, the liquid was poured into a funnel equipped with a filter which was weighed with a labelled sample vessel, beforehand. Any remaining solid residue inside the reactor was scrapped off utilizing a spatula and put into the filter. All filters were, then, dried inside a drying oven at 40 °C for 24 h and afterwards weighed. The solid samples were utilized for elemental analysis (see section **6.4.4** for more details) and the liquid samples primarily for gas-chromatography coupled with mass-spectrometry, but also for Karl-Fisher-titration, gel-permeation-chromatography, or pH value analysis.

6.3.1.2 Batch stirred-tank reactor 100 mL (Setup 2)

Experimental plant for Setup 2

The 3-fold plant consists of three stainless steel (1.4571) reactors, each with a volume of 100 mL, manufactured by *HALMOSI GmbH*, and is depicted in **Figure 6-2**. In contrast to the 10-fold plant, each reactor contains a gas entrainment stirrer manufactured by *Parr Industries* and a stirring motor being a *Microstar 20 Control* unit by *IKA GmbH & Co. KG*. The main sealings for the reactors are disposable graphite sealings called *Novaphit* by *Erwin Telle GmbH*, while all other sealings are made of Teflon. For heating each reactor is provided with its heating jacket which is detachable. The peripherals (valves, pipes, screwing) utilized are made of stainless steel (1.4571). Each reactor possesses both an analogous (PI1 – PI3) and a digital

pressure gauge (PIR1.2 – PIR3.2) manufactured by *WIKA SE & Co. KG* which is connected to a *Eurotherm 3216i* control unit. Additionally, each reactor is equipped with two temperature sensors, one measuring the reactor shell temperature (TIR1.1 – TIR3.1) and the other one measuring and controlling the inside temperature of the reactor (TIRC1.0 – TIRC3.0). All temperature sensors are also connected to an *Eurotherm 3216/Eurotherm 3216i* control unit. Both temperature and pressure data are recorded by an internal software called *Flexlab*, which also allows controlling the reactor temperature. For safety reasons, each reactor is equipped with a rupture disc (RD1 – RD3) manufactured by *Schlesinger GmbH* bursting at 120 ±10 % bar and a check-valve (CV1 – CV3) to prevent oxygen-containing gas flowing into the nitrogen pipes. For pressurizing the reactors, each reactor contains a valve for oxygen or synthetic air (V1.2 – V3.2) and one for nitrogen (V1.1 – V3.1). To switch from oxygen to synthetic air, valve V0.1 can be used. For depressurizing the reactors, each reactor is equipped with two valves, the first being utilized for gas sampling (V1.3 – V3.3) and the second one acting as an exhaust (V1.4 – V3.4).

Experimental procedure for Setup 2

Similarly to the 10-fold plant, all reactors were filled with the substrate, catalyst and solvent. The graphite sealings were examined and switched, if necessary, before closing the reactor. For this, the movable bottom of the reactor was aligned with the top part and all five screws were tightened in a star-shaped order to prevent any tilting. Afterwards, each heating jacket was attached to the reactor. Before continuing, all valves were checked and closed, if necessary. To purge the reactors with oxygen, the corresponding pressurizing valve (V1.2, V2.2, or V3.2) was slowly opened until a pressure of 20 bar was reached. Similarly, the exhaust valves (V1.4, V2.4, or V3.4, respectively) were opened to depressurize the reactors. This procedure can also be done for nitrogen by opening the corresponding valves V1.1, V2.1, or V3.1, respectively.

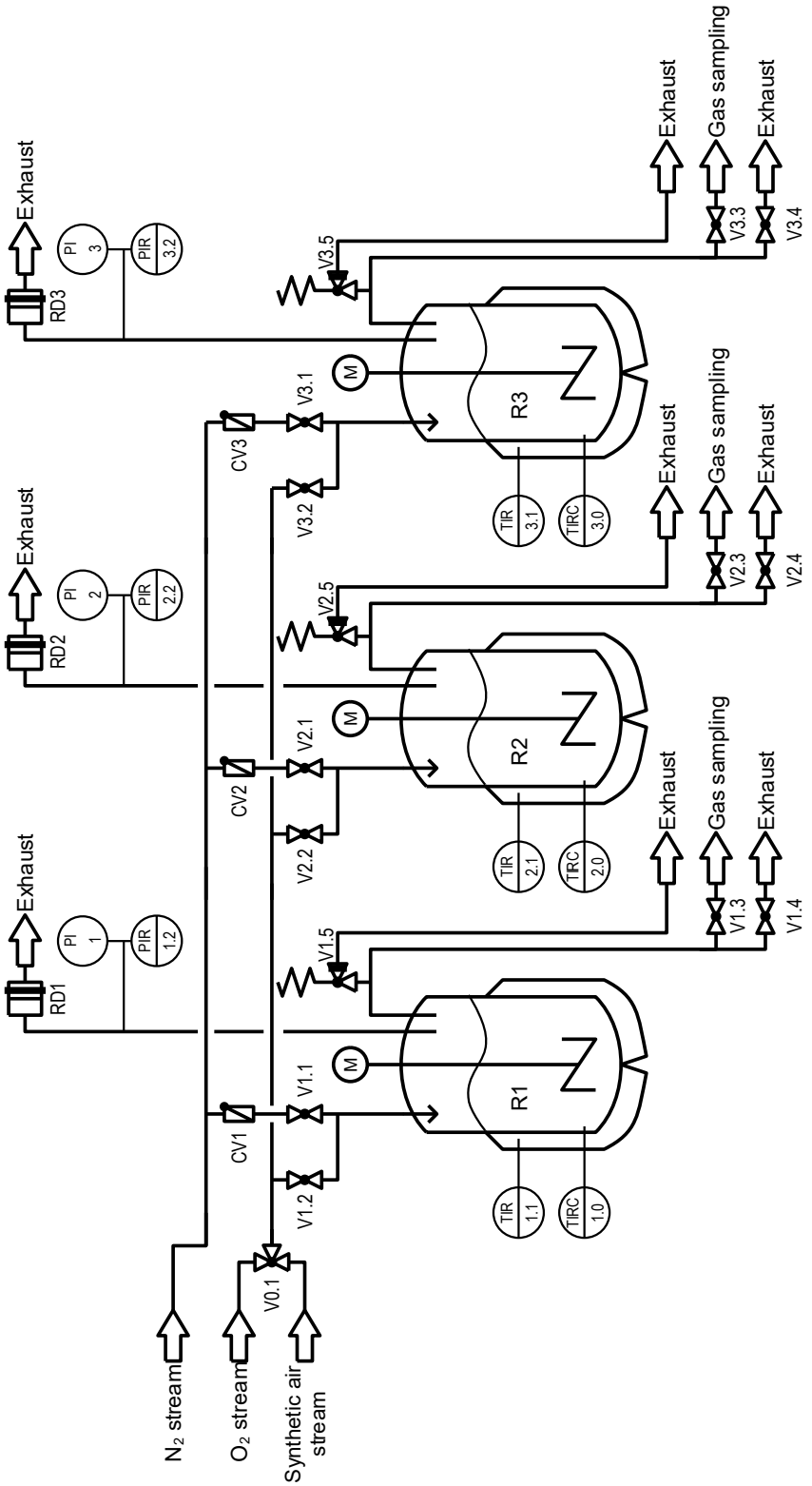

Figure 6-2: P&ID of the 3-fold plant (Setup 2).

The purging was repeated two more times, however, the third time the pressure was increased to 50 bar to do a leak test, parallelly. If no leaks were observed, the desired pre-reaction pressure

was applied. Exemplarily for a reaction pressure of 20 bar at 140 °C, a pre-reaction pressure of 14 bar was employed. Before starting the reaction, all temperature and pressure thresholds in the *Flexlab* software were examined and adjusted if necessary. The stirrers were switched on, set to 300 rpm and the temperature was set to the desired value in *Flexlab*. The temperature usually was reached within 15 min, marking the time of reaction start. At this point, the stirrer was set to 1000 rpm.

To terminate the reaction, the temperature was switched off in *Flexlab*, the heating jackets were detached, and a stream of pressurized air was utilized to increase the reactor's cooling rate. Once cooled down, both temperature and pressure were noted and a gas sample for each reactor was taken. For this, the sample gas bag could be directly fitted onto a silicon tubing which was already attached to the exit of the gas sampling tube. The gas bag was opened and valves V1.3, V2.3, or V3.3, respectively, were slowly opened to prevent any liquid sample being pulled upwards. Once the gas bag was full, its valve as well as the previously opened valves were thoroughly closed. Any excess pressure remaining in the reactors could be released by opening the exhaust valves V1.4, V2.4, or V3.4, respectively. Similarly to the procedure in section **6.3.1.1**, the reactors were opened after evacuation, and the liquid sample was poured onto a previously weighed filter which was placed in a funnel directed into a labelled sample vial. Remaining solid residue in the reactor was scraped off with a spatula and added to the filter. After finishing the filtration, the liquid sample vial was closed, and the filters were dried in an oven at 40 °C for 24 h. Then, the filters were again weighed, the solid sample was transferred to a labelled solid sample vial, and briefly grinded by a spatula. All samples produced in Setup 2 were characterized equally to those from Setup 1.

6.3.1.3 Continuous stirred-tank reactor 450 mL (Setup 3)

Experimental plant for Setup 3

To further validate the feasibility of lignin depolymerisation developed with the first two setups, Setup 3 was utilized. This plant was designed and built in collaboration with Tobias Esser and commissioned as a part of this thesis and should demonstrate the continuous depolymerisation of lignin.

In **Figure 6-3**, the piping and instrumentation diagram is depicted, and the plant can be divided into four sections:

1. Gas supply and exhaust
2. Upstream processing
3. Main reactor setup
4. Downstream processing and recycling

The gas supply section is located at the top-centre in **Figure 6-3**. Here, valves V3 and V5 can be opened for oxygen or nitrogen, respectively. Each pipe is equipped with a mass-flow-controller (MFC1 and MFC2) which each require a particle filter beforehand (F2 and F3). By utilizing mass-flow-controllers a defined amount of gas flow for continuous reactions can be ensured. To circumvent the MFCs each pipe has a by-pass line which requires opening valves V3 for oxygen and V8 and V9 for nitrogen. Additionally, there is an overall by-pass gas pipe for nitrogen to allow automatic purging of the reactor during an alarm with inert nitrogen gas – this by-pass line is equipped with valve V6 which is always open to a certain degree enabling slow purging in case of an emergency shutdown of the plant. Again for safety reasons, several apparatuses are installed, as well. Each gas line and the nitrogen purging line are equipped with a check valve (CV2 – CV4) and the oxygen and by-pass pipe have a security valve (V4 and V7) of which V4 closes and V7 opens during a plant shutdown. This stops oxygen and purges the reactor with nitrogen preventing any ongoing reactions and further temperature rise.
The exhaust section contains a line for excessive pressure increase which is equipped with a rupture disc (RD1). In case of an irregularity which causes the pressure to increase slowly, there is a pressure control valve (V22) installed which opens at a predetermined pressure of 60 bar. With V12 a gas sample can be taken, or the reactor can be depressurized while additionally opening V13. For additional safety measurements, the security valve V11 opens in case of an emergency shutdown. The reactor slowly depressurizes into the exhaust, while V10 is always slightly opened.
The upstream processing can be found in the top-left of **Figure 6-3**. Here, the substrate solution is poured into container C1, a 5 L plastic tank, which is at atmospheric pressure and stirred. The substrate solution is pre-solubilized in a 2 L stirred tank reactor. With V1 usually open the peristaltic pump P1 pumps the substrate solution into the mixing container C2, a sealed 500 mL glass bottle. Additionally, a catalyst solution, coming from the downstream processing, is pumped into C2 via peristaltic pump P4. From the mixing container the now reaction ready solution is guided to a particle filter (F1) and to a high-performance liquid-chromatography

(HPLC) pump (P2) manufactured by *Techlab GmbH*. The solution is pumped into the reactor passing a check valve (CV1) to protect the pump from any counter-pressure.

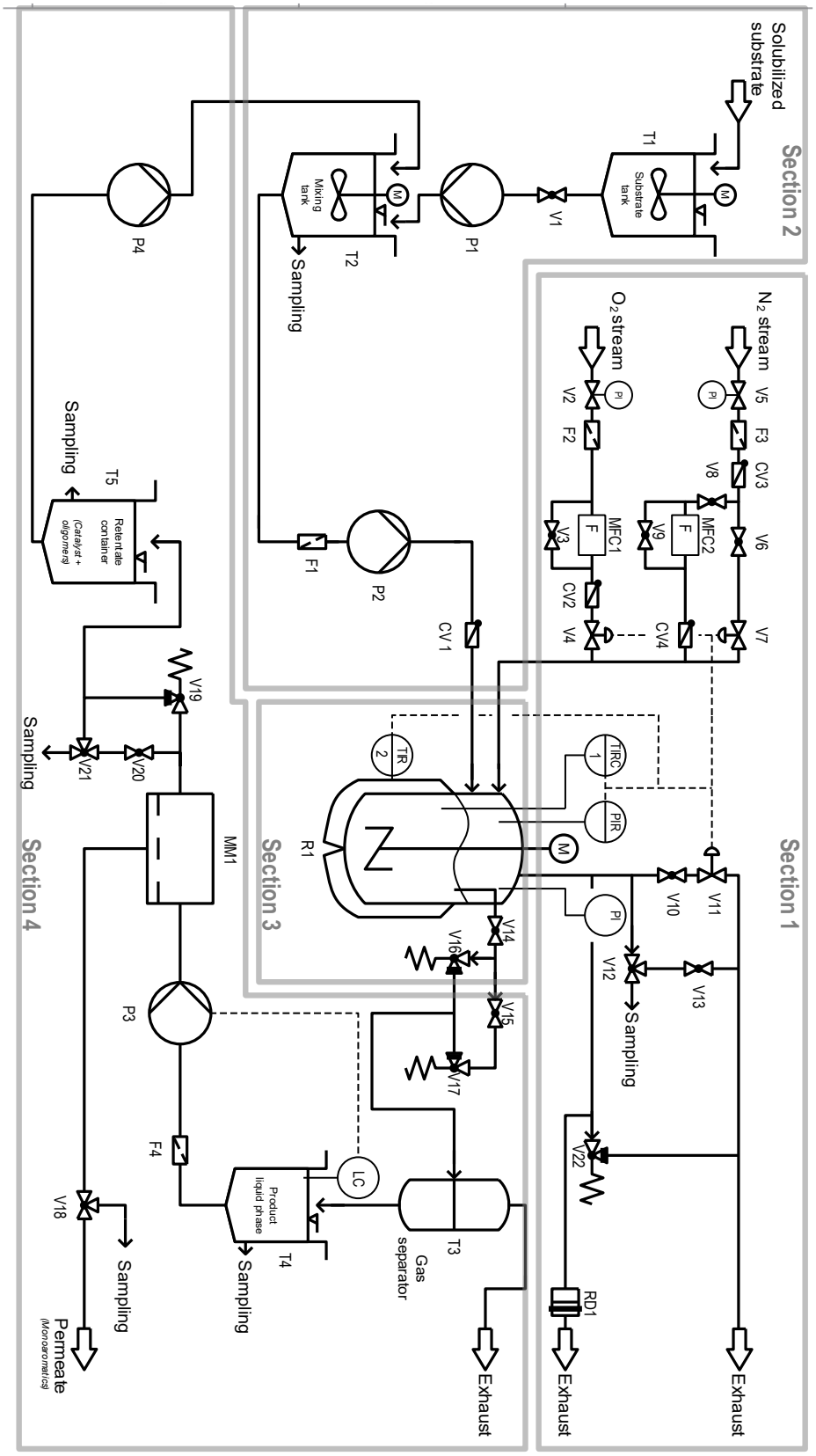

Figure 6-3: P&ID of the continuous lignin depolymerisation plant (Setup 3).

The main reactor setup consists of the 450 mL Hastelloy C-276 stainless-steel reactor (R1). It is manufactured by *Parr Industries*, equipped with a gas entrainment Hastelloy C-276 stirrer, sealed by a perfluoroelastomeric (FFKM) sealing and heating is provided by a heating jacket. Temperature is measured and controlled by two Pt-100 sensors at the outside reactor wall (TIR2) and inside the reactor`s solution (TIRC1). To measure the pressure, two pressure gauges are installed, an analogous (PI3) and a digital one (PIR4).

The downstream processing is located at the bottom of **Figure 6-3**, starting at the reactor exit though. Here, a riser pipe is installed allowing the inflowing liquid, increasing the level inside the reactor, to be pushed out of the gas phase. This is ensured by two relief valves (V16 and V17) of which the first one opens at a predetermined pressure of 25 bar. The second one is added due to redundancy and for process modification, i.e. changing the reaction pressure. To completely close the reactor V14 can be utilized and to switch between the two relief valves V15 is used. The exiting liquid is directed to the gas separator C3, a 2 L stainless-steel vessel. Here, the gas phase following the liquid is relaxing and rises towards the exhaust. The liquid phase is flowing downwards into the product liquid phase container C4, a sealed 500 mL glass bottle. The liquid phase accumulates here until reaching a certain level which is detected by a ultrasonic sensor (zws-24/CI/QS) manufactured by *Microsonic GmbH*. Upon reaching the calibrated level, the sensor activates the HPLC pump (P3) manufactured by Bischoff GmbH. The liquid then passes through a filter (F4) and is pumped into a membrane cell (MM1), consisting of stainless-steel module, a membrane, and a steel mesh to ensure sufficient space on the permeate side. While the membrane cell is not in use, all connections must be closed and inside there must be the solvent (methanol) to allow swelling of the membrane. A detailed description of the membrane module can be found in section **6.3.3**. The permeate is directed towards V18 utilized for direct sampling or to be collected in a storage tank. On the other side, the retentate is collected in container C5, a sealed 500 mL glass bottle, passing V20 (to switch between manual and automatic mode) and V21 (for direct sampling or container collection) or the relief valve V19 set to 30 bar (for automatic mode). From container C5, the retentate stream is recycled towards container C2 via a peristaltic pump (P4).

Experimental procedure for Setup 3

Initially, the pre-solubilized lignin solution had to be prepared. This was carried out in a 2 L stainless-steel stirred reactor which was not part of this plant and commissioned by *Leon Schidowski*, PhD student at the research group of Prof. Albert. The desired amount of lignin

was weighed and transferred to the reactor, as well as the desired amount of methanol. Next, the reactor was purged three times with 20 bar of pure nitrogen to prevent any oxidation taking place and a nitrogen pressure of 15 bar retained afterwards. The stirrer was switched on to 300 rpm and a temperature of 100 °C was set. The pre-treatment was specified for 1 h at 100 °C. At the end, the heating was switched off, the heating jacket was removed, and external quenching water was applied to increase cooling rate. Once reaching room temperature, the stirrer was switched off, all excess pressure was slowly released into the fume hood, and the reactor content was poured into container C1. To decrease start-up time of the continuous reaction, reaction-ready solutions were prepared in container C2 and in reactor R1. The desired catalyst concentration was mixed in these containers with the solubilized lignin. Additionally, a pure catalyst solution was prepared in container C5. Then, the reactor R1 was purged with oxygen three times, while the third time a pressure of 50 bar was applied to additionally check for any leakages. Afterwards an oxygen pressure of 14 bar was applied, the stirrer was set to 300 rpm and the temperature was set to 160 °C using TIRC1.

Once reaching this temperature, the reaction time started, all data recording was initialized and pumps P1, P2 and P4, as well as the level sensor and control of container C4 were switched on. Further, the mass-flow controller MFC1 was switched on. Due to the increasing liquid level inside the reactor and the increasing pressure as of the mass-flow controller, a certain amount of reactor content periodically was transferred to container C4 by opening relief valve V17. Directly before reaching the fill level, at which the sensor switches on HPLC pump P3, all solvent inside the membrane cell MM1 was removed and the stirrer of the membrane module was switched to 1,000 rpm. The solvent was removed to prevent dilution of the product stream and to avoid drying of the membrane, which could potentially close the pores. Throughout an experiment, liquid samples of retentate and permeate were taken regularly and immediately analysed quantitatively by GC-MS. This was done to determine stationary state of the plant as soon as possible and to be able to then tweak reaction parameters observing the plant's behaviour.

To terminate the continuous reaction, the temperature was set to 0 °C and the pumps, the mass-flow controller and the fill level controller were switched off. After reaching room temperature, the stirrer was switched off too and the remaining excess pressure was slowly released into the fume hood. All plant parts (containers, reactor, membrane cell) were detached and thoroughly rinsed and cleaned with methanol, water and, lastly acetone. Afterwards everything was

assembled again, and a mixture of water and acetone was pumped through the pipes to completely remove all remaining lignin. These pipes were then dried with nitrogen, according to the purging section above.

For the membrane cell, the membrane had to be replaced after each experiment and each membrane had to be conditioned prior to continuous experiments which is discussed in detail in section **6.3.3**.

6.3.2 Experimental procedure: Extraction

All extraction experiments were conducted in a 1 L glass separatory funnel. Several beakers and glass bottles were also utilized for product storage. For this, the synthetic product solution, the synthetic catalyst solution or the actual reaction solution were prepared beforehand. Both synthetic solutions were depicting averaged concentration of aromatic products (each aromatic product with a concentration of 1 mg/mL) and catalyst (with a concentration of 20 mg/mL). The actual reaction solution was produced in the 10-fold or 3-fold plant according to section**s 6.3.1.1** and **6.3.1.2**. The solvent for the synthetic and reaction solution was a mixture of methanol and water in a 95:5 volume ratio. As extraction solvents ethyl acetate, toluene, n-hexane, octyl amine, and 1-heptanol were selected based on literature research [168–171] and simulations of ternary diagrams of methanol, water and solvent – more on this in section **7.3.1**. Additionally, demineralized water was additionally necessary to reach the miscibility gap of the ternary mixture.

First, 90 mL of synthetic product, catalyst or actual reaction solution was added to the beaker, directly followed by 180 mL of demineralized water. The separatory funnel was closed with a plug and thoroughly shaken for 1 minute and then settled for 20 min. After visual verification that no precipitate has been formed, 270 mL of extraction solvent was added to the separatory funnel. The funnel was again closed and thoroughly shaken for 30 seconds, but then the time necessary for complete phase separation was observed. Once everything was settled, the filling levels of each phase were marked, and a beaker was placed beneath the separatory funnel for the raffinate phase. The valve of the separatory funnel was slowly opened to remove almost all of the raffinate phase which was then closed again. To prevent any contamination of the respective other phase, an additional beaker was used for a mixture phase. For this, all remaining raffinate phase and a little of the extract phase were removed from the funnel into the mixture beaker. The remaining extract phase in the funnel was then removed into the extract

beaker. All contents of the mixture beaker were considered waste. If necessary, rudimentary density measurements were then conducted of the extract and raffinate.
For the evaluation of the suitability of extraction the following analytical characterization was conducted. For the organic extract phase, the quantification of aromatic products by GC-MS (section **6.4.9**), water content by Karl-Firscher titration (section **6.4.10**), and catalyst concentration by elemental analysis, specifically ICP-OES (section **6.4.6**)

6.3.3 Experimental procedure: Membrane separation

The membrane separation was carried out in a membrane plant commissioned by *Dr. Tobias Esser*, a former PhD student at the research group of Prof. Albert. At its core, the plant is equipped with a membrane cell manufactured by PI Prozesstechnik GmbH provided with a magnetic stirrer. Three measuring cylinders were utilized for feed, retentate and permeate solutions. The piping is provided by polymer tubes suited for high-pressure applications. From the feed, a tube equipped with a ceramic microporous filter is leading towards an HPLC pump manufactured by Bischoff GmbH pumping the feed into the membrane cell. On the side of the retentate tubing, a relief valve is installed which is set to the desired operating pressure (usually 30 bar). Alternatively, a needle valve can be utilized to fine-tune the operating pressure while the relief valve is completely closed by another ball valve. Especially for the start-up, a bypass is utilized to recycle the retentate stream into the feed solution at atmospheric pressure. Otherwise, the tubing then leads to the retentate and permeate measuring cylinders. For the separation in the previously described Setup 3, an additional membrane separation setup was built and commissioned as describe in section **6.3.1.3**.

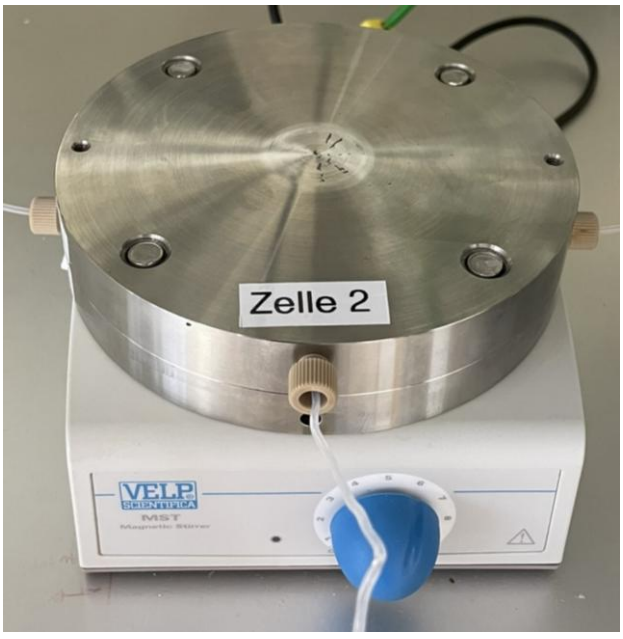

Figure 6-4: Picture of the installed membrane cell also showing all connections, being the feed (right plug), permeate (bottom plug) and retentate (left plug), and the stirring plate beneath the cell.

In **Figure 6-4**, the installed membrane cell is shown. In operation, the feed

stream enters the cell at the right side of the bottom layer of the cell. The feed is separated by the membrane in a retentate stream flowing to the exit on the left side, and a permeate stream leaving the cell through the bottom connection. Additionally, the dismantled membrane cell is shown in **Figure 6-5** where small parts like stirrer, metal mesh or polymer membrane are depicted.

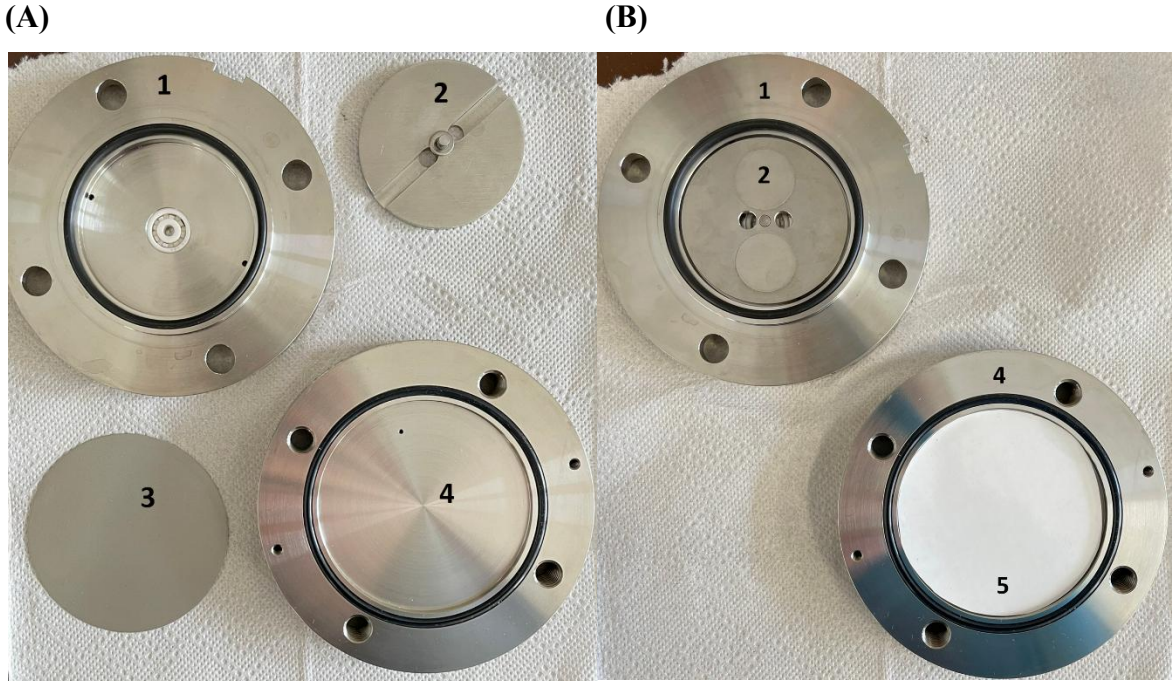

Figure 6-5: (A) Picture of the completely dismantled membrane cell showing the feed/retentate side (1) with two small orifices being for feed and retentate, the stirring plate (2), a metal mesh (3) ensuring enough space between the later installed membrane and the permeate exit shown on the permeate side (4). (B) Picture of the partly assembled membrane cell. The stirrer (2) is inserted into the feed/retentate side (1), and the mesh (3) was inserted onto the permeate side (4) but is obscured by the already implemented polymer membrane (5).

To condition the membrane, it was installed inside the membrane cell and the cell was connected to the membrane plant. The solvent (in this case the methanol-water-mixture) was pumped through the retentate side of the membrane with active stirring (1000 rpm) for 15 min at atmospheric pressure. Afterwards, the pressure was increased to 35 bar for 30 min allowing the solvent to also flow through the permeate side of the membrane. To allow full conditioning, all connections were closed for at least 24 h to allow membrane swelling. The module was then stored until further used in separation experiments.

For the membrane performance experiments, the cell containing a conditioned membrane (described in the next paragraph) was installed in the membrane plant. During this step, all

solvent inside the cell was removed. Again, both synthetic aromatic product solutions and synthetic catalyst solutions were created previously, just like in the extraction section **6.3.2**. Pre-weighed measuring cylinders were placed at the permeate and retentate exits and sealed by a plug which has a borehole for the respective exit stream tube. The synthetic solution was poured into the remaining pre-weighed measuring cylinder and closed by a plug, such as for the other cylinders. The solution then needed to be primed into the HPLC pump by syringe. The bypass on the retentate side was opened so that all feed could be recycled into the feed cylinder. The HPLC pump was set to 15 mL/min and switched on. Once the membrane cell was filled with feed, the stirred was switched on and slowly set to 1000 rpm. This feed recycling was carried out for 5-10 min to ensure a complete homogeneous distribution inside the tubing. Then the bypass was closed, leading to the desired pressure build-up and the relief valve, which has been set to 30 bar before, opens. At this point, a timer was started recording the operating time. Once, either the permeate or retentate cylinders were full, or the feed cylinder was empty, the pump was switched off and the timer was stopped. All cylinders were removed and again weighed to determine the mass flow of permeate and retentate. For each solution, a rudimentary density measurement was then conducted to receive a volume flow rate. Each solution was then stored inside glass bottles. The plant then needed to be purged and cleaned, first with the pure methanol-water-mixture and then with pure water. At last, all sections of the plant were then emptied. The membrane cell was opened to inspect the membrane and, if necessary, to clean it. For all samples produced from synthetic aromatic product solutions, product quantification by GC-MS was conducted. For the samples produced from synthetic catalyst solutions, elemental analysis by ICP-OES was conducted.

For the conditioning of a membrane, it was installed inside the membrane cell, the cell was connected to the membrane plant. Similar to the typical membrane performance experiments, the solvent (in this case the methanol-water-mixture, no other contaminants) was pumped through the retentate side of the membrane with active stirrer (1000 rpm) for 15 min at atmospheric pressure. Afterwards the pressure was increased to 35 bar for 30 min allowing the solvent to flow through the permeate side of the membrane, as well. To allow full conditioning, the cell was disconnected from the plant and all connections were closed for at least 24 h to swell the membrane. The module was then stored until further used in separation experiments.

6.4 Analytical procedures

Throughout the present work various analytical devices were utilized to characterize lignin feedstocks or validate process performances. In this section a concise overview of each analytical methodology including technical devices will be discussed.

6.4.1 Compositional analysis (for lignins)

Throughout the compositional analysis the contents of acid-soluble, acid-insoluble lignin, carbohydrates, proteins and ash were determined following the instructions of the National Renewable Energy Laboratory (NREL). [172] This analysis is vital for the calculation of lignin conversion and aromatic product yield. The compositional analysis for all lignin feedstocks was carried out as a part of the supervised master thesis of Shreya Desai.

First, the biomass samples were dried at 105 °C including the determination of moisture content. The samples were then grinded and sieved to achieve a particle size between 180 µm and 850 µm. The samples were then hydrolysed in a two-step procedure. During the first step, the biomass samples were treated in 72 % sulphuric acid at 30 °C for 1 h. This step is targeted to destroy the intermolecular connections of lignocellulose. Subsequently, the solution was diluted with demineralized water to reach 4 % sulphuric acid concentration, and the solution was further treated at 121 °C for 1 h. This second step shall hydrolyse all polysaccharides into monomeric sugars. After this hydrolysis treatment, all remaining solid residues were separated by vacuum filtration. The cake represents acid-insoluble lignin (AIL) also containing ash and the filtrate contains acid-soluble lignin (ASL) and all carbohydrates. The cake was dried at 105 °C, weighed, subsequently burned in an oven at 600 °C and again weighed. The remaining residue represents the ash content. The mass difference between dried cake and ash content portrays the actual AIL content. For the determination of the ASL content, the filtrate was measured by ultraviolet-visible (UV-vis) spectroscopy usually at a wavelength of 205 nm. Afterwards a provided extinction coefficient was utilized to calculate the AIL concentration. For the determination of carbohydrates, the filtrate was analysed by HPLC. For the determination of protein content, the overall elemental analysis was employed. The nitrogen content was then converted to a protein content utilizing a provided conversion factor. For the calculation of reaction yields the sum of AIL and ASL were utilized.

6.4.2 Infrared spectroscopy (for lignins and catalysts)

Fourier-transformed infrared spectroscopy (FTIR) was performed for lignin feedstocks, reaction residues and synthesized POM catalysts. For the lignin feedstocks, specifically the comparison of spectrograms was observed to distinguish different biomass sources and lignin pulping processes. For the reaction residues, the comparison to the original lignin feedstock regarding the alteration of bond types was observed. Lastly, for the synthesized POM catalysts, FTIR was conducted to ascertain the successful synthesis.

A Shimadzu IR-Spirit equipped with a Shimadzu QATR-S crystal was utilized. For the measurement a few milligrams of solid sample were placed on the dedicated area of the plate and fixated on the ATR crystal by a stamp. The transmission was measured in the wavelength range of 4000-400 cm^{-1} at a resolution of 0.9 cm^{-1} and 32 scans. For the data analysis the software LabSolution by Shimadzu was used.

6.4.3 Thermogravimetric analysis (for lignins and catalysts)

Thermogravimetric analysis (TGA) was performed to determine the moisture content of lignin feedstock samples and the crystal water content of synthesized POM catalysts. A Netzsch TG209 device was used for this. Approx. 20-30 mg of fine dispersed sample were weighed into the provided aluminium oxide crucible (for lignin samples) or quartz glass crucible (for synthesized POM catalyst). The mass was recorded by the internal scale. For lignin samples, the temperature started at 30 °C for 15 min, increased to 130 °C at a heating rate of 5 K/min, stayed at 130 °C for 15 min and lastly decreased the temperature to 30 °C at a heating rate of -5 K/min. The software provided by Netzsch was utilized for data analysis.

6.4.4 Organic elemental analysis (for lignins and reaction products)

Organic elemental analysis was carried out for all lignin feedstocks and reaction residues, allowing mass balance closure. Specifically, the content of the elements carbon, hydrogen, nitrogen, sulphur and oxygen (CHNSO) were measured, however for oxygen a different method needs to be employed. All measurements were performed by the department of central elemental analysis at University of Hamburg utilizing an *EA3000* elemental analyser manufactured by *EuroVector*. Approx. 1 mg of sample was burned with pure oxygen (for the elements CHNS) at high temperatures around 1,000 °C. All formed gases were subsequently separated by gas-chromatography and quantitively measured by a thermal conductivity detector

(TCD). For the determination of oxygen a pyrolysis mode was employed, utilizing an inert atmosphere and a contact to a dispersed carbon. At temperatures around 1,300 °C carbon monoxide was formed which is then measured in a TCD.

6.4.5 Gel-permeation-chromatography (for lignins and reactions products)

For the determination of the molecular weight distribution (M_w, M_n) gel-permeation chromatography (GPC), alias size-exclusion chromatography (SEC), was conducted. As the solubility of the relevant materials was not uniform, two setups and methods were applied.

The first method was conducted by *Xuang Tung Do* in the department of natural sciences at the Bonn-Rhein-Sieg University of Applied Sciences. The method employed is based on the publication of *Rumpf* et al. [173] The setup consisted of an Agilent 1260 based PSS GPC equipped with a pre-column (PSS MCX 8x50 mm 5 µm), a main column (PSS MCX 8x300 mm 5 µm), a multiple wavelength detector (MWD) and a refractive index detector (RID), all operated at 35 °C. As eluent a 0.1 molar sodium hydroxide solution at 0.7 mL/min was utilized. Each sample was solubilized in that eluent at 2.5 g/L concentration and an internal standard (ethylene glycol) was added at 1 g/L concentration. Due to lignins being mostly soluble at alkaline conditions, this method was employed to screen the molecular weight distribution of all lignin feedstocks.

The second method was conducted in-house and mainly utilized for tetrahydrofuran-soluble lignins and reaction samples. The setup was self-assembled, utilizing a degasser by *Knauer*, a pump by *FLOM*, an autosampler by *Knauer*, a MWD by *Merck* and a RID by *Schambeck*. The pre-column was an Agilent PLgel 10 µm and the main column consists of two Agilent PLgel 10 µm MIXED B columns. As eluent tetrahydrofuran (THF) was utilized with a flow rate of 1 mL/min. All solid samples were solubilized at 1 g/L concentration and all reaction solutions were diluted with THF in a 1:1 volume ratio. As an internal standard, toluene was added. For data evaluation the software Chromatographica was applied.

6.4.6 Inorganic elemental analysis (for catalysts)

The determination of inorganic elements was conducted by the department of central elemental analysis at University of Hamburg. Here, both inductively coupled plasma optical emission spectroscopy (ICP-OES) and flame atomic absorption spectrometry (F-AAS) were carried out to quantitively measure the contents preferably of Mo, P and Ni, but also of Si, W, V, Mn, Nb, and In. The devices utilized were ARCOS by *Spectro* (ICP-OES) and Solaar S Series by *Thermo Scientific* (F-AAS). The samples were ideally provided in an aqueous solution. If the samples were in solid form, they were solubilized in water with a pre-determined weight if possible. Otherwise, i.e. if the sample is not soluble in water or is already dissolved in organic solvents, a complete molecular breakdown was necessary which was achieved by adding nitric acid or aqua regia supported by microwave heating. Subsequently, all organic compounds were evaporated leaving behind an aqueous solution with its inorganic elements.

6.4.7 pH value (for catalysts and reaction products)

Within this work, the pH value was occasionally measured for reaction samples or catalyst solutions. For this, a Winlab Excellent Line pH Meter manufactured by *Windhaus Labortechnik GmbH & Co. KG* was utilized. The calibration of the pH-meter was conducted at room temperature with buffer solutions of pH value of 4, 7 and 10.

6.4.8 Gas chromatography (for reaction products)

The composition of the gas phase of all depolymerisation experiments was quantitively determined by gas chromatography (GC). The measurements were carried out in the gas chromatograph Varian 450-GC equipped with a Restek Shin Carbon Column (2 m x 0,53mm inner diameter, ST 80/100). The sample taken via gas bag directly from the reactors was injected onto the column utilizing a 250 µL sample loop. Argon was used as a carrier gas at a column pressure of approx. 5 bar. After the injection at 220 °C, the sample was directed towards the column inside the oven which was held at 40 °C for 2.5 min. The temperature was then increased to 140 °C at a rate of 15 K/min which was then hold for 3 min, lastly. The device was equipped with a TCD operating at 200 °C and detecting the permanent gases carbon dioxide, carbon monoxide and oxygen. All chromatograms were recorded, and the volumetric fractions of each gas were quantitively determined by the Galaxie Chromatography Software. The calibrations necessary for this can be found in the appendix in **Figure B-9** and **Figure B-10**.

6.4.9 Gas chromatography coupled with mass spectrometry (for reaction products)

Similarly to the previous section, the composition of the liquid phase was analysed by GC, however, here it was coupled with mass spectrometry (MS). The device was an Agilent 8860 GC system coupled with an Agilent 5977B GC/MSD. It is equipped with two columns, an Agilent HP-5MS-UI (for non-polar components) and an Agilent DB-WAX-UI (for more polar components). The carrier gas was helium at a flow rate of 1.2 mL/min and the sample was injected into either column at a temperature of 250 °C through a Agilent Ultra Inert Liner (5190-2295). For measurements on the DB-WAX-UI the starting oven temperature was 50 °C, hold for 1 min, increased to 250 °C at a rate of 10 K/min, and lastly hold at 250 °C for 4 min. For measurements on the HP-5MS-UI the starting oven temperature was 40 °C and the final temperature was 200 °C. The MS transfer line, the MS source and the MN quadrupole had a temperature of 250 °C, 220 °C, and 150 °C, respectively.

To allow quantification of components, each sample was prepared with the following procedure. For non-polar components, an internal standard solution was prepared utilizing methylparaben (methyl 4-hydroxybenzoate) in HPLC-grade methanol at a concentration of 10 mg/mL. Then, 2x 720 µL of sample and 1x 160 µL of internals standard were injected into the GC-vial by an Eppendorf micropipette. For more polar components, pure THF was utilized as an internal standard. 1.000 µL of sample and 10 µL of internals standard were injected into the GC-vial, again by micropipette. All chromatograms and spectrograms were recorded, and the concentration of each calibrated component was quantitatively determined by the Agilent MassHunter Software. All calibrations can be found in the appendix in **Figure B-1** to **Figure B-8**.

6.4.10 Karl-Fischer-titration (for reaction products)

For the determination of water content in reaction or extraction samples Karl-Fischer-titration (KFT), specifically the volumetric KFT, was utilized. The measurements were conducted on a Metrohm Titrando 835 with a 803 Ti module. The reagents and solvents necessary for the titration were Hydranal™ products produced by Honeywell. For all samples, three measurements were conducted, which were saved and analysed by the Metrohm tiamo software.

6.5 Reaction engineering parameters and calculations

In this section the mathematical formulas utilized for the analysis and assessment of all conducted experiments are described. This can be divided into three fields, being the depolymerisation, the membrane separation and the extraction.

Starting with the depolymerisation experiments, the key performance indicators were the yield Y_i of each monomer product i and the carbon balance fraction w_j of each product j, determined as shown in **Eq. 6-1** and **Eq. 6-2,** respectively. For **Eq. 6-1**, β_i is the mass concentration, $V_{Product\ solution}$ the volume of the reaction solution, m_{lignin} the initial mass of weighed lignin, and $w_{True\ lignin}$ the actual lignin content in the substrate. For **Eq. 6-2**, m_j is the mass, $w_{Carbon\ in\ j}$ the carbon content in product j, m_{lignin} the initial mass of weighed lignin, and $w_{Carbon\ in\ lignin}$ the carbon content in the lignin.

$$Y_i = \frac{\beta_i \cdot V_{Product\ solution}}{m_{lignin} \cdot w_{True\ lignin}} \qquad \textbf{Eq. 6-1}$$

$$w_j = \frac{m_j \cdot w_{Carbon\ in\ j}}{m_{lignin} \cdot w_{Carbon\ in\ lignin}} \qquad \textbf{Eq. 6-2}$$

Additionally, for the evaluation of kinetic experiments and the continuous depolymerisation plant both the residence time τ and the space-time-yield STY were considered and calculated as in **Eq. 6-3** and **Eq. 6-4**, respectively. For **Eq. 6-3**, V_R is the reactor volume and $\dot{V}$ the volume flow rate. For **Eq. 6-4**, m_j is the mass of product j, V_R is the reactor volume, and t_R is the reaction time at which the product mass m_j was acquired.

$$\tau = \frac{V_R}{\dot{V}} \qquad \textbf{Eq. 6-3}$$

$$STY = \frac{m_j}{V_R \cdot t_R} \qquad \textbf{Eq. 6-4}$$

For the evaluation of extraction experiments both the separation factor α for compound i and the rejection factor R for compound i were considered and calculated as in **Eq. 6-5** and **Eq. 6-6**,

respectively. For both, $\beta_{i,Extract}$ is the mass concentration of component i in the extract and $\beta_{i,Feed}$ the mass concentration of component i in the feed.

$$\alpha = \frac{\beta_{i,Extract}}{\beta_{i,Feed}} \quad \textbf{Eq. 6-5}$$

$$R = 1 - \frac{\beta_{i,Extract}}{\beta_{i,Feed}} \quad \textbf{Eq. 6-6}$$

The experiments for the membrane separation were evaluated similarly to allow for a direct comparison between these two product isolation approaches. Therefore, the separation factor α and the rejection factor R were calculated as **Eq. 6-5** and **Eq. 6-6**, respectively, with the index *Extract* being changed to *Permeate*. Additionally, for the performance comparison of membranes utilized, the specific permeate volume flow rate J was determined as in **Eq. 6-7**. $\dot{V}_{Permeate}$ is the volume flow rate of the permeate and $A_{Membrane}$ the area of the membrane sheet.

$$J = \frac{\dot{V}_{Permeate}}{A_{Membrane}} \quad \textbf{Eq. 6-7}$$

6.6 Design of experiments - Box-Behnken design

In this work a so-called Design of Experiments (DoE) study was conducted. DoE is a systematic and statistical method to study the effects of multiple factors on a response or outcome. Multiple factors can be varied simultaneously, unlike traditional one-factor-at-a-time (OFAT) approaches which require a higher experimental effort and usually provide no insights into interactions of multiple factors. DoE, on the other hand, aims to maximize information gained with minimal experimental effort, while also providing insights on factor interactions. Additionally, the results are statistically analysed to assess the significance of each factor's influence and allowing the same level of accuracy compared to the OFAT approach. [174,175]

$$n = 2k \cdot (k-1) + c_0 \quad \textbf{Eq. 6-8}$$

The approach considered within this work was the Box-Behnken-Design (BBD). The BBD is particularly suited towards exploring quadratic response surfaces making it effective in optimizing processes with multiple influencing parameters while limiting the amount of factor combinations to a minimum. For all influencing factors three levels are observed (usually low, medium and high). Additionally, the centre point (all factors at medium level) is observed multiple times to assess the experimental error and the overall robustness of the model. With **Eq. 6-8** the required experiments n for k factors at three levels with c_0 centre points are calculated – for three factors and three centre points the overall number of experiments equals 15 [174]. This BBD plan is depicted in **Figure 6-6** where the three axes represent each factor. It is apparent that the corners of the model are not observed while the middle setting of each edge is resulting in the desired consideration of quadratic responses. During the design plan one factor stays at its medium level while the others are varied. The repetition of the centre point is necessary for the calculation of statistical variance within the utilized setup. This variance or standard deviation is applied to all other experimental points to determine the outcome's significance. This statistical procedure is conducted within an Analysis Of Variance (ANOVA). Overall, the application of the BBD allows the consideration of parameter influence and interaction and was utilized specifically for the optimization of product yield within this work. [174,175]

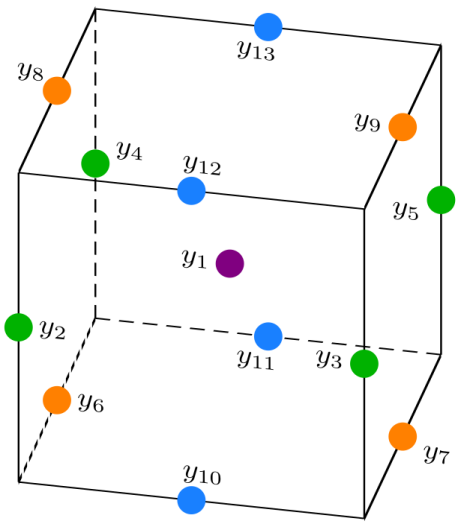

Figure 6-6: Illustration of the Design of Experiment Box-Behnken-design with three factors, one for each coordinate axis, and the centre point (violet). [174]

6.7 Consideration of error

Generally, all devices and procedures are subject to errors. This, of course, includes inaccuracies of the procedures themselves as well as direct deviations of measuring devices. Because of these complex procedures which include differing quantifying devices, the consideration of error cannot be easily done. For this reason, this consideration will be conducted exemplarily.

For experimental procedures of lignin depolymerisation, errors are induced during weighing and measuring the reaction solvents, as the scale shows a relative error of 0.1 % and the graduated pipette a relative error of 0.2 %. However, these errors are only applicable for experiments on Setup 1 (cf. section **6.3.1.1**). During up-scaling to Setup 2 (section **6.3.1.2**) or Setup 3 (section **6.3.1.3**) larger amounts of feedstock, catalyst and solvent are used which are measured by larger instruments showing a maximum relative error of 1.0 %. While pre-setting the pressure before starting the experiments, each reactor's pressure must be adjusted individually leading to slightly differing reaction pressure and to a relative error of 1-3 %. After the reaction and during the measurement of the temperature, an acute error might arise for experiments in the 10-fold plant, as this temperature is measured on the outside reactor wall. The relative error cannot be determined here, unfortunately. Then, while taking a gas sample the connecting the tube of gas bag and pressurized vessel is not evacuated leading to a small portion of air inside the gas sample decreasing the volumetric product amount measured later. The relative error here is varying as the remaining pressure inside the reactor and thus the amount of gas sample is dependent on the reaction. Again, the relative error for this cannot be calculated but estimated to a maximum of 5 %. For the quantification of these gaseous products, the GC calibration curves of CO_2 and CO can be found in the appendix in **Figure B-9** and **Figure B-10**. The yield of liquid phase products, on the other hand, are subject to a larger amount of relative error. First, the quantification via GC-MS yielding the mass concentration of these products showed to be rather inaccurate due to the catalyst being unable to evaporate and thus disturbing the evaporation process of said liquid phase products. The calibration curves of the pure substances showed statistical significance and can be found in the appendix from **Figure B-1** to **Figure B-8**.To increase the reliability of liquid phase products, each sample was measured three times. The relative error observed lied between 5-10 %. Subsequently, this mass concentration was utilized for the calculation of the absolute mass of product. For this, the solvent volume must be utilized. Due to the organic solvent being a light boiler, thus evaporating and leaving the reactor during gas sampling, and subject to side-reactions forming

esters and water being formed during reaction, the initial volume of solvent had changed. The estimated error of volume change must therefore be estimated to an amount of 1-5 %. The solid residue of the depolymerisation experiments, however, show a small relative error. As the amount is weighed on a pre-weighed filter by precision-scale the relative error is 0.1-1 %.

For the experimental procedures of extraction and membrane separation large volumes were utilized leading to a maximum relative error of 1 %.

The elemental analyses conducted showed a high precision and accuracy for all elements leading to a maximum relative error of 1 %, provided that the element's concentration lied within the range of calibration.

7. Results and discussion

In this chapter, all experimental results of the present thesis will be described and discussed in detail. The investigation on oxidative lignin depolymerisation can be distinguished into four parts. The first one being the characterization of the acquired technical lignins. The second one being a sensitivity study of the lignin depolymerisation including a substrate, solvent and catalyst screening as well as an investigation on the influence of reaction parameters and its optimization. In the third part the two concepts of extraction and membrane separation will be examined for the isolation of monoaromatic products. Lastly, in the fourth part the planning, commissioning and testing of a continuous lignin depolymerisation plant will be discussed.

7.1 Characterization of lignin substrates

Throughout this section the characterization of the lignin substrates will be discussed. It must be mentioned that all substrates are technical lignins and not model substances. All these technical lignins were acquired from industrial partners and other research institutions. An overview of all lignin substrates can be seen in **Table 7-1**. Throughout the characterization, specifically the elemental composition (elements C, H, N, S), the structural composition by NREL method and the molecular weight distribution by GPC were examined and will be discussed in the following sections. Additionally, the functional composition by FT-IR were analysed for some lignins. These results can be found in the appendix in section **B.3**.

7.1.1 Elemental composition

The knowledge of elemental composition of the lignin substrates is necessary in order to evaluate the lignins but also to consider carbon mass balances later during the depolymerisation experiments. This analysis was conducted for all acquired technical lignins and the results are shown in **Table 7-2**. The range of the carbon weight fraction lied between 55-65 % independent on biomass or pulping type. There are a few outliers which were substrate S7, S14, S15, S18A and S18B showing lower carbon contents of 15-30 %. The reason for this was a considerable amount of moisture of up to 60 % in these substrates resulting in a highly viscous liquid substrate. All substrates showed a typical amount of hydrogen with 5-8 % and a neglectable amount of nitrogen between 0-1 % originating from remaining proteins. The sulphur content lied within the expected range of 2-3 % for kraft lignins, at 0 % for organosolv lignins and between 5-8 % for sulphite lignins. The sulphur content for all hydrolysis lignins, the 2G

biorefinery lignin and the ionic liquid lignin was expectedly close to 0 % as no sulphur containing materials were applied during acidification to precipitate and isolate the lignin. Noteworthy is the sulphur content of the soda lignin (S13) which was expected to be at 0 %. A reason for this elevated value of 1.1 %could be the downstream processing while isolating the lignin. Potentially, acidification by sulphuric acid was applied for lignin precipitation resulting in any incorporation of sulphates.

Table 7-1: Overview of acquired lignin substrates including provider, biomass type and pulping type information.

Substrate #	Provider	Biomass type	Pulping type
S1	FAU Erlangen	Softwood	Organosolv
S2	Merck	Softwood	Kraft
S3	Merck	Softwood	Kraft
S4	Fraunhofer CBP, Leuna	Beech wood	Organosolv
S5	Fraunhofer CBP, Leuna	Spruce wood	Organosolv
S6	LignoPure, Hamburg	Softwood	Hydrolysis
S7	LignoPure, Hamburg	Hardwood	Sulphate
S8	LignoPure, Hamburg	Softwood	Kraft
S9	Fraunhofer CBP, Leuna	Beech wood	Organosolv
S10	LignoPure, Hamburg	Birch wood	2G Biorefinery
S11	LignoPure, Hamburg	Spruce wood & wheat straw	Enzymatic
S12	LignoPure, Hamburg	Beech Wood	Hydrolysis
S13	LignoPure, Hamburg	Wheat straw	Purified Soda
S14	Lenzing, Czech Republic	Softwood	Mg-Sulphate
S15	Lenzing, Austria	Softwood	Mg-Sulphate
S16	Fraunhofer CBP, Leuna	Beech wood	Organosolv
S17	Lixea, Sweden	Softwood	Ionic liquid fractionation
S18A	Essity, Mannheim	Straw residues	Essity-process
S18B	Essity, Mannheim	Straw residues	Essity-process
S19	Mercer, Rosenthal	Softwood	LignoBoost

Aside from the high moisture substrates, all lignins showed an oxygen content of 30 to 40 wt.-%. These were expected results, as the monomers of lignin show a lower oxygen content of 21, 27 and 30 wt.-% for coumaryl alcohol, coniferyl alcohol and sinapyl alcohol, respectively. Due to random and additional ether bonds and aliphatic hydroxy groups the

oxygen content in the macromolecule increases. Additionally, any impurities of carbohydrates (i.e. cellulose and hemicellulose) increase the oxygen content significantly, since these show oxygen contents of approx. 50 %.

As lignin from hardwood generally consists of higher amounts of *S* units (syringyl) which shows a higher relative oxygen content than the *G* units (guaiacyl) more commonly found in softwoods, the assumption that these hardwood-based lignins should contain higher amounts of oxygen can be made. However, there is no clear trend observable that would confirm this assumption.

Overall, the results of the elemental analysis are in accordance with literature and will be applied for the evaluation of depolymerisation experiments. [176,177]

Table 7-2: Elemental composition of all lignin substrates including carbon, hydrogen, nitrogen, sulphur and oxygen (CHNSO). C, H, N, S were measured, and O is calculated by the remaining amount.

Substrate #	Lignin description	C in wt-%	H in wt-%	N in wt-%	S in wt-%	O in wt-%
S1	Organosolv softwood	60.1 %	6.1 %	0.3 %	0.0 %	33.6 %
S2	Kraft softwood	52.4 %	5.1 %	0.0 %	2.7 %	39.8 %
S3	Kraft softwood	61.7 %	5.7 %	0.5 %	1.8 %	30.3 %
S4	Organosolv beech	60.4 %	6.1 %	0.0 %	0.0 %	33.5 %
S5	Organosolv spruce	64.1 %	5.9 %	0.0 %	0.0 %	30.0 %
S6	Hydrolysis softwood	61.6 %	5.8 %	0.0 %	0.0 %	32.7 %
S7	Sulphate hardwood	30.3 %	5.7 %	0.0 %	6.9 %	57.1 %
S8	Kraft softwood	63.2 %	5.9 %	0.0 %	1.9 %	29.1 %
S9	Organosolv beech	60.4 %	6.4 %	0.6 %	0.0 %	32.6 %
S10	2G Biorefinery birch	56.2 %	6.5 %	0.7 %	0.2 %	36.3 %
S11	Enzymatic spruce&wheat	57.3 %	6.2 %	0.4 %	0.2 %	36.0 %
S12	Hydrolysis beech	57.3 %	6.3 %	0.6 %	0.0 %	35.9 %
S13	Soda wheat	59.1 %	6.0 %	0.7 %	1.1 %	33.1 %
S14	Mg-sulphate softwood	26.5 %	7.2 %	0.0 %	4.3 %	62.0 %
S15	Mg-sulphate softwood	27.0 %	6.9 %	0.0 %	5.0 %	61.0 %
S16	Organosolv beech	63.6 %	6.0 %	0.3 %	0.0 %	30.1 %
S17	Ionic liquid softwood	65.3 %	5.5 %	0.3 %	0.4 %	28.5 %
S18A	Essity straw solid	32.8 %	4.8 %	0.9 %	0.2 %	61.3 %
S18B	Essity straw liquid	15.5 %	8.0 %	0.5 %	0.1 %	75.9 %
S19	LignoBoost softwood	62.3 %	6.0 %	0.15 %	2.4 %	29.2 %

7.1.2 Compositional analysis

The compositional analysis of the lignin substrates was mandatory in order to evaluate impurities of carbohydrates, moisture and ash. As these impurities cannot be converted to aromatic products, their measured quantity must be considered while calculating product yields. In **Figure 7-1**, the results of the compositional analyses for the substrates S1 to S13 are shown (as these analyses were conducted externally and the substrates S14-S19 were acquired at a later stage, those substrates have not been analysed). The exact numbers are included in the appendix in **Table B-2**.

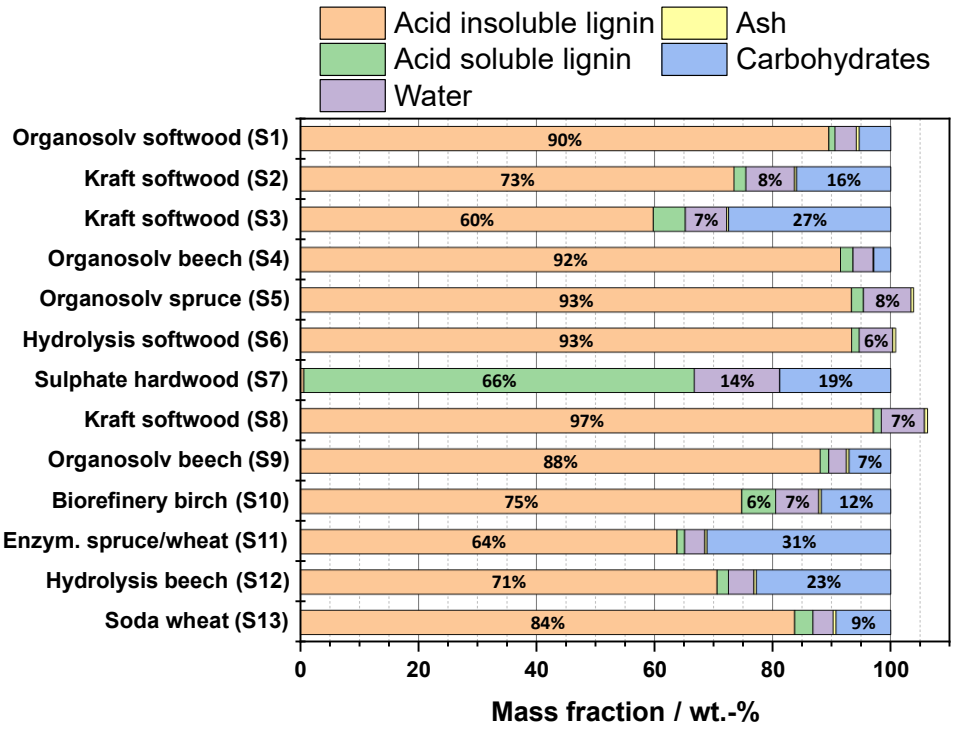

Figure 7-1: Mass distribution for acid insoluble lignin, acid soluble lignin, water or moisture, ash and carbohydrates in lignin substrates S1 to S13.

The organosolv lignins (substrates S1, S4, S5, S9) all showed a high purity with approx. 90 wt.-% being specifically acid insoluble lignin. The content of acid soluble lignin was close to 0 wt.-% for all organosolv substrates. This is an expected result due to the pulping treatment involving organic solvents which do not cause an increased solubility in aqueous media. The impurities comprise carbohydrate or moisture. There is no clear difference of soft- or hardwood lignins observable.

The kraft lignins (S2, S3, S8) and soda lignin (S13), on the other hand, show larger deviations from each other. Even though their lignin content was comprised by acid insoluble lignin again,

the content ranges from 60 to 97 wt.-%. Substrates S2 and S3 showed larger contents of carbohydrates being 16 and 27 wt.-%, respectively, while substrate S8 and S13 showed none or 9 wt.-%, respectively. The moisture content was coherent for all three kraft lignins being between 4 and 8 wt.-%. The large contents of carbohydrates for S2 and S3 potentially indicate an insufficient treatment of the softwood during pulping leading to increased concentrations of long-chained carbohydrates which might co-precipitate with the lignin. The other potential reason might be a too harsh precipitation method leading to a co-precipitation of carbohydrates. This again shows the significant influence on the pulping process – even the same process can result in varying lignin qualities.
Substrates S10, S11, S12, which all underwent a hydrolysis-similar process, showed moderate lignin contents ranging from 64 to 75 wt.-%, again being acid insoluble lignin. For all these substrates the majority of impurities was comprised by carbohydrates. This is again a sign for an incomplete hydrolysis treatment leading to recondensation of lignin-carbohydrate complexes as described by *Feng* et al. [178]. These complexes might also precipitate causing the high carbohydrate content determined during the compositional analysis. The presence of such complexes might also influence the depolymerisation process developed throughout this thesis.

Lastly, the lignosulphonate S7 showed no acid insoluble lignin at all and only acid soluble lignin with 66 wt.-%. This highlights the inorganic sulphite groups enhancing the water solubility tremendously. Besides this, the substrate showed high concentrations of residual water and also impurities, specifically carbohydrates, with an amount of 14 and 19 wt.-%, respectively.

Overall, the results of the compositional analysis will help both understanding the results of the lignin depolymerisation and deciding what lignins will most likely have the maximum product yield.

7.1.3 Molecular weight distribution

In this section, the analysis of molecular weight distribution of different lignin substrates will be discussed and compared. These results are shown in **Table 7-3**. Here, all lignins except for substrates S14, S15 and S17-S19 were measured by gel-permeation chromatography (again, as this analysis was conducted externally and these substrates were acquired at a later stage).

The organosolv lignins showed weight average molecular weight (M_w) values of 1,800 to 3,000 Da, number average molecular weight (M_n) values of 800 to 1,100 Da and polydispersities (D) between 2.0 and 3.2. The values for the molecular weight are in accordance with literature, however, the polydispersities showed reduced valued compared to literature. [52,55,60–65]

The kraft lignins exhibited M_w values of 5,400 to 6,700 Da, M_n values of 1,300 to 1,500 Da and polydispersities of 4.3 to 4.6. Especially the values for M_w and D are significantly larger compared to literature values shown in section **4.2.2**. [52,55,60–65]

Table 7-3: Overview of the molecular weight by number, by weight and its polydispersity of different lignin substrates by pulping process type.

Substrate #	Lignin description	M_n / Da	M_w / Da	D / .-
S1	Organosolv softwood	864	2513	2,9
S2	Kraft softwood	1260	5391	4,3
S3	Kraft softwood	1378	6177	4,5
S4	Organosolv beech	800	2234	2,8
S5	Organosolv spruce	1133	3607	3,2
S6	Hydrolysis softwood	475	1111	2,3
S7	Sulphate hardwood	783	3717	4,7
S8	Kraft softwood	1456	6680	4,6
S9	Organosolv beech	852	3049	3,6
S10	2G Biorefinery birch	844	7215	8,6
S11	Enzymatic spruce&wheat	705	1613	2,3
S12	Hydrolysis beech	977	9348	9,6
S13	Soda wheat	1212	5910	4,9
S16	Organosolv beech	884	1809	2,0

Contrarily, the sulphite lignin showed significantly smaller values for M_w (3,700 Da), Mn (800 Da) and D (4.7). In literature, values usually mentioned are 20,000-50,000 Da for M_w, 3,000-8,000 Da for M_n and 6-8 for the polydispersity. [52,55,60–65]
The hydrolysis lignins showed large differences with M_w values of 1,100 to 9,300 Da, M_n values of 500 to 1,000 Da and polydispersities of 2.3 to 10. This can be explained by the various number of approaches and fractionation techniques within hydrolysis pulping. This leads to a broad range of possible molecular weight distributions as the native lignin is chemically modified in different ways.

Lastly, the results of GPC analysis of the soda lignin are in accordance with literature. [52,55,60–65]

In summary, the characteristic parameters for molecular weight show discrepancies with values from literature. [52,55,60–65] Reasons for this are diverse and cannot be pinpointed. Generally, the biomass origin, the pulping process details, the lignins purity and of course the GPC methodology all have a significant influence on the results.

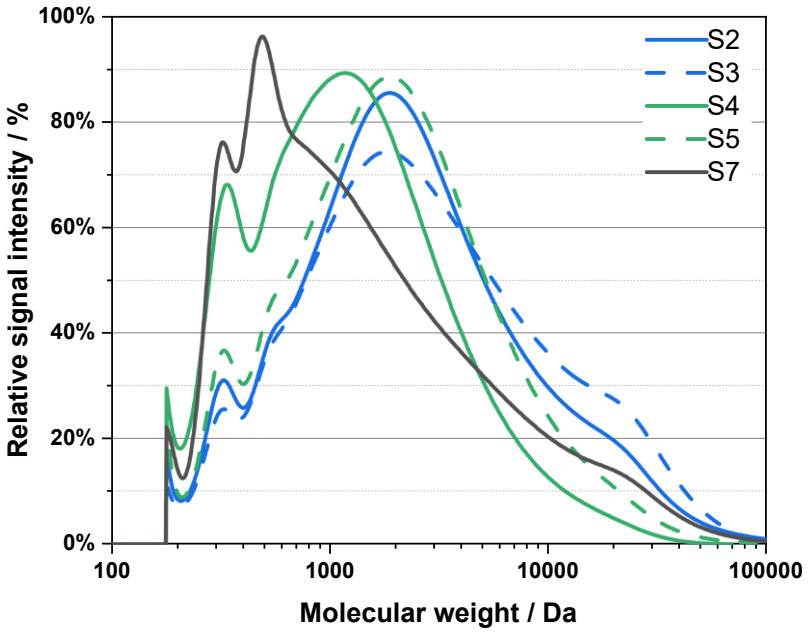

Figure 7-2: Molecular weight distribution of two softwood kraft lignins (S2 and S3), one beech wood organosolv lignin (S4), one spruce wood organosolv lignin (S5) and a softwood sulphite lignin (S7).

In **Figure 7-2** the molecular weight distribution is exemplarily shown for two kraft lignins, two organosolv lignins and a sulphite lignin. The two kraft lignins (S2 and S3) show small deviations leading to the diverging results from **Table 7-3**. The quantity of molecules in the range of 2,000 Da is lower for S3. On the other hand, the quantity of molecules in the range of 20,000 Da are significantly higher for S3. These two lignins not only were produced by the same pulping process but also originate from a similar biomass being softwood. Surely, softwood is an inaccurate description, however, usually spruce and pine wood are utilized as a softwood feedstock for pulping processes. [179] This means that even the specific plant type results in a significant difference for the molecular weight distribution. Additionally, even seasonal or geographic conditions have an impact on lignin characteristic, as discussed in section **4.1.1**.

The two organosolv lignins originated from beech wood (S4) and spruce wood (S5). Here, a clear difference in their molecular weight distribution can be observed. While the overall course of the distribution is similar, the beech wood lignin shows higher quantities in molecular weight smaller than 2,000 Da, while the spruce wood lignin shows higher quantities in molecular weight larger than 2,000 Da. This is in accordance with literature, as softwood lignins show higher molecular weights than hardwood lignins due to softwood lignin being more branched and cross-linked. [180,181]
Lastly, the sulphite lignin (S7) shows high quantities of molecular weights below 1,000 Da which is contradicting with literature as values between 20,000 to 100,000 Da are reported here. [52,55,182] A reason for this significant deviation might be the GPC method. As reported by *Guizani* et al. [182] an alkaline treatment of sulphite lignin can reduce the molecular weight distribution substantially. The GPC method applied here indeed involved the dissolution of lignins in aqueous and alkaline solutions at pH 12. This might have caused a chemical modification of the lignin explaining the deviation to literature values.

Overall, all lignins show characteristic shoulders at 200, 300, 500, 2,000, and 25,000 Da. Regarding the depolymerisation of these lignins to monomeric aromatics, this finding means that specific fractions of these lignins need less or more depolymerisation time compared to the average in order to be converted to the desired monomeric aromatics. Thus, the desired products are formed at different reaction times and must be separated throughout the process to prevent any degradation to undesired products.

7.1.4 Discussion on applied characterization techniques

In this section, several key parameters were analysed to characterize lignin, with the goal of supporting the evaluation of subsequent depolymerisation experiments. Among these parameters, the elemental composition (C, H, N, and S) and the compositional analysis were particularly critical. Elemental analysis, and specifically the carbon content, was used to assess the carbon efficiency of the developed process, which is essential for evaluating the distribution and yield of carbon-containing product groups. The compositional analysis, on the other hand, provided insights into the actual lignin content and the presence of impurities such as carbohydrates, water, and ash. Since the formation of desired monoaromatic products is derived exclusively from the lignin fraction, this analysis was indispensable prior to conducting depolymerisation experiments.

In contrast, the determination of the molecular weight distribution proved less informative in the context of experimental evaluation. No clear correlation between molecular weight distribution and the observed depolymerisation results could be established. Furthermore, direct comparison between the feedstock and product molecular weight distribution was not feasible due to methodological inconsistencies. Gel permeation chromatography (GPC), the technique employed, is highly sensitive to the utilized methodology. Consequently, the analysis of reaction products, performed in organic solvents, differed substantially from that of the lignin feedstock, which was analysed under aqueous conditions. This disparity prevented reliable comparison between the two datasets.

In summary, both elemental composition and compositional analysis were found to be essential for the meaningful interpretation of depolymerisation results. However, given that compositional analysis is time-intensive, the implementation of improved or more efficient analytical methods, such as those proposed by *Nisar* et al. [183], could enhance analytical throughput. For molecular weight analysis to contribute effectively to process evaluation, methodological consistency between feedstock and product characterization would be required to ensure comparability and reliability of the data.

7.2 Sensitivity study of oxidative depolymerisation of lignin

In this section the results of the sensitivity study for the oxidative depolymerisation of lignin towards monomeric, aromatic compounds is discussed. This includes the definition of target parameters by which the depolymerization reactions can be assessed. Then, various screening experiments for the selection of a substrate, a solvent system and a catalyst were conducted. These are then utilized for the optimization of process parameter conditions which are reaction time, oxygen partial pressure, up-scaling, temperature, stirring speed, catalyst loading and substrate loading. These optimized process conditions are lastly applied to all other substrates again.

7.2.1 Definition of target parameters

In order to develop a process for the homogeneous, oxidative depolymerisation of technical lignins towards the compounds Va, Sy and their derivatives, target parameters must be defined to evaluate the influence of the various process conditions.

Lignin is a heterogeneous biopolymer showing a diverse functionalisation which is propagated due to different pulping processes. Thus, the solubility of lignin is not only restricted in both organic and aqueous solvents but also varying depending on the applied pulping process. Accordingly, the lignin content in the liquid phase is a suitable target parameter as the effective depolymerisation takes place in the liquid phase driven by the homogeneous POM catalyst. This lignin content is measured by the carbon balance indicating how much carbon inside the lignin stayed in the solid phase, was solubilized towards the liquid phase and how much carbon was over-oxidized towards the gas phase. Overall, the goal is to maximize the carbon content in the liquid phase, while minimizing the carbon content in the solid and gas phase.

The second target parameter for the sensitivity study is more straightforward, being the yield of the desired aromatic compounds and undesired smaller compounds (with a base carbon chain length of C1-C5) which are all located inside the liquid phase. This parameter thus is a further refinement of the prior described carbon balance and indicates the progression of the depolymerisation inside the liquid phase. Obviously, the yields of the aromatic compounds (both the sum and individually) are to be maximized while the undesired smaller sized compounds shall be minimized.

The target parameters can be summarized as follows:

- Maximizing carbon content in liquid phase
- Maximizing yield of desired monoaromatic products (Va, MeVa, Sy, MeSy)
- Minimizing yield of degradation products

7.2.2 Selection of substrate (Setup 1)

Initially, 13 technical lignins were available for experimental testing. The process development for the oxidative depolymerisation of lignin is an extensive undertaking and it does not make sense to conduct this procedure for all these lignins, separately. Therefore, the number of promising lignins was narrowed down by a substrate screening. The depolymerisation of all lignins was experimentally tested both without a catalyst and using a reference POM catalyst ($H_8PV_5Mo_7O_{40}$ abbreviated as HPMo-V_5). The goal in this substrate screening was to determine lignins showing the highest carbon content inside the liquid phase after catalytic depolymerisation. The control substrate screening, containing no catalyst, is meant to determine the influence of the POM catalyst. As described in section **4.4.2**, the HPMo-V_5 shows both Brønsted acidity and RedOx potential inducing both acidic hydrolysis and oxidation of the lignin substrates leading to a varying conversion behaviour compared to a reaction with no POM catalyst. The comparison of these two screenings, thus, might allow a further understanding of the depolymerisation reaction itself.

Table 7-4: Overview of the standard parameters for the screening of technical lignins for the oxidative depolymerisation towards vanillin, syringaldehyde and their derivatives in 10-fold plant of Setup 1.

Reaction parameter	Parameter value	Details
Time	24 h	
Partial pressure	20 bar	Oxygen
Temperature	140 °C	
Substrate mass	500 mg	
Catalyst mass	0 mg or 200 mg	Blank or HPMo-V_5
Solvent volume	10 mL	Methanol
Stirring speed	0 rpm	Does not contain stirrer

The screening experiments were all conducted in Setup 1 containing ten 20 mL batch reactors. The depolymerisation reaction time was 24 h at an oxygen partial pressure of 20 bar and a

temperature of 140 °C. The substrate and catalyst mass were 500 mg and 200 mg, if any, respectively and these were immersed in 10 mL of methanol. As in these small reactors only magnetic stirrers are feasible, these were entirely neglected since they would not move while being immersed in the solid lignin (as previously tested). These reaction parameters are additionally summarized in **Table 7-4** and were determined based on both preliminary work of the research group of *Prof. Albert* and a thorough literature research. [184–197]

The results of the control substrate screening containing no catalyst are shown as the carbon balance in **Figure 7-3**. Here, the carbon content in the gas, liquid and solid phase are depicted for the utilized substrates which are grouped by pulping process for an easier comparison. The first thing to notice is that all phases are present for each substrate. However, the carbon content in the gas phase does not exceed 8 wt.-% (for S7). This means that the applied reaction conditions without using a catalyst already suffice for an occasional full oxidation of carbon towards CO_2 and CO. On the other hand, the distribution of liquid and solid phase is more diverse. For the kraft lignins (S2, S3, S8) the carbon content in the liquid phase lies between 50 and 67 wt.-% while the carbon content in the solid phase lies between 31 and 47 wt.-%.

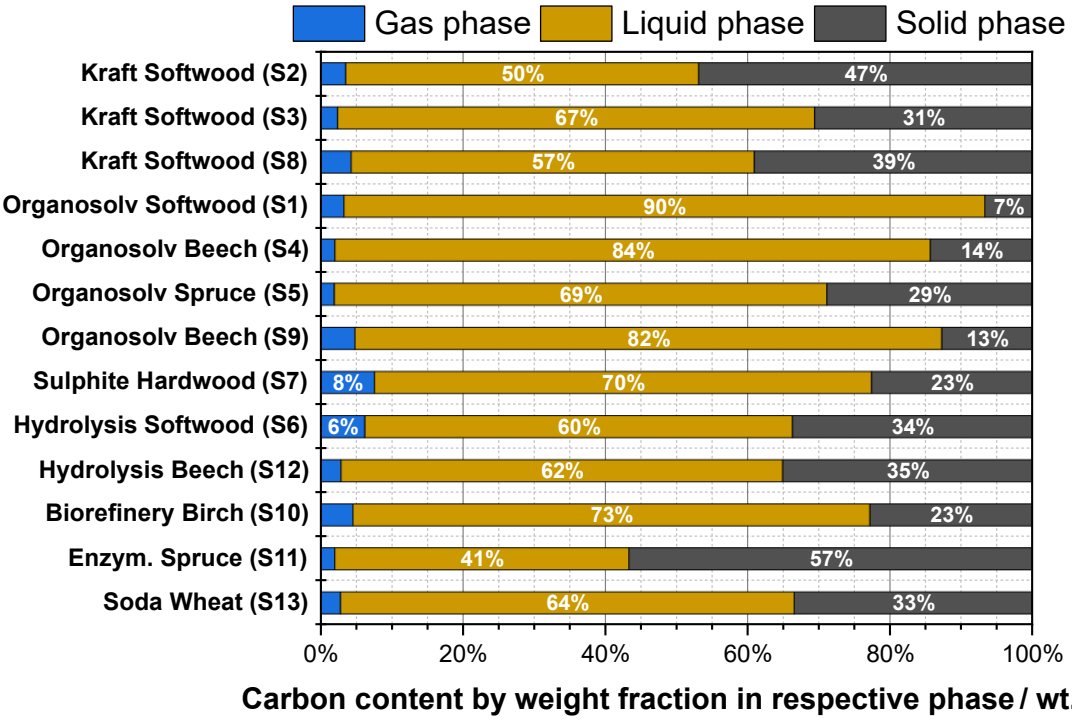

Figure 7-3: Carbon balance of the initial lignin substrate screening (including substrates S1-S13) for the oxidative depolymerisation with no catalyst as a control experiment. The substrates are grouped by pulping process. Reaction conditions were 140 °C, 20 bar oxygen partial pressure, 24 h, 0 rpm, 10 mL MeOH, 500 mg substrate, no additional catalyst.

The organosolv lignins (S1, S4, S5, S9) show a carbon content in the liquid and solid phase of 69 to 90 wt.-% and 7 to 29 wt.-%, respectively, which shows that the organosolv lignin are significantly more soluble in the reaction solvent being methanol. However, this is an expected result as the organosolv pulping involves a thermal solvolysis treatment including acidic conditions and organic solvents, whereas the kraft lignins were produced by a treatment including alkaline conditions and water as solvent. The remaining substrates overall lie between the results of the kraft and organosolv lignins. Though, S11 originating from an enzymatic fractionation of spruce shows a significantly lower carbon content in the liquid phase with 41 wt.-%.

As previously described, this substrate screening was repeated with the addition of the reference POM catalyst HPMo-V_5. The results of the carbon balances are shown in **Figure 7-4** again for the gas, liquid and solid phase. Comparing the two screening experiments, it is apparent that the carbon content in the gas phase shows no significant change. This means that even though the oxidizing power is potentially increased by the catalyst, the oxidation towards CO_2 and CO is not changed. This indicates that the catalyst does not facilitate the reaction towards CO_2 and CO which has been shown by *Albert* et al. in various biomass conversions. [141,155,198]

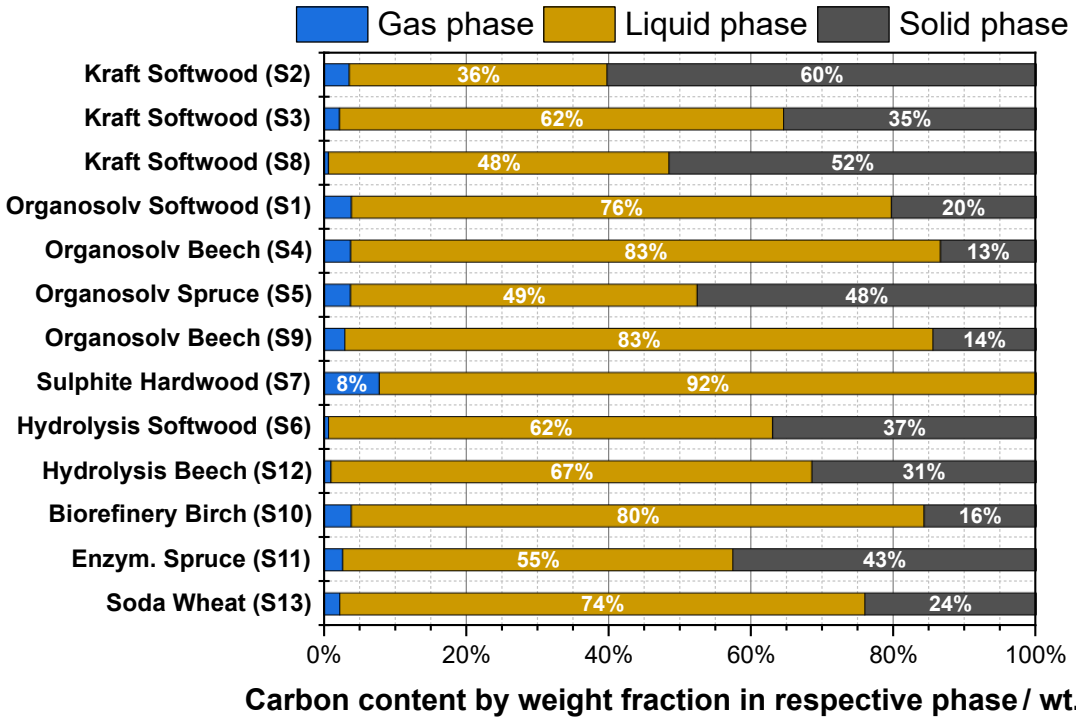

Figure 7-4: Carbon balance of the follow-up lignin substrate screening (including substrates 1-13) for the oxidative depolymerisation with HPMo-V_5 as POM catalyst. Reaction conditions were 140 °C, 20 bar oxygen partial pressure, 24 h, 0 rpm, 10 mL MeOH, 500 mg substrate, 200 mg catalyst.

The sulphite lignin (S7) explicitly stands out, here. The carbon content of the solid phase for this substrate entirely disappeared and was allegedly converted to the liquid phase reaching 92 wt.-%. This is an expected result as sulphite lignins contain a considerable amount of inorganic sulphur functionalization leading to a high solubility in aqueous solutions at any pH value. This is also shown in the compositional analysis where the sulphite lignin is the only substrate showing a high solubility in acidic environments (cf. **Figure 7-1**). As the POM catalyst contains crystal water which might be released at reaction conditions and facilitates the formation of reaction water due to etherification or esterification by its Brønsted acidity, the water content in the solvent might increase enough for the solubilization of the sulphite lignin (S7).

As indicated, the carbon content in the liquid phase is more variable for the remaining substrates. All kraft lignins (S2, S3, S8), the organosolv lignins S1 and S5 and the hydrolysis softwood lignin S6 show a decreased amount in the liquid phase and an increased amount in the solid phase. The increased amount in the solid phase suggests that condensation or repolymerisation reactions of the lignin might occur more frequently utilizing the catalyst. This might result in an increased amount of humin-like compounds, similarly to pseudo-lignin. These are formed by condensation reactions while processing carbohydrate compounds (cellulose or hemicellulose) at too harsh conditions, as described in literature. [199–201]
The organosolv lignins S4 and S9 not only perform almost equally between each other, they also show no significant change of carbon balance when compared to the control experiments. This could mean that the catalyst does not change anything and suggests an equal rate of formation of pseudo-lignin and depolymerisation to dissolvable compounds. Overall, the carbon content in the liquid phase for both substrates is promising at 83 wt.-%.

The substrates S10 to S13 all show a slight increase of carbon content in the liquid phase (7 to 14 wt.-%). The reason for this is not clear. One potential reason would be applicable for the substrates S11 and S12. The compositional analysis for both substrates shows a considerable amount of carbohydrates. As *Albert* et al. [155] have shown, these carbohydrates can be converted to formic acid and derivatives, excellently, when using the HPMo-V_5 as a catalyst. Thus, the increased carbon content in the liquid phase could be caused by the addition of the catalyst. Unfortunately, this reason is not applicable for S10 and S13 as these show only minor amounts of carbohydrates.

Overall, the substrate screening provided an overview of the carbon balance allowing for a pre-determination of substrates for further process development. From these 13 tested lignins, three were selected mostly based on the highest carbon content in the liquid phase. One additional requirement was to include one kraft lignin in order to have one representative technical lignin from the most utilized pulp process. The substrates selected for the next step were the kraft lignin S3, the organosolv lignin S4 and the sulphite lignin S7.
On another note, the influence of the POM catalyst was negligible regarding the carbon balance and thus, the benefit of the catalyst was absent at this stage. No clear trend of improvement of carbon content in the liquid phase was observable, and contrary to expectations, the carbon content in the solid phase increased for some lignins (e.g. S2, S3, S8). However, only the carbon balance was observed for now, which will be considered throughout the next sections.
Next, the influence of different solvent systems usually applied in literature was tested and the yields of the desired monoaromatic products were analysed.

7.2.3 Influence of solvent (Setup 1)

The selection of a suitable solvent is an essential step throughout the process development because of several reasons. The desired products must show high solubility in said solvent system, similarly to the lignin substrate. Otherwise, the substrate cannot be depolymerized optimally, and the aromatic products might precipitate decreasing yield and potentially causing hotspots in the reactor. In terms of specific solvents, the aromatic products show considerable solubility in polar organic solvents, such as methanol or ethanol. For the lignin substrate, the preferable solvent vastly depends on the pulping process – while organosolv or hydrolysis lignins are exceptionally soluble in methanol or ethanol, kraft lignins are only soluble at alkaline and aqueous conditions. Lastly, as POMs are crystalline salts in its basic form, they show full solubility in aqueous media.

In summary, the solvent ideally is a mixture of a polar organic solvent and water. In literature similar approaches are described underlining the methodology applied here. [168,191,197] The defined solvent systems based on this are (1) pure methanol, (2) a volumetric 1:1 mixture of methanol and water, (3) pure ethanol and (4) a volumetric 1:1 mixture of ethanol and water. These were used for the depolymerisation of the substrates S3, S4 and S7 as selected in the previous section. The adjusted process conditions are shown in **Table 7-5**.

Table 7-5: Overview of the parameters for the selection of a suitable solvent for the oxidative depolymerisation of the kraft softwood lignin S3, the organosolv beech lignin S4 and the sulphite hardwood lignin S7.

Reaction parameter	Parameter value	Details
Time	24 h	
Partial pressure	20 bar	Oxygen
Temperature	140 °C	
Substrate mass	500 mg	Kraft softwood lignin (S3) Organosolv beech lignin (S4) Sulphite hardwood lignin (S7)
Catalyst mass	200 mg	HPMo-V_5
Solvent volume	10 mL	Methanol Methanol/Water (1:1 v/v) Ethanol Ethanol/Water (1:1 v/v)

The results of the carbon balance for these experiments are shown in **Figure 7-5**. In methanol, the carbon content in the liquid phase rises being 66, 84 and 97 wt.-% for S3, S4 and S7, respectively, similarly to the previous findings in **Figure 7-4**. This also shows that the results so far are reproducible. When changing the solvent to the 1:1 mixture of methanol and water, several aspects change. The carbon content in the solid phase significantly increases for S3 and S4 by 8 and 24 wt.-%, respectively. This can be either a result of a decreased solubility or an increase of recondensation and formation of pseudo-lignin. Secondly, the carbon content in the gas phase significantly increased to 10, 9 and 17 wt.-%, respectively. This indicates an increase of the unselective conversion towards CO_2 and CO. This could be an effect of the catalyst showing higher activities in highly aqueous solvents.

When changing from methanol to ethanol, the carbon balance was affected similarly as in the methanol/water system. The carbon content in the solid phase significantly increased to 35, 48 and 41 wt.-%, respectively for S3, S4 and S7. Even for the highly soluble sulphite hardwood lignin S7 a significant amount of carbon in the solid phase was found. When anticipatorily comparing to the result of the ethanol/water mixture, the primary reason for the increase of solid phase is its insolubility in ethanol. The gas phase for the ethanol system, on the other hand, does not change substantially when compared to the methanol system, although a slight increase of CO_2 and CO was observed. Lastly, when changing the solvent from pure ethanol to the 1:1 mixture of ethanol/water, the effects were similar as to the change from methanol to

methanol/water for substrates S3 and S4. The increased water content lead to a significant rise of carbon in solid phase for S3 and S4, again indicating the reduced solubility of these substrates in more aqueous solvents and acidic conditions. On the other hand, the carbon in the liquid phase for S7 substantially increased, compared to the pure ethanol system, to almost 100 wt.-%. This shows that S7 is highly soluble at aqueous conditions and likely insoluble in pure EtOH.

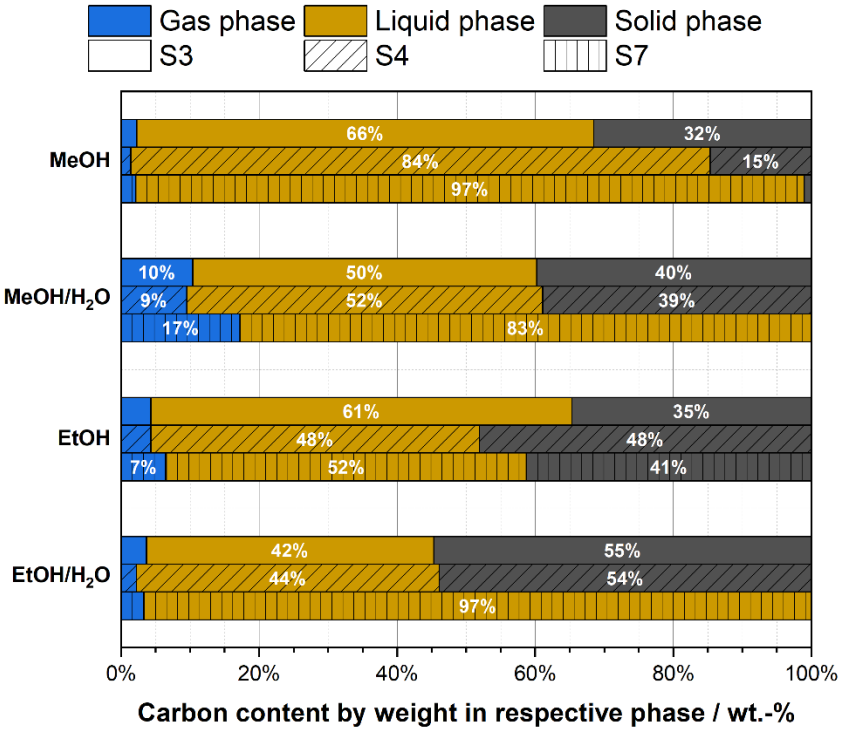

Figure 7-5: Carbon balance of the experiments for the selection of a suitable solvent for the oxidative depolymerisation of the kraft softwood lignin (S3), the organosolv beech lignin (S4) and the sulphite hardwood lignin (S7) carried out in Setup 1. Reaction conditions were 140 °C, 20 bar oxygen partial pressure, 24 h, 0 rpm, 10 mL solvent (MeOH, MeOH/H_2O 1:1 v/v, EtOH, EtOH/H_2O 1:1 v/v), 500 mg substrate (S3, S4, S7), 200 mg catalyst (HPMo-V_5).

When comparing the results of each solvent, the highest average carbon content in the liquid phase was achieved for pure methanol. Thus, the liquid samples of these phases were further analysed by GC-MS to (1) determine reactions products and (2) quantify these by the addition of a selected internal standard (cf. section **6.4.9**). In **Figure 7-6** the chromatograms of these measurements for the liquid phase samples in pure methanol of substrates S3, S4 and S7 are shown. The chromatograms for the remaining three solvents can be found in the appendix in **Figure B-25**, **Figure B-26**, and **Figure B-27**, respectively.

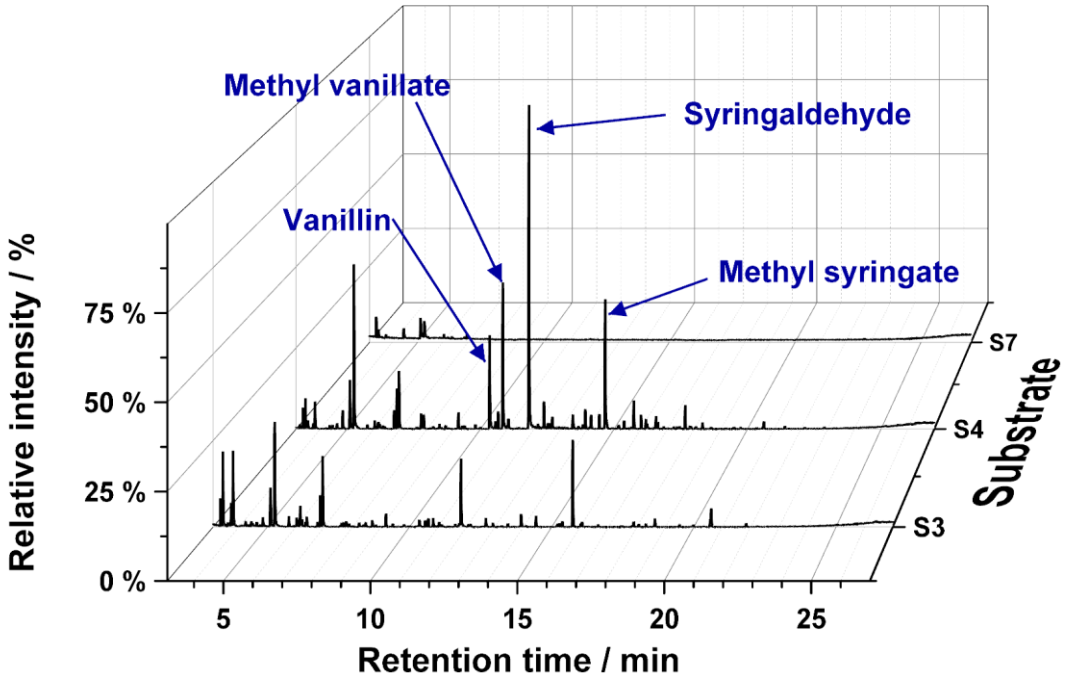

Figure 7-6: Chromatograms by GC-MS for the product liquid phases of the conversion of kraft softwood lignin (S3), organosolv beech lignin (S4) and sulphite hardwood lignin (S7) in the pure methanol solvent carried out in Setup 1. Reaction conditions were 140 °C, 20 bar oxygen partial pressure, 24 h, 0 rpm, 10 mL solvent (MeOH, MeOH/H_2O 1:1 v/v, EtOH, EtOH/H_2O 1:1 v/v), 500 mg substrate (S3, S4, S7), 200 mg catalyst (HPMo-V_5).

Deducted from the GC-MS library, three product groups can be defined in regard to the retention time. From 3 to 10 min, mostly aliphatic hydrocarbons with a maximum base carbon chain length of 6 are present. These are mostly further functionalized methyl ester groups. From 10 to 15 min mostly monoaromatic compounds were found and any reaction products beyond 15 min retention time were not possible to determine, although these are likely dimeric, trimeric or oligomeric products.

The results in **Figure 7-6** clearly show that only for S4 considerable amounts of all four targeted monoaromatic compounds were found, while for S3 only syringaldehyde in reduced quantities and for S7 no monoaromatics at all were detected. For both S3 and S4 various other monoaromatic compounds in lower quantities were measured, however. The oligomeric compounds are negligible for all three substrates, besides a significant signal at approx. 16 min for S3 for which the determination was not possible. The methyl ester group (mostly signals before 10 min retention time) shows signals for all three substrates, while the chromatograms of S3 and S4 indicate considerable quantities compared to the monoaromatics, and S7 again showing negligible signals. Compounds suggested by the GC-MS library were for example dimethyl succinate, dimethyl maleate, dimethyl malonate, or 2-Methoxysuccinic acid dimethyl

ester. As the GC-MS signal area is a function of both the concentration and the ionizability of a substance, a direct comparison of areas can be misleading. However, the strong signal suggest similar orders of magnitude in terms of concentration.

Generally, S7 almost shows no signals in the chromatograms and according to **Figure 7-5** only produced a minor amount of carbon in the gas phase. Still, the majority of carbon content remains in the liquid phase. This indicates that for S7 compounds were formed which were not detectable using the utilized GC-MS device and, thus, could be more polar products such as methyl or ethyl formate. The products of the depolymerisation for S3, on the other hand, likely show the highest quantities in the methyl ester group when comparing signal strength. In combination with the results of **Figure 7-5**, this hints that the remaining oligomeric compound rather tends to recondensate forming an insoluble pseudo-lignin or is further depolymerized towards additional methyl ester compounds. Admittedly, as the analysis does not depict all possible depolymerisation products, missing monoaromatic products might be present, but were not determinable by the established procedure. Lastly, S4 shows the most promising results with the allegedly highest product quantities in the monoaromatic product group, when comparing the signal intensities.

Thus, S4 was selected for (1) the previously mentioned quantification of monoaromatic products and (2) the further process development continuing in section **7.2.4**. The results of the monoaromatics quantification for S4 conversion in all four solvents are shown in **Figure 7-7**. For a start, the depolymerisation of S4 towards the monoaromatic compounds Va, MeVa, Sy and MeSy works for all solvents at least at low yields. While the methanol-water, the ethanol, and the ethanol-water-mixtures all performed similarly with summed yields between 1.5 and 1.75 wt.-%, the pure methanol solvent almost doubles the yield to approx. 3.0 wt.-%. Additionally, the yields of the methyl esters MeVa and MeSy were considerably higher in pure MeOH compared to the aldehydes, while for the methanol-water mixture all yields were relatively close to each other. To add to that, in both ethanolic solvents this trend becomes even clearer as the methyl esters each showed less than 0.5 wt.-% yield.

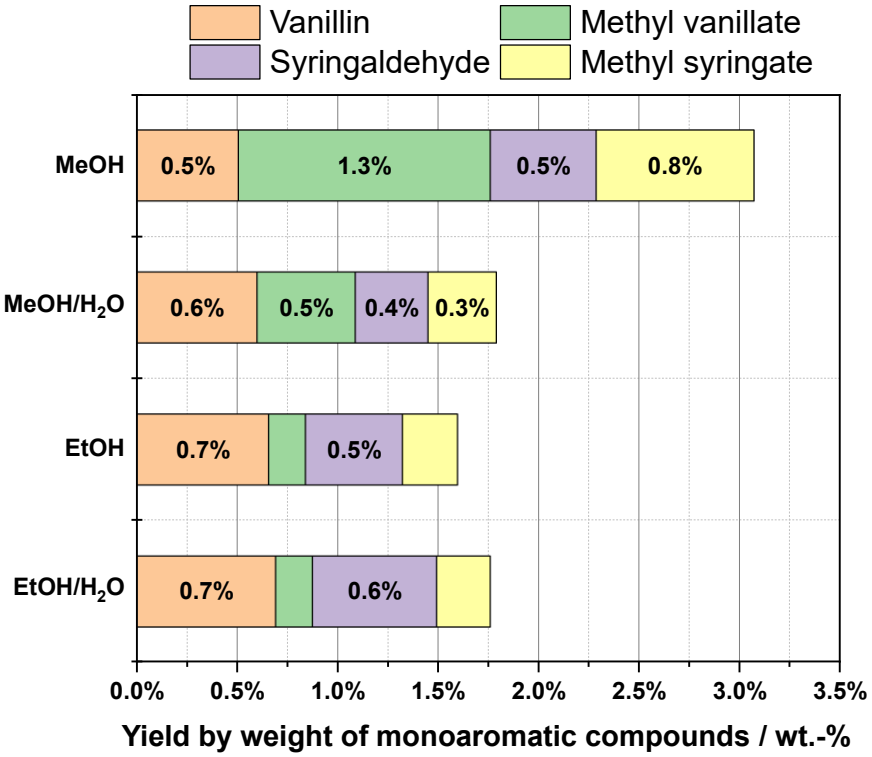

Figure 7-7: Yield by weight of the desired monoaromatic compounds for the solvent screening with the organosolv beech lignin (S4) carried out in Setup 1. Reaction conditions were 140 °C, 20 bar oxygen partial pressure, 24 h, 0 rpm, 10 mL solvent (MeOH, MeOH/H_2O 1:1 v/v, EtOH, EtOH/H_2O 1:1 v/v), 500 mg substrate (S4), 200 mg catalyst (HPMo-V_5).

Discussion on reaction network:

These observations indicate that methanol plays a crucial role for the formation of MeVa and MeSy which is likely due to the esterification of carboxylic derivatives of Va and Sy formed by the overall oxidative conditions during reaction. A potential reaction network is proposed in **Scheme 7-1** showing that the methyl esters are a secondary product derived from Va and Sy. At first, the lignin is solubilized and partially depolymerized towards oligomers by the overall thermal, oxidative and acidic conditions. These are then further depolymerized towards the desired products Va and Sy, likely originating from the guaiacyl and syringyl units, respectively. Subsequently, Va and Sy are oxidized to their respective carboxylic acid (vanillic and syringic acid). These compounds were not found due to an unsuitable GC-column which could not detect any kind of carboxylic acid. Lastly, induced by the acidic conditions and presence of methanol, the carboxylic acids are esterified to the products MeVa and MeSy. This reaction network would explain the increased presence of MeVa and MeSy as reaction products for the pure methanol solvent system. As esterifications are equilibrium reactions forming both the ester and water, the absence of water and the hyperstoichiometric concentration of methanol

shifts the equilibrium towards the ester side and thus outlines the increased presence of MeVa and MeSy when comparing the methanol systems.

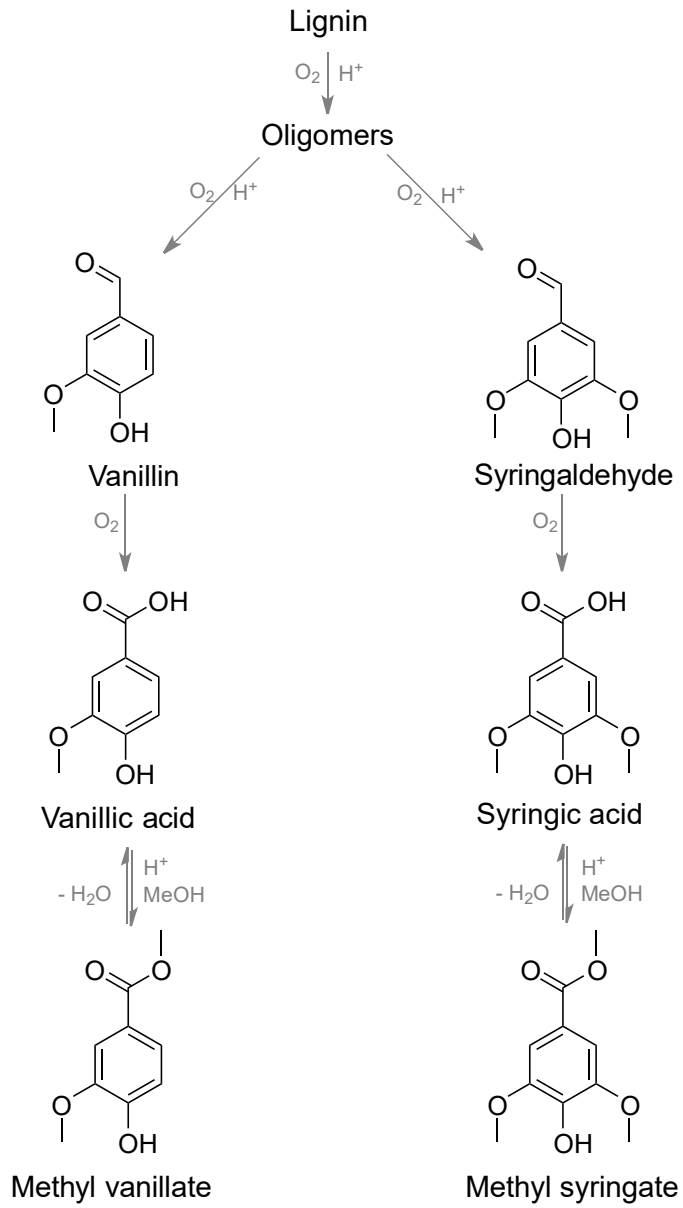

Scheme 7-1: Proposed reaction network describing the formation of all four monoaromatic products originating from the lignin substrate.

Consequently, methyl esters are significantly less likely to be formed in the ethanolic solvent due to the absence of methanol. In accordance with the proposed reaction network, the formation of ethyl esters by the esterification of ethanol and the formed carboxylic acids should occur and, indeed, a signal originating from ethyl syringate was observed for S3 at approx. 16 min, as can be seen in **Figure 7-6**. This signal, however, was significantly lower compared to the MeSy signal for S4.

In general, this further product modification potentially exhibits one key benefit being the promotion of chemical stability for the desired products. The aldehyde groups of Va and Sy seem to be more susceptible to further chemical modification, as shown by the oxidation towards the carboxylic acid. This could lead to degradation resulting in a decreased yield of monoaromatic compounds. Contrary, the formation of the methyl ester derivatives reduces this risk as ester functions exhibit higher chemical stability than aldehydes e.g. due to higher steric hindrance. Thus, the reaction network forming methyl ester derivatives describes an advantageous effect when using pure alcohols, in this case methanol, for the solvent resulting in considerable higher yields of the desired monoaromatics.

On a side note, this finding of methanol being a reactant rather than only a solvent is a crucial aspect when thinking about future process development. Not only was methanol consumed during the reaction, which must be considered in material balances, additionally water is formed at significant quantities, which likely has an influence on the solvent composition and consequently on the solubilization of lignin.
Nonetheless, methanol in pure or predominant concentrations was selected as solvent system and for the subsequent step of catalyst screening.

7.2.4 Selection of catalyst (Setup 1)

Overview:
In this section, the results of the screening experiments in Setup 1 for the selection of the most suitable catalyst will be discussed. The process parameters selected for this screening were based on the results of the previous sections with one exception. Instead of applying the proposed pure methanol as a solvent, a small and defined fraction of water was during this screening.

Table 7-6: Overview of the parameters for the selection of a catalyst for the oxidative depolymerisation of the organosolv beech lignin S4.

Reaction parameter	Parameter value	Details
Time	24 h	
Partial pressure	20 bar	Oxygen
Temperature	140 °C	
Substrate mass	500 mg	Organosolv beech lignin (S4)
Catalyst mass	200 mg	Described in **Table 7-7** and **Table 7-8**
Solvent volume	10 mL	Methanol/Water (95:5 v/v)

This is due to the reason that for the majority of POM catalysts utilized in this screening there is no excessive knowledge about their chemical behaviour, specifically regarding their solubility. Due to their crystalline nature all POMs show a high solubility in water, as previously described. But their solubility in methanol at reaction temperatures is unknown. To ensure full solubility of all POM catalysts a volume fraction of 5 % is added to the solvent. This leads to the reaction parameters shown in **Table 7-6**.

Overall, 26 different POM catalysts were screened within this investigation. All utilized catalysts are listed in **Table 7-7** and **Table 7-8**, also showing their respective abbreviations. The list is ordered by the incorporated metal. Besides the control experiment and those utilizing the commercially available POMs, the following metals, each with different degree of substitution, were incorporated: V, Co, Mn, Ni, Nb, In, and mixtures thereof.

Table 7-7: Overview of the utilized catalysts ordered by incorporated metal. Part I.

Category	Chemical formula	Abbreviation
Control	Blanc	
Commercial	$H_3PMo_{12}O_{40}$	HPMo-0
(no substitution)	$H_3PW_{12}O_{40}$	HPW-0
	$H_4SiW_{12}O_{40}$	HSiW-0
Vanadium	$H_4PV_1Mo_{11}O_{40}$	HPMo-V_1
	$H_5PV_2Mo_{10}O_{40}$	HPMo-V_2
	$H_6PV_3Mo_9O_{40}$	HPMo-V_3
	$H_7PV_4Mo_8O_{40}$	HPMo-V_4
	$H_8PV_5Mo_7O_{40}$	HPMo-V_5
Cobalt	$H_7PCo_1Mo_{11}O_{40}$	HPMo-Co_1
	$H_{11}PCo_2Mo_{10}O_{40}$	HPMo-Co_2
	$H_{15}PCo_3Mo_9O_{40}$	HPMo-Co_3
	$Na_7PCo_1Mo_{11}O_{40}$	NaPMo-Co_1
	$Na_{15}PCo_3W_9O_{40}$	NaPW-Co_3

The mass for all catalysts was fixed to 200 mg, even though this could result in varying molar amounts of each POM. This was done as the catalyst does not have clearly defined active sites which could change with varying metals incorporated and with degree of incorporation. Additionally, the Brønsted acidity strongly varies depending on incorporated metals. Thus, a fixed mass was applied to eventually allow considerations of mass-based productivity.

To further understand the abbreviations for each POM catalyst, **Scheme 7-2** can be utilized. The abbreviation can be separated into four information digits. The first one showing the cation of the POM which typically can be H^+, K^+ or Na^+. The second digit shows the heteroatom in

the centre of the POM, either being P or Si. The third digit shows the fundamental framework metal, being either Mo or W. Lastly, the fourth digit shows which metal has been incorporated into the POM structure (and thus substituting a framework metal) and to what degree (how many metals have been incorporated).

Table 7-8: Overview of the utilized catalyst ordered by incorporated metal. Part II.

Category	Chemical formula	Abbreviation
Manganese	$H_7PMn_1Mo_{11}O_{40}$	HPMo-Mn_1
	$H_{11}PMn_2Mo_{10}O_{40}$	HPMo-Mn_2
Nickel	$H_7PNi_1Mo_{11}O_{40}$	HPMo-Ni_1
	$H_{11}PNi_2Mo_{10}O_{40}$	HPMo-Ni_2
	$H_{15}PNi_3Mo_9O_{40}$	HPMo-Ni_3
Niobium	$Na_6PNb_3Mo_9O_{40}$	NaPMo-Nb_3
Indium	$H_{15}PIn_4Mo_8O_{40}$	HPMo-In_4
Bisubstituted	$H_8PV_1Mn_1Mo_{10}O_{40}$	HPMo-V_1Mn_1
	$H_{12}PV_1Mn_2Mo_9O_{40}$	HPMo-V_1Mn_2
	$H_{14}PV_3Mn_2Mo_7O_{40}$	HPMo-V_3Mn_2
	$H_{12}PV_5Mn_1Mo_6O_{40}$	HPMo-V_5Mn_1
	$H_{11}PNi_1Mn_1Mo_{10}O_{40}$	HPMo-Ni_1Mn_1
	$H_{11}PNi_1Co_1Mo_{10}O_{40}$	HPMo-Ni_1Co_1

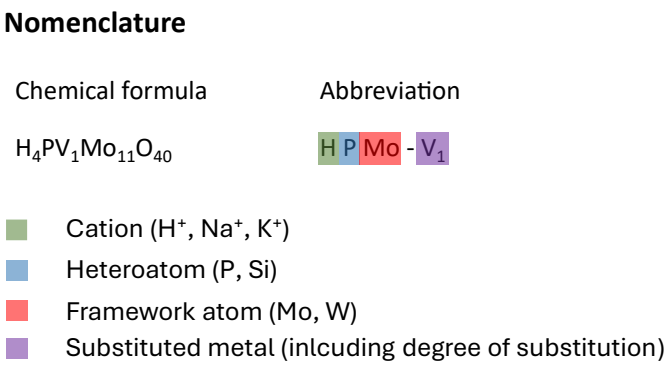

Scheme 7-2: Explanation of the nomenclature for the POMs utilized in this section.

Results of yields and carbon balance:

In **Figure 7-8**, the yields of the desired monoaromatic compounds and in **Figure 7-9**, the carbon balances for each phase are shown for the catalyst screening.

The results are similarly ordered as in **Table 7-7** and **Table 7-8**. Overall, the yields significantly vary between approx. 2 and 8 wt.-%, while the carbon balance is more uniform with a few outliers having increased carbon content in the solid phase. This overall trend indicates that the depolymerisation of lignin towards monoaromatic compounds works for all tested POM catalysts in principle.

Looking at the control experiment (Blank), it is shown that the oxidative depolymerisation is possible without a catalyst, however, resulting in the lowest yields. The formation of Va and Sy, thus, is possible simply by the thermal solvolysis and the presence of oxygen. The subsequent oxidation and esterification towards MeVa and MeSy also occur, however, at significantly lower ester concentrations compared to the previous reference experiments. This is probably due to the oxidation of Va and Sy being less likely in the absence of a POM, and due to the absence of free protons preventing the acidic catalysed esterification of the carboxylic acid derivatives.

In contrast to this control experiment the addition of the commercially available, unsubstituted POM catalysts (HPMo-0, HPW-0 and HSiW-0) results in a similar yield for Va and Sy, however, in a significantly higher yield of MeVa and MeSy approx. doubling the overall yield of monoaromatic compounds. This increase of methyl ester concentration is a consequence of the higher Brønsted acidity induced by the POM catalysts. Comparing these three catalysts with each other, both tungsten-based POMs show similar yields to each other but reduced yields of MeVa and MeSy compared to the molybdenum-based POM. Further, the carbon content in the solid residual phase almost linearly increases from HPMo-0 to HPW-0 and HSiW-0, as shown in **Figure 7-9**. This trend is similar to the Brønsted acidity induced by these catalysts which should similarly increase in the order listed. As tungsten is larger than molybdenum, and silicon is larger than phosphorous (according to the periodic table), the size of the POM structure should increase from HPM-0 to HSiW-0 increasing delocalization of polarity, the potential of dissociation and thus the Brønsted acidity. This suggested higher Brønsted acidity could result in an increased formation of instable intermediates and subsequently to recondensation forming insoluble pseudo-lignin, as previously described. The key insight of these two observations is that a minimum of Brønsted acidity is necessary for the formation of the aromatic methyl esters. On the other hand, excessive Brønsted acidity likely results in the formation of undesirable

pseudo-lignin. Because of this, specifically molybdenum-based POMs (with one exception) were considered for the remaining catalyst screening experiments.

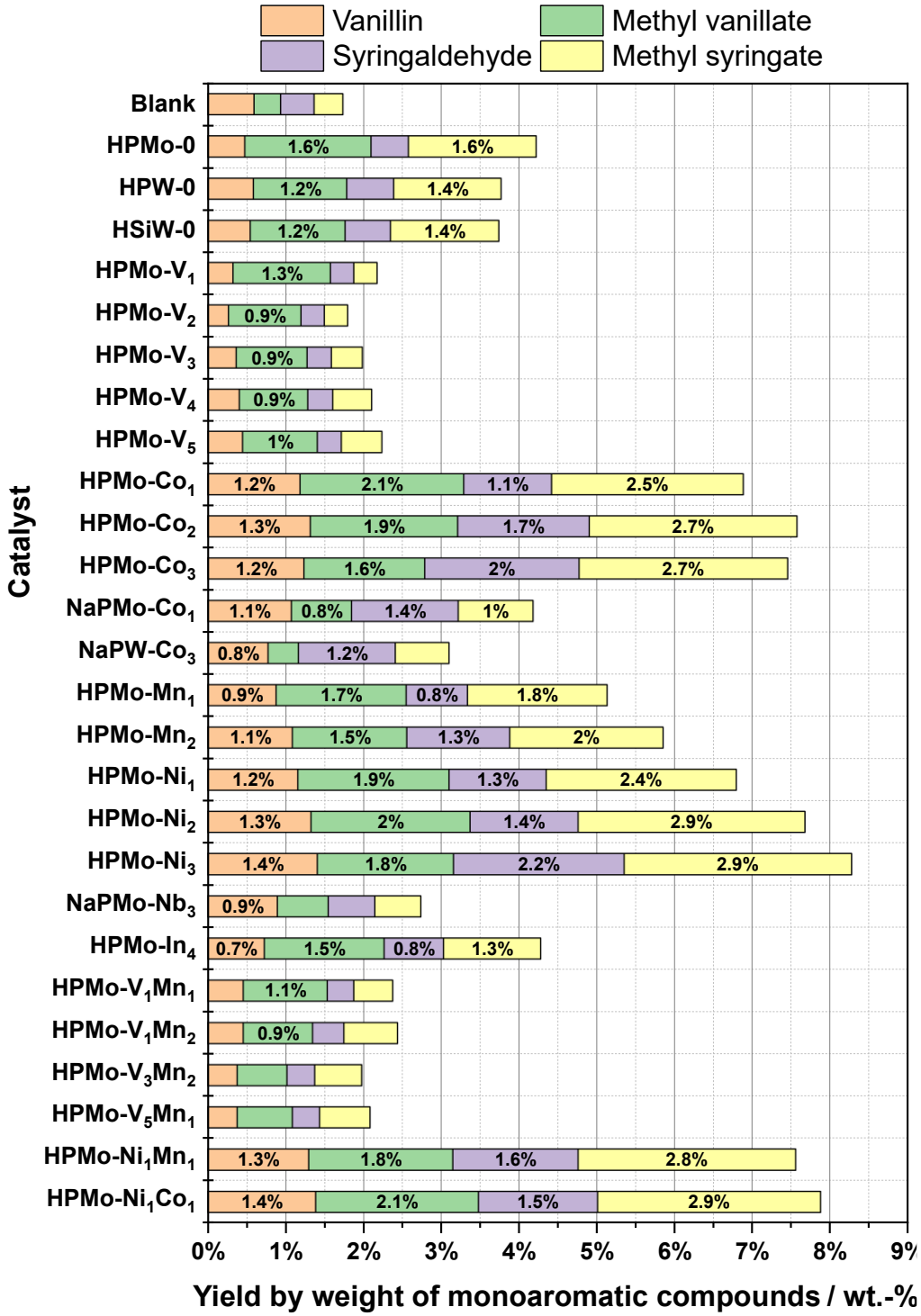

Figure 7-8: Yield by weight of the desired monoaromatic compounds for the catalyst system screening carried out in Setup 1. Reaction conditions were 140 °C, 20 bar oxygen partial pressure, 24 h, 0 rpm, 10 mL solvent (MeOH/H_2O 95:5 v/v), 500 mg substrate (organosolv hardwood lignin S4), 200 mg catalyst.

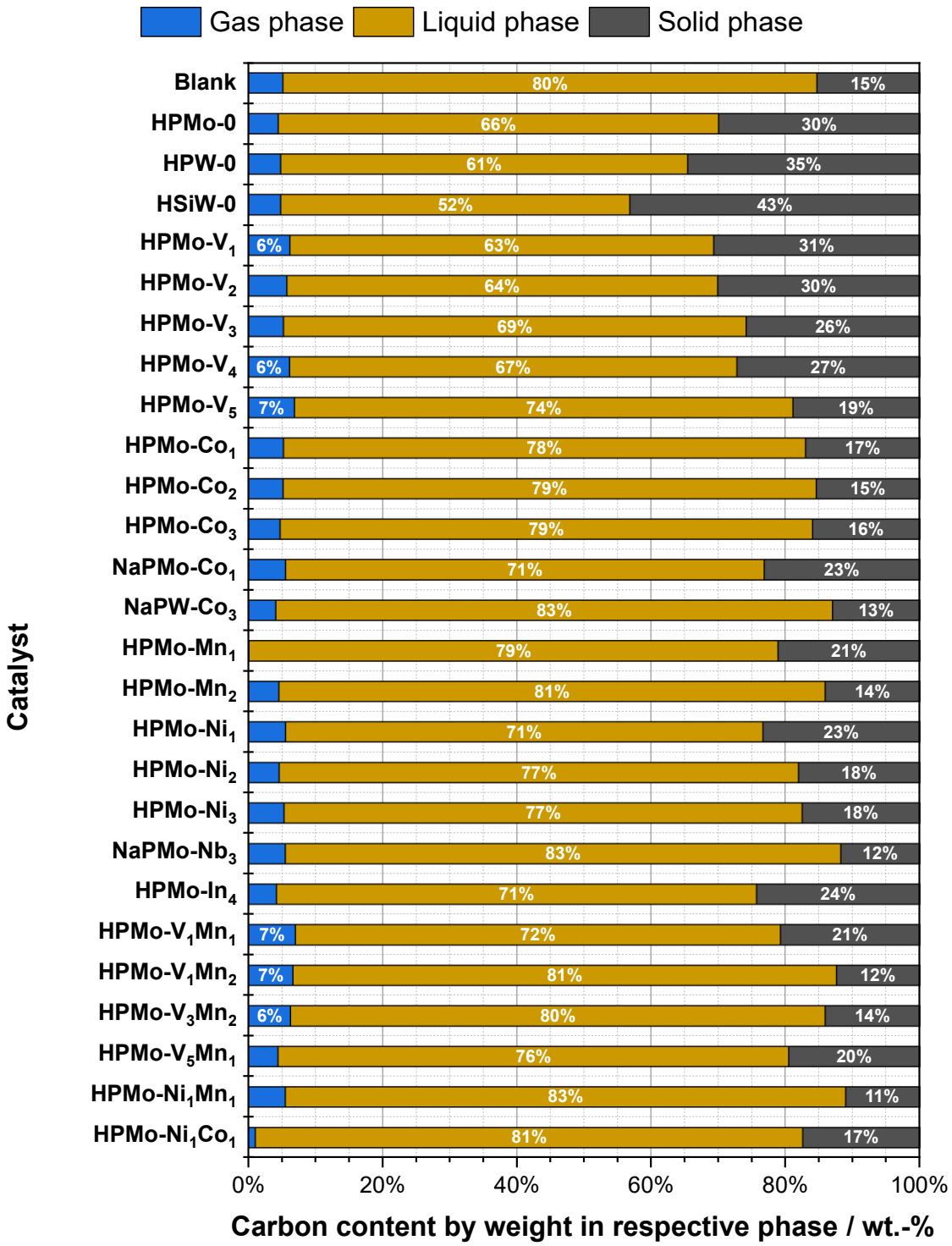

Figure 7-9: Carbon balance by weight and phase for the catalyst system screening carried out in Setup 1. Reaction conditions were 140 °C, 20 bar oxygen partial pressure, 24 h, 0 rpm, 10 mL solvent (MeOH/H_2O 95:5 v/v), 500 mg substrate (organosolv hardwood lignin S4), 200 mg catalyst.

The next group is that of the vanadium-substituted POMs. The aromatic yields are significantly lower than for the commercial POMs, and rather similar to that of the control experiment, although the product distribution is shifted. The predominant aromatic product is MeVa, while

Va, Sy and MeSy are similarly low. Within this group, all catalysts performed comparably considering the aromatic yields and the carbon content in the solid phase shows a slight decreasing trend with increasing vanadium substitution. A potential reason for these observations could be the high RedOx activity of the vanadium species leading to a further degradation of the target aromatic monomers and of the compounds formed by recondensation, which occurs at highly acidic environments as suggested by *Shinde* et al. [201]

Next is the group of cobalt-substituted POMs. Besides the molybdenum-based Brønsted acidic POMs, two additional with sodium as a counter-ion were tested, one of which also is a tungsten-based POM. With respect to the carbon balance, most of these cobalt-based catalysts achieve low carbon contents in the solid phase when compared to the previous catalysts. With one exception all catalysts result in carbon content in solid phase between 13 and 17 wt.-% (the exception being the NaPMo-Co_1 catalyst which results in a higher carbon content of 23 wt.-%). Thus, these cobalt-based POM catalysts achieve comparably lower carbon contents in the solid phase than all the previous catalysts which is a key benefit. Additionally, the Brønsted acidic molybdenum-based cobalt-POMs achieve significantly higher yields of the desired monoaromatic compounds ranging between 7 and 7.5 wt.-%. The two sodium salts result in significantly lower yields of MeVa and MeSy, again confirming the necessity of free protons for this esterification. Additionally, the yields of Sy and MeSy are substantially higher for the Brønsted acidic cobalt-POMs when compared to the previous catalysts. This might be an indication for a milder depolymerisation when utilizing cobalt-POMs for the following reason. As beech wood is a hardwood which generally shows higher amounts of syringyl units (as described in section **4.2.1**), the yields of Sy and/or MeSy should generally be higher than those of Va and MeVa. This was not applicable for the previous catalysts, indicating an increased degradation potential for compounds originating from syringyl units. This aspect is changed when using these cobalt-POMs, hence, indicating a less severe depolymerisation activity. This again is a key benefit for the formation of the targeted monoaromatics.

The manganese-POMs achieve similar results for the carbon balance but decreased monoaromatic yields between 6 and 7 wt.-% when compared to the cobalt-POMs. Both the niobium- and indium-POMs achieve even lower yields.
The nickel-POMs act similar as the cobalt-POMs achieving considerable monoaromatic yields with 7, 7.5 and 8 wt.-%, respectively for HPMo-Ni_1, HPMo-Ni_2 and HPMo-Ni_3. Thus, the

HPMo-Ni3 achieves the highest yields, so far, while showing similar characteristics as the cobalt-POMs.

Lastly, bi-substituted POMs are considered. As the incorporation of manganese results in a boost of the yield, the combination with vanadium might be of interest as vanadium shows high applicability for the oxidative depolymerisation of lignocellulosic biomass, as shown by *Albert* et al. [139]. However, the combination does not achieve the expected benefit, still resulting in low yields between 2 and 2.5 wt.-%. Next, the combination of nickel with each cobalt and manganese is considered since all of these metals result in a significant increase of monoaromatic yield. The addition of either manganese or cobalt does increase the yield of the one-fold substituted HPMo-Ni_1. However, the yields are not higher than that of the two-fold substituted HPMo-Ni_2, but rather similar. Thus, the combination of these transition metals does not lead to an additional beneficial effect and further bi-metallic incorporation is not considered. In summary, this catalyst screening extended the understanding of the applied depolymerisation and lead to an improvement of product yield from approx. 2 to 8 wt.-% when utilizing the HPMo-Ni_3 catalyst.

Discussion about catalyst functionalities:

In **Table 7-9** the pH values of the reaction media (solvent and catalyst) are shown before and after reaction for selected catalysts (HPMo-0, HPMo-V_2, HPMo-V_5, HPMo-Mn_2, HPMo-Co_2, and HPMo-Ni_2). For a better visualization, the reaction media before the reaction, excluding any biomass, are shown in **Figure 7-10**. While the pH values of the reaction media after the reaction are consistent between 1.50 and 1.75, the values significantly differ prior to reaction. The commercial HPMo-0 and both V-substituted HPMo catalysts result in pH values between 1.13 and 1.22. The pH then increased during reaction indicating both the dilution by reaction water formed by esterification, and the formation of less Brønsted acidic carboxylic acids. On the other hand, the POMs substituted with Mn, Co or Ni show significantly higher pH values before reaction ranging between 4.28 and 4.58. Thus, these POMs show lower acidity and dissociation compared to the other POMs. This could be a key advantage as described above due to excessive depolymerisation and repolymerisation being prevented. Besides that, the pH values decrease during reaction either confirming the above-mentioned formation of carboxylic acids or being caused by the degradation of the Mn-/Co-/Ni-POM towards other POM species with a higher Brønsted acidity. No clear evidence for the POM degradation was found, while compounds such as formic or acetic acid were found in GC-MS analysis.

Table 7-9: pH values of the reaction media before and after reaction for selected catalysts with reference to the appearance of the reaction media before reaction in **Figure 7-10**.

Catalyst	Corresponding number in Figure 7-10	pH value	
		Before reaction	After reaction
HPMo-0	1	1.13	1.50
HPMo-V_2	2	1.17	1.71
HPMo-V_5	3	1.22	1.75
HPMo-Mn_2	4	4.58	1.75
HPMo-Co_2	5	4.36	1.65
HPMo-Ni_2	6	4.28	1.56

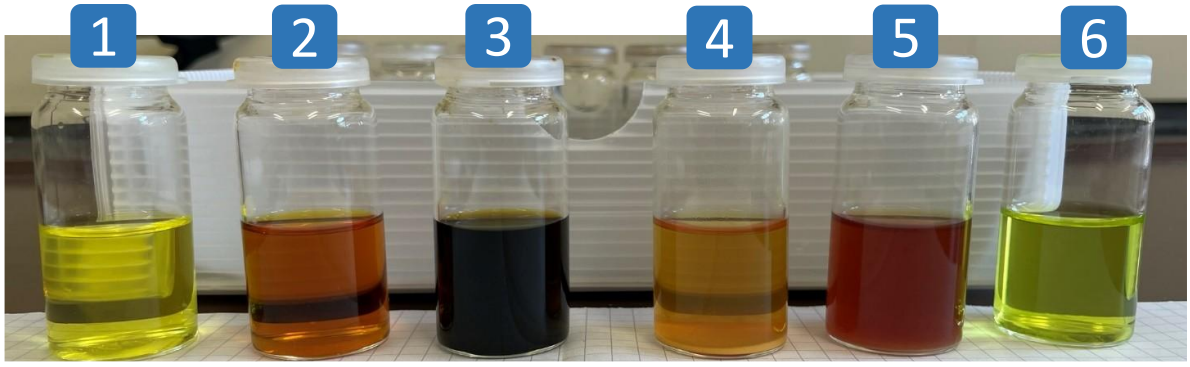

Figure 7-10: Depiction of reaction media before reaction for the selected catalysts HPMo-0 (1), HPMo-V_2 (2), HPMo-V_5 (3), HPMo-Mn_2 (4), HPMo-Co_2 (5), and HPMo-Ni_2 (6) prior to biomass addition. The numbers correspond to the pH values described in **Table 7-9**.

Besides their investigated Brønsted acidity and oxidation capability, there might be a third functionality specifically for the POMs showing an amount of hydrogen atoms in their formula higher than 12. For clarity, the structure of a Keggin POM is depicted in **Figure 7-11** showing the terminal oxygen atoms from 1 to 12.

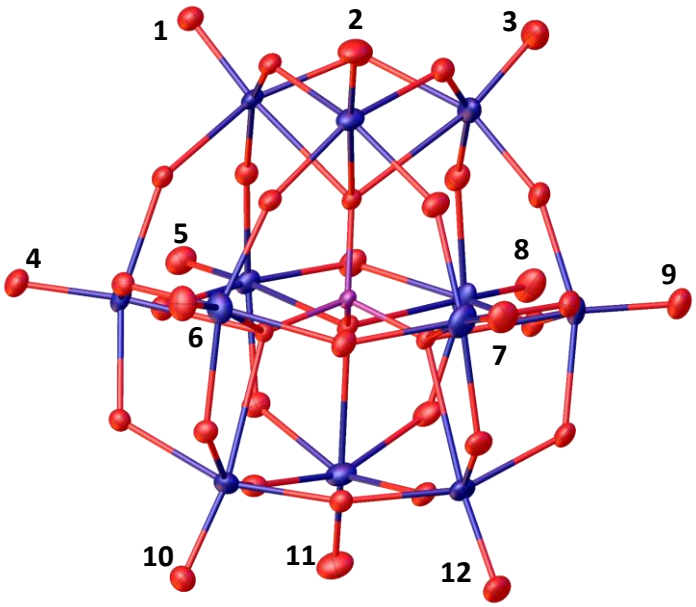

Figure 7-11: Illustration of the structure of a Keggin polyoxometalate showing the central heteroatom in purple, the framework metal atoms in blue and the oxygen atoms in red. All terminal oxygen atoms are numbered from 1 to 12. Adapted from [146].

The Keggin POM structure contains twelve terminal oxygen atoms, each capable of forming a bond with a cation to balance the negative charge of the POM. This implies that a maximum of twelve cations can be coordinated to the structure. However, in the cases of HPMo-Ni_3 or HPMo-Co_3, the anion cluster exhibits a negative charge of -15, necessitating the binding of fifteen cations to neutralize the charge – three more than the available terminal oxygen atoms. A plausible solution to this discrepancy is the binding of two cations (specifically protons) to a single terminal oxygen, forming an oxonium group ($–OH_2$) that can release water (H_2O) upon dissolution in aqueous solutions. This process creates a vacancy at the metal centre within the framework. This could then function as a Lewis acid. In addition to their oxidative properties and Brønsted acidity, this mechanism would introduce a third functionality to the POM, establishing it as a trifunctional catalyst.

Optimization of solvent:

Throughout the catalyst screening, the highest yields of the desired monoaromatics were achieved with the HPMo-Ni_3 catalyst. As the previous solvent optimization was not conducted using this catalyst, this step was now repeated. The overall solvent, being a methanol-water-mixture, and all other parameters remained unchanged, but the solvent volume ratios were altered. The yields of monoaromatics and the carbon balance of this solvent optimization is shown in **Figure 7-12** and **Figure 7-13**, respectively.

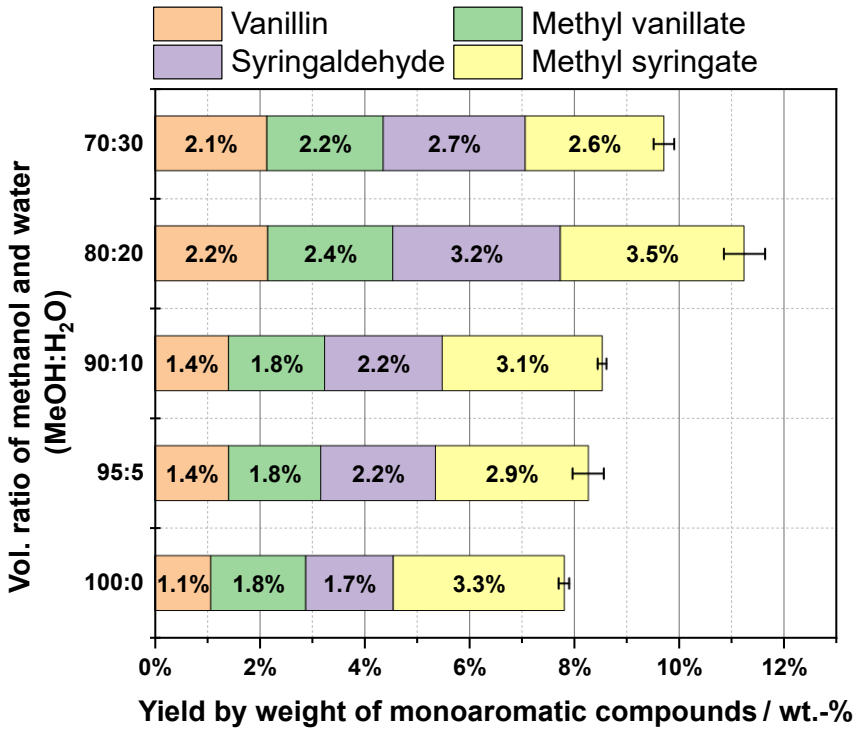

Figure 7-12: Yield by weight of the desired monoaromatic compounds for the optimization of solvent for the selected POM catalyst HPMo-Ni_3 in Setup 1. Reaction conditions were 140 °C, 20 bar oxygen partial pressure, 24 h, 0 rpm, 10 mL solvent, 500 mg substrate (organosolv hardwood lignin S4), 200 mg catalyst (HPMo-Ni_3).

Unlike the reference catalyst HPMo-V_5, pure methanol achieves the lowest yields of monoaromatics for the considered solvent ratios. The yields increased with increasing water fraction until a MeOH:H_2O ratio of 8:2 (v/v) was reached achieving the so far highest yields of approx. 11 wt.-%. Further increasing the water ratio, on the other hand, reduced the yield.

Looking at the carbon balance, two things stand out. First, with increasing water ratio the carbon content in the gas phase was also increasing. Second, this also applied to the carbon content in the solid phase. As both contents increased, a suitable explanation would be a reduction of catalyst selectivity, and thus an increase of catalyst activity, resulting in the formation of CO_2, CO and insoluble pseudo-lignin. Additionally, due to the increased water content more lignin compounds become insoluble, further increasing the contents in the solid phase.

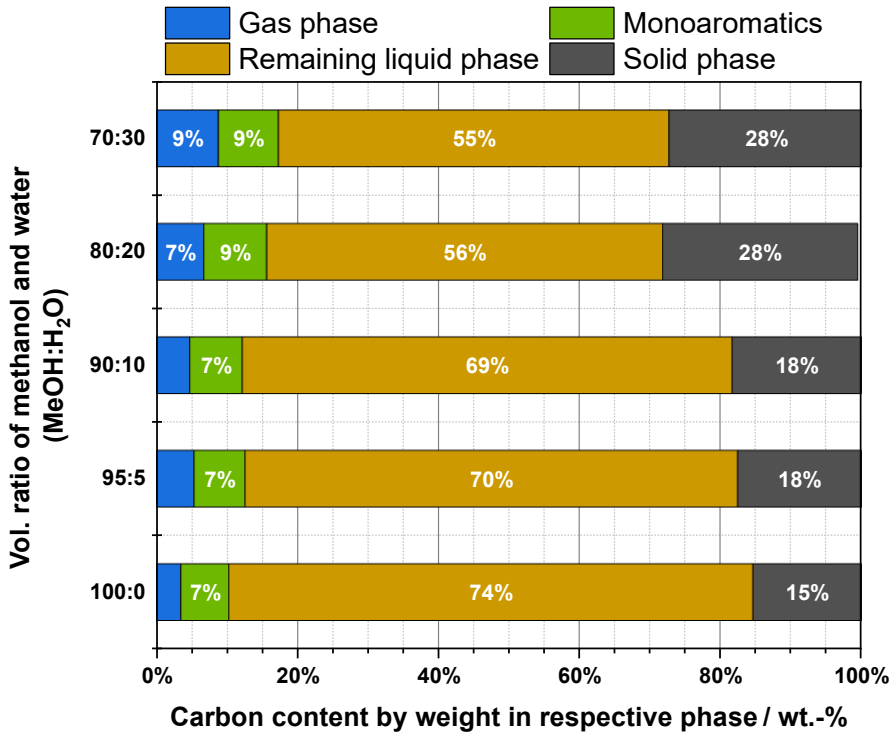

Figure 7-13: Carbon balance by weight and phase for the optimization of the solvent for the selected POM catalyst HPMo-Ni_3 in Setup 1. Reaction conditions were 140 °C, 20 bar oxygen partial pressure, 24 h, 0 rpm, 10 mL solvent, 500 mg substrate (organosolv hardwood lignin S4), 200 mg catalyst (HPMo-Ni_3).

In summary, 26 POM catalysts were examined throughout this section and the HPMo-Ni_3 catalyst was selected for further investigations as it achieved the so far highest monoaromatic yields of up to 8 wt.-% with an unchanged solvent. The effect of the pH value on lignin depolymerisation, as well as a potential third catalyst functionality was described. Lastly, the optimization of the solvent was repeated for the newly selected catalyst. At a methanol-water ratio of 8:2 (v/v), the so far highest monoaromatic yields of approx. 11 wt.-% were achieved. At this point, the chemical system for the lignin depolymerisation was set and more reaction engineering-oriented parameters had to be observed. First, the influence of reaction time was considered in the next section.

7.2.5 Influence of reaction time (Setup 1)

For the optimization of reaction-engineering parameters, which will be applied for the implementation in a continuous process, it is important to have sufficient lignin substrate available in order to compare results to the corresponding batch reactions. The so far utilized substrate (S4) was not sufficiently available for all consecutive process development stages. For this reason, an additional substrate selection was conducted for organosolv lignins. The

results are attached to the appendix in **Figure B-28**. Here, the influence of the substrate's origin was clearly observable as the monoaromatic yields decrease from approx. 11 wt.-% for S4 to just approx. 5 wt.-% for S1 with the second highest yield. Nonetheless, substrate S1 (organosolv softwood lignin) was selected for the remaining process development due to being sufficiently available.

The reaction conditions for the investigation on reaction time are summarized in **Table 7-10**. The time considered lied between 2 and 24 hours and each reaction time corresponds to an individual experiment and reactor. All other parameters were according to previous experiments.

Table 7-10: Overview of reaction parameters for the investigation on reaction time influence. Experiments were conducted in Setup 1.

Reaction parameter	Parameter value	Details
Time	2-24 h	
Partial pressure at T_R	20 bar	Oxygen
Temperature	140 °C	
Substrate (mass)	500 mg	S1 – Organosolv softwood
Catalyst (mass)	200 mg	HPMo-Ni_3
Solvent volume	10 mL	Methanol/Water (8:2 v/v)

The yields obtained throughout this reaction time screening are shown in **Figure 7-14**. Overall, the yields started low at around 2.2 wt.-% between 2 and 4 hours reaction time, ramping up until 20 hours reaching approx. 6 wt.-% yield and by then becoming more asymptotic approximating around 6 wt.-% yield. This course was equivalent to classical equilibrium-limited batch reaction.

In terms of monoaromatic distribution, there were some shifts observable depending on reaction time. In the beginning approx. 75 % of the formed desired monoaromatics was syringaldehyde. Throughout increasing reaction time, the absolute concentration of syringaldehyde stayed constant, while the concentrations of vanillin, methyl vanillate and methyl syringate constantly increase. This indicates that the reaction rate of the formation of syringaldehyde was equal to the degradation rate. The concentration of vanillin also stagnated, however, only after 14 hours, again indicating equal speed of formation and degradation. Lastly the methyl esters appeared

to be slowly but continuously increasing in concentration, implying no degradation but stability of said compounds.

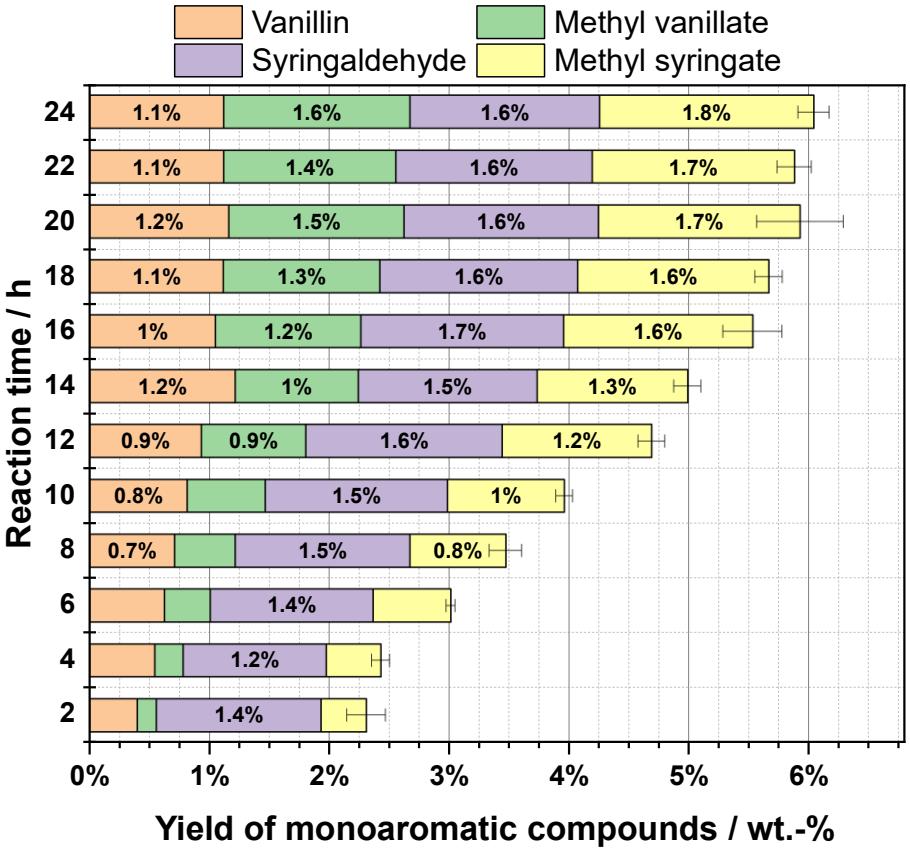

Figure 7-14: Yield by weight of the desired monoaromatic compounds for the investigation of reaction time influence in Setup 1. Reaction conditions were 140 °C, 20 bar oxygen partial pressure, 2-24 h, 0 rpm, 10 mL solvent (8:2 v/v MeOH:H_2O), 500 mg substrate (organosolv softwood lignin S1), 200 mg catalyst HPMo-Ni_3.

The slow concentration increased of the methyl esters supports the previous hypothesis of their subsequent formation starting from vanillin and syringaldehyde, respectively, as suggested by **Scheme 7-1**. Additionally, it was shown that syringaldehyde not only was degraded towards syringic acid but also to vanillin and subsequently methyl vanillate in a separate experiment. By exposing pure syringaldehyde to standard reaction conditions at reduced reaction times (<6 h). The main product was MeSy (skipping the acid through immediate esterification) but also significant concentrations of Va and MeVa were present as shown in the appendix in **Figure B-29**.

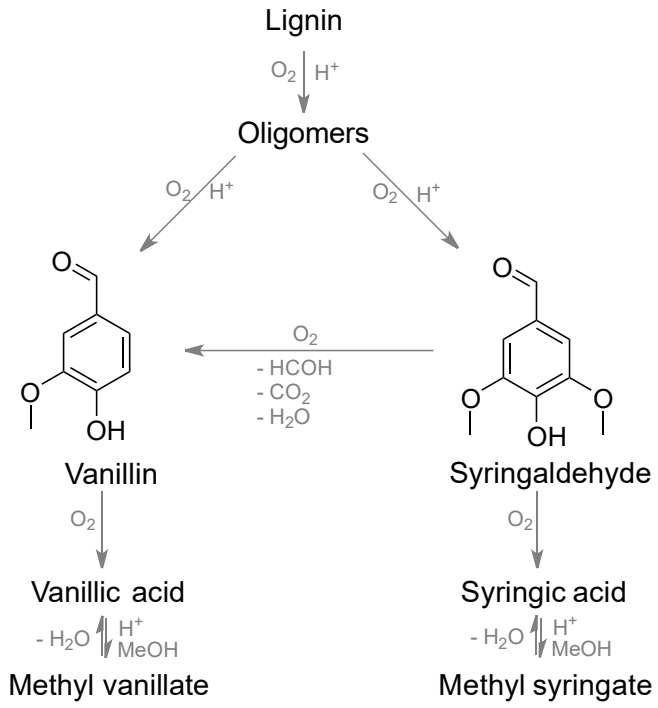

Scheme 7-3: Updated proposed reaction network describing the formation of all four monoaromatic products originating from the lignin substrate including the formation of vanillin from syringaldehyde.

This reaction step might be induced by oxidation of one of the methoxy groups towards either formaldehyde at mild oxidation conditions or even towards carbon dioxide at harsher conditions, as shown in the updated reaction network in **Scheme 7-3**. This additional reaction pathway forming vanillin would mean a potentially significant amount of formaldehyde was formed. Due to the harsh oxidative conditions present during reaction, the further oxidation of said formaldehyde to formic acid is likely. Equally, the subsequent esterification with the solvent methanol, forming methyl formate is likely. This and several other short-chained methyl ester compounds were detected in a separate GC-column throughout this reaction time screening and, as a result, quantified. The results of all quantified compounds are shown in **Figure 7-15**. As can be seen, the yields of both CO & CO_2 and methyl formate (MF) equally increased with reaction time as the yield of monoaromatics. Due to the reduced carbon content in these side products, the molar amount exceeded that of the monoaromatics substantially. This likely means that these side products were not only formed by the oxidation of one of syringaldehyde's methoxy groups, but also during the depolymerisation process. This explains the presence of both side products at 2 hours reaction time. The question arises if the reaction conditions in combination with the catalyst can oxidize formic acid or methyl formate to CO_2, as well. Studies of *Maerten* et al. [202] have shown this does not occur in solvent systems majorly containing methanol, allowing for a selective formation of formic acid derivatives if desired. Still, the formation of CO & CO2 is significant and most likely occurring during depolymerisation where crosslinking ether bonds are cleaved.

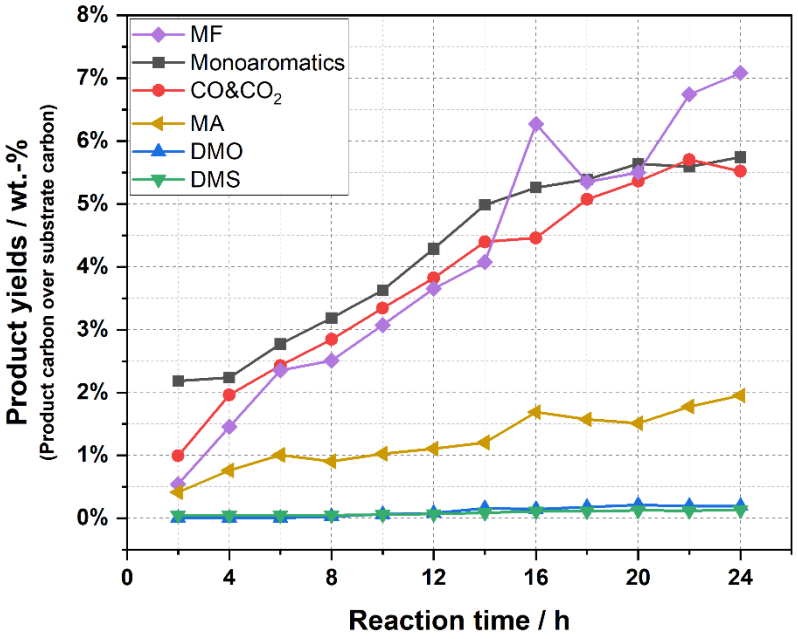

Figure 7-15: Yields for all quantified gas phase and liquid phase products, being MF (methyl formate), the sum of all monoaromatics, CO and CO_2, MA (methyl acetate), DMO (dimethyl oxalate) and DMS (dimethyl succinate), plotted over reaction time. Reaction conditions were 140 °C, 20 bar oxygen partial pressure, 2-24 h, 0 rpm, 10 mL solvent (8:2 v/v MeOH:H_2O), 500 mg substrate (organosolv softwood lignin S1), 200 mg catalyst HPMo-Ni_3.

Additionally, methyl acetate (MA) was found, however, at reduced concentrations compared to methyl formate. Due to lignin consisting of phenylpropanoid units, the formation of C2 components through cleavage of propanoid units is to be expected. Lastly, both dimethyl succinate and dimethyl oxalate were found after 14 hours, although their concentration remained negligible. While the oxalate can again be formed by cleavage of propanoid units, the succinate requires a different explanation as it consists of four carbon atoms at its basis. Two approaches come to mind. First, a propanoid unit could be cleaved leading to a radical which reacts with another propanoid unit leading to carbon chain lengths higher than C3. As the solvent methanol shall act as a radical acceptor and due to the surplus of methanol, this first approach is unlikely. The second approach comprises the degradation of a benzene ring leading to a maximum possible chain length of C9 (C6 for benzene, plus C3 for the propanoid unit). While this could explain the presence of ≥C4 alkyl units, there is no clear evidence of this benzene degradation as no other alkyl components with chains lengths of ≥C4, besides the succinate, were found. A clear reaction pathway for the formation of succinates, therefore, could not be suggested.

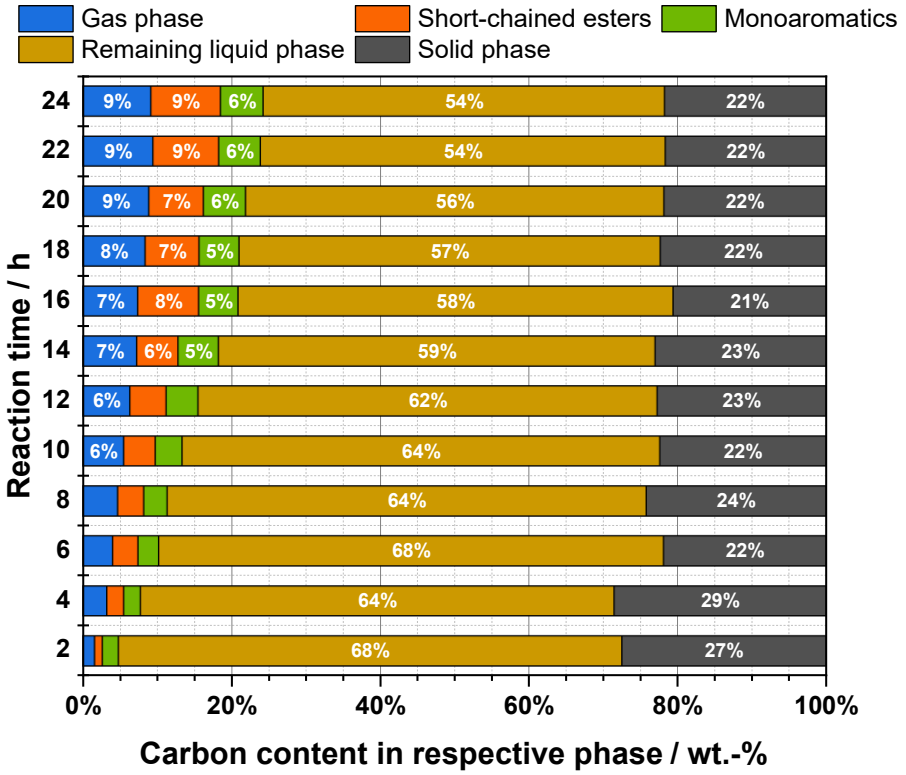

Figure 7-16: Carbon balance by phase for the investigation on reaction time influence in Setup 1. Reaction conditions were 140 °C, 20 bar oxygen partial pressure, 2-24 h, 0 rpm, 10 mL solvent (8:2 v/v MeOH:H_2O), 500 mg substrate (organosolv softwood lignin S1), 200 mg catalyst (HPMo-Ni_3).

In **Figure 7-16** the carbon balance of the reaction time screening is shown including the quantification of short-chained methyl esters. Here, especially the remaining liquid phase and the solid phase are of interest. During the first couple of hours, the carbon content in the liquid phase decreased indicating the solubilization requiring 4 to 6 hours. However, with longer reaction times, the solid carbon contents remained rather constant. As the compositional analysis showed negligible amounts of acid soluble lignin, it is suggested that at least a portion of this remaining solid carbon is pseudo-lignin formed by repolymerisation. The amount of solid carbon then remained constant if depolymerisation and repolymerisation occur to the same degree.

On the other hand, the carbon in the remaining liquid phase slowly but steadily decreased with reaction time while a large portion of the substrate's carbon was rapidly solubilized within the first 2 hours. The solubilization and the depolymerisation towards monomeric compounds, thus, appeared to be two separatable processes. This concept of pre-solubilizing was already proposed by *Du* et al. [203] and was also considered in preparation for the continuous process.

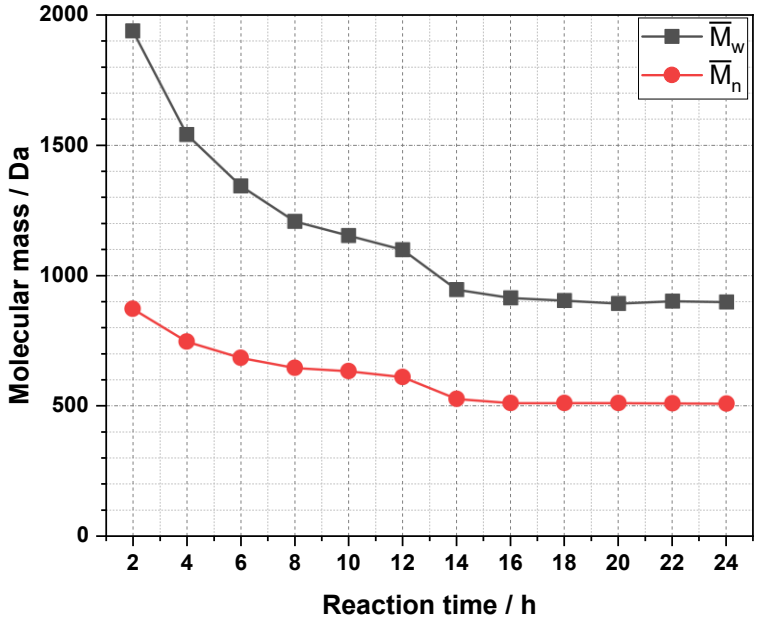

Figure 7-17: Course of average molecular mass over reaction time measured by GPC for the reaction solutions obtained at following reaction conditions: 140 °C, 20 bar oxygen partial pressure, 2-24 h, 0 rpm, 10 mL solvent (8:2 v/v MeOH:H_2O), 500 mg substrate (organosolv softwood lignin S1), 200 mg catalyst HPMo-Ni_3.

Further, the reaction solutions were measured by GPC analysis and the results of the average molecular weight are shown in **Figure 7-17**. The value of the original substrate is here not included because the molecular weight distribution of the substrates was originally measured with an alkaline method whereas the reaction product samples were measured with THF as eluent. Additionally, the substrate was not measured in THF as it was not entirely soluble.

As can be seen, the mass average molecular weight started quite high at approx. 2,000 Da, while the number average molecular weight only started at approx. 900 Da. This shows that there was a significant amount of lower molecular weight compounds while there are a few significantly heavy compounds present at the reaction start, displaying an inhomogeneous depolymerisation. The two average molecular weights approximate with increasing reaction time showing that the described heavy compounds are more likely to be depolymerised than the lighter compounds. At 16 hours reaction time, the molecular weight distributions became stagnant. This indicates a decrease of excessive depolymerisation perhaps due to activation energy being too high compared to cleaving monomeric compounds, or the reaction rate of depolymerisation and repolymerisation being equal, as proposed earlier. Nonetheless, the overall average molecular weight in the liquid phase remained rather high at 900 and 500 for M_w and M_n, respectively. The number of oligomers in liquid phase, thus, was still significant but beyond 16 hours reaction time, it did not change. Additionally, the molecular weight distribution is shown in the appendix in **Figure B-30**.

In summary, a few discoveries have been made throughout this section. (1) It was discovered that vanillin was formed from syringaldehyde by elimination of a methoxy group, which likely is converted to CO_2 or formaldehyde and consequently to formic acid and methyl formate. (2) Indeed, several short-chained ester compounds, such as methyl formate, were detected and quantified. With increasing reaction time, especially methyl formate and methyl acetate significantly increased in concentration, and methyl formate even reached higher yields by weight than the sum of the desired monoaromatics. Hence, the reaction time was reduced to 16 hours to limit this formation of byproducts. (3) The analysis of molecular weight showed that even at a reaction time of 24 hours, the weight-average molecular weight with $900\,\frac{g}{mol}$ is still significantly higher than that of the desired monoaromatics. This again put emphasize on the large quantity of oligomeric fraction, which potentially could be converted to the desired monoaromatics. However, the concentration of monoaromatics started to stagnate around 24 hours. For this reason, the so-called just-in-time product separation is required so that the monoaromatics are not further degraded once formed.
Next, the influence of the oxygen partial pressure was investigated.

7.2.6 Influence of oxygen partial pressure (Setup 1)

The oxygen partial pressure directly influences the desired oxidative depolymerisation. As described by *Henry's* law, the partial pressure of a gas over a liquid phase proportionally determines the amount of said gas dissolved in the liquid phase. [204] Thus, increasing the oxygen partial pressure also increases the amount of oxygen dissolved in the methanol-water solvent. As oxygen is participating in the reaction as a reactant, its concentration directly influences the kinetics of the reaction. For this reason, the influence of oxygen partial pressure on the depolymerisation was also considered in this section.
So far, the oxygen partial pressure at reaction temperature was kept at 20 bar corresponding to an initial oxygen partial pressure at standard conditions of 14 bar which was typically applied prior to temperature increase. In this context, two additional initial partial pressures, 5 and 27.5 bar, were considered to observe the influence on both monoaromatic yield and carbon balance. The remaining reaction conditions were at standard values and summarized in **Table 7-11**.

Table 7-11: Overview of reaction parameters for the investigation on influence of oxygen partial pressure. Experiments were conducted in Setup 1.

Reaction parameter	Parameter value	Details
Time	24 h	
Initial partial pressure at standard conditions	5, 14, 27.5 bar	Oxygen (for 5 bar oxygen, 9 bar of nitrogen were added)
Temperature	140 °C	
Substrate (mass)	500 mg	S1 – Organosolv softwood
Catalyst (mass)	200 mg	HPMo-Ni_3
Solvent volume	10 mL	Methanol/Water (8:2 v/v)

The results of the monoaromatic yields and carbon balance are depicted in **Figure 7-18** and **Figure 7-19**, respectively. For the yields, at 5 bar initial oxygen partial pressure the sum of monoaromatics was reduced by approx. 0.75 % compared to the reference at 14 bar, while the even higher pressure of 27.5 bar did not show any deviation to the sum of monoaromatic yields. At 5 bar the main component was syringaldehyde while the vanillin-based compounds showed comparably reduced yields. This means that the availability of oxygen contained in the liquid phase had more influence on the formation of vanillin (and its derived product) than for syringaldehyde. This is again an indication for oxidation and elimination of syringaldehyde's methoxy group towards vanillin, as suggested by **Scheme 7-3**. This hypothesis was further supported by the results at 14 and 27.5 bar. Here, the increased oxygen partial pressure lead to decreased yields of syringaldehyde while enhancing the yields of all other three monoaromatics. At 27.5 bar even more so than for 14 bar. Additionally, the reduction of methyl syringate yield at 27.5 compared to 14 bar further hints that methyl syringate could also be oxidized towards methyl vanillate. To summarize the results of the yields, a minimum oxygen partial pressure was required to maximize the overall monoaromatic yield. Further increasing the partial pressure did not boost the overall yield but influenced the distribution of monoaromatics – at higher pressures it was in favour of vanillin and methyl vanillate while at lower pressures it is in favour of syringaldehyde and methyl syringate.

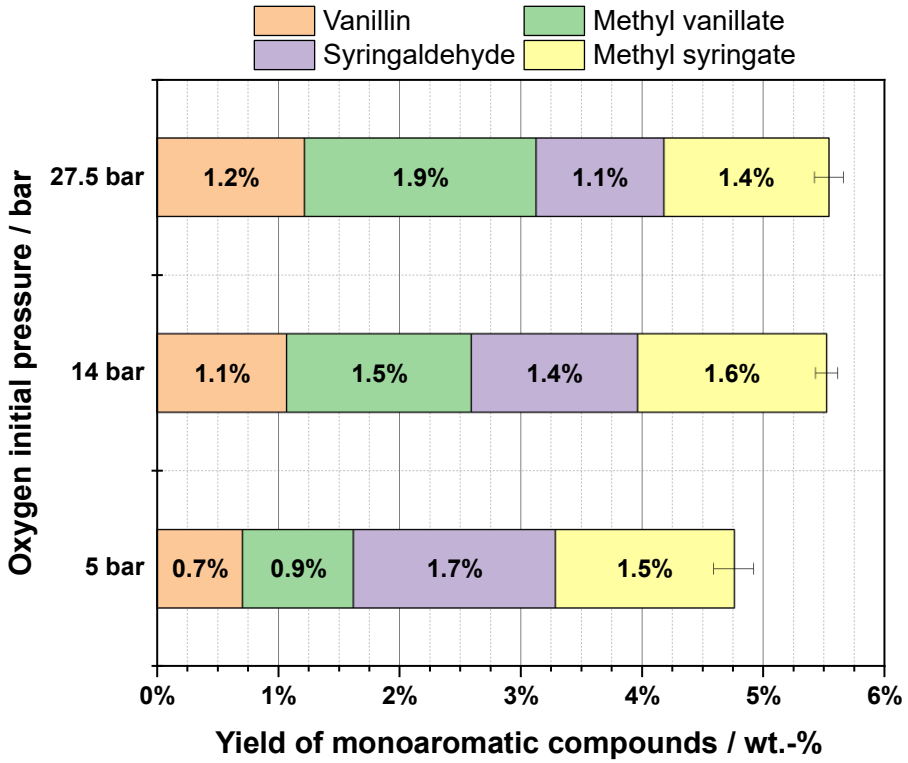

Figure 7-18: Yield by weight of the desired monoaromatic compounds for the investigation on oxygen partial pressure influence in Setup 1. Reaction conditions were 140 °C, 5/14/27.5 bar oxygen initial partial pressure, 24 h, 0 rpm, 10 mL solvent (8:2 v/v MeOH:H_2O), 500 mg substrate (organosolv softwood lignin S1), 200 mg catalyst HPMo-Ni_3.

For the carbon balance, similar effects were observable. At a reduced initial oxygen partial pressure of 5 bar the carbon content in the solid phase was significantly increased at 32 wt.-% compared to the typical 23 wt.-% at 14 bar. This indicates the necessity of oxygen for the lignin solubilization and depolymerisation. Further increasing the oxygen partial pressure also lead to further reduction of solid carbon content which is a beneficial effect and supports the previous observation. On the other hand, with increasing oxygen partial pressure the formation of CO & CO_2 naturally also increased which is undesirable as the gas phase carbon content, especially in CO & CO_2, can be seen as a loss of product yield.

For the decision of what initial oxygen partial pressure to use for the further process development, not only these scientific results but also technical/commercial aspects were considered. The gas phase of this process basically is off-gas which usually requires purification treatment before emitted into the atmosphere which increases both capital and operating expenditures (CAPEX & OPEX) of a perspective commercial plant. The increased amount of off-gas at higher oxygen pressure in combination with the increased consumption of oxygen

leading to even higher OPEX, leads to the conclusion to set the oxygen partial pressure to 14 bar for the remaining process development.

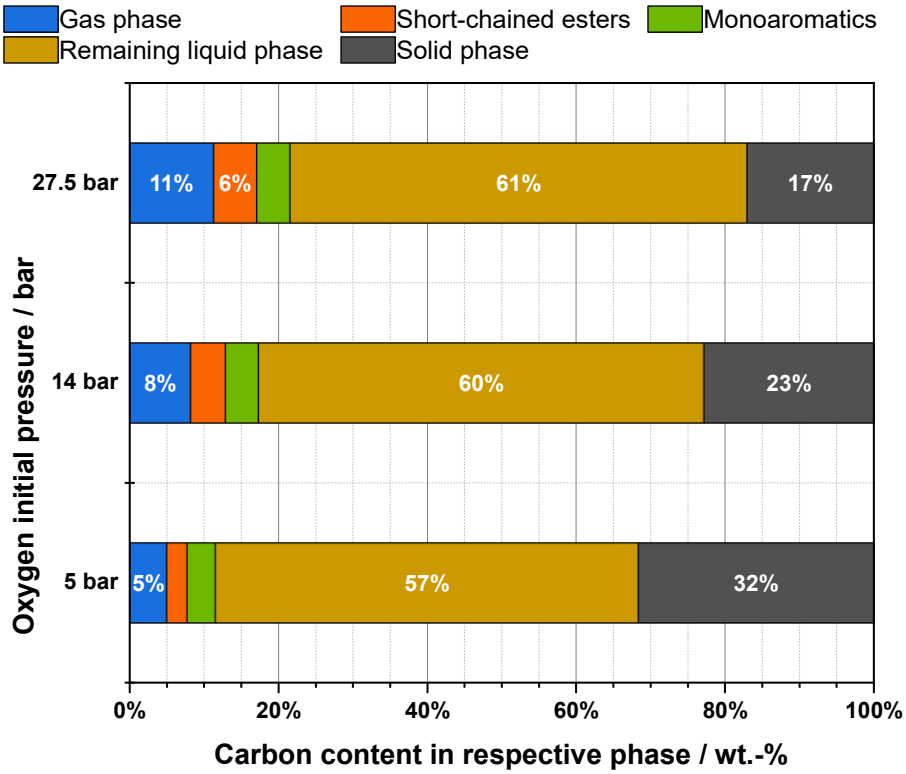

Figure 7-19: Carbon balance by phase for the investigation on oxygen partial pressure influence in Setup 1. Reaction conditions were 140 °C, 5/14/27.5 oxygen initial partial pressure, 24 h, 0 rpm, 10 mL solvent (8:2 v/v MeOH:H_2O), 500 mg substrate (organosolv softwood lignin S1), 200 mg catalyst HPMo-Ni_3.

Now, that both oxygen partial pressure and reaction time were set, the influence of up-scaling and process parameters as temperature, stirrer and catalyst loading was studied in the next sections utilizing Setup 2.

7.2.7 Influence of up-scaling (Setup 2)

In order to evaluate further process parameters and to diminish relative statistical error due to work up procedures, the influence of up-scaling shall be investigated within this section. So far, only Setup 1 was utilized within the sensitivity study of section **7.2** which consisted of 20 mL reactors. This reactor volume was now increased to a maximum of 100 mL in Setup 2 which consisted of three reactors containing *in-situ* temperature sensors and a gas-entraining stirrer made of stainless-steel. A comparison of the sizes of the reactors can be seen in **Figure 7-20**.

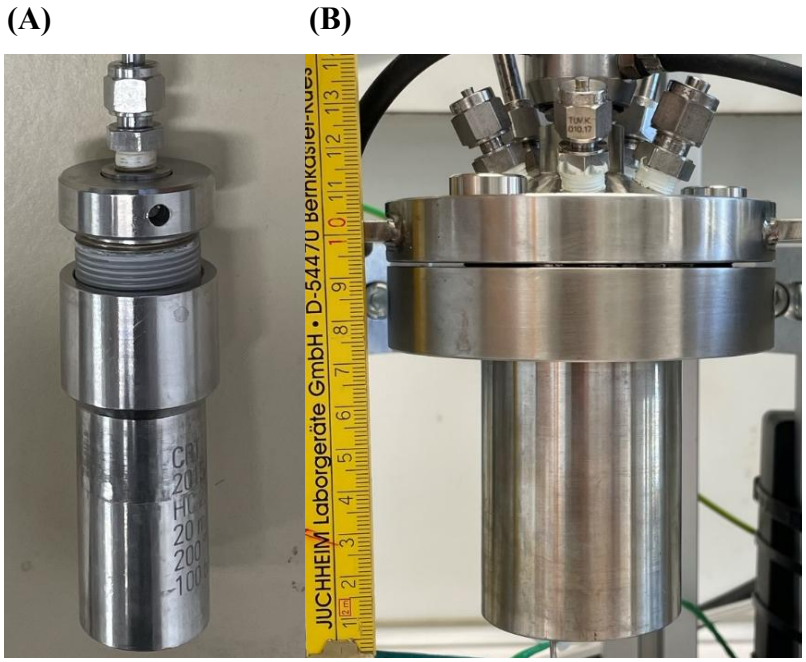

Figure 7-20: Comparison of one of the reactors from Setup 1 with approx. 20 mL reactor volume (A) and one of the reactors from Setup 2 with approx. 100 mL reactor volume (B). Reference of scale is applicable to both reactors.

In general, all process conditions had to be kept constant in order to provide comparability. The scale of the reaction in Setup 2 was threefold, resulting in the process conditions summarized in **Table 7-12**. One thing to note is that the scale-up potentially could have been larger, however, this results in a higher consumption of substrate which was limited in quantity and had to be sufficient for all remaining experiments.

Table 7-12: Overview of reaction parameters for the comparison of Setup 1 and Setup 2.

Reaction parameter	Parameter value	Details
Time	16 h	
Partial pressure at T_R	20 bar	Oxygen
Temperature	140 °C	
Substrate (mass)	500 / 1,500 mg	S1 – Organosolv softwood
Catalyst (mass)	200 / 600 mg	HPMo-Ni_3
Solvent volume	10 / 30 mL	Methanol/Water (8:2 v/v)
Stirring speed	0 rpm	Setup 1 did not contain stirrer Setup 2 was set to 0 rpm

The monoaromatic yield comparison is shown in **Figure 7-21**. The yields appeared to improve in the scaled-up system reaching approx. 6.75 wt.-% from approx. 5.5 wt.-% in Setup 1. While this was an excellent finding, the reason for this beneficial effect was mostly unclear. During scale-up most ratios were kept constant, such as substrate and catalyst loading, process conditions and solvent. Two thing comes to mind when examining the setups in detail. (1) The ratio of reactor ground surface area to lignin volume might be different for the setups. The reactor ground area is the surface on which the lignin is weighed on in the reactor prior to adding the solvent. If through reactor geometry the lignin is placed on more relative surface in Setup 2 compared to Setup 1, the lignin likely has more area of contact with the solvent system potentially leading to an advantageous solubilization effect. The higher the degree of solubilization the more monoaromatics can be formed and indeed, it is found that the carbon content in the solid phase is only at approx. 16 wt.-% in Setup 2 compared to the 21 wt.-% observed in Setup 1 in section **7.2.5** allowing this hypothesis to not be refuted.

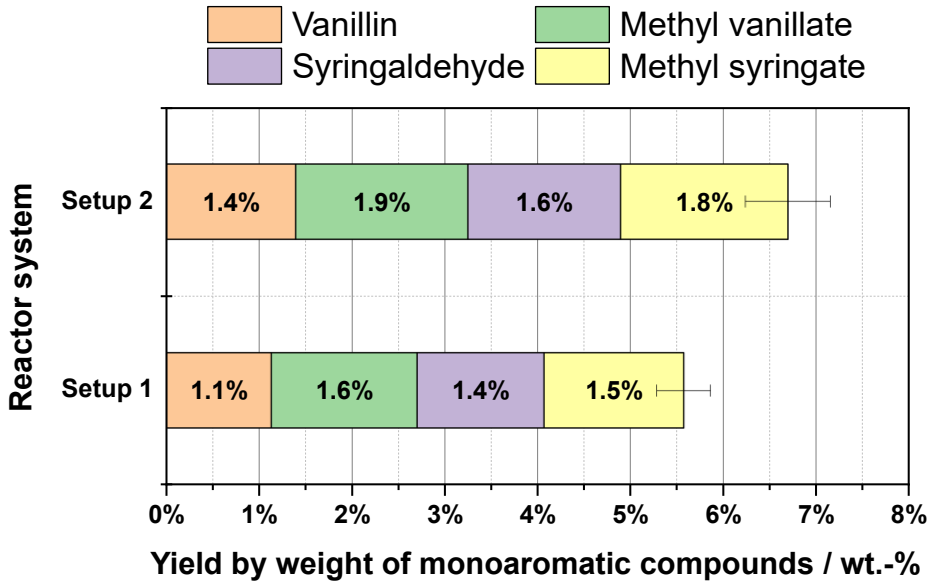

Figure 7-21: Comparison of yields by weight of the desired monoaromatic compounds investigated in Setup 1 & Setup 2. Reaction conditions were 140 °C, 20 bar oxygen partial pressure, 16 h, 0 rpm, 10&30 mL solvent (8:2 v/v MeOH:H_2O), 500&1500 mg substrate (organosolv softwood lignin S1), 200&600 mg catalyst HPMo-Ni_3.

(2) Additionally, the ratio of head space and solvent volume differentiates between the two plants. While in Plant 1, the ratio was 1:1 (~10 mL of both head space and solvent volume), the ratio in Plant 2 was >2:1 (~ 70 mL head space and ~30 mL solvent volume). This lead to a higher absolute amount of oxygen in the system. While the equilibrium concentration of dissolved oxygen was not changed by this due to equal partial pressure, the consumption of

oxygen during the reaction was partly buffered and might lead to higher oxygen availability in the liquid phase at later reaction times.
This concept of potentially increasing solvent contact and/or mixing was considered in the next section where a process parameter optimization was conducted.

7.2.8 Parameter optimization utilizing design of experiments (Setup 2)

Results of design of experiment study:

To further assess the influence of process parameters on the oxidative depolymerisation of lignin towards the desired monoaromatics, a design of experiment study (DoE) was conducted within this section. This provides the benefit of reducing the number of experiments while still observing the influence of each parameter. Additionally, both parameter combinations and quadratic influences can be investigated when applying the Box-Behnken design, as explained in section **6.6**.
The parameters considered were (A) the reaction temperature, (B) the stirring speed which was neglected altogether so far, and (C) the substrate to catalyst ratio which basically just alters the amount of catalyst mass as the substrate mass was set constant. The remaining parameter values correspond to the previous investigations summarized in **Table 7-21**. An overview of the DoE experiments is provided with **Scheme 7-4**. For the three parameters three levels at equidistant gaps were considered resulting in the temperatures 120, 140, and 160 °C, in the stirring speeds 0, 500, and 1,000 rpm, and in the catalyst ratio 1, 2.5, and 4. This resulted in 15 experiments including 3 experiments at centre point (CP) conditions as indicated by the orange points in the scheme.

Table 7-13: Standard process parameter conditions for the design of experiment study, excluding the variable parameters temperature, stirring, catalyst mass (ratio).

Reaction parameter	Parameter value	Details
Time	16 h	
Initial partial pressure at standard conditions	14 bar	Oxygen
Substrate (mass)	1,500 mg	S1 – Organosolv softwood
Solvent (volume)	30 mL	Methanol/Water (8:2 v/v)

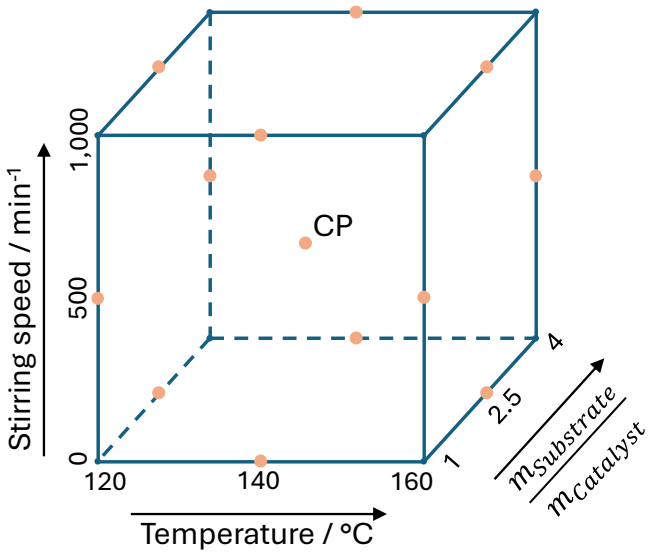

Scheme 7-4: Schematic drawing of experimental points in Box-Behnken design of experiments. CP stands for the centre point.

The experiments were performed in Setup 2 according to the DoE plan and the results of the monoaromatic yields, carbon yield of CO, CO_2 and short-chained carbon esters, and carbon yield in solid phase are attached in the appendix in **Table B-4**. The DoE model was selected based on suggestions of the software Design Expert resulting in a quadratic model.

Further, the overall p-values also show significance basically meaning no significant outliers were observed. A summary of the ANOVA is attached in the appendix in **Table B-5**. Looking at each parameter's statistical values, it becomes clear that the stirring speed did not show a significant influence on the yields of monoaromatics while both reaction temperature and catalyst ratio did.

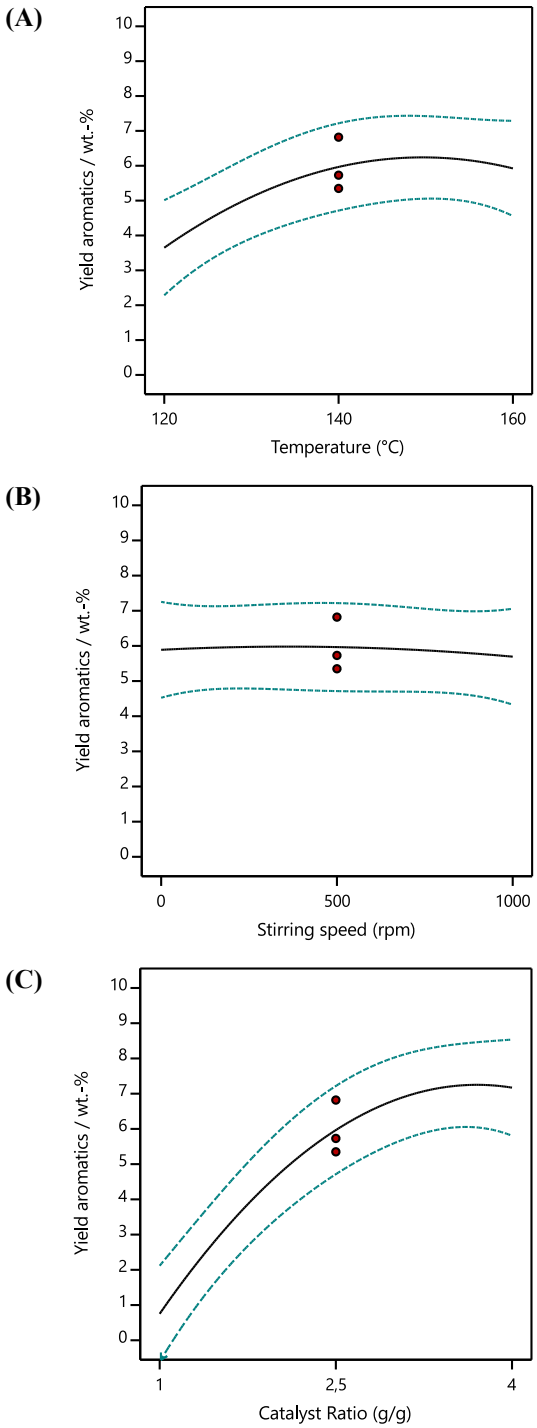

Figure 7-22: Comparison of process parameter influence on yield of monoaromatics. Shown are the effect of temperature (A), stirring speed (B) and substrate to catalyst ratio (C).

These aspects are observable when the monoaromatic yield was plotted over the respective reaction parameter as shown in **Figure 7-22** for temperature (A), stirring speed (B) and catalyst ratio (C). As only the influence of one parameter was considered in these graphs, the additional ranges achieved through altering remaining reaction parameters is shown with the blue dotted line. The red dots represent the triplicate centre points. As can be clearly seen, the stirring speed showed no influence on the yield. Due to the stirrer increasing the available oxygen in the liquid phase, this means that no mass transfer limitations regarding the oxygen was present in the observed parameter ranges. On the other side, both with increasing temperature and catalyst ratio (so, meaning reducing catalyst loading) the yields could be significantly boosted. Both seemingly approximate an asymptote and even falling a little at the edge of considered parameter range. This means that while increasing reaction temperature or lowering catalyst mass, the kinetics of the depolymerisation towards the monoaromatics were higher compared to the degradation towards short-chained methyl esters or CO & CO_2. Thus, the depolymerisation was more driven by temperature while the degradation was more driven by the catalyst leading to the question if further increasing the catalyst ratio (or decreasing the mass of catalyst) would result in further monoaromatic yield. This question was investigated later.

Now that the parameter influence has been investigated, the next step was to maximize the monoaromatic yield. As the stirrer had negligible effect, it was set to 0 rpm. The results of varying both temperature and catalyst ratio on the yields are depicted in **Figure 7-23** in a 3D-graph.

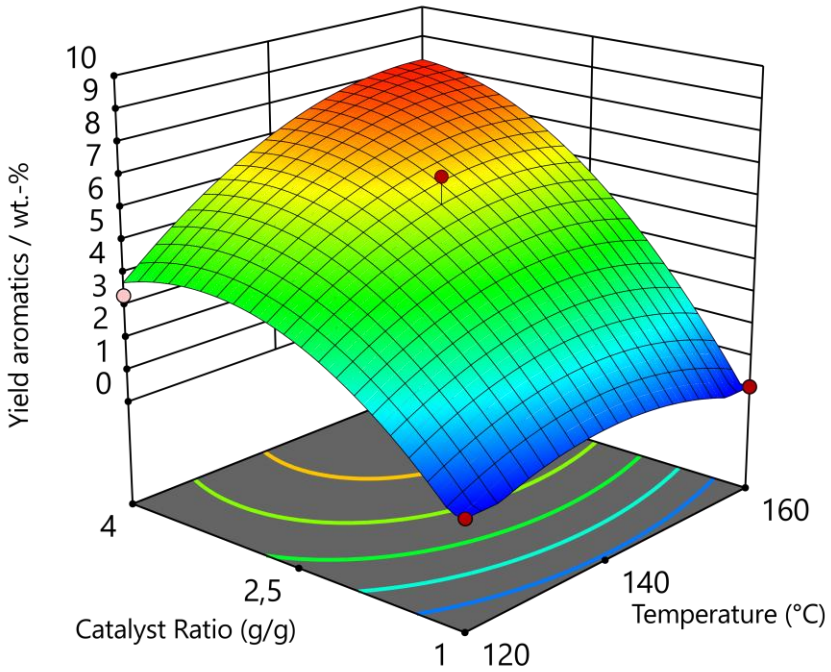

Figure 7-23: 3D-graph showing the influence on yield of aromatics for parameters temperature and substrate to catalyst ratio.

As can been, at the minimum catalyst ratio (highest catalyst loading) the monoaromatic yields reached 0 wt.-% independently on temperature. On the other hand, at the highest catalyst ratio the yields increase from 120 to 160 °C reaching yields of >8 wt.-%. Utilizing the Design Expert software to predict the maximum yield possible within the parameter ranges, the result was 8.7 wt.-% at 160 °C, 0 rpm and catalyst ratio of 4. These process parameters were tested to confirm the model's prediction. The monoaromatic yield reached a value of 8.3 wt.-% which is in the range of error, thus not contradicting the model.

Further points to mention are the measured summed carbon yields of CO, CO_2 and short-chained methyl esters (hereinafter called degradation products), and the carbon yield in the solid phase. For both, the experiment's data were also fed to the DoE software, however, they did not result in significant models. Nonetheless, the data shows tendencies which shall now be briefly discussed. For the carbon yield of degradation products both stirring speed and catalyst

ratio did not show significant effects. The temperature, though, notably influenced the yields of degradation products, specifically of methyl formate and CO_2. While at 120 °C the carbon yield of these degradation products was between 8 to10 wt.-%, the yields increased to 21 to 23 wt.-% at 160 °C. The reason for this was likely an increased selectivity of the POM catalyst for the formation of formic acid and CO_2 at elevated temperatures rather than the selective oxidative depolymerization towards monoaromatics. Further, at elevated temperatures the formation of oxygen radicals increased, also leading to unselective oxidation and, thus, to CO_2. Even though the degradation products were not the primary products within this study, the potential loss of carbon in these products at elevated temperatures was accepted as the monoaromatics yields increase with rising temperatures, as well. [198,205–207]

The mentioned second point of interest was the carbon yield in the solid phase. It was primarily affected by stirring speed and catalyst ratio. Increasing stirring speed and decreasing catalyst ratio (so increasing catalyst mass), reduced the amount of carbon in the solid phase. The first parameter likely did show effects on the solubilization, decreasing both total solid mass and, thus, carbon yield in the solid phase. The catalyst ratio, on the other hand, did not necessarily show influence on the total solid mass but on the elemental mass distribution in the solid mass. At high catalyst loading the relative carbon content in the solid phase was as low as 20 wt.-% and at low loading the content reached 50 wt.-%. This clearly shows that the utilized HPMo-Ni_3 catalyst directly affects the oxidation reactions.

Reflection on DoE methodology:

Overall, the DoE study proved excellent optimization capabilities and improved the yield significantly. However, with additional efforts prior to this parameter optimization, two aspects of this DoE could have been improved. (1) An initial screening of parameters' significance would have allowed to switch the stirring speed for e.g. the oxygen partial pressure, which was investigated outside of this optimization, or the lignin loading. (2) The boundaries of significance for each parameter could also have been investigated previously. Then, a broader range of temperature could have been investigated and for the catalyst on the other side, the investigation could have focused on the lower catalyst loadings, which was then investigated separately.

Further catalyst loading optimization:

While these observations are interesting, they do not change any of the previously determined process conditions for maximizing monoaromatic carbon yield. This DoE procedure was now

finished but one aspect, mentioned above, is still unclear which is the further increase of substrate-catalyst-ratio, or the reduction of catalyst mass. For this, the catalyst loading was consecutively decreased until a maximized monoaromatic yield was observed. The results are shown in **Figure 7-24**.

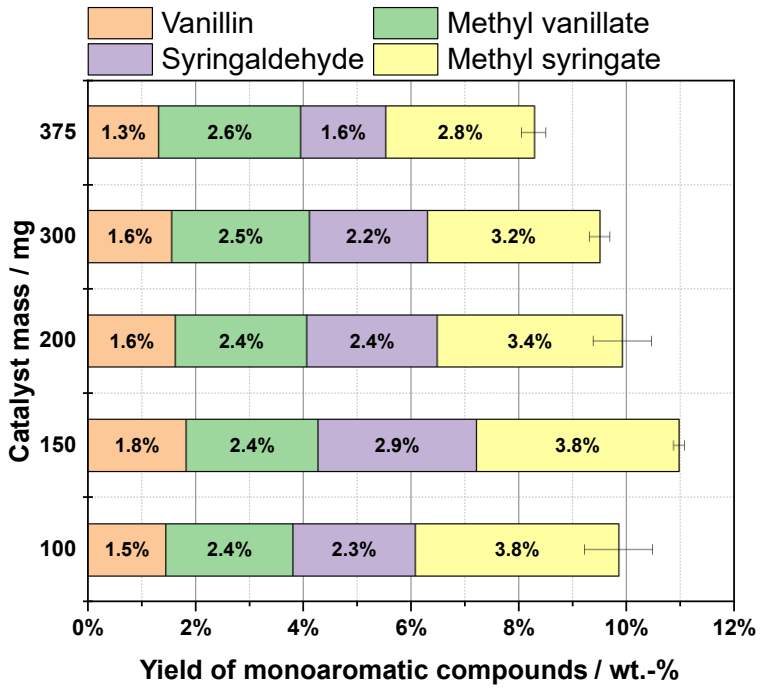

Figure 7-24: Monoaromatic yields for further catalyst loading optimization. Reaction was carried out in Setup 2 and conditions were 160 °C, 14 bar oxygen partial pressure at T^0, 16 h, 0 rpm, 30 mL solvent (8:2 v/v MeOH:H_2O), 1500 mg substrate (organosolv softwood lignin S1), 375;300;200;150;100 mg catalyst HPMo-Ni_3.

The monoaromatic yields at a catalyst loading of 375 mg correspond to the highest substrate-catalyst-ratio (being 4:1) of the DoE study. As can be seen, the yields further increased with decreasing catalyst loading until a loading of 150 mg. Here, the yields reached a total value of approx. 11 wt.-%. Further decreasing the catalyst loading resulted in a loss of monoaromatics. The optimized loading thus is at 150 mg, corresponding to a ratio of 10:1.

Further, the monoaromatic's distribution shifted throughout adjustment of catalyst loading. While the ratio of each aldehyde to its respective methyl ester is approx. at a factor of two, this ratio decreased while lowering the catalyst loading. For the compounds Va and MeVa this occurs at an almost constant yield for MeVa while the yield of Va increases consecutively until 150 mg catalyst loading. This means the formation of Va is promoted at lower catalyst concentrations while the esterification towards MeVa is not. A plausible explanation would be the decreased Brønsted acidity by lowering catalyst loading. However, this observation is

contradicted when looking at the compounds Sy and MeSy. Here, both the aldehyde and the methyl ester grew in yield while lowering the catalyst loading. The esterification to MeSy is thus not hindered at lower catalyst concentrations. The overall observation indicates that the catalyst is actively participating in the conversion of Sy which seems to be an instable component.

Throughout this extensive study it was possible to increase the monoaromatic yields from approx. 6.5 to approx. 11 wt.-% for the softwood organosolv lignin S1. For the previously utilized hardwood organosolv lignin S4, this value was already reached without further process parameter optimization. This shows that the results of this process are highly dependent on feedstock quality and characteristics. The obtained process parameters listed below were utilized for the experiments conducted in the continuous plant in section **7.4**.

- Reaction temperature: 160 °C
- Residence time: 16 h
- Stirring speed: 50 rpm (to enable homogeneity)
- O_2 partial pressure at T^0: 14 bar
- Solvent system: Methanol/water at 8:2 v/v ratio
- Solvent volume: 30 mL
- Substrate: Softwood organosolv lignin S1
- Substrate mass: 1,500 mg
- Catalyst: HPMo-Ni_3
- Catalyst mass: 150 mg

Before going into the next chapter for further process development, a brief kinetic study elaborating order of reaction and activation energy was provided for the studied system. Additionally, the obtained optimized reaction parameters were applied to all initially screened lignins.

7.2.9 Determination of reaction order and activation energy (Setup 2)

In this section both the effective order of reaction and activation energy were determined for the selected chemical system at optimized process conditions. For this the basis of **Eq. 7-1** was utilized where *r* is the reaction rate, *i* is component i, *T* temperature, *c* is concentration, *t* is reaction time, *k* is reaction constant, and *m* is partial order of reaction for component i.

$$r_i(T,c) = \frac{dc_i}{dt} = k(t) \cdot \prod_{i=1}^{j} c_i^{m_i} \qquad \textbf{Eq. 7-1}$$

As the considered system of lignin depolymerisation is highly complex going through several steps of reactions with unknown oligomeric compounds, the effective reaction rate was utilized summarizing the relevant reaction network to lignin and monoaromatic products. Further, oxidized catalyst (and thus also oxygen for re-oxidation of catalyst) and methanol were required for the reactions. [208] Selecting a sufficient partial pressure of oxygen allows the oxidation of the lignin being the rate-limiting step, rather than the catalyst reoxidation. This means that the concentration of oxidized catalyst and methanol are assumed to be constant during reaction. All constants (k, $c_{ox.catalyst}$, $c_{methanol}$) can be summarized to k'_{eff} leading **Eq. 7-2**, where r_{eff} is the effective reaction rate, k'_{eff} the effective reaction constant, and c^m_{Lignin} is the concentration of lignin with the partial order of reaction m.

$$r_{eff} = k'_{eff} \cdot c^m_{Lignin} \qquad \textbf{Eq. 7-2}$$

$$\ln(r_{eff}) = \ln(k'_{eff}) + m \cdot \ln(c_{0,Lignin}) \qquad \textbf{Eq. 7-3}$$

After applying the natural logarithm, **Eq. 7-3** is obtained, which can be used for the graphical plotting of experimental data to determine the reaction order. This was done by varying the initial lignin concentration resulting in the final concentration of the desired monoaromatic compounds, shown in **Table 7-14**, at otherwise optimized reaction conditions. This data was used to generate **Figure 7-25**. As shown, the measured data points are well aligned with a linear fit, yielding a high coefficient of determination R^2.

Table 7-14: Summary of initial lignin concentration and monoaromatic concentrations after reaction during the determining of reaction order. Reaction conditions were Setup 2, 160 °C, 14 bar initial oxygen partial pressure, 16 h, 50 rpm, 30 mL solvent (8:2 v/v MeOH:H_2O), varying substrate mass (organosolv softwood lignin S1), 600 mg catalyst HPMo-Ni_3.

Experiment #	Initial lignin concentration / $\frac{mg}{mL}$	Monoaromatic concentration / $\frac{mg}{mL}$
1	33.2	1.1
2	50.2	2.2
3	66.7	3.7
4	83.4	5.9

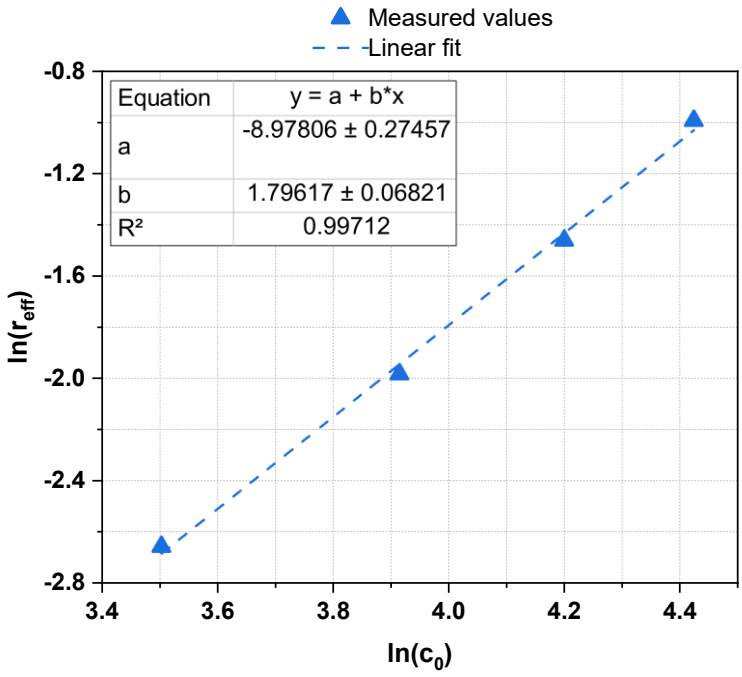

Figure 7-25: Logarithmic plot of the effective reaction rate over the initial lignin concentration including four measured data points and a linear fit. Reaction conditions were Setup 2, 160 °C, 14 bar initial oxygen partial pressure, 16 h, 50 rpm, 30 mL solvent (8:2 v/v MeOH:H_2O), varying substrate mass (organosolv softwood lignin S1), 600 mg catalyst HPMo-Ni_3.

The slope *b* of the linear fit represents the partial reaction order *m*, as shown in **Eq. 7-2.** The obtained value of *m* is approx. 1.8, indicating that the reaction rate increased more than linearly but not exactly quadratically with lignin concentration. This suggests a complex reaction mechanism involving intermediate steps and potentially the formation of radicals [209]. Compared to previous studies, the partial reaction order observed here was significantly higher. While literature typically reports values close to 1 [210–213], the discrepancy can be attributed

to differences in the chemical system. Most studies on lignin oxidation focus on kraft lignin under aqueous and alkaline conditions, whereas this study investigated organosolv lignin under acidic conditions in organic solvents, complicating direct comparisons.

Another possible explanation for the high partial reaction order was the varying lignin-to-oxygen ratio throughout the study. Although oxidation shall be primarily driven by the catalyst, dissolved molecular oxygen, considerably soluble in organic solvents [214–216], may also contribute. Since the oxygen partial pressure was kept constant, its relative concentration compared to lignin and reaction products decreased with increasing initial lignin concentration. As monoaromatic compounds might undergo further degradation, the observed partial reaction order may suggest that the selected oxygen partial pressure was too high for optimal monoaromatic yield. This insight highlights a potential approach for process optimization in future investigations. Specifically, this approach could be tested by consecutively increasing the initial lignin concentration or decreasing the oxygen partial pressure and checking for the reaction rate growth (exponent *m*) to reach a value of 1.

Next, the activation energy was investigated. This was achieved at optimized reaction conditions but varying the temperature from 140 °C to 170 °C, in 10 °C steps, as suggested in **Table 7-15**, leading to the shown monoaromatic concentrations. The basis of this procedure to calculate the activation energy is the Arrhenius equation shown in **Eq. 7-4** where A is the pre-exponential factor, E_A the activation energy, R the universal gas constant, and T the temperature. Applying the natural logarithm yields **Eq. 7-5**, a linear equation where $\frac{-E_A}{R}$ is the slope.

$$k'_{eff} = A \cdot e^{\frac{-E_A}{R \cdot T}} \qquad \textbf{Eq. 7-4}$$

$$\ln k'_{eff} = \ln A \cdot \frac{-E_A}{R} \cdot \frac{1}{T} \qquad \textbf{Eq. 7-5}$$

Eq. 7-5 was utilized to calculate the effective rate constants at different temperatures. These are plotted over $\frac{1}{T}$, shown in **Figure 7-26** and a linear fit was applied. As can be seen, the linear fit aligned well with the observed data points leading to a R^2 of 0.997. Rearranging the slope $\frac{-E_A}{R}$ yields an activation energy of $E_A = 12.7\ \frac{kJ}{mol}$.

Table 7-15: Summary of reaction temperature variation and its effect on monoaromatic concentrations after reaction. Reaction conditions were Setup 2, 140-170 °C, 14 bar initial oxygen partial pressure, 16 h, 50 rpm, 30 mL solvent (8:2 v/v MeOH:H_2O), 1,500 g substrate (organosolv softwood lignin S1), 600 mg catalyst HPMo-Ni_3.

Experiment #	Reaction temperature / °C	Monoaromatic concentration / $\frac{mg}{mL}$
1	140	3.0
2	150	3.3
3	160	3.5
4	170	3.9

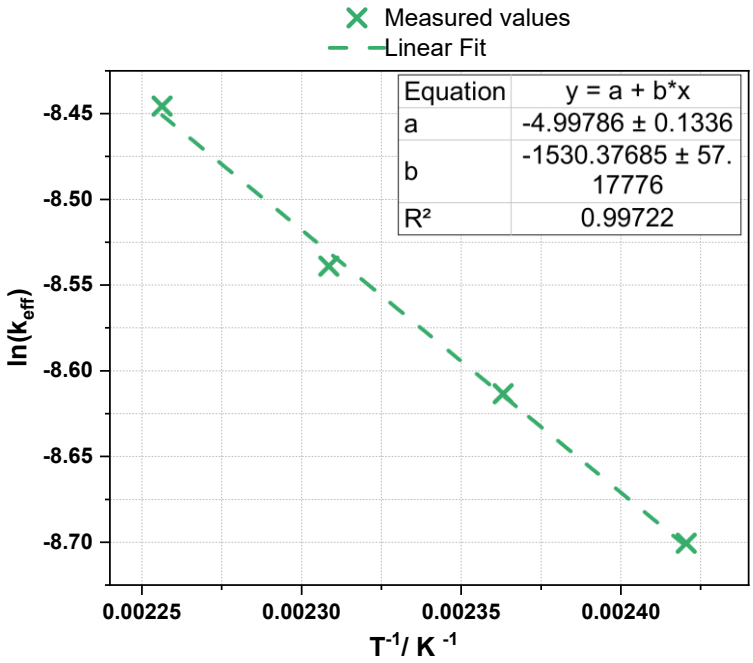

Figure 7-26: Logarithmic plot of the effective rate constant over one over reaction temperature including four measured data points and a linear fit leading to an activation energy of E_A=12.7 kJ/mol. Reaction conditions were Setup 2, 140-170 °C, 14 bar initial oxygen partial pressure, 16 h, 50 rpm, 30 mL solvent (8:2 v/v MeOH:H_2O), 1,500 g substrate (organosolv softwood lignin S1), 600 mg catalyst HPMo-Ni_3.

In literature, not many investigations on activation energy for the oxidative lignin depolymerisation are to be found and those discovered show a large discrepancy in activation energy values. *Fargues* et al. and *Werhan* et al. found activation energies of 29.1 $\frac{kJ}{mol}$ and 170.8 $\frac{kJ}{mol}$, respectively [168,212]. For both investigations, the vanillin production specifically was observed, unlike in this study. *Fargues* et al. utilized an alkaline system with sodium

hydroxide as catalyst for the depolymerisation of kraft lignin. Both the catalyst and the substrate show a significant deviation to the observed system in this study. *Werhan* et al. on the one hand also used a kraft lignin, on the other hand a polyoxometalate catalyst in a methanol-based solvent was applied showing more similarities in terms of the chemical system. The large discrepancy of the activation energy from *Werhan* et al. and this study cannot be clearly explained. However, the selection of lignin substrate shows a significant influence on the depolymerisation and the solubility of organosolv lignin is considerably higher than of kraft lignin easing the subsequent depolymerisation. Further, four monoaromatic compounds were observed and a more sophisticated catalyst was applied, here. Lastly, *Werhan* et al. utilized a microreactor opposed to the stirred tank reactor from this work. This might have an influence on oxygen availability and, thus, potentially on the reaction-limiting step, as well.

In summary, the observed system showed a low activation energy compared to literature highlighting the benefit of the selected substrate and catalyst combination. In this context, the question arises, if the optimized reaction conditions in combination with the newly found catalyst also provide a benefit for the other lignin substrates initially screened in section **7.2.2**. This topic was investigated in the next section.

7.2.10 Substrate screening with optimized reaction parameters (Setup 1)

To observe the influence of the reaction parameter optimization on the different lignin substrates, another substrate screening similar to that of section **7.2.2** was conducted again in Setup 1. The reaction parameters are summarized in **Table 7-16**. It is to note that the absolute monoaromatic yields are expected to be reduced compared to the values of the parameter optimization (section **7.2.8**) due to the downscaling, as described in section **7.2.7**. The results of the screening are summarized in **Figure 7-27**.

As can be seen, the monoaromatic yields of the so far developed process are significantly dependent on the lignin substrate. While for the organosolv lignins the expected high yields of approx. 7 to 8 wt.-% were observed (excluding S5 which achieves considerably lower yields), other lignins such as S18A/B achieve yields close to 0 wt.-%. Notably, even within the same pulping type substantial variations were observable, e.g. for S3 as a kraft lignin or S5 as an organosolv lignin. This suggests that both the biomass origin and the specific pulping process conditions strongly influence lignin depolymerisation.

The kraft lignins (S2, S3, S8) only showed significant concentrations of Va and MeVa. The reason for this might be the reduced content of syringyl units in softwood. On the other hand, the softwood organosolv lignins show considerable yields of Sy and MeSy. This either means that these compounds are formed from other units, which is unlikely, or that the syringyl units were not initially present in the kraft lignin. This is in accordance with *Kondo* et al. who have shown that the β-O-4 bond degradation of syringyl-syringyl-units is significantly faster than syringyl-guaiacyl- or guaiacyl-guaiacyl-units during alkaline processes such as kraft or soda pulping which potentially leads to a decreased syringyl content in the precipitated lignin. [217] When comparing the FT-IR spectra (in the appendix in section **B.3**) of kraft lignins S2, S3 or S8 and organosolv lignin S1, the characteristic signal of syringyl units at approx. 1325 cm^{-1} was not present for the kraft lignin while it was for the organosolv lignin. [218–220] This explains the missing monoaromatic products of Sy and MeSy for the kraft lignin substrates. The same concept can be applied to the differing organosolv lignin S5, the hydrolysis lignin S6, and the enzymatic fractionated lignin S11 which showed no characteristic band for syringyl units. This brings up the question if S1, claimed to be a softwood lignin, is rather a mixture of both softwood and hardwood. Unfortunately, this question could not be answered due to unclear origin.

Table 7-16: Process parameters for substrate screening at optimized reaction parameters.

Reaction parameter	**Parameter value**	**Details**
Plant setup		Setup 1
Time	16 h	
Initial partial pressure	14 bar	Oxygen
Temperature	160 °C	
Stirring	0 rpm	
Substrate mass	500 mg	
Catalyst mass	50 mg	HPMo-Ni_3 ($H_{15}PNi_3Mo_9O_{40}$)
Solvent volume	10 mL	MeOH/H_2O (8:2 v/v)

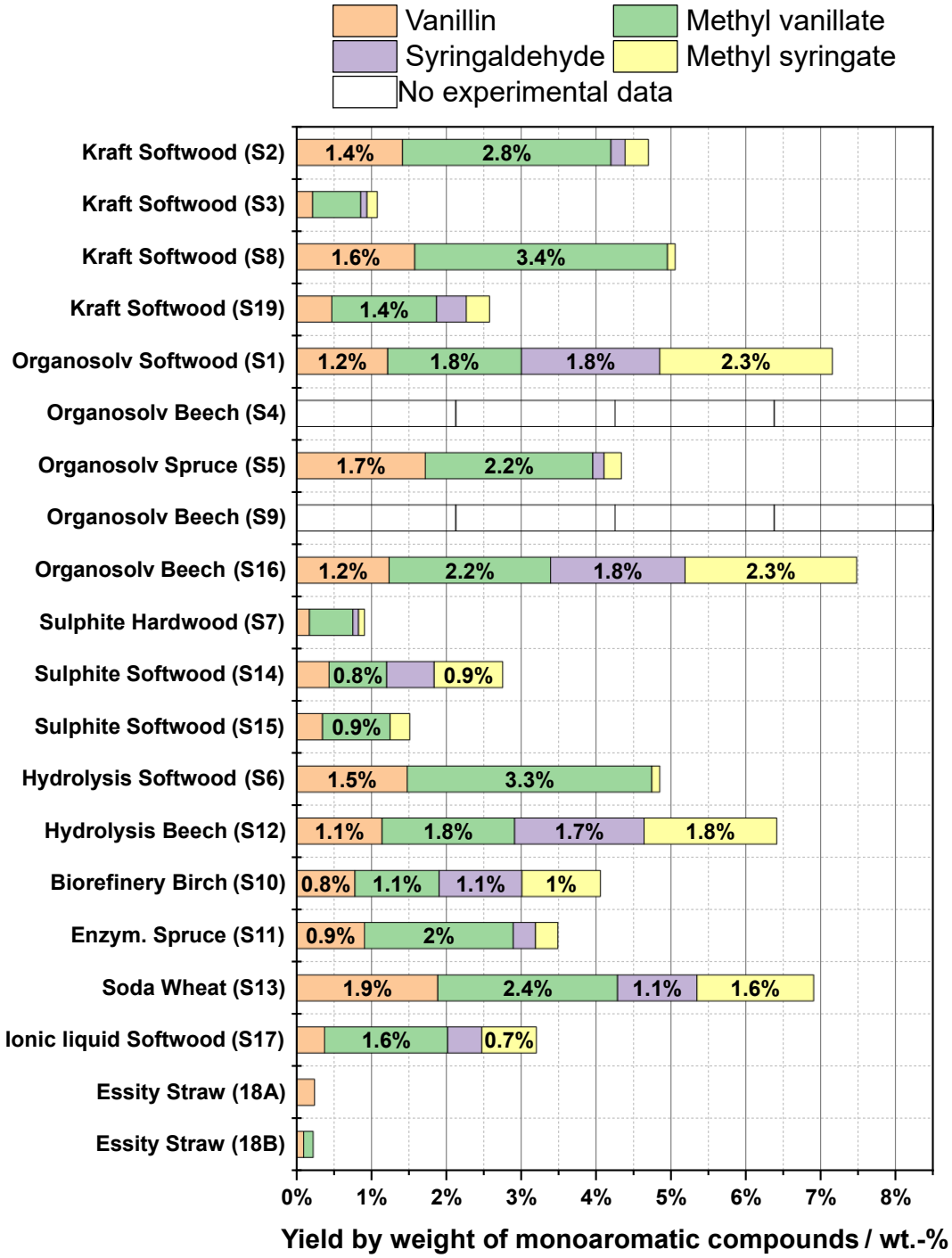

Figure 7-27: Monoaromatic yields of the substrate screening at optimized reaction conditions. Reaction was carried out in Setup 1 and conditions were 160 °C, 14 bar oxygen partial pressure at T^0, 16 h, 0 rpm, 10 mL solvent (8:2 v/v MeOH:H_2O), 500 mg substrate, 50 mg catalyst HPMo-Ni_3.

The sulphite lignins (lignosulphonates) S7, S14, and S15 exhibited very limited monoaromatic yields, as indicated by the GC-MS data discussed in section **7.2.3**. This may be due to their high solubility, which could accelerate depolymerization, leading to the rapid degradation of the desired monoaromatics.

Overall, this screening showed and confirmed that organosolv lignins produce the highest yields of the desired monoaromatics which does make sense as the process optimization was conducted with and for an organosolv lignin. On the other hand, this also shows that the process development for this oxidative, homogeneous depolymerisation is highly dependent on the specific substrate and would need to be adjusted for each substrate. Further, the selection of a lignin stemming from a hardwood material is also advantageous due to an increased content of syringyl units which likely are depolymerised to the product Sy and MeSy.

This concludes the sensitivity study for the oxidative depolymerisation of different technical lignins to the monoaromatic products vanillin, methyl vanillate, syringaldehyde and methyl syringate. Utilizing an organosolv lignin (S1) monoaromatic yields of approx. 11 wt.-% were achieved. However, as these studies were conducted in batch mode, the monoaromatics are likely to be further degraded towards non-aromatic products, unless separated from the reaction mixture. Especially with the overall goal in mind to develop an entire process for the lignin depolymerisation, the product separation and isolation is a crucial step which was further investigated in section **7.3**.

7.3 Concept selection for product isolation and catalyst recycling

As previously mentioned, the separation or isolation of the desired monoaromatics from the remaining catalytic system is a crucial step for the overall process development. This is due to the monoaromatics basically being an intermediate product which can be further degraded towards small-sized methyl esters as can be seen in **Figure 7-16** – as with increasing time, the concentration of these methyl esters also rises. For this consideration of product separation, the methods of liquid-liquid-extraction (LLE) and membrane separation were investigated, starting with the extraction.

7.3.1 Liquid-liquid-extraction of monoaromatic compounds from reaction solutions

The methodology of LLE is a well-known, industrially-applied technique for the separation of products utilizing their varying solubility in different solvents. [221,222] Even for the separation of formed products during lignin depolymerisation, LLE has been a common technique and both methodology and extraction solvent selection were based on this literature. [168–171] To allow an initial comparison of LLE and membrane separation, the following extraction solvents were selected based on these studies:

- Ethyl acetate
- Toluene
- n-hexane
- Octyl amine
- 1-heptanol

The experimental procedure was developed based on the tertiary diagram of ethyl acetate, methanol and water, being the extraction solvent and the reaction solvent, respectively. The procedure is shown in **Figure 7-28**. The starting point represents the initial reaction mixture (at this project stage the mixture still consisted of 95 vol.-% methanol and 5 vol.-% water) with 90 mL of volume. To allow reaching the miscibility gap, additional water is necessary which is why in Step 1 180 mL of water were added. Then, in Step 2, the ethyl acetate with a volume of 270 mL was added shifting the mixture into the miscibility gap. After proper phase separation, the aqueous phase (Point 3) and the organic phase (Point 4) were obtained. The remaining ternary diagrams are shown in the appendix (**B.8**).

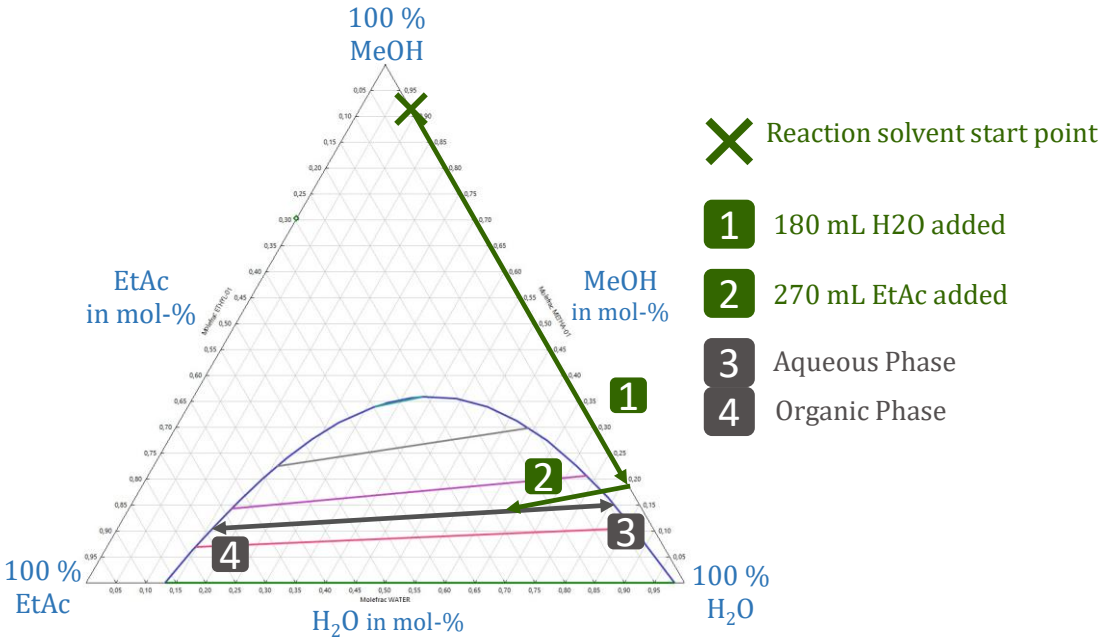

Figure 7-28: Ternary phase diagram of the compounds methanol (MeOH), water (H_2O), and ethyl acetate (EtAc) (in mol-%) showing the miscibility gap at the bottom generated in Aspen Plus. Point X represents the initial mixture of the reaction solvent (at this point, 95 % MeOH and 5 % H_2O). In step 1, 180 mL of H_2O were added. In step 2, 270 mL of ethyl acetate were added, shifting the mixture into the miscibility gap. After phase separation points 3 (aqueous) and 4 (organic) were formed.

The overall procedure was kept constant for each extraction solvent due to the miscibility gaps being favourable for this procedure for the remaining solvents as can be seen in the appendix (**B.8**). For the consideration of monoaromatic separation with extraction, the investigation was conducted in three steps and evaluated by means of separation factor α (basically extraction yield). First, the extraction was validated using stock solutions only consisting of the methanol-water solvent and the monoaromatics at representative concentrations (1 mg/mL). The three best performing extraction solvents were then utilized in the second step again with stock solutions but now also including the catalyst at reaction concentration (at this stage of the project still being 20 mg/mL). In the third step the two best performing extraction solvents were validated utilizing real reaction solutions from previously carried out lignin depolymerisation.

7.3.1.1 Extraction of stock solutions only containing monoaromatics

In **Figure 7-29** the individual and overall extraction yields for the monoaromatic compounds during the first step of extraction method evaluation are shown. As can be seen, the yield significantly varied depending on selected extraction solvent. The overall yields approx. range from 50 % for n-hexane to 85 % for toluene.

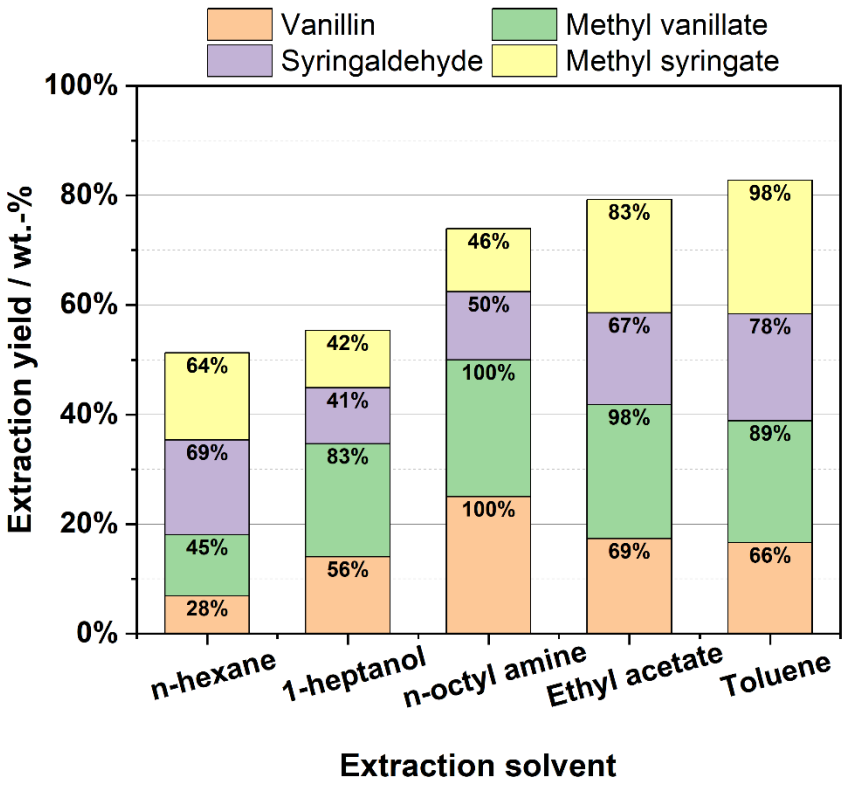

Figure 7-29: Average extraction yields and that of each desired monoaromatic compounds starting with a stock solution of methanol/water (95:5) containing 1 mg/mL of each monoaromatic. Extraction was carried out in a glass separating funnel. 90 mL of stock solution were diluted with 180 mL of water and then further diluted with 270 mL of the respective extraction solvent.

The low polarity of n-hexane as an extraction solvent explains the overall low yields. Observing the individual yields, these significantly differ between vanillin compounds and syringaldehyde compounds. The increased yields for the Sy units might be explained due to a potential decrease of polarity by shielding the hydroxy group through the additional methoxy group. This could also be a reason for the yield increase from Va to MeVa as the polar aldehyde group or rather the oxygen of it can be shielded by the methyl ester in MeVa.

These observations are consistent with the results of 1-heptanol which exhibits a moderately polar terminal hydroxy group. For this extraction solvent, the monoaromatic yields are opposite to that of n-hexane with higher yields for the vanillin compounds.

The extraction solvent n-octyl amine reached overall yields of 75 % with an exceptional extraction efficiency for the vanillin compounds while it stayed at similar values for the syringaldehyde compounds compared to 1-heptanol. A possible reason for the exceptional solubility of the vanillin compounds compared might be the formation of hydrogen bonds between the hydroxy and the amine group. However, this formation should also be possible for the extraction solvent 1-heptanol where significantly reduced extraction yields for the vanillin

compounds were observed. This aspect, thus, might be a factor for the differing yields, however, not a clear explanation.

The solvent ethyl acetate reached extraction yields of 80 % while showing quite evenly distributed individual yields. However, both yields for the methyl ester monoaromatics (MeVa, MeSy) were higher compared to the aldehyde monoaromatics (Va, Sy). Ethyl acetate being an ethyl ester and thus showing higher solubilities for similar functional groups might be the reason for this.

Lastly, toluene showed the highest overall extraction yields at approx. 85 %. The combination of aromaticity and hydroxy group, thus, showed the highest solubility for the monoaromatic compounds. In case toluene proved to be a viable extraction solvent, a potential optimization could be achieved by tweaking the extraction compound by an ester group to further increase extraction efficiency.

Overall, 1-octyl amine, ethyl acetate and toluene achieved moderate to high extraction yields which is why these three solvents were selected for the next step in which the catalyst was added to the stock solution.

7.3.1.2 Extraction of stock solutions containing monoaromatics and catalyst

The reason for this additional step of adding catalyst to the stock solution is to see the influence of the increased polarity in the reaction solvent. The polyoxometalate HPMo-Ni_3 potentially has a positive charge of +15 in aqueous environments and, thus, poses a significant change in molecule interaction during solvent extraction. In **Figure 7-30**, the extraction yields for the solvents 1-octyl amine, ethyl acetate and toluene are shown for stock solutions containing both monoaromatics and catalyst at reaction-similar concentrations (1 mg/mL for aromatics, 20 mg/mL for catalyst).

Observing the extraction yields, two aspects immediately stick out. First, for 1-octyl amine no extraction yields were obtained due to no phase separation or rather second phase formation occurring. Second, the extraction yields for ethyl acetate and toluene were significantly lower compared to the initial extraction solvent screening.

Starting with the first point, during the extraction utilizing 1-octyl amine no second phase was formed. The catalyst typically exhibited a light green colour when dissolved and no change of colour throughout the liquid contents in the separation funnel was observed. However, at least a change of colour intensity should be observed as the catalyst is a salt highly soluble in water

but not in less polar organic solvents. Since the liquid in the separation funnel uniformly remained in the characteristic green colour, the hypothesis of no second phase formation was made. The first idea for a reason would be that by the addition of the catalyst, the ternary solvent system would fall out of the miscibility gap. However, through the addition of the catalyst the water content would rather increase since it does contain a limited amount of crystal water. Looking at the ternary diagram of the methanol, water, 1-octyl amine system (c.f. **Figure B-33**) shows that even at an increase of water content the system should remain in the miscibility gap.

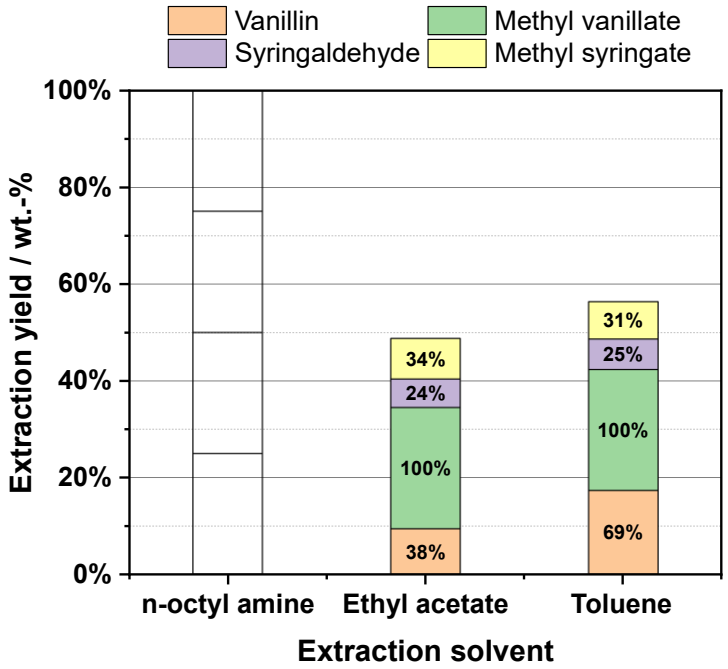

Figure 7-30: Average extraction yields and that of each desired monoaromatic compounds starting with a stock solution of MeOH:H_2O (95:5) containing 1 mg/mL of each monoaromatic and the polyoxometalate catalyst HPMo-Ni_3 ($H_{15}PNi_3Mo_9O_{40}$) with the three best performing solvents from the previous screening. Extraction was carried out in a glass separating funnel. 90 mL of stock solution were diluted with 180 mL of water and then further diluted with 270 mL of the respective extraction solvent.

Another reason for this disappearance of miscibility, might be a pseudo-formation of a surfactant disturbing a clear phase separation. [223] This surfactant might be formed through the coordination of the 1-octyl amine, already showing a non-polar octyl tail and a moderately polar amine, to the polarity of the polyoxometalate. In detail, the non-bonded electron pair of the amine could coordinate at the positively charged polyoxometalate cluster. By this, a compound would be formed showing both non-polarity through the alkyl-tail and high polarity through the polyoxometalate cluster. This aspect, even though quite interesting, was not pursued to be proven as the determination of a feasible monoaromatic separation was the overall goal for this chapter.

A second phase with subsequent phase separation was observed for ethyl acetate and toluene. The presence of the polyoxometalate catalyst significantly alters the polarity of the aqueous phase, which, in turn, affects the extraction yields. However, this effect was detrimental, reducing the yields to approx. 50 % and 55 % for ethyl acetate and toluene, respectively. Given that the target monoaromatic compounds are relatively non-polar compared to the dissolved polyoxometalate species, they are more likely to partition into a non-polar phase. In the case of ethyl acetate, the organic phase retains a considerable amount of water (c.f. **Figure 7-28**), suggesting that at least a fraction of the catalyst dissolves into the organic phase, thereby increasing its polarity. This may lead to reduced selectivity of the extraction solvent, explaining why ethyl acetate performs worse than toluene, which contains only trace amounts of water in its organic phase (cf. **Figure B-31**).
Another possible reason for the overall reduction in extraction yields is the catalytic activity. In these experiments, the catalyst and monoaromatic compounds exist in an isolated system without lignin or its oligomers, increasing the likelihood of monoaromatic degradation. Previous studies suggest that syringaldehyde is particularly unstable under reaction conditions and may degrade during extraction. This could explain the significantly lower extraction yields of Sy MeSy), while Va and MeSy maintain high yields.

Overall, this study demonstrates that the polarity induced by the polyoxometalate catalyst has a significant impact on extraction efficiency and can even hinder phase separation. Consequently, both ethyl acetate and toluene were selected for the next stage, where real reaction solutions will be used for extraction.

7.3.1.3 Extraction of real reaction solutions

In this section the results of the extraction experiments utilizing real reaction solutions will be discussed. It was observed in the last section that the presence of the polyoxometalate catalyst significantly influenced the extraction yields. The extraction was conducted for both real reaction solutions containing either no catalyst, or catalyst. As 90 mL of reaction solution per experiment are required, several depolymerisation experiments in Setup 1 were conducted according to section **7.2.4**. The experiments not containing the catalyst were primarily done to provide a visual comparison of the extraction. The monoaromatics were not quantified as the concentrations were significantly lower compared to the depolymerisation containing the catalyst.

In **Figure 7-31**, photos of the extraction for both solvents and catalyst setting are shown with a brief time lapse. On the top side the extraction is shown for ethyl acetate (left) and toluene (right) for the reaction solutions containing no catalyst, and on the bottom side the extraction is shown for solutions containing the catalyst. For the extraction with ethyl acetate and no catalyst (top left), a clear distinction between organic phase with a dark colour, a mixed phase still containing all solvents in a reddish tone, and the aqueous phase with a yellow colour can be seen. After approx. 60 min the mixed phase completely vanishes and leaves behind separated organic and aqueous phase with a clear phase separation. Comparing this to the extraction with ethyl acetate and catalyst (bottom left), the colour of the phases is not as distinguishable as it was for the previous extraction. Even after 60 min of phase separation the phases did not change visually, unless a flashlight was held behind the solution. Only then a difference of phases was observable and even a clear phase separation was formed showing that the addition of the catalyst did not completely prevent phase separation as it did for other extraction solvents in previous experiments.

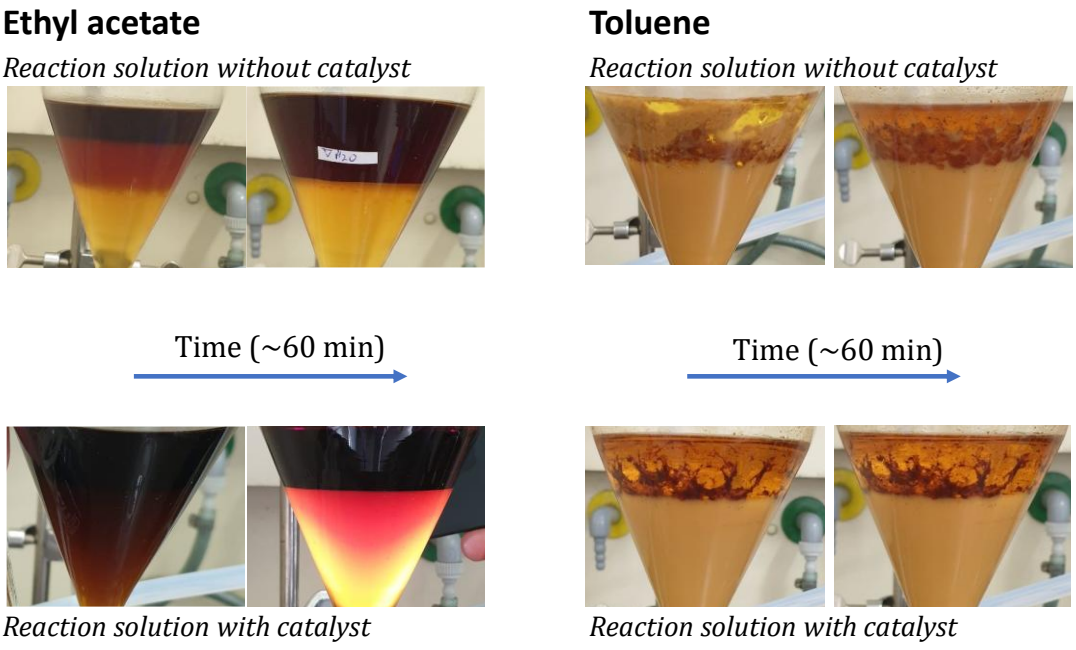

Figure 7-31: Photos of the extraction solutions stemming from real reaction solutions for both ethyl acetate and toluene, and reaction solutions containing catalyst or no catalyst.

The results of the extraction with toluene (right side) show a significant difference to that of ethyl acetate. While a phase separation was observable overall, a clear phase separation is not present. In the organic phase being in the upper section, the formation of precipitate can be seen in all four photos. Specifically for the extraction with catalyst (bottom right), the formed

precipitate did not change over time while a transition was observable for the extraction without catalyst (top right). Comparing the miscibility gaps with ethyl acetate and toluene (**Figure 7-28** and **Figure B-31**), there was a significant difference for the organic phase as with toluene the organic phase predominantly consisted of toluene and methanol. It thus might be that components initially well-soluble in a water-methanol solution reach their solubility limits when the water fraction is significantly reduced, potentially resulting in the observable formation of precipitate.

The aqueous phase, on the other hand, looks equal in all four photos showing an opaque dispersion in a brownish colour. During workup of the experiment, there was no clear evidence of particles in this aqueous phase meaning that this liquid might rather be an emulsion than a suspension. For an emulsion to be formed, it typically requires surface active compounds reducing any interface tension on the phase boundary. [224–226] As this already occurred throughout previous experiments, this might be an explanation for this behaviour in the aqueous phase. However, in this case the question arises why the organic phase was still present then. This again enables the theory that the aqueous phase was indeed a suspension showing finely dispersed particles which is supported by the precipitation already observed in the organic phase. Potentially, these particles might be the same precipitate observable in the organic phase but simply not agglomerated and rather finely dispersed.

For the technical feasibility, the formation of solid particles during extraction makes the extraction solvent toluene unviable as clogging might be a result during continuous reaction. For this reason, the organic phase of the toluene extraction was also not measured and quantified to prevent damage to the analytical devices. For the ethyl acetate extraction, the results are shown in **Figure 7-32**, however.

As can be seen, no extraction yields are depicted for the toluene extraction due to the poor technical feasibility. For the ethyl acetate extraction, an overall extraction yield of approx. 45 % was achieved which is similar to the results of the previous extraction step with stock solutions and catalyst. The yield distribution, however, significantly changed compared to the previous extraction. Here, the compounds Sy and MeSy showed higher yields than those of Va and MeVa which is exactly the opposite to the previous extraction step. One potential reason for this might be that both Sy and MeSy, even though showing a certain instability, were not degraded at these conditions caused by the presence of lignin and its oligomers. These oligomers might prevent the Sy and MeSy degradation through sheer availability as their concentration was likely

significantly higher as the lignin starting concentration is at 50 mg/mL while the monoaromatics typically show concentration of 1 to 2 mg/mL.

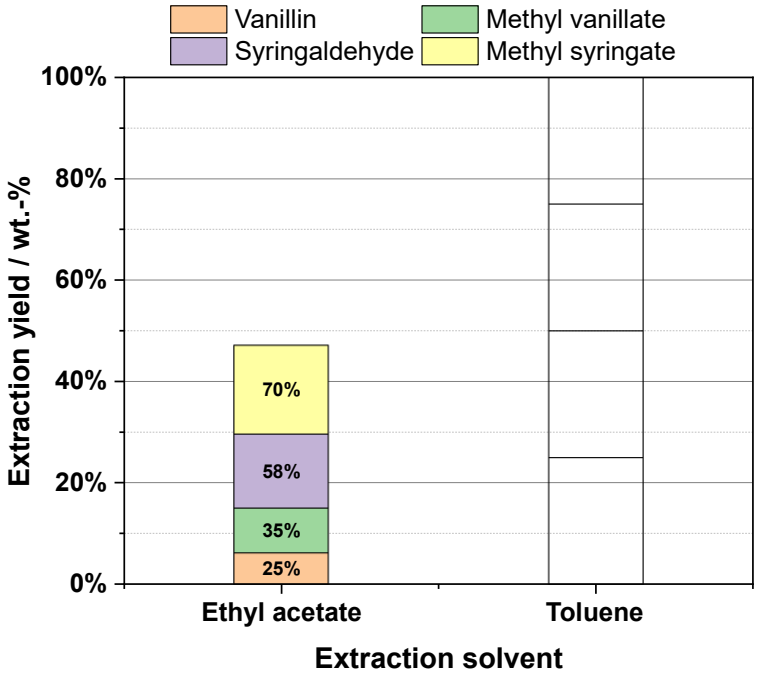

Figure 7-32: Average extraction yields and that of each desired monoaromatic compounds starting with real reaction solutions acquired depolymerizing lignin. Extraction was carried out in a glass separating funnel. 90 mL of stock solution were diluted with 180 mL of water and then further diluted with 270 mL of the respective extraction solvent.

Another reason for the extraction yield distribution to change might be the change of polarity and pH value in the organic and aqueous phase. [226] As the lignin oligomers likely showed no solubility in the aqueous phase, they remained in the organic phase because of their low polarity compared to water. On the other hand, all compounds formed containing carboxylic acid groups migrated to the aqueous phase due to their higher polarity which further reduced the pH value of the aqueous phase. This would result in highly differing phases concerning their polarity and pH value. It thus might be that the compounds Sy and MeSy show higher solubilities in extremely non-polar environments (perhaps due to the additional methoxy group) while Va and MeVa tend to have higher solubility in a more polar solvent.

Table 7-17: Results of elemental analysis for nickel, phosphorous, and molybdenum (Ni, P, and Mo) for the organic and aqueous phase formed during the extraction utilizing ethyl acetate and real reaction solutions containing catalyst.

	Concentration of element in respective phase / wt.-%		
Element	Ni	P	Mo
Organic phase	0.1 %	49.1 %	4.4 %
Aqueous phase	99.9 %	50.9 %	95.6 %

Another performance parameter to consider is the catalyst separation. As the catalyst is an acid it is likely to enrich in the aqueous phase which is why high yields in the water phase are expected. In **Table 7-17**, the mass concentration for the elements Ni, P, and Mo are shown for both phases. The phosphorous showed a low separation factor with concentration of 49.1 and 50.9 % in the organic and aqueous phase, respectively. The reason for this is the surplus of phosphoric acid during synthesis which means that the minority of this phosphorous originates from the catalyst. On the other side, both nickel and molybdenum remain in the aqueous phase with concentrations of 99.9 and 95.6 wt.-%, respectively. As during synthesis no surpluses of any was utilized since they should have equal values. This might either stem from inaccuracies of the elemental analysis or be an indicator of catalyst instability in the selected extraction system. If the extraction method would be selected for the continuous process, this aspect of catalyst instability would need to be investigated. This could be done by the comparison of ^{31}P-NMR and FT-IR of the catalyst prior and after the extraction. A change in the characteristic bands in the spectra could confirm the suspicion of catalyst instability. In this case, repeated extraction experiments should also be conducted for confirmation.

At this stage, however, the separation efficiency of catalyst and monoaromatics was to be compared to the second approach for product isolation being membrane separation, first. This approach will be discussed in the next section.

7.3.2 Membrane separation of monoaromatic compounds and catalyst

While liquid-liquid-extraction utilizes the varying solubility of compounds in different solvents, membrane separation, on the other hand, primarily utilizes its pore size to separate compounds smaller from compounds larger than this pore size. Of course, and depending on the membrane other properties such as polarity of the compounds also play role. In **Scheme 7-5**, a schematic overview of the membrane separation setup can be found. A feed vessel containing the solution of catalyst and/or monoaromatics is supplied to an HPLC pump which conveys the feed solution

at a pressure of 30 bar and a volume flow rate of 15 mL/min to the membrane module. This separates the feed into a retentate with enriched catalyst concentration and a permeate with enriched monoaromatic concentrations.

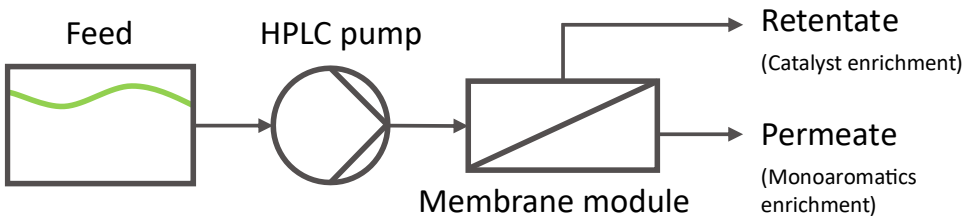

Scheme 7-5: Scheme of the experimental setup for the consideration of membrane separation to separate the desired monoaromatics and catalyst.

Initially, eight polymer membranes from three manufacturers were acquired for a first screening which are listed in combination with their product name and pore size in **Table 7-18**. All three membranes from *Evonik* show an identical pore size distribution of 280-600 Da which likely means that the membrane's material is differing allowing for varying selectivities depending on compounds. Similarly, the two membranes from *Suez Water Technologies and Solutions* show identical pore size distribution of 200-300 Da. Lastly, the three membranes from *Mann+Hummel* likely allow a fine tuning in terms of pore size as these range from 300-500 to 600 and 1000 Da.

Table 7-18: Overview of tested polymer membrane including manufacturer, product name and pore size ranges.

Entry #	Manufacturer	Membrane product name	Pore size / Da
1	Evonik	PuraMem Performance	280 – 600 Da
2	Evonik	PuraMem Selective	280 – 600 Da
3	Evonik	PuraMem Flux	280 – 600 Da
4	Suez Water Tech.&Sol.	DK-Series	200 – 300 Da
5	Suez Water Tech.&Sol.	DL-Series	200 – 300 Da
6	Mann+Hummel	XN45	300 – 500 Da
7	Mann+Hummel	NADIR	~ 600 Da
8	Mann+Hummel	UA60	~ 1000 Da

Regarding the experimental procedure, the following thought process was conducted. The polyoxometalate catalyst (M≈1726 g mol^{-1}) is significantly larger than the monoaromatic compounds (M≈212 g mol^{-1} for the largest compound methyl syringate) in terms of molecular weight and the molecular weight can be seen as an indicator for the molecular size. For this reason, at first suitable membranes were to be found that reject the POM catalyst allowing for an enrichment in the retentate. As the monoaromatics are significantly smaller, they are likely not to be rejected allowing the enrichment in the permeate. Consequently, all membranes were initially screened with only POM in the methanol-water solution. At this stage of the project, catalyst concentration has not been optimized, and 20 mg/mL were used for this membrane screening. The concentrations of the elements Ni, Mo and P were determined by elemental analysis (ICP-OES) for the feed, retentate and permeate solutions and the rejection was calculated according to **Eq. 6-6**. The results of the rejection are shown in **Table 7-19**. As can be seen, there are no values for entries 1-3. The three membranes from *Evonik* did not show any permeability of the reaction solution leading to no separation and thus 100 % retentate. It was concluded that the reason for this is the impermeability of methanol for these membranes, as it was indeed permeable for only aqueous solutions previously studied by *Dr. Tobias Esser*.

Table 7-19: Catalyst rejection factors for the membranes of entries 4-8, as entries 1-3 were not methanol soluble. Rejection is shown as weight percent of each element remaining in the retentate. Nickel – Ni, molybdenum – Mo, phosphorous – P.

Entry #	Membrane name	Rejection of element / wt.-%		
		Ni	Mo	P
4	DK-Series	89 %	84 %	84 %
5	DL-Series	94 %	96 %	100 %
6	XN45	99 %	99 %	89 %
7	NADIR	99 %	99 %	86 %
8	UA60	100 %	99 %	83 %

Due to the catalyst showing a distinctive green colour, a first visual assessment was possible by looking at the permeate solutions, as shown in **Figure 7-33**. While the feed shows the described green colour, the permeate solutions all show a decrease of colour and from entry 4 to entry 6 it appears that the colour continuously decreases. From entry 6 to 8 no visible change was observed anymore as the solution already appears to be free of any colour. These visual observations were confirmed by the elemental analysis results in **Table 7-19**. While both

membranes from manufacturer *Suez Water Techn. & Sol.* (entry 4 and 5) certainly show high rejections between 84 and 96 % for nickel or molybdenum, these values were even improved by any of the three membranes from manufacturer *Mann+Hummel* (entry 6-8) which all show rejections ≥99 % for Ni and Mo.

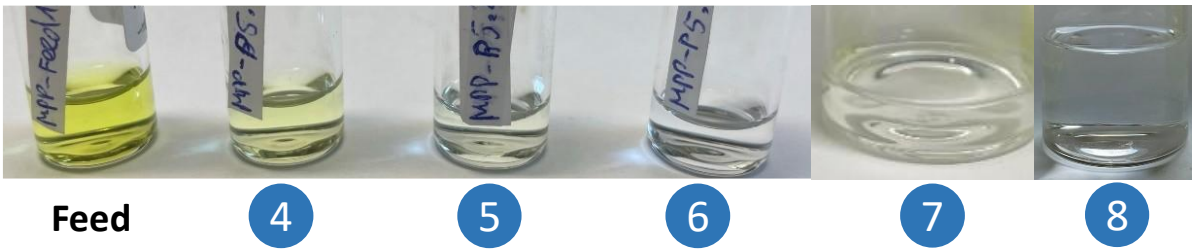

Figure 7-33: Photos of the feed and respective permeate solutions containing the catalyst with the corresponding entry numbers. The greenish colour stemming from the catalyst is increasingly reduced in the permeate showing the improvement of catalyst rejection.

Similarly to the extraction, excess phosphate during synthesis could explain the limited rejection of phosphorous for entries 4 and 6-8. As phosphate is considerably smaller than the cluster of a POM, it may migrate through the membrane into the permeate. The continuous process in mind, this should not be an issue as all free phosphate would then be separated and the overall concentration in the system should decrease after ramp-up time. For entry 5, however, a sudden rejection of 100 % for phosphorous was observed. A potential reason for this might be additional absorptive effects of the membrane material allowing full rejection of free phosphates by absorbing the compounds inside the membrane. [227]

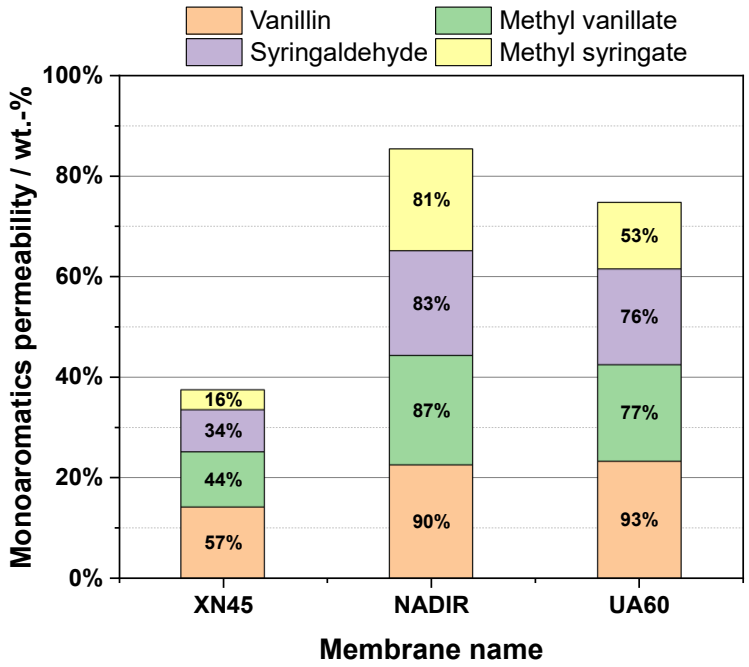

Figure 7-34: Permeability of the desired monoaromatic compounds for the three membranes of manufacturer Mann+Hummel.

As the membranes of manufacturer *Mann+Hummel* showed the most promising catalyst rejection, only these three were tested for their permeability through the membranes. These experiments were conducted similarly to the extraction experiments with a stock solution of monoaromatics. The results of these experiments are shown in **Figure 7-34**. As can be clearly seen, both the pore size and the membrane material had a significant influence on the permeability as the separation yields vastly differ for these three tested membranes. The XN45 membrane exhibits a pore size of 300-500 Da and shows a yield of approx. 38 %. The permeability decreases with increasing monoaromatic size as the yields for vanillin is the highest while for methyl syringate the lowest. Overall, this result indicates that the membrane's pore size is not sufficiently large leading to a higher degree of monoaromatic rejection. This is significantly changed when switching to the NADIR membrane which exhibits a pore size of approx. 600 Da. The average separation yield is increased to approx. 85 % proving that the pore size has a significant influence on the monoaromatic permeability. Similarly to the XN45 membrane, the yields again decrease with increasing size of the aromatic compound. Lastly, for the UA60 membrane, which exhibits the largest pore size with approx. 1,000 Da, permeability is shifted to only approx. 75 %. Assuming that the provided pore sizes of the manufacturers are correct, this observation indicates that besides the pore size also the

membrane material has a significant influence on the permeability. [228–230] The overall trend of decreasing permeability with increasing compound's size is again confirmed.
At this stage, the consideration of real reaction solutions for the membrane separation would be the next step, especially when compared to the procedure of the liquid-liquid-extraction. As membrane separation is primarily influenced by physical parameters such as flow rate, surface area, or concentration gradient, it was assumed that the separation efficiency would not be changed significantly when utilizing real reaction solutions. Aspects such as long-term efficiency and fouling would rather be investigated over larger time frames in the continuous plant.

In summary, eight membranes were tested for the rejection of POM catalyst and permeability of monoaromatics. Five of these membranes showed considerable catalyst rejection, while all three membranes of manufacturer *Mann+Hummel* showed exceptional catalyst rejection. For this reason, these membranes were tested for monoaromatic permeability. The NADIR membrane stood out achieving monoaromatic separation yields of approx. 85 % while the other two membranes achieved lower yields.

7.3.3 Discussion on selected concept for product isolation and catalyst recycling

Throughout the last sections both liquid-liquid-extraction and membrane separation were validated for the product isolation and catalyst recycling in a prospective continuous process. In both studies, a selection of chemical and physical systems was experimentally narrowed down to one system for each concept which should now be compared for a final decision. For the LLE concept, the extraction with ethyl acetate is the most promising system, while for the membrane separation concept, this was the case for the NADIR membrane of manufacturer *Mann+Hummel*.
In **Table 7-20**, a direct comparison of the catalyst rejection and the monoaromatic permeability are shown for both selected approaches. As can be seen, the catalyst rejection performs similarly for both approaches, although the rejection of phosphorous does behave differently reaching a significantly higher rejection for the NADIR membrane. A potential reason for this reduced diffusion of proposedly free phosphates might be the polarity. As membranes not only separate by molecule size but also by polarity, depending on the membrane material, the considerable polarity of phosphates might reduce the migration through the membrane and, thus, increase the rejection.

Table 7-20: Comparison of catalyst rejection and monoaromatic permeability for the selected systems of liquid-liquid-extraction (extractant ethyl acetate) and membrane separation (NADIR membrane from Mann+Hummel). Ni: nickel, Mo: molybdenum, P: phosphorous, Va: vanillin, MeVa: methyl vanillate, Sy: syringaldehyde, MeSy: methyl syringate.

Separation concept	Catalyst rejection / wt.-%			Separation factor / wt.-%				
	Ni	Mo	P	Va	MeVa	Sy	MeSy	Avg.
Extraction Ethyl acetate	99	96	51	25	35	58	70	47
Membrane NADIR	99	99	86	90	87	83	81	85

For the permeability of the monoaromatics, the yields behave contrary for the two separation approaches. While the extraction with ethyl acetate achieves lowest yields for Va and highest for MeSy, the NADIR membrane achieves highest yields for Va and lowest for MeSy. This behaviour is easily explained for the membrane, as the smaller sized products show higher permeability and the key property for the separation is molecular size, here. The improvement of permeability for the methyl esters does make sense in the context of ethyl acetate also being an ester. The increased solubility of the syringaldehyde-based compounds is likely due to the addition of a methoxy group aligning the polarity to that of ethyl acetate. On average, the permeability of the monoaromatics is significantly better for the NADIR membrane system with approx. 85 % yield. Even when compared to the adequate extraction system (cf. **7.3.1.2**) where similarly ~50 % yield was achieved in ethyl acetate.

An additional performance parameter, which has not been mentioned yet, is the remain of lignin oligomers. While no specific analysis has been conducted for confirmation, it is likely that at least a portion of the oligomers similarly migrate to the organic phase during LLE, whereas these oligomers are likely not able to diffuse through the membrane and thus remain in the retentate. For the extraction, this would mean that a large fraction of the reactant is separated from the reaction mixture, whereas this is not the case for the membrane separation where the oligomers likely stay in the catalyst-rich retentate which is recycled to the reactor.

To conclude, the membrane separation achieves similar results as the extraction for the catalyst rejection, and significantly improved separation yields of the monoaromatic compounds. Additionally, this technique allows the recycling of lignin oligomers to the reactor potentially increasing overall product yields. Because of these reasons, the membrane separation technique was selected as a unit operation for the downstream processing of the continuous plant. The further development of this continuous plant will be described in the next section.

7.4 Continuous process (Setup 3)

In the following section, the previously developed technical processes shall be translated to a continuous process. For this, the generally known steps for process plant design were applied, however, summarized in concept planning, plant assembly and commissioning. [231] These aspects will be described in the next sections, followed by the execution of lignin depolymerisation in the developed continuous plant.

7.4.1 Concept planning and plant assembly

Based on the previous studies within this work, a basic flow diagram was created for the initial concept planning of the continuous plant. An overview is given in **Scheme 7-6** which separates the plant into an upstream processing, the catalytic depolymerization, and a downstream processing. In the upstream processing, the continuous feed of oxygen gas, lignin and reaction solvent are included. The oxygen is necessary for the oxidation, the lignin shall be oxidized, and the reaction solvent system must be supplied as there is a loss in the downstream processing, at this stage. Additionally, a solvolysis step of the lignin was added to allow a homogeneous feed into the reactor.

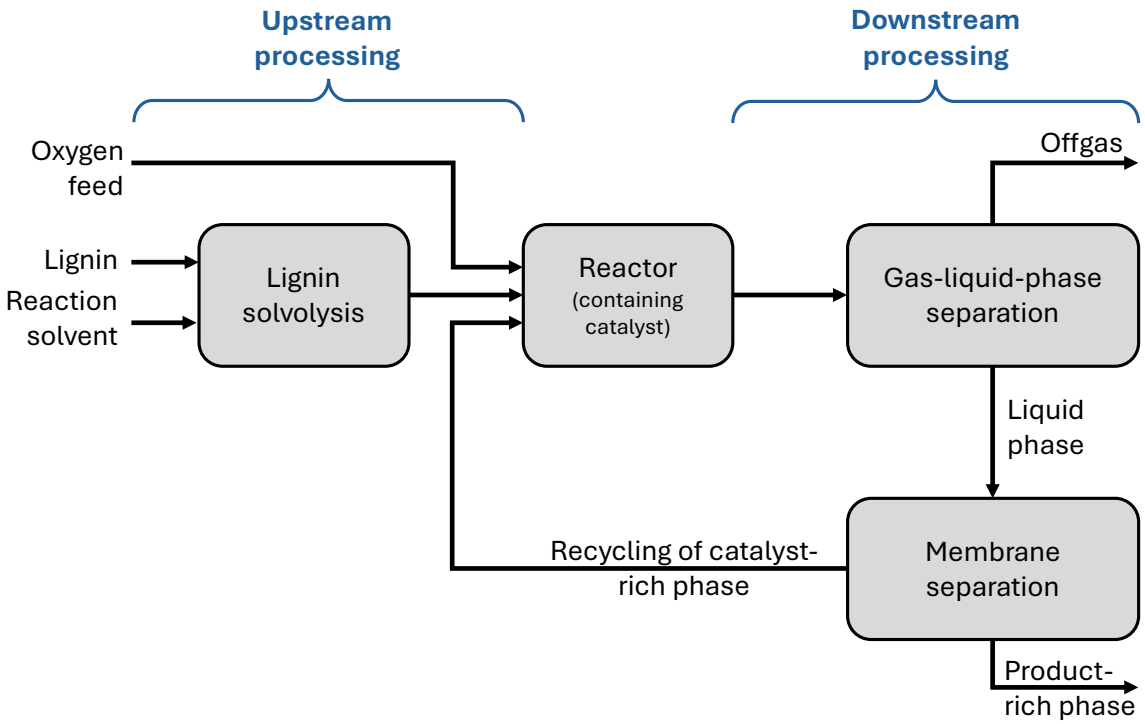

Scheme 7-6: Overview of the initial basic flow diagram for the continuous plant of oxidative lignin depolymerisation divided into upstream processing, reaction, and downstream processing.

So far, this solvolysis step has not been investigated and, thus, was explored within this section. The reaction itself was thoroughly developed in section **7.2**.
For the downstream processing, a reactor effluent stream containing both gas and liquid phase was planned. These phases must then be separated resulting in an off-gas stream and in a liquid phase which were separated into a product-rich and a catalyst-rich phase by membrane separation. The product-rich phase contains the monoaromatics, while the catalyst-rich phase is to be recycled into the reaction.
Throughout the next sections, those unit operations, which have not been discussed within this work yet, shall be elaborated starting with the upstream processing.

7.4.1.1 Lignin solvolysis (upstream processing)

Due to the fact, that this process should run continuously and under high pressure, a continuous supply of the solid lignin proves to be challenging. One approach, which has been conducted in literature already, is a preceding solvolysis step followed by the separation of the remaining solids and the liquid phase. Similarly to the approach of *Du* and *Tricker* et al., an initial step of pretreatment was considered at milder reaction conditions. [203] The pretreatment reaction was carried out in Setup 2 with the following reaction conditions:

- Temperature: 100 °C
- Pressure: 10 bar of N_2 (at room temperature)
- Time: 2 h
- Stirrer: 300 rpm
- Loading: 0.5 g/mL (standard biomass to solvent loading)
- Solvent: 8:2 (v/v) MeOH:H_2O

The acquired suspension containing both dissolved lignin and insoluble lignin was filtered to receive a particle free filtrate. This was then used as a feedstock for the subsequent catalysed experiment according to section **7.2.8**. The monoaromatic yields of this two-step process were compared to the typical depolymerisation without prior solvolysis in **Figure 7-35**.
Overall, the yields were considerably similar. Both the sum and the respective yields did not show significant deviations from the reaction without prior solvolysis. One anomaly was the standard deviation for the sample of the two-step process. This, however, can be explained by technical difficulties in the GC-MS device after the first measurement, leading to the high

deviation. Excluding the repetitive measurements would result in an even higher yield. For the purpose of transparency, all measurements were included in these results. Due to aging of the sample repeating measurements were not possible, after the device was fixed.

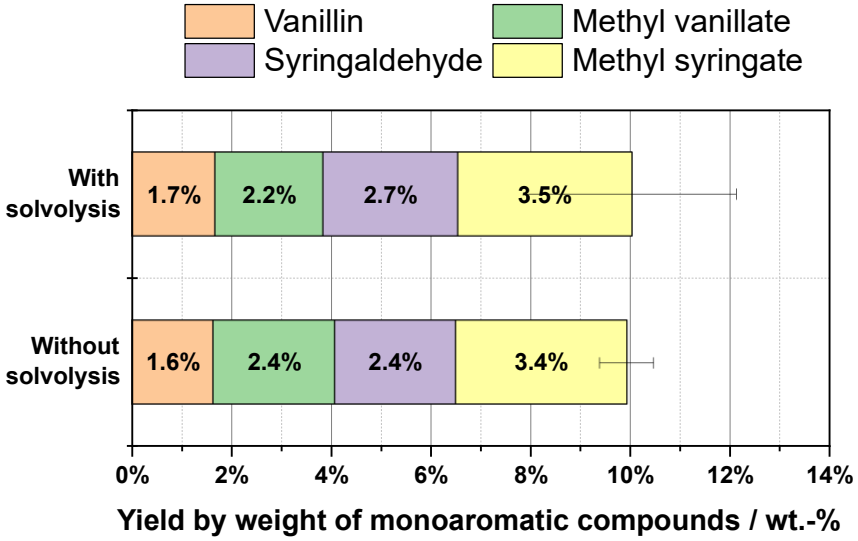

Figure 7-35: Comparison of monoaromatic yields for a two-step lignin depolymerisation process including an initial solvolysis step and typical one-step depolymerisation process. For the solvolysis the conditions were 100 °C, 10 bar initial pressure of N_2, 2 h, 300 rpm, 0.5 g/mL biomass loading, 8:2 (v/v) MeOH:H_2O solvent system. For the depolymerisation, reaction conditions were in Setup 2 160 °C, 14 bar initial oxygen partial pressure, 16 h, 50 rpm, 30 mL solvent (8:2 v/v MeOH:H_2O), varying substrate concentration (organosolv softwood lignin S1), 600 mg catalyst HPMo-Ni_3.

These results confirmed the approach of a preceding solvolysis step of lignin. The monoaromatic yields were not altered significantly, while it was possible to provide a particle-free, liquid feedstock which can be pumped into the reactor. To avoid a build-up of filter cake (insoluble lignin) in the continuous plant, it was decided to utilize a separate batch reactor for the first step of solvolysis, initially. The suspension was then to be filtered, and the filtrate was stored in a feed container of the continuous plant. With this, the concept of the upstream processing was outlined and a further look on the downstream processing units is given in the next section.

7.4.1.2 Gas-liquid separation (downstream processing)

As it was planned to have a combined effluent stream containing both gas and liquid phase, the separation of these two phases was necessary as indicated by **Scheme 7-6**. Not only is there a considerable amount of gas volume per liquid volume. Due to the high partial pressure of oxygen, a significant amount is likely dissolved in the liquid phase, as well. For an effective

separation of gaseous compounds and liquid phase, a pressure relief was thus necessary. This could be achieved by a pressure letdown vessel which basically was a container with a large volume compared to the volume of the entering medium. This increase of volume lead to a sudden pressure relief resulting in a separation of gas and liquid phase. By two exits located at the top and bottom of the vessel, the two phases were separated.
As the reaction and the product-catalyst-separation have been investigated in section **7.2** and **7.3**, respectively already, all unit operations of the continuous plant have now been investigated individually. To evaluate if existing equipment can be utilized, the requirements of the equipment's materials are discussed in the next section.

7.4.1.3 Resistance requirement of materials

Based on the previously applied reaction conditions and reaction media, a moderate to high corrosivity was expected due to a high availability of oxygen and highly acidic environment potentially leading to surface corrosion. For this reason, the materials utilized during plant assembly were selected accordingly to prevent corrosion. The most critical parts were those in contact with the reaction media at elevated temperatures which primarily is the reactor. Due to an existing plant being modified, as described later in section **7.4.1.5**, the material of the reactor was C276 which shows exceptional corrosion resistance not only against surface corrosion, but also pitting corrosion, crevice corrosion, and stress corrosion cracking due to the high content of nickel. [232,233] Plant components, which do not underly significant thermal stress but still pressure, are primarily the piping, valves, and the pressure letdown vessel. For these, the material stainless steel 1.4571 was selected as it still shows considerable corrosion resistance. For the depressurized area of the plant, the piping and containers remain. For this piping, the plastic material perfluoroalkoxy alkanes was selected as still a considerable chemical resistance was required. For the containers, either a borosilicate glass 3.3 or a high-density polyethylene (HDPE) material was selected to provide required chemical resistance but also being shatterproof. For sealing conventional fluoropolymers, such as PTFE, FKM and FFKM, were selected.

7.4.1.4 Estimated pressure drop

The estimation of pressure drop was required for the selection of suitable pumps in the plant. For this, the so-called Moody diagram (cf. **Figure B-35**) was utilized to assess the Darcy friction factor (f). At first, the Reynolds number was calculated by estimated flow velocities, as

shown in **Eq. 7-6**, where v is the axial velocity, d the inner diameter of the pipe and ϑ the kinematic viscosity of the liquid medium. The results lie between 2.7 and 4.8 showing a clear laminar flow behaviour.

$$Re = \frac{v \cdot d}{\vartheta} \qquad \textbf{Eq. 7-6}$$

According to the Moody diagram, the Darcy friction factor at laminar flows (f_{lam}) can be calculated as shown in **Eq. 7-7**. Utilizing this factor the estimated pressure drop was then calculated with **Eq. 7-8** (where l is the pipe length, d its inner diameter, ρ the density of the liquid medium, and v the axial velocity) resulting in a negligible pressure drop of approx. 1 mbar. The exact calculations can be found in the appendix in **Table B-6**.

$$f_{lam} = \frac{64}{Re} \qquad \textbf{Eq. 7-7}$$

$$\Delta p = f_{lam} \cdot \frac{l}{d} \cdot \frac{\rho}{2} \cdot v^2 \qquad \textbf{Eq. 7-8}$$

As these initial estimations showed no significant pressure drop, no further calculations were conducted. As a result of this, the selection of pumps for the continuous plant did not have any further requirements. The next step was the plant assembly which is discussed in the next section.

7.4.1.5 Modification of existing plant

For the assembly of the continuous plant, rather than completely building a new plant, an existing plant was modified to the required needs. The existing plant was the so-called *Michel*-plant and is shown in the PID in **Figure 7-36**. The original plant is shown in black whereas all changes made are shown in grey (cf. **Figure 6-3**).

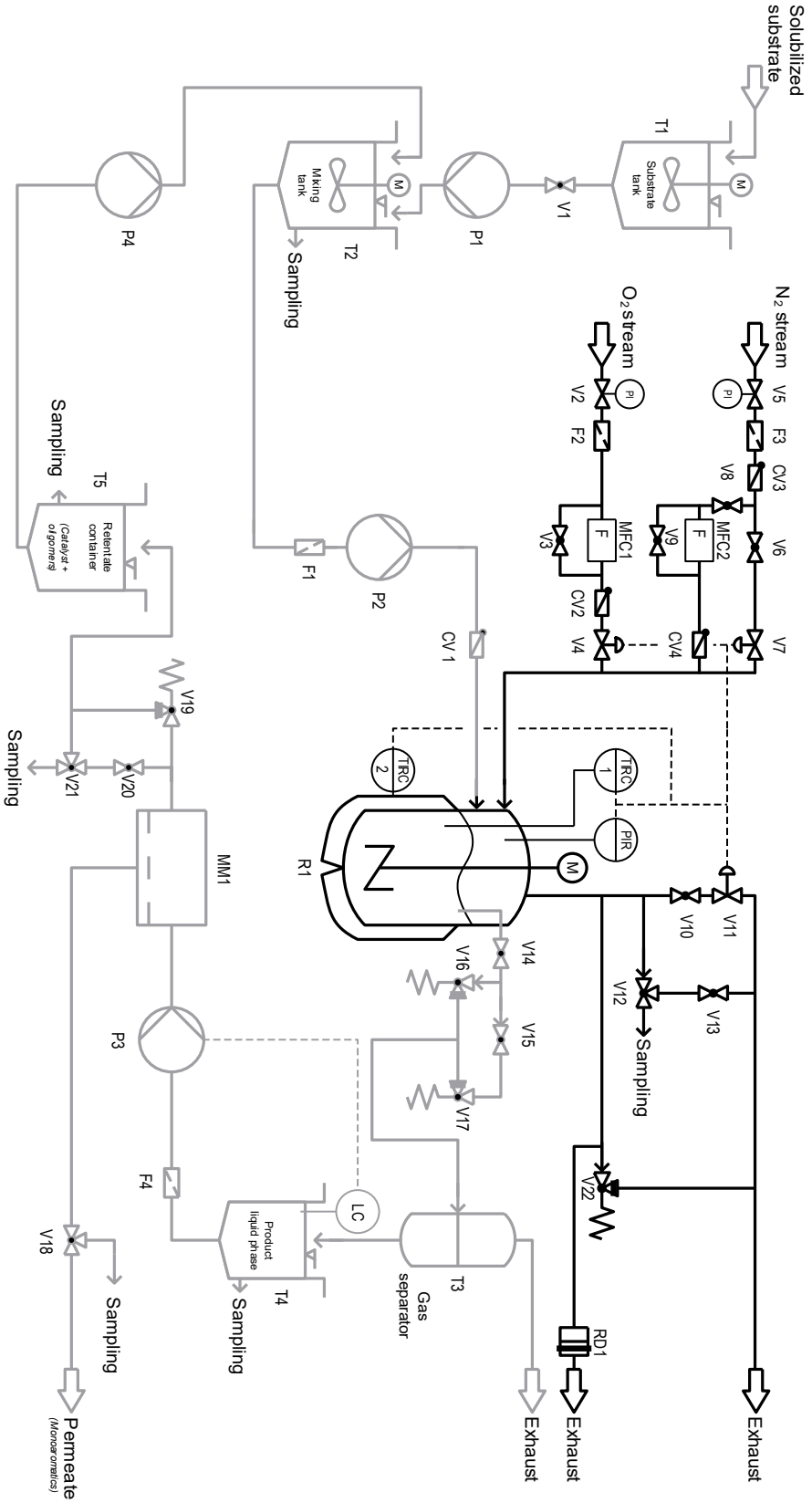

Figure 7-36: Piping and instrumentation diagram of the existing *Michel*-plant (in black) which was previously utilized for biomass conversion in batch mode. It consists of a gas feed section on the left, a 450 mL reactor in the centre, and a gas effluent and gas sample section to the right. All modifications towards a continuous plant are marked in grey.

The *Michel*-plant was a batch plant and consisted of a 450 mL high-pressure reactor equipped with a gas feed section (including mass flow controllers allowing semi-batch mode) and a gas effluent and gas sample section. Instrumentation and controlling of the plant were already available and connected to the control box. As can be seen, the batch plant lacks some unit operations necessary for the continuous experiments which are the feed section (including lignin and recycled catalyst), a gas separator, the product isolation by membrane separation and the catalyst recycling.

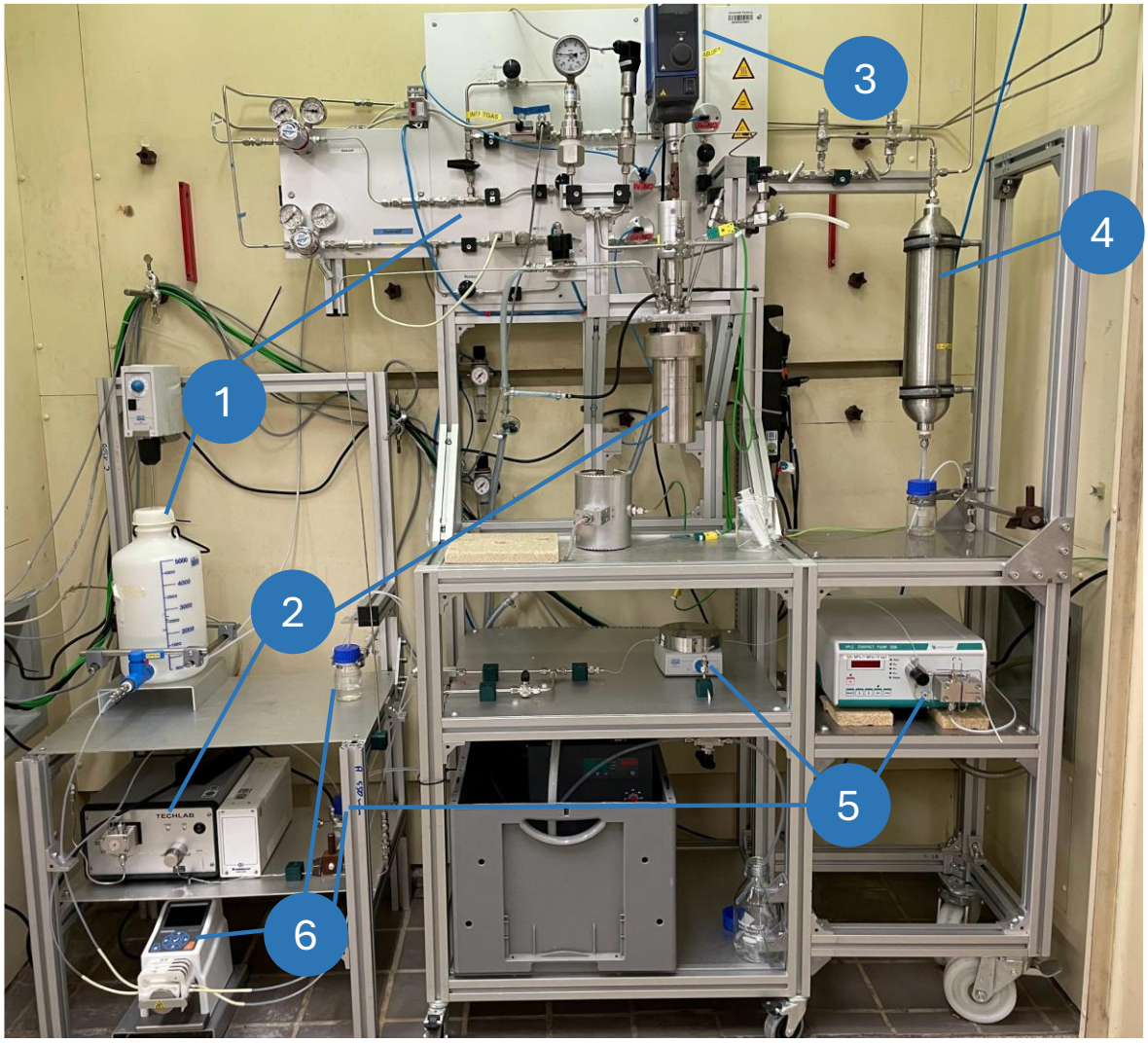

Figure 7-37: Photo of the modified *Michel*-plant for the continuous depolymerisation of lignin. (1) shows the feed container of the lignin solution and the gas feed. (2) shows the HPLC pump feeding the reactor. (3) shows the gas effluent and sampling. (4) shows the gas-liquid separator. (5) shows the membrane separation setup including an HPLC pump, the membrane cell, and a retentate container. (6) shows the catalyst recycling via a peristaltic pump into a mixing container.

During this modification several containers, two peristaltic pumps, two high-pressure pumps, a liquid level control in the reactor, a gas separator and a membrane module were installed,

leading to the plant shown in the photograph in **Figure 7-37**. Further details are described in section **6.3.1.3**. Following the assembly, several aspects of the commissioning will be discussed in the next section.

7.4.2 Commissioning

During the commissioning phase, several key activities were performed: calibration of the pumps, adjustment of pressure control valves, implementation of level control, execution of a HAZOP study, preparation of operating instructions, and finally, water trial runs to test the reactor outlet and determine the residence time.

Pump calibration

All four pumps were calibrated using an 8:2 (v/v) methanol/water mixture. The conveyed mass was measured over a 10-minute interval, following prior determination of the mixture's density using a volumetric pipette and mass measurement. The measured mass flow was converted to a volumetric flow rate, assuming a linear relationship with pump power. The resulting calibration curve and corresponding factors are provided in the appendix in **Eq. B-1** and **Table B-7**, respectively.

Pressure control valves

The plant includes four pressure control valves: V16, V17, V19, and V22. Valve V22 serves as a safety device, set to open at 60 bar in the event of a thermal runaway. Valve V19 controls the pressure in the membrane cell and was set to 30 bar, consistent with the pressure used in membrane separation experiments. Valves V16 and V17 regulate the reactor pressure, with V17 set to the design pressure of 22 bar at reaction temperature and V16 initially set to 25 bar to allow for pressure variation. These settings were achieved by adjusting system pressure via the gas inlet and tuning the valve springs using a digital pressure gauge to correspond to the desired opening pressures.

Level control for membrane separation

Due to the higher flow rate in the membrane separation unit compared to the reactor effluent rate, level control was deemed necessary. An ultrasonic sensor was employed to measure the distance to the liquid surface and integrated into a Siemens LOGO! 12-24RCE controller with an AM2 module. This setup enabled automated control of the HPLC feed pump of the

membrane unit based on the detected liquid level. The control logic was implemented using LOGO! Soft Comfort software, and the circuit diagram is presented in **Figure B-36** in the appendix.

Water trial run

Following the completion of the HAZOP and operating procedures, water trial runs were performed to verify the operability of all components, particularly the reactor effluent stream mechanism – a critical element of the plant. Operability was confirmed by monitoring reactor pressure during simultaneous gas and liquid flow. Results are shown in **Figure 7-38**.

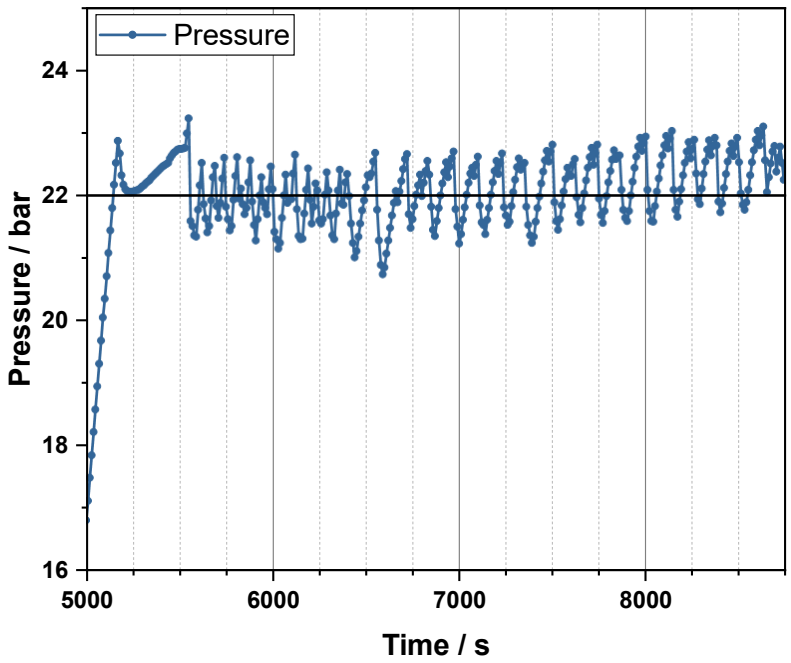

Figure 7-38: Reactor pressure during initial water trial run showing the operability of the reactor effluent stream mechanism.

During the first 30 minutes, the reactor was heated to the target reaction temperature (160 °C), causing a steady increase in pressure. At 23 bar, the pressure control valve opened; initially, only gas exited the reactor due to insufficient liquid presence. Once the liquid flow commenced, pressure regulation stabilized, as seen from approx. 5,500 seconds onward. Pressure remained well-regulated for the duration of the trial, indicating successful commissioning of the reactor outlet.

Residence time:

Theoretical residence time, determined in section **7.2.5,** is 16 h. The feed pump was calibrated accordingly. However, due to potential deviations from ideal mixing, experimental verification was also performed. The plant was first flushed with deionized water, after which a potassium chloride (KCl) tracer solution was introduced into the feed tank. Upon pump activation, a timer was started, and the effluent's electrical conductivity was continuously recorded, forming a step-response experiment. The normalized conductivity data yielded the cumulative residence time distribution F(t), shown in **Figure 7-39**. Numerical differentiation produced the residence time density function E(t).

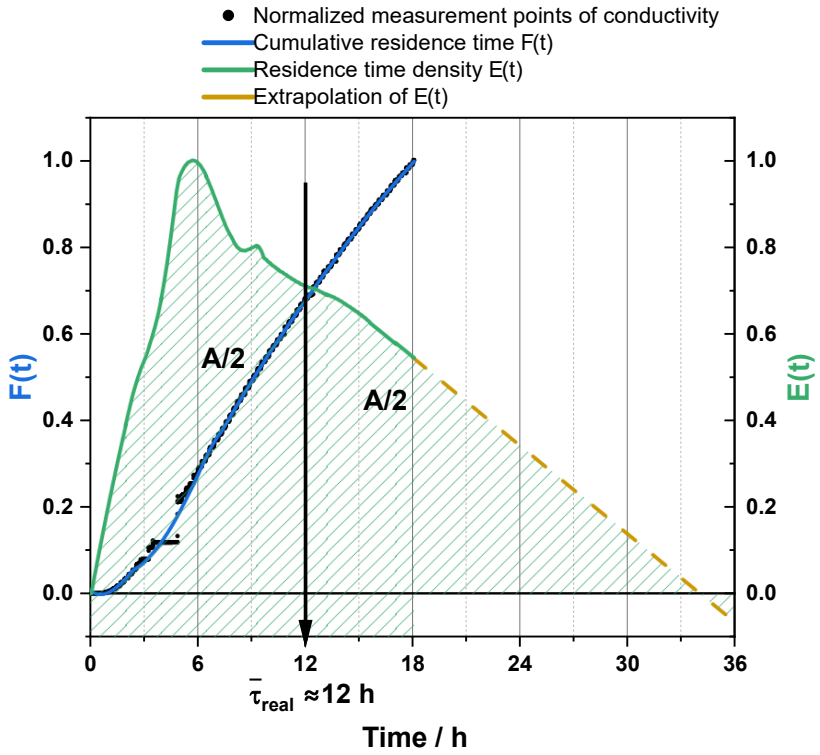

Figure 7-39: Determination of reactor residence time by plotted, normalized electrical conductivity over time. Change of conductivity was induced by step experiment with a potassium chloride solution.

Due to technical limitations, conductivity measurements were halted at 18 hours. Consequently, the E(t) curve was linearly extrapolated to zero. Integration of E(t), with its area divided into two equal halves, resulted in an estimated residence time of approx. 12 hours. While this value is lower than the theoretical expectation, it is likely an underestimate due to the typically near-asymptotic nature of E(t), which suggests additional long-tail residence time contributions. Nevertheless, the feed flow rate was not adjusted at this point and remains an open parameter for subsequent optimization studies.

With the continuous plant fully constructed and commissioned, the next phase involved continuous lignin depolymerization, discussed in the following section.

7.4.3 Continuous depolymerization of lignin to monoaromatic compounds

In this chapter the procedure and results of the continuous lignin depolymerization experiments will be discussed. The process parameters selected for the initial experiments are shown in **Table 7-21** which were determined in section **7.2.8**.

Table 7-21: Process parameters for continuous depolymerisation of technical lignins in Setup 3.

Reaction parameter	**Parameter value**	**Details**
Plant setup		Setup 3
Feed volume flow rate	0.365 mL/min	
Reaction partial pressure	22-23 bar	Oxygen (14 bar at room temp.)
Gas phase flow rate	50 NmL/min	
Temperature	160 °C	
Stirring	100 rpm	
Solvent		MeOH/H_2O (8:2 v/v)
Substrate concentration	50 mg/mL (during pretreatment)	1. Kraft lignin S19 2. Sulphite lignin S14 3. Organosolv lignin S1
Catalyst concentration	5 mg/mL	HPMo-Ni_3 ($H_{15}PNi_3Mo_9O_{40}$)

The required lignin pretreatment, described in section **7.4.1.1,** is not part of the continuous plant. For this reason, this process step is considered and discussed separately in the next section.

7.4.3.1 Selection and pretreatment of lignin feedstocks

Selection of lignin feedstocks

For the continuous experiments, multiple lignin feedstocks were tested to investigate the influence of lignin characteristics on the continuous depolymerization process. Since all process optimization in this work has been carried out using the organosolv softwood lignin S1, this feedstock unquestionably served as a reference in the continuous trials.

In addition to S1, two other lignin types were included based on their technical and industrial relevance: a kraft lignin and a sulphite lignin. The kraft lignin S19 was selected primarily due to the availability of sufficient sample quantity, making it the only viable candidate from this category. The sulphite softwood lignin S14 was chosen based on its performance in preliminary studies, where it exhibited the highest monoaromatic yields among the tested sulphite lignins (cf. section **7.2.10**).

Pretreatment of lignin feedstocks

As previously described in section **7.4.1.1,** it was decided that a pretreatment of the lignin by solvolysis was conducted to allow a precipitate-free feedstock in the continuous plant. For this step, a separate batch reaction plant consisting of a 2 L Hastelloy reactor was utilized. The pretreatment conditions and procedure are described in section **6.3.1.3** and the lignin solutions are depicted in **Figure 7-40**. All solutions were free of precipitate and specifically for the sulphite lignin the entire lignin sample completely dissolved in the methanol-water-solution prior to pretreatment. This is likely due to the high solubility of sulphite lignin in aqueous solutions. The solvolysis of each lignin was separately conducted before each corresponding continuous experiment to avoid any aging effects.

At this stage, the solvolysis yields were not calculated as the residual lignin solids were not collected and weighed. The monoaromatic yields in Setup 3 still refer to the initial solid lignin mass, however. Prospectively, these solvolysis yields are of importance for further upscaling and techno-economic analysis, though. Following the pretreatment, the continuous experiments were consecutively conducted starting with the kraft lignin S19, as discussed in the next section.

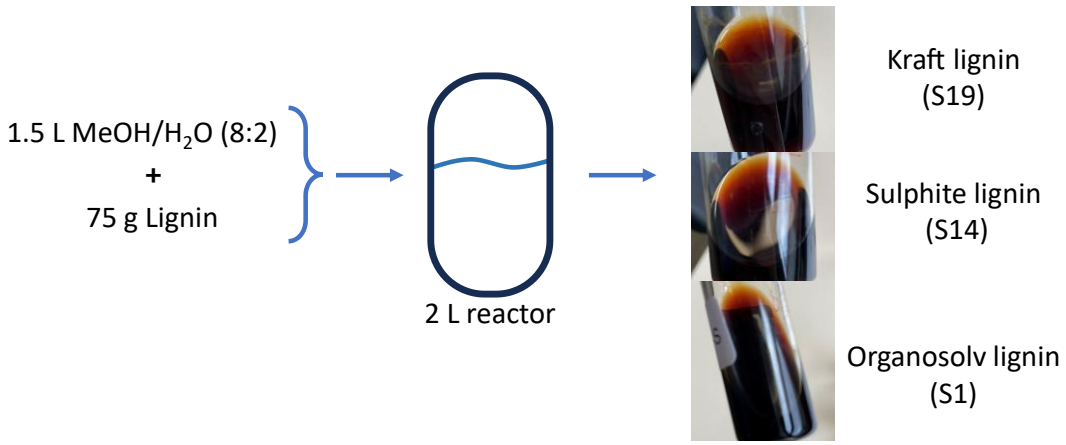

Figure 7-40: Representation of lignin pretreatment by solvolysis and the resulting solutions for lignins S19, S14, and S1. MeOH stands for methanol and H_2O for desalted water.

7.4.3.2 Continuous depolymerisation of kraft lignin (S19)

Besides the lignin feedstock container, the reactor itself was also filled with the particle-free pretreatment solution of lignin S19 to allow reaching steady-state faster. Once everything else was prepared, the reactor heating and stirrer were switched on and upon reaching the desired temperature, all feed pumps were switched on – for more details on experimental procedure, compare to section **6.3.1.3**.

For a measure of process stability, the reactor pressure curve is plotted over the reaction time in **Figure 7-41**. As can be seen, the reactor reached operating pressure after 30 minutes and showed stable behaviour until approx. 4 hours. From then on, the pressure relief system showed significant hiccups. Especially at 6 hours, the pressure increased to 27 bar and decreased to 20 bar after relief. Thereafter, the pressure curve showed more stable behaviour. However, at 7 hours reaction time the reaction was stopped due to clogging at the membrane module HPLC pump which will be discussed later.

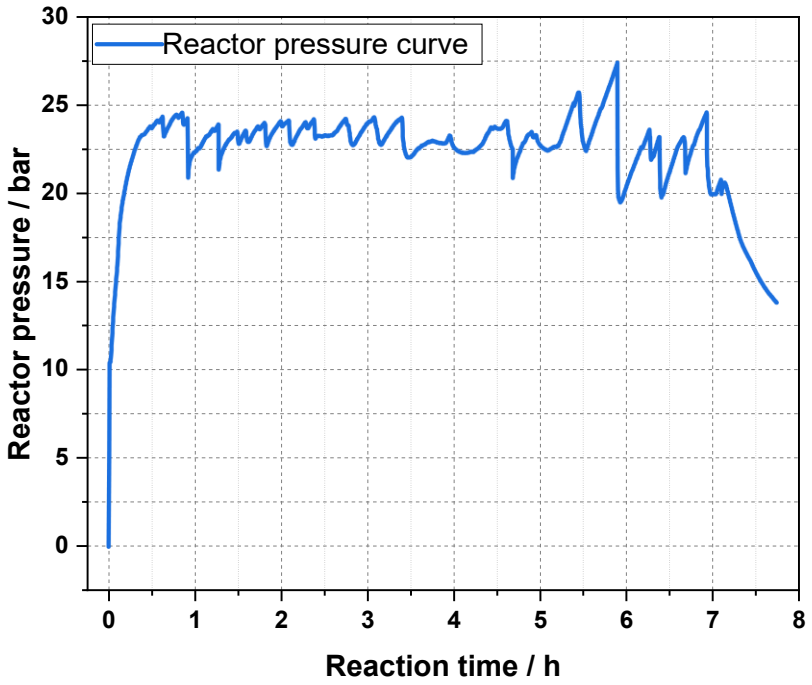

Figure 7-41: Reactor pressure curve during the first experiment of continuous depolymerisation of kraft lignin S19.

At approx. 6 hours, permeate and retentate samples were taken of the membrane module. Sample volume and sampling time were recorded, catalyst and monoaromatic concentration were determined by ICP-OES and GC-MS, respectively. The results are shown in **Table 7-22**

and compared to the isolated experiment reference from section **7.3.2**. As can be clearly seen, the performance of the membrane module is significantly worse indicated by the reduced permeate flow rate, catalyst rejection and monoaromatic permeability. The reason for this likely is the clogging of the suction side of the membrane module feed pump leading to inconsistent module pressure and flow rates. This is also indicated by the deviation of membrane module feed flow rate being 15.6 mL/min (sum of permeate and retentate flow rate) as opposed to the set flow rate of 15 mL/min.

Table 7-22: Results of membrane separation performance and overall monoaromatic yield during continuous depolymerisation of kraft lignin S19. Samples were taken at approx. 6 h reaction time. Reference refers to experiments from section **7.3.2**.

	Membrane flow rates / mL/min	**Catalyst rejection / wt.-%**	**Separation factor monoaromatics / wt.-%**	**Monoaromatic yield / wt.-%**
Permeate	2.5	-	20 %	1.3 %
Retentate	13.1	> 92 %	-	
Reference Permeate	*4.2*	-	*85 %*	*2.6 %*
Reference Retentate	*10.8*	*> 99 %*	-	-

Another performance indicator is the monoaromatic yield shown in the last column. The reference refers to the yield acquired during substrate screening in section **7.2.10** and, thus, with a reaction time of 16 hours. The yield acquired during the continuous experiment being 1.3 wt.-% was obtained after a maximum of 6 hours residence time, so approx. half the yield compared to the batch experiment.

In section **7.2.5** the influence of reaction time on the depolymerisation is discussed. Similarly to the yield results here, the yield at 6 hours is approx. half the amount achieved at the desired reaction time of 16 hours. This potentially means that even though the performance of the membrane separation is impaired, the monoaromatic yield stayed consistent. However, due to the preliminary termination of the reaction due to clogging, only the presented results were acquired.

During workup procedure after the experiment's termination, various photos were taken to show the formed precipitate – these are shown in **Figure 7-42**. As can be clearly seen in photo

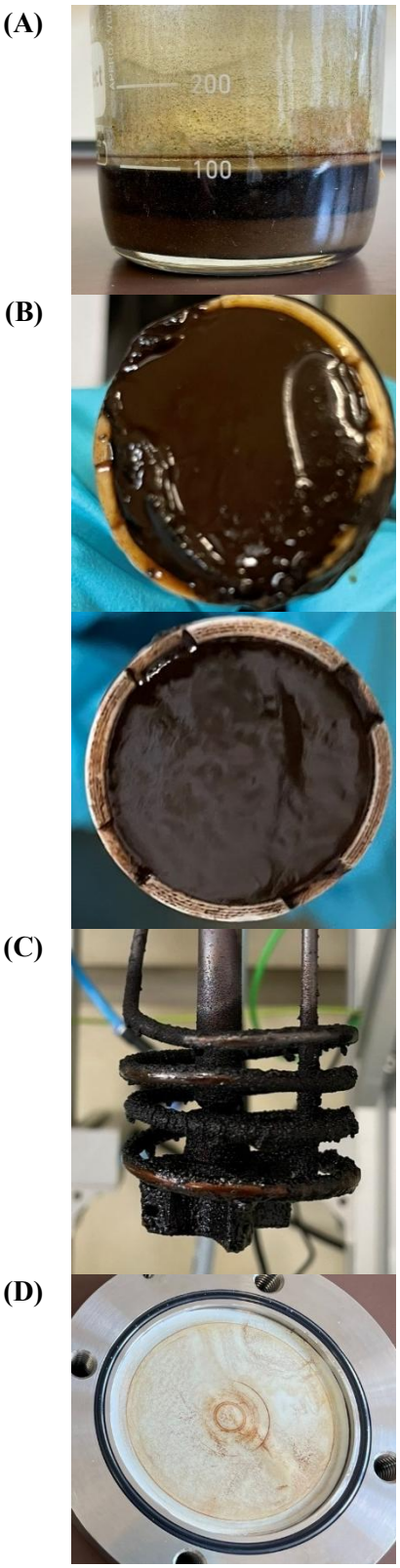

Figure 7-42: Representation of precipitation formed during continuous depolymerisation of kraft lignin S19. (A) shows the liquid product container T4, (B) shows the particle filter of the membrane module inlet side before and after cleaning, (C) shows the stirrer and cooling coil inside the reactor, and (D) the membrane sheet.

(A), a significant amount of precipitate was formed, approx. 50 mL. Due to the suction of the membrane feed pump, notable amounts of solids aggregated on the membrane feed filter as shown in photo (B) with a comparison of the filter being cleaned. The occurred precipitation in this container arises the question for the reason. As this container is not heated and under atmospheric pressure, these aspects could be reasons. Formed oligomers during depolymerisation potentially show soluble behaviour only at elevated temperatures. Additionally, the sudden decrease of pressure in the gas-liquid-separator could lead to an unequal evaporation of methanol and water leading to a change of the solvent system mixture and thus changed solvating properties.

Opening the reactor showed that the precipitation was not limited to the downstream processing, as significant quantities of solids were formed in the reactor, too. This can be seen in photo (C) showing the reactor's cooling coil and gas-entraining stirrer. This finding can have two reasons. First, the chemical system inside the reactor could be altered compared to the dissolved lignin system from section **7.4.3.1** Selection and

pretreatment of lignin feedstocks. A reason for this could be the addition of polyoxometalate catalyst increasing the water fraction due to crystal water and the overall polarity of the solvent. The second reason could be occurring repolymerisation reactions of previously formed oligomers. As no excess precipitation was observed in mixing container T2, the second reason is more likely to be the case. This means that at a temperature of 160 °C, presence of oxygen and a catalyst, the formation of radicals is occurring leading to repolymerisation, as no solids were present in the feed solution, initially. Lastly, photo (D) shows the membrane of the opened membrane module. It clearly shows deposition of solid particles which is another reason for decreasing performance of the membrane besides the clogging of the filter.

Overall, this experiment showed that the continuous depolymerisation is fundamentally possible. However, due to the formation of precipitate, clogging of filters occurred leading to the termination of the experiment. The question arises if by the utilization of another lignin type, which shows higher solubility, the formation of precipitate can be prevented. For this reason, the sulphite lignin S14 was selected for the second run of the continuous plant which will be discussed in the next section.

7.4.3.3 Continuous depolymerisation of sulphite lignin (S14)

The experimental procedure for the continuous depolymerisation of sulphite lignin S14 was identical to that used for kraft lignin S19, as detailed in section **6.3.1.3.** As in the kraft lignin experiments, reactor pressure was continuously monitored to provide process oversight and control – the profile is shown, in **Figure 7-43**.

At the start of the reaction, both temperature and pressure increased steadily to the target values. After approx. 30 minutes, the system reached a pressure of 23.5 bar, triggering the relief valve and initiating the intended pressure regulation cycle. This cycle remained relatively stable for the next 11 hours. During this period, several samples were collected for further analysis, as discussed below.

However, after approx. 11 hours of reaction time, an undesired stagnation in pressure was observed. This irregularity went unnoticed until the 23-hour mark, as it occurred during the night when the laboratory was unattended. Around 23 hours into the reaction, the anomaly was identified and monitored, but no effluent was observed exiting the reactor during the subsequent hour as the feed pump repeatedly switched off. Consequently, the experiment was terminated after a total reaction time of 24 hours.

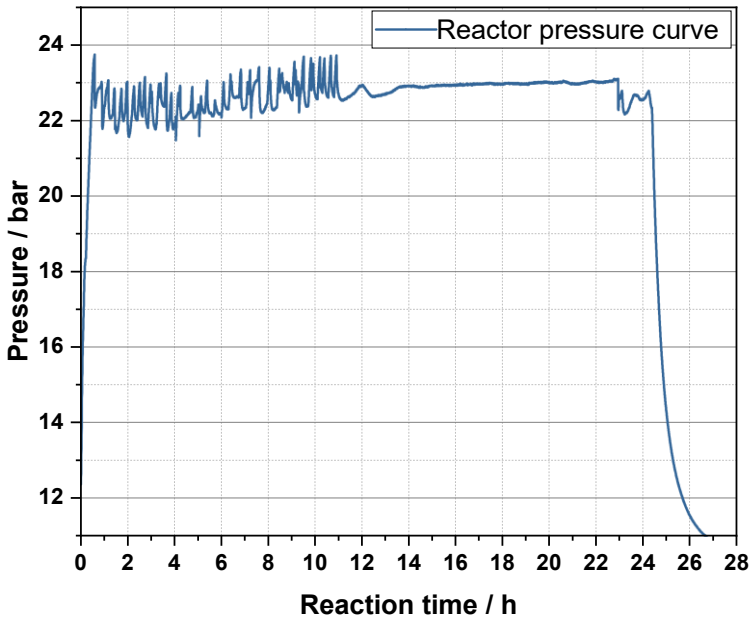

Figure 7-43: Reactor pressure curve during the continuous depolymerisation of sulphite lignin S14 over reaction time.

In **Figure 7-44**, the previously mentioned samples are shown. For the first sample, taken at one hour, only the permeate is shown as at this stage the membrane cell only contained the pure methanol water mixture. This is because these membranes require being wet at all times to allow membrane swelling, necessary to achieve the desired separation performance. As a result, both permeate and retentate samples at one hour showed no reaction products. As can be seen, the colour of the samples 2-5 is then changed from the first sample. The brown opaque colour of the retentate samples resembles the colour of the reaction solutions acquired after batch experiments. The lighter and transparent colour of the permeate has not been seen so far. This difference in colour clearly indicates a varying composition of dissolved compounds and potentially even shows that smaller sized compounds exhibit lighter colours.

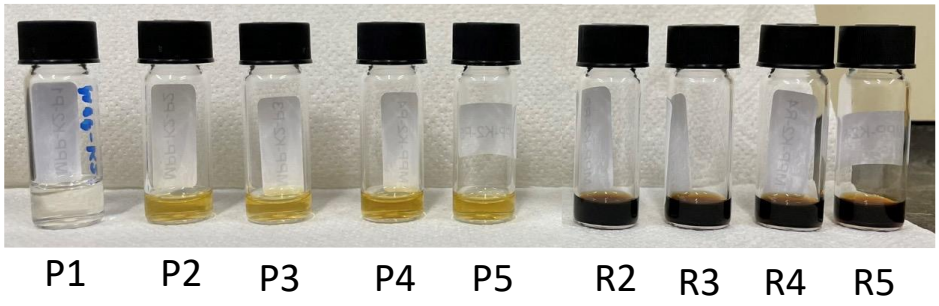

Figure 7-44: Photo of the permeate (P) and retentate (R) samples taken during continuous depolymerisation of sulphite lignin S14. Samples were taken at approx. 1; 3.5; 4.5; 7; 9 hours, respectively.

During sample collection, the flow rates of permeate and retentate were recorded and the catalyst concentrations were measured to calculate rejection. These results are shown in **Figure 7-45**. The catalyst rejection (in blue) showed constant and high values of approx. 98-99 % throughout the entire run which is an improvement to the depolymerisation of kraft lignin.
Until clogging (around 11 hours) the retentate flow rate stayed consistent in contrast to the permeate flow rate which continuously decreased over the first 9 hours which is a sign for deposition on the membrane sheet inhibiting the diffusion through the membrane. After clogging, one additional sample was taken at 23 hours at which the catalyst rejection stayed consistent. However, both permeate and retentate flow rate decreased indicating a reduced pump performance which might again be due to deposition on the pump suction filter. These hypotheses will be later checked during workup procedure of the plant.

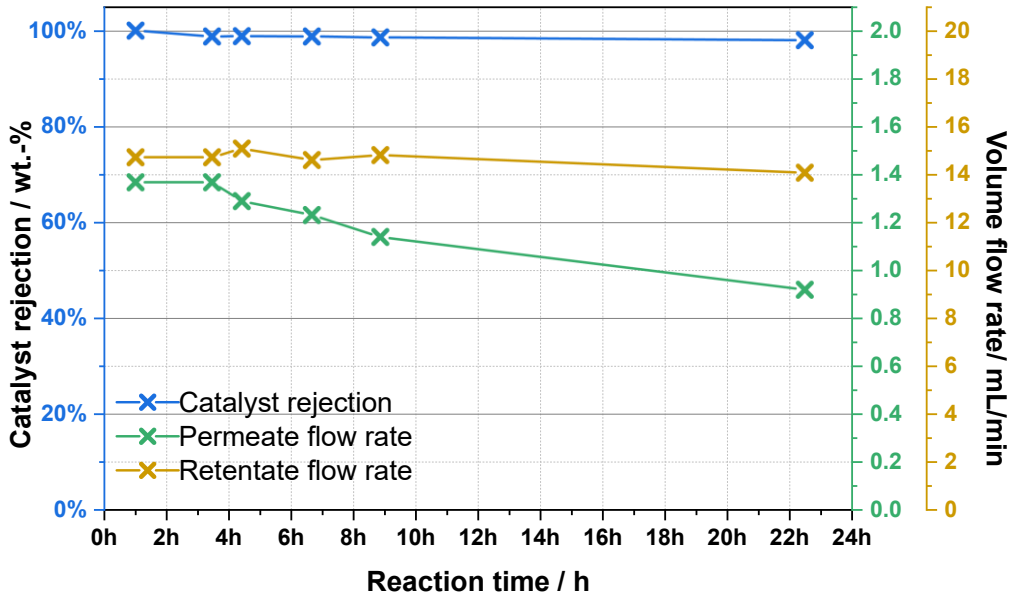

Figure 7-45: Membrane separation performance for catalyst rejection, permeate and retentate flow rate over course of reaction time during continuous depolymerisation of sulphite lignin (S14).

First, the permeate samples were measured and quantified for reaction products. In contrast to the expected monoaromatic yield of approx. 3 wt.-%, discussed in section **7.2.10**, no monoaromatics were found in these permeate samples at all. This either means that the selected reaction conditions, specifically the reaction/residence time, were too moderate to sufficiently depolymerize the lignin, or that the selected conditions were too harsh leading to premature degradation of the monoaromatics. Speaking for too moderate conditions is the expected elevated molecular weight distribution of sulphite lignins in comparison to other lignin types,

as discussed in section **7.1.3**. Molecular weight distribution On the other hand, the presence of smaller-sized compounds such as formic or acetic acid and their derivatives, as shown in **Figure 7-46**, speak for too harsh depolymerisation.

As can be seen, the concentrations of both methyl formate and methyl acetate (neglecting the first measurement point) consistently increase throughout the first 9 hours. These compounds are formed through the esterification of the respective acids and the solvent methanol, similarly to the formation of MeVa and MeSy (cf. **Scheme 7-1**).

The approximation of the respective permeate and retentate concentrations between 9 and 23 hours is likely the result of diffusion and, thus, concentration balance as the membrane module was not active in this time. Due to this, the compounds naturally diffused through the membrane according to the concentration gradient.

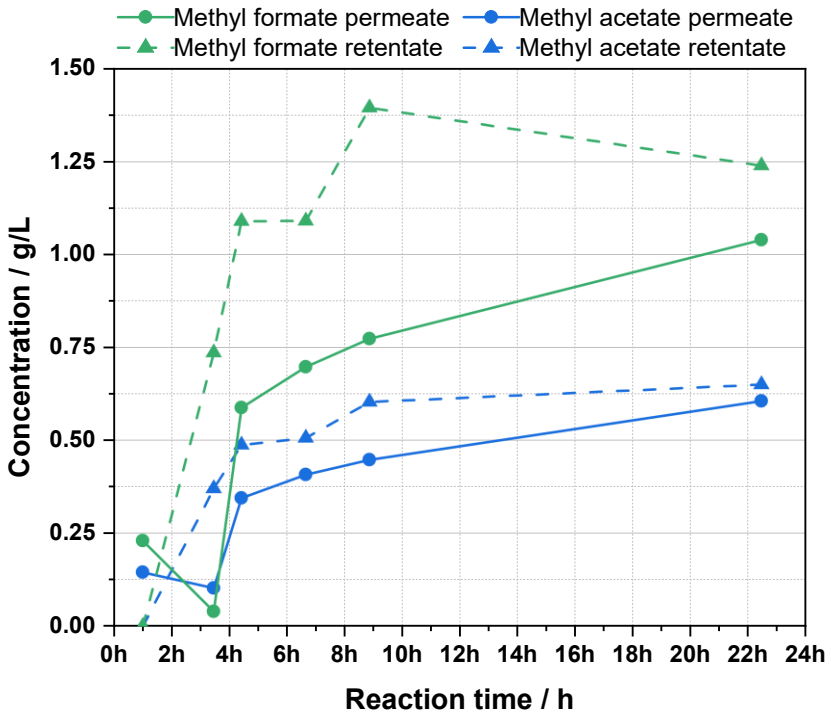

Figure 7-46: Course of concentrations for methyl formate and methyl acetate over reaction time during continuous depolymerisation of sulphite lignin (S14).

Overall, the formation of methyl formate and methyl acetate simply show the oxidative depolymerisation and does not give any insights on why no monoaromatics were found. A potential reason for this, as already described, might be an elevated molecular weight requiring longer residence times for a sufficient depolymerisation. In this experiment however, the sample with the longest residence time in the reactor was at 9 hours, since after 11 hours no new effluent exited the reactor due to inlet clogging. Nonetheless, even at this residence time,

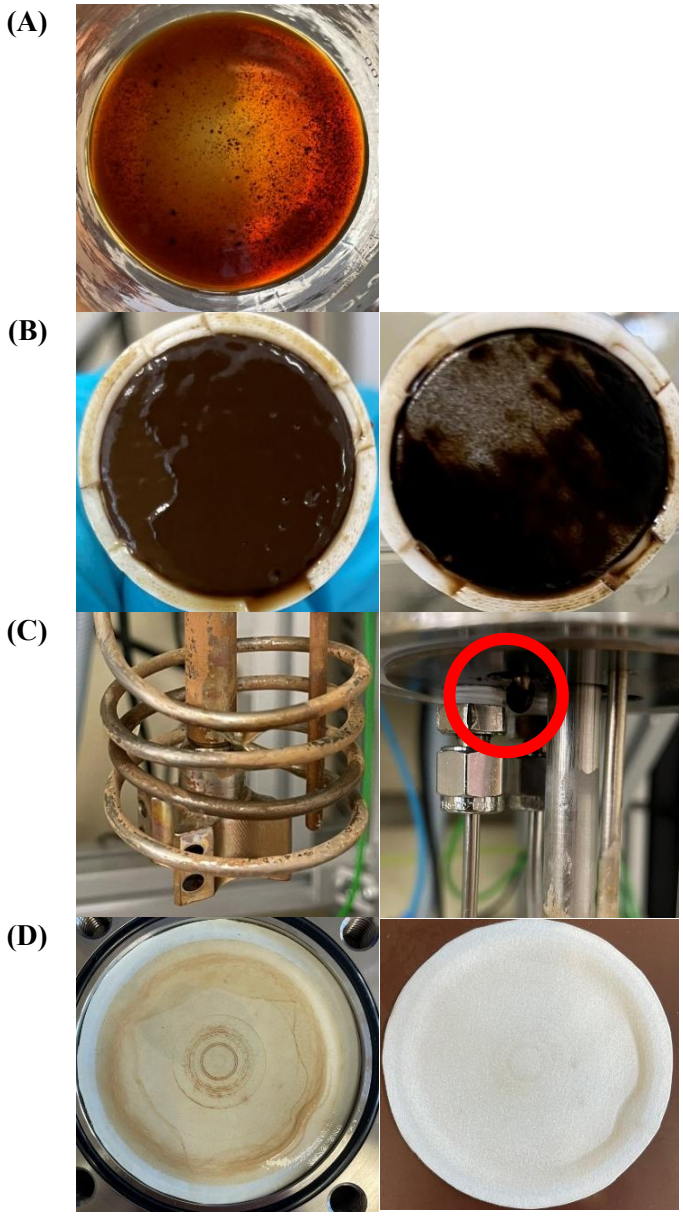

Figure 7-47: Representation of precipitation formed during continuous depolymerisation of sulphite lignin S14. (A) shows the liquid product container T4 from above, (B) shows the particle filter of the membrane module before and during cleaning, (C) shows the stirrer and cooling coil, and the liquid feed inlet inside the reactor, and (D) the membrane sheet, left retentate side, right permeate side.

monoaromatics should already be detectable. So, it was not possible to find a clear reason at this stage.

During the workup and cleaning procedure of the reactor, again various photos were taken and are shown in **Figure 7-47**. In photo (A) it can be seen that even though the sulphite lignin appeared to be entirely soluble, precipitate has been formed in the liquid effluent container T4. As to be expected, some of this precipitate deposited on the particle filter of the membrane module's suction side, as shown in photo (B). In this instance, however, there was significantly less deposit, especially considering the elevated reaction time compared to the kraft lignin experiment. This precipitate was soluble in water contrary to the kraft lignin deposit, as expected. [234,235] Potentially, this deposit only formed after a certain dwell time (e.g. because of the reduced temperature in container T4) which would then lead to the deposition on the filter and reduced overall membrane flow rate as suggested by **Figure 7-45**.

The stirrer, cooling coil and liquid feed inlet are shown in photo (C). Compared to the first experiment, there is significantly less precipitate formed during this reaction. However, as indicated by the red circle a plug was formed at the tip of the reactor feed inlet. This plug led to a pressure increase of the feed pump reaching 100 bar leading to an emergency shutdown. This pump shutdown was the reason why no further liquid feed was pumped into the reactor,

leading to no liquid effluent exiting the reactor and subsequently to the stagnant pressure curve after 9 hours. Basically, only oxygen entered the reactor which immediately left it through the relief valve.
The membrane's retentate and permeate side are shown in photo (D), left and right respectively. As can be clearly seen, precipitate only deposited on the retentate side. This deposition might be the reason for the continuously decreasing permeate flow rate while the retentate flow rate stayed constant, at least for the first 9 hours (cf. **Figure 7-45**). Contrary to the kraft lignin experiment and unexpectedly, this membrane sheet was not cleanable as the deposit did not show solubility in water, acetone or ethanol. As other precipitate did show this solubility, this suggests that these particles deposited deep inside the membrane, potentially even formed inside the membrane through the change of properties in the solvent. These properties could include the change of methanol-water-ratio, of polarity through catalyst rejection, or of other organic compounds.

In summary, the continuous depolymerisation of the sulphite lignin S14 started to be more promising due to high solubility of the lignin in the solvent system. Unfortunately, the reason for the experiment's termination is again precipitation – this time however, in the feed inlet. Additionally, the depolymerisation towards the monoaromatics was not observable entirely. The formation of smaller compounds such as methyl formate and methyl acetate was observed, however. Lastly, the membrane suffered severe fouling likely caused by precipitation inside the membrane.
Prospectively, the feed inlet pipe should be increased in diameter to prevent such clogging. In this reactor setup, this would lead to significantly reduced residence time. Specifically for the sulphite lignin this adjustment could clarify the question of too mild or too severe depolymerisation. Reducing the residence time would result in a milder depolymerisation. If then monoaromatics are found, the initial reaction parameters were too severe.
In the next section, the depolymerisation of the organosolv lignin will be discussed.

7.4.3.4 Continuous depolymerisation of organosolv lignin (S1)

Again, the experimental procedure of the continuous depolymerisation of organosolv lignin (S1) was identical to that of the two previous depolymerisations. This was done to acquire an improved understanding of the behaviour of different technical lignins. Similarly, the pressure curve of the reactor is depicted in **Figure 7-48**.

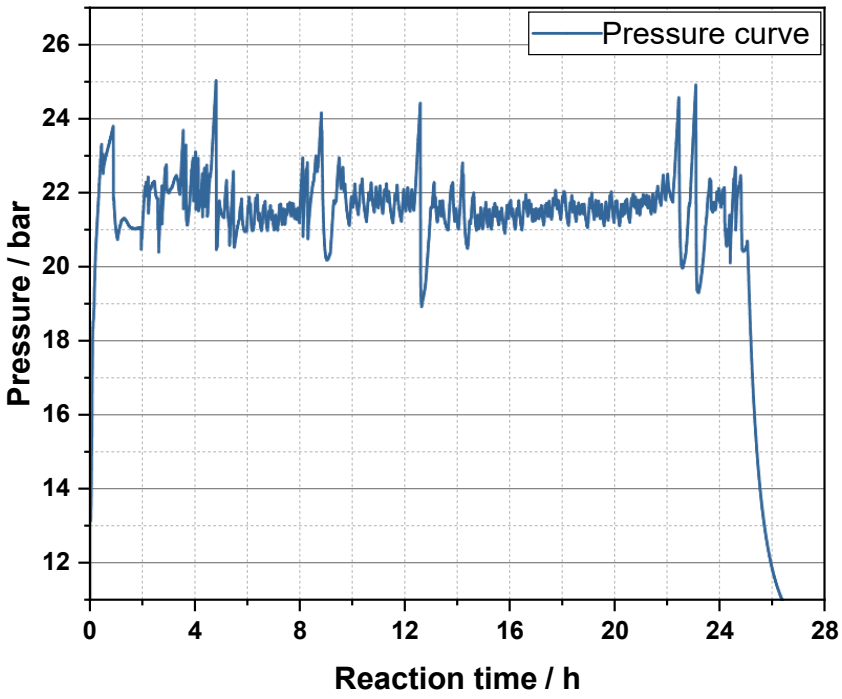

Figure 7-48: Reactor pressure curve during the continuous depolymerisation of organosolv lignin (S1) over reaction time.

As can be seen, the reactor reached process pressure after around 30 minutes. Besides some irregularities every few hours, the pressure stayed rather constant between 21 and 23 bar. These irregularities, meaning the occasional pressure increases, could already be a sign for precipitation in the reactor and clogging of the effluent pipe. Throughout the pressure increase, the pipe might be dislodged returning to the normal pressure curve behaviour, afterwards. Because of technical issues the experiment was terminated at approx. 26 hours which will be discussed later in this section.

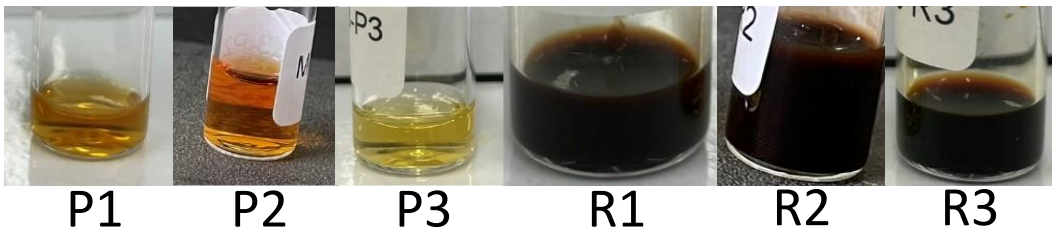

Figure 7-49: Photo of the permeate (P) and retentate (R) samples taken during continuous depolymerisation of organosolv lignin S16. Samples were taken at 4.2, 8.4, and 23.1 hours, respectively.

Throughout the experiment, three retentate and permeate samples were taken from the membrane module after approx. 4, 8 and 23 hours which are shown in **Figure 7-49**. The retentate samples R1 – R3 show uniform colour and are comparable to both the retentate

samples from previous depolymerisations and the liquid feedstock which suggests that the retentate majorly contains large oligomeric compounds. On the other hand, the permeate samples show unexpected course of appearances. The first sample (P1) shows a dark yellow colour, the second sample (P2) is then changing the colour to a darker, reddish tone, and lastly, the third sample (P3) is still transparent, however, shows a lighter yellow than the first sample. As the presence of colour and its intensity is a sign of conjugated electron systems (including aromatic compounds), darker colours suggest higher concentrations of aromatics compounds in this case. [236] This would mean that from P1 to P2 the concentration of aromatic compounds increased, and from P2 to P3 decreased again. As the catalyst itself also emits a colour, which typically is green, its presence might also have an influence. For this reason, the performance of the membrane module is depicted in **Figure 7-50**.

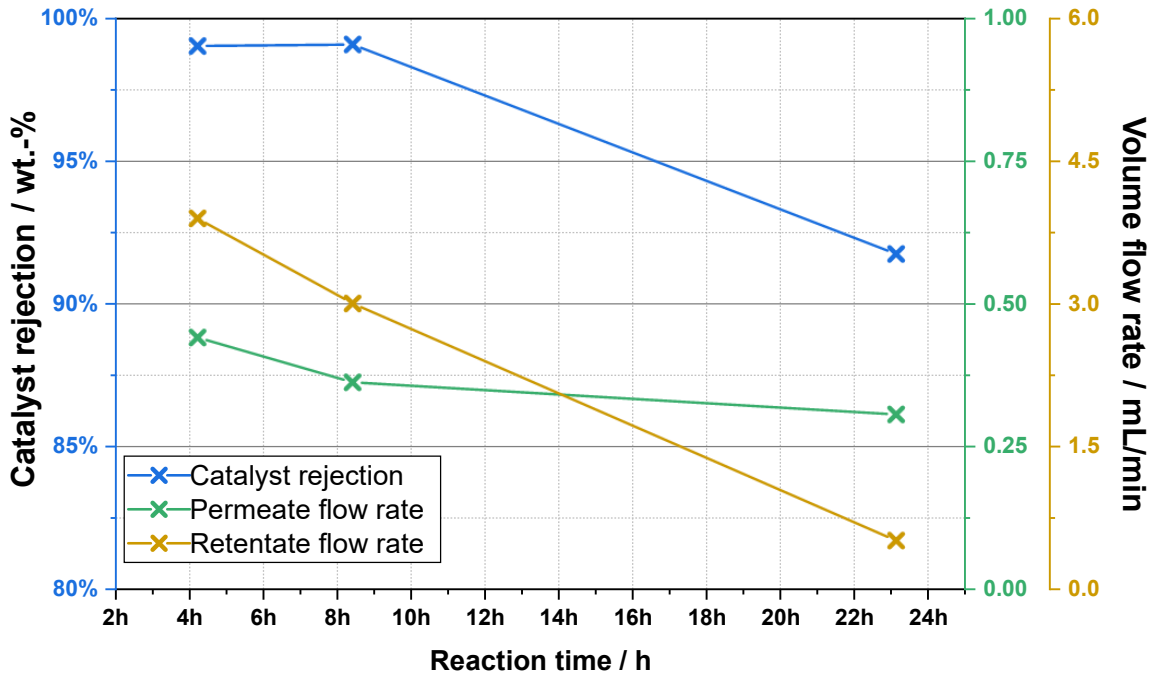

Figure 7-50: Membrane separation performance for catalyst rejection, permeate and retentate flow rate over course of reaction time during continuous depolymerisation of organosolv lignin (S1)

The catalyst rejection, shown in blue, stayed consistent with results of the membrane screening for the first two samples being >99 %, but then significantly decreased to approx. 92 % at 23 hours. This means that in permeate sample P3, a significantly larger amount of catalyst was present. Overall, previous experiments showed that reaction solutions are still active when catalyst is present. This could explain the change of colour for P3, as the catalyst might continue to depolymerize aromatic and/or oligomeric compounds.

Besides this, **Figure 7-50** shows the volume flow rate of permeate and retentate in green and yellow, respectively. Already during the first sample, the overall flow rate (in sum approx. 5 mL/min) was significantly lower than the set flow rate of 15 mL/min and continued to decrease throughout the course of the reaction. This again indicates the clogging of the particle filter on the pump suction side, which will be picked up later in this section.

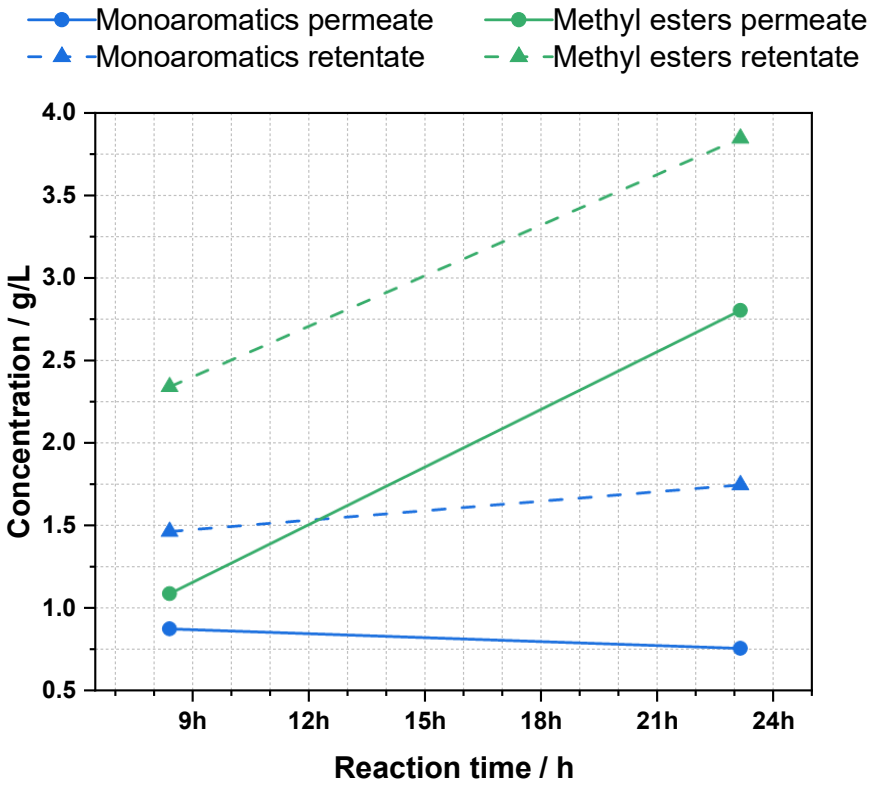

Figure 7-51: Course of concentrations for the monoaromatics (Va, MeVa, Sy, MeSy) and methyl esters (methyl formate, methyl acetate, dimethyl succinate, dimethyl oxalate) plotted over reaction time during continuous depolymerisation of organosolv lignin (S1).

In **Figure 7-51**, the course of product concentrations in the permeate and retentate is shown at approx. 8 and 23 hours. The concentration of methyl esters expectedly increases with time as these compounds likely will not be degraded any further. This leads to the increase in both permeate and retentate. On the other hand, the monoaromatic's concentration slightly increases in the retentate whereas it slightly decreases in the permeate. A reason for this might be fouling of the membrane caused by deposition of precipitate similarly to the previous experiments. These product concentrations in the respective phase led to the yields shown in **Table 7-23**. While for the methyl esters no separation factor was determined in the batch experiments, the factor for the monoaromatics significantly decreased in the continuous experiment compared to the batch. Similarly, the product yields significantly decrease in the continuous run from 7.5

to 0.8 % for the monoaromatics and from 10.8 to 3.0 % for the methyl esters. As the concentrations in the permeate and retentate are in the same order of magnitude for the desired monoaromatics, the most probable reason for this is an incomplete depolymerisation or repolymerisation in the reactor and the effluent-collecting vessel.

Table 7-23: Comparison of monoaromatics and methyl esters yield for the continuous depolymerisation of organosolv lignin (S1) and the batch run (cf. section **7.2.10**)

	Separation factor / wt.-%		**Product yield / wt.-%**	
	Monoaromatics	Methyl esters	Monoaromatics	Methyl esters
Continuous run	55 %	81 %	0.8 %	3.0 %
*Batch run (*section ***7.2.10****)*	*85 %*	*- (not measured)*	*7.5 %*	*10.8 %*

Potentially, this can be adjusted by varying process temperature, residence time in the reactor, and residence time in the effluent-collecting container T4, as precipitation again was the sole reason for the experiment's termination. Apparently, the particle filter suction side was clogged to such an extent that the HPLC pump (P3) built up a vacuum on the suction side. To prevent any damage on the pump, the experiment was then terminated.

Again, photos were taken during the workup procedure which are shown in **Figure 7-52**. In photo (A) considerable quantities of precipitate can be seen which explains the clogging of the particle filter, depicted in photo (B). As can be seen, a thick layer of solids has deposited on the filter which, retrospectively, led to the blockage of the pump's suction side. After opening the reactor, similar amounts of precipitate were found compared to container T4. This could be an indication for two things. First, the solids formed through repolymerisation induced by the exposure to elevated temperatures and presence of oxygen, or second, the composition of the solvent system changed so that dissolved oligomers were not solubilized anymore leading to precipitation. As in the mixing container T2, no solids were observed, the addition of catalyst did not lead to the necessary change of polarity to induce precipitation. On the other hand,

Figure 7-52: Representation of precipitation formed during continuous depolymerisation of organosolv lignin S1. (A) shows the liquid product container T4 from above, (B) shows the particle filter of the membrane module before cleaning, (C) shows the stirrer and cooling coil inside the reactor, and (D) the membrane sheet, top retentate side, bottom permeate side.

continuously withdrawing the gas phase through the relief valve might change the ratio of methanol and water, as methanol shows a significantly increased vapor pressure at process temperature. A clear explanation was not found, and further studies would be necessary. In photos (C), again the precipitation on reactor's stirrer and cooling coil is shown. Additionally, in photo (D) quite high deposition of precipitate on the membrane sheet can be seen on both retentate and permeate side.

The continuous depolymerisation of the softwood organosolv lignin (S1) was only moderately successful. It was shown that the continuous setup works. Monoaromatics were formed and subsequently separated from the reaction mixture, and the catalyst was recycled to the reactor. However, the performance of the membrane and the overall yields are significantly reduced to the reference batch experiments. Additionally, the formation of solids again was an issue and ultimately led to the termination of the experiment.

At this stage, the project came to an end which is the reason why no further experiments or further studies regarding the solubility of lignin and its degradation products were conducted. In the next section, the findings of the continuous experiments will be summarized for prospective follow-up projects.

7.4.4 Prospective improvements of the continuous setup

Frankly, the continuous experiments all suffered of the formation of solid particles which led to the clogging of inlet or effluent pipes, or the particle filters. This precipitation occurred independently on lignin type, even though the selected types (kraft, sulphite, and organosolv) show extremely varying solubility behaviour.

For all three lignins, solid particles deposited on the particle filter in container T4 to higher and lower extents. As the opening of the effluent pipe is at the surface level of the reactor's fluid content, entraining of solid particle formed in the reactor is unlikely. This leads to the conclusion, that the precipitation takes place inside container T4. To prevent this, various setup improvements could be applied. First, the residence time of the effluent inside container T4 could be reduced by e.g. reducing the total volume or adjusting the membrane module setup to convey continuously instead of repeatedly. Second, applying an inert gas phase in the container to ensure the absence of oxygen which likely facilitates repolymerisation and subsequently precipitation. And third, applying a container heating to increase the solubility of any dissolved compounds. Overall, a pipe heating system could further limit any precipitation.

As for all lignins precipitation formed inside the reactor as well, a few potential adjustments are proposed. First, reducing the process temperature likely results in reduced formation of solids. On the other side, higher temperatures resulted in higher yields, as observed in section **7.2.8**. A balance between these two factors must be found, then. Second, to further inhibit repolymerisation, additives could be added that act as radical scavengers, as suggested by *Dizhbite* et al., and *Rusdipoetra* et al. [237,238] Lastly, to prevent clogging of the inlet pipe, the mixing container T2 could be omitted and the lignin feed and catalyst recycling stream could directly go into the reactor. To further understand the precipitation, the formed solids could be examined, in the context of its solubility in varying solvents, temperatures and catalyst concentrations.

With these suggestions the continuous plant could be improved in a follow-up project for the depolymerisation of lignin. This brings the section **7.4** and the continuous depolymerisation of lignin to an end. In the next chapter, a concise outlook including these and the findings of the previous chapters will be given.

8. Conclusion and Outlook

Conclusion

In the first part of the study, the reaction system was established by systematically evaluating different lignin types, catalysts, solvents, and reaction conditions. The most critical parameters influencing product yields were the lignin feedstock and the POM catalyst. While monoaromatic yields ranged from 2 to 8 wt.-% depending on the catalyst, the type of lignin caused an even broader range from 0.5 to 8 wt.-%. These findings underscore the importance of feedstock-specific process design, with organosolv lignins demonstrating the most compatibility. It was shown that yield optimization is possible through the adjustment of process parameters such as reaction temperature, residence time, and substrate-to-catalyst ratio. Overall, this section has established a robust chemical framework and identified the most impactful parameters to guide future process adaptation for various lignin types.

The second part focused on downstream processing, particularly the separation of products and catalysts. Both solvent extraction and membrane separation were explored. Extraction yields declined significantly when moving from stock to real reaction solutions, primarily due to the influence of catalysts and product compounds on polarity and phase behaviour – sometimes preventing phase separation entirely. Toluene, for example, caused precipitation, while ethyl acetate proved to be the most viable solvent. However, due to the co-extraction of oligomeric intermediates, which could otherwise be further converted into monoaromatics, membrane separation was pursued as an alternative. The PuraMem membranes from *Evonik* exhibited methanol impermeability, but among those that were suitable, membrane separation demonstrated superior performance, with separation factors nearly twice those of extraction. Consequently, membrane separation was selected as the preferred downstream processing method with the NADIR membrane by *Mann+Hummel*.

In the third part, knowledge was gained regarding the implementation of a continuous process. Contrary to expectations, kraft lignin yielded higher monoaromatic outputs than organosolv lignin. While kraft lignin achieved approx. 50 % of the yield of the batch process, organosolv lignin just reached 10 %. The cause remains unclear, but residence time and membrane clogging likely played a role. All lignin types tested caused varying degrees of precipitation, resulting in clogging of pipes and filters, and ultimately in the termination of the experiments. Both kraft and organosolv lignins exhibited substantial solids formation, while sulphite lignin produced

considerably less, showing the increased solubility in aqueous systems. However, even sulphite lignin led to clogging, particularly at the reactor inlet. While sulphite lignin presented the best technical compatibility, its lower conversion efficiency limits its potential. These findings reinforce the conclusion that each lignin type necessitates specific process modifications to achieve optimal performance and avoid operational issues such as precipitation.

Outlook

The continuous process demonstrated technical feasibility but requires significant refinement, particularly in mitigating precipitation. Given the differences in solubility and behaviour among lignin types, future work should consider optimizing the process for a single, widely available lignin source. Kraft lignin or hydrolysis lignin would be promising candidates – kraft as it is the predominant process type in pulping industry, and hydrolysis lignin due to its increasing availability from the growing bioethanol market. [239]

From a technical standpoint, preventing precipitation on the membrane module's particle filter is essential. Measures such as container stirring, container heating, or even complete pipe heating should be investigated. In the case of kraft lignin, substantial reactor precipitation suggests a possible need to revise the chemical system, possibly through the addition of free-radical scavengers. These additives, however, must remain chemically inert to avoid unintended consumption and operating cost increases.

Beyond technical adjustments, a techno-economic assessment comparing batch and continuous processes should be undertaken to evaluate economic feasibility. This will provide crucial insights into whether a continuous setup offers genuine advantages over batch operations.

In conclusion, while the core concept has been validated, further work is required to address operational challenges and confirm the economic viability of scaling the process for industrial application.

A. Bibliography

[1] M. Elsner, G. Atkinson, S. Zahidi, *Global Risks Report 2025* **2025**.

[2] M. Grömling, H. Bardt, M. Beznoska, M. Demary, R. Henger, T. Hentze, M. Hüther, T. Obst, J. Pimpertz, H. Schäfer, S. Seele, *Konjunktur im Desorientierungsstress: IW-Konjunkturprognose Frühjahr 2025*, Cologne/Berlin **2025**.

[3] T. Grothmann, P. Ruppel, C. Harms, G. Reese, *Die mentalen Auswirkungen des Klimawandels und die Bereitschaft zur Anpassung*, Umweltbundesamt **2025**.

[4] REN21 Renewable Energy Policy Network for the 21st Century, *REN21 Renewables 2011 Global Status Report* **2011**.

[5] F. J. Richter, *Mineralöl in Deutschland*, Berlin **2015**.

[6] S. Oltulular, *Energy Strategy Reviews* **2024**, *53*, 101386. DOI: 10.1016/j.esr.2024.101386.

[7] J. Laherrère, C. A. Hall, R. Bentley, *Current Research in Environmental Sustainability* **2022**, *4*, 100174. DOI: 10.1016/j.crsust.2022.100174.

[8] *Valorization of Biomass to Value-Added Commodities: Current Trends, Challenges, and Future Prospects* (Eds: M.O. Daramola, A.O. Ayeni), 1st ed., Green Energy and Technology, Springer International Publishing; Imprint Springer, Cham **2020**.

[9] J. Harrandt, M. Carus, C. vom Berg, *Evaluation of Recent Reports on the Future of a Net-Zero Chemical Industry in 2050*, Renewable Carbon Initiative (RCI) **2024**.

[10] Paul Münnich, Julian Somers, Julia Metz, Utz Tillmann, Camilla Oliveira, Ronja Hermanns, Aline Kalousdian, Raoul Meys, André Bardow, Benedikt Winter, *Chemicals in transition: The three pillars for transforming chemical value chains* **2023**.

[11] A. Behr, T. Seidensticker, *Chemistry of Renewables*, Springer Berlin Heidelberg, Berlin, Heidelberg **2020**.

[12] M. Kaltschmitt, H. Hartmann, H. Hofbauer, *Energie aus Biomasse*, Springer Berlin Heidelberg, Berlin, Heidelberg **2016**.

[13] D. S. Bajwa, G. Pourhashem, A. H. Ullah, S. G. Bajwa, *Industrial Crops and Products* **2019**, *139*, 111526. DOI: 10.1016/j.indcrop.2019.111526.

[14] A. Behr, D. W. Agar, J. Jörissen, A. J. Vorholt, *Einführung in die Technische Chemie*, Springer Berlin Heidelberg, Berlin, Heidelberg **2016**.

[15] *Kirk-Othmer encyclopedia of chemical technology: Vanillin* (Eds: D. Havkin-Frenkel, A. Seidel, R.E. Kirk, D.F. Othmer), 5th ed., A John Wiley & Sons, Inc., publication, Vol.12, Wiley-Interscience, Hoboken, NJ **2005**.

[16] J. M. Pepper, J. A. MacDonald, *Can. J. Chem.* **1953**, *31 (5)*, 476–483. DOI: 10.1139/v53-064.

[17] W. Schutyser, T. Renders, S. van den Bosch, S.-F. Koelewijn, G. T. Beckham, B. F. Sels, *Chemical Society reviews* **2018**, *47 (3)*, 852–908. DOI: 10.1039/c7cs00566k.

[18] J. Albert, P. Wasserscheid, *Green Chem.* **2015**, *17 (12)*, 5164–5171. DOI: 10.1039/C5GC01474C.

[19] Y. M. Bar-On, R. Phillips, R. Milo, *Proceedings of the National Academy of Sciences of the United States of America* **2018**, *115 (25)*, 6506–6511. DOI: 10.1073/pnas.1711842115.

[20] S. V. Vassilev, D. Baxter, L. K. Andersen, C. G. Vassileva, T. J. Morgan, *Fuel* **2012**, *94*, 1–33. DOI: 10.1016/j.fuel.2011.09.030.

[21] R. C. Saxena, D. K. Adhikari, H. B. Goyal, *Renewable and Sustainable Energy Reviews* **2009**, *13 (1)*, 167–178. DOI: 10.1016/j.rser.2007.07.011.

[22] G. Döring, G. Renger, J. Vater, H. T. Witt, *Zeitschrift fur Naturforschung. Teil B, Chemie, Biochemie, Biophysik, Biologie und verwandte Gebiete* **1969**, *24 (9)*, 1139–1143. DOI: 10.1515/znb-1969-0911.

[23] A. Stoll, E. Wiedemann, *Fortschr. chem. Forsch.* **1952** *(2)*, 538–608. DOI: 10.1007/BFb0051797.

[24] S. V. Vassilev, D. Baxter, L. K. Andersen, C. G. Vassileva, *Fuel* **2010**, *89 (5)*, 913–933. DOI: 10.1016/j.fuel.2009.10.022.

[25] *Biomass as a sustainable energy source for the future: Fundamentals of conversion processes*, Wiley, Hoboken, New Jersey **2014**.

[26] D. A. Da Silva, E. Eloy, B. O. Caron, P. F. Trugilho, *Floresta Ambient.,* in press. DOI: 10.1590/2179-8087.020116.

[27] S. V. Vassilev, D. Baxter, L. K. Andersen, C. G. Vassileva, T. J. Morgan, *Fuel* **2012**, *94*, 1–33. DOI: 10.1016/j.fuel.2011.09.030.

[28] I. Urbina, J. Sardans, C. Beierkuhnlein, A. Jentsch, S. Backhaus, K. Grant, J. Kreyling, J. Peñuelas, *Environmental and experimental botany* **2015**, *111*, 63–73. DOI: 10.1016/j.envexpbot.2014.10.005.

[29] L. León-Sánchez, E. Nicolás, I. Prieto, P. Nortes, F. T. Maestre, J. I. Querejeta, *Journal of Ecology* **2020**, *108 (1)*, 47–60. DOI: 10.1111/1365-2745.13259.

[30] L. Sun, B. Zhang, B. Wang, G. Zhang, W. Zhang, B. Zhang, S. Chang, T. Chen, G. Liu, *Ecological Engineering* **2017**, *106*, 448–457. DOI: 10.1016/j.ecoleng.2017.06.018.

[31] F. W. Lichtenthaler, in *Ullmann's Encyclopedia of Industrial Chemistry*, Wiley-VCH Verlag GmbH & Co. KGaA, Weinheim, Germany **2000**.

[32] *Bioökonomie für Einsteiger* (Ed: J. Pietzsch), Lehrbuch, Springer Spektrum, Berlin **2017**.

[33] K. P. C. Vollhardt, N. E. Schore, *Organische Chemie,* 5th ed., Wiley-VCH-Verlag GmbH & Co. KGaA, Weinheim **2011**.

[34] *Glycoscience: Chemistry and Chemical Biology I-III* (Ed: B.O. Fraser-Reid), Springer, Berlin, Heidelberg **2001**.

[35] J. Cai, Y. He, X. Yu, S. W. Banks, Y. Yang, X. Zhang, Y. Yu, R. Liu, A. V. Bridgwater, *Renewable and Sustainable Energy Reviews* **2017**, *76*, 309–322. DOI: 10.1016/j.rser.2017.03.072.

[36] F. H. Isikgor, C. R. Becer, *Polym. Chem.* **2015**, *6 (25)*, 4497–4559. DOI: 10.1039/C5PY00263J.

[37] A. Yousuf, D. Pirozzi, F. Sannino, in *Lignocellulosic biomass to liquid biofuels* (Eds: A. Yousuf, D. Pirozzi, F. Sannino), Academic Press, London, San Diego, Cambridge, MA, Oxford **2020**.

[38] V. B. Agbor, N. Cicek, R. Sparling, A. Berlin, D. B. Levin, *Biotechnology advances* **2011**, *29 (6)*, 675–685. DOI: 10.1016/j.biotechadv.2011.05.005.

[39] P. Bajpai, *Pretreatment of Lignocellulosic Biomass for Biofuel Production*, Springer Singapore, Singapore **2016**.

[40] S. Moraïs, E. Morag, Y. Barak, D. Goldman, Y. Hadar, R. Lamed, Y. Shoham, D. B. Wilson, E. A. Bayer, *mBio,* in press. DOI: 10.1128/mBio.00508-12.

[41] A. Barakat, H. de Vries, X. Rouau, *Bioresource technology* **2013**, *134*, 362–373. DOI: 10.1016/j.biortech.2013.01.169.

[42] D. M. Alonso, J. Q. Bond, J. A. Dumesic, *Green Chem.* **2010**, *12 (9)*, 1493. DOI: 10.1039/c004654j.

[43] T. Li, S. Takkellapati, *Biofuels, bioproducts & biorefining Biofpr* **2018**, *0*, 1–32. DOI: 10.1002/bbb.1913.

[44] CALVIN WOODINGS, *Kirk-Othmer Encyclopedia of Chemical Technology: Fibers, Regenerated Cellulose,* Wiley online library, Wiley, New York **2013**.

[45] K. A. Chu, S. H. Yalkowsky, *Current drug metabolism* **2009**, *10 (10)*, 1184–1191. DOI: 10.2174/138920009790820110.

[46] H. V. Scheller, P. Ulvskov, *Annual review of plant biology* **2010**, *61*, 263–289. DOI: 10.1146/annurev-arplant-042809-112315.

[47] L. J. Gibson, *Journal of the Royal Society, Interface* **2012**, *9 (76)*, 2749–2766. DOI: 10.1098/rsif.2012.0341.

[48] A. Ebringerová, Z. Hromádková, T. Heinze, in *Polysaccharides I* (Ed: T. Heinze), Advances in Polymer Science, Springer-Verlag, Berlin/Heidelberg **2005**.

[49] J. L. McCarthy, A. Islam, in *Lignin: Historical, Biological, and Materials Perspectives*.

[50] *Pretreatment of Lignocellulosic Biomass for Biofuel Production* (Ed: P. Bajpai), SpringerBriefs in Molecular Science Ser, Springer Singapore, Singapore **2016**.

[51] S. Kumaravel, P. Thiruvengetam, K. Karthick, S. S. Sankar, A. Karmakar, S. Kundu, *Biotechnology progress* **2021**, *37 (2)*, e3111. DOI: 10.1002/btpr.3111.

[52] *Functional materials from lignin: Methods and advances* (Eds: X.J. Loh, D. Kai, Z. Li), Sustainable chemistry series, volume 3, World Scientific, Singapore **2018**.

[53] C. Bonechi, M. Consumi, A. Donati, G. Leone, A. Magnani, G. Tamasi, C. Rossi, in *Bioenergy Systems for the Future*, Elsevier **2017**.

[54] P. Figueiredo, K. Lintinen, J. T. Hirvonen, M. A. Kostiainen, H. A. Santos, *Progress in Materials Science* **2018**, *93*, 233–269. DOI: 10.1016/j.pmatsci.2017.12.001.

[55] J. D. Gargulak, S. E. Lebo, T. J. McNally, in *Kirk-Othmer Encyclopedia of Chemical Technology* (Ed: J. W. &. S. Inc), John Wiley & Sons, Inc, Hoboken, NJ, USA **2000**.

[56] Z. Jin, K. S. Katsumata, T. B. T. Lam, K. Iiyama, *Biopolymers* **2006**, *83 (2)*, 103–110. DOI: 10.1002/bip.20533.

[57] K. Singh, S. Mehra, A. Kumar, *Green Chem* **2022**, *24 (24)*, 9629–9642. DOI: 10.1039/D2GC03207d.

[58] J. A. Okolie, S. Nanda, A. K. Dalai, J. A. Kozinski, *Waste Biomass Valor* **2021**, *12 (5)*, 2145–2169. DOI: 10.1007/s12649-020-01123-0.

[59] S. Sen, S. Patil, D. S. Argyropoulos, *Green Chem.* **2015**, *17 (11)*, 4862–4887. DOI: 10.1039/C5GC01066G.

[60] H. Zhang, S. Fu, Y. Chen, *International journal of biological macromolecules* **2020**, *147*, 607–615. DOI: 10.1016/j.ijbiomac.2020.01.105.

[61] P. Mousavioun, W. Doherty, *Industrial Crops and Products* **2010**, *31 (1)*, 52–58. DOI: 10.1016/j.indcrop.2009.09.001.

[62] J. Ruwoldt, K. Syverud, M. Tanase-Opedal, *Sustainable Chemistry for the Environment* **2024**, *6*, 100102. DOI: 10.1016/j.scenv.2024.100102.

[63] J. Sameni, S. A. Jaffer, M. Sain, *Composites Part A: Applied Science and Manufacturing* **2018**, *115*, 104–111. DOI: 10.1016/j.compositesa.2018.09.016.

[64] C. Inkrod, M. Raita, V. Champreda, N. Laosiripojana, *Bioenerg. Res.* **2018**, *11 (2)*, 277–290. DOI: 10.1007/s12155-018-9895-2.

[65] S. K. Singh, P. L. Dhepe, *Bioresource technology* **2016**, *221*, 310–317. DOI: 10.1016/j.biortech.2016.09.042.

[66] T. Saito, R. H. Brown, M. A. Hunt, D. L. Pickel, J. M. Pickel, J. M. Messman, F. S. Baker, M. Keller, A. K. Naskar, *Green Chem.* **2012**, *14 (12)*, 3295. DOI: 10.1039/c2gc35933b.

[67] A. Eraghi Kazzaz, P. Fatehi, *Industrial Crops and Products* **2020**, *154*, 112732. DOI: 10.1016/j.indcrop.2020.112732.

[68] G. Gellerstedt, G. Henriksson **2008**, 201–224. DOI: 10.1016/B978-0-08-045316-3.X0001-4.

[69] J. Zakzeski, P. C. A. Bruijnincx, A. L. Jongerius, B. M. Weckhuysen, *Chemical reviews* **2010**, *110 (6)*, 3552–3599. DOI: 10.1021/cr900354u.

[70] C. Xu, F. Ferdosian, in *Conversion of Lignin into Bio-Based Chemicals and Materials* (Eds: C. Xu, F. Ferdosian), Green Chemistry and Sustainable Technology, Springer Berlin Heidelberg, Berlin, Heidelberg **2017**.

[71] J. Ruwoldt, M. Tanase Opedal, *Industrial Crops and Products* **2022**, *185*, 115102. DOI: 10.1016/j.indcrop.2022.115102.

[72] *Conversion of Lignin into Bio-Based Chemicals and Materials* (Eds: C. Xu, F. Ferdosian), Green Chemistry and Sustainable Technology, Springer Berlin Heidelberg, Berlin, Heidelberg **2017**.

[73] P. Bajpai, *Paper and board making,* Biermann's handbook of pulp and paper / Pratima Bajpai, consultant pulp & paper, Kanpur, India, volume 2, Elsevier, Amsterdam, Oxford, Cambridge, MA **2018**.

[74] Theodor N. Kleinert *US3585104A*, **1971**.

[75] *Industrial Lignin Production and Applications: Status Quo and Future Directions* (Ed: E.K. Pye), 1st ed., Wiley-VCH, Weinheim, Bergstr **2008**.

[76] Gobley, *Journal de Pharmacie Chimie* **1858** *(34)*, 401–405.

[77] N. J. Walton, M. J. Mayer, A. Narbad, *Phytochemistry* **2003**, *63 (5)*, 505–515. DOI: 10.1016/s0031-9422(03)00149-3.

[78] Hans Evju *US4151207A*, **1979**.

[79] Á. Cabeza Sánchez, O. Trygve Berglihn, E. Ottaviano, T. Rücker, T. Pettersen, B. Wittgens, A. Aliko, L. Gálvez, M. López, *Open Res Europe* **2024**, *4*, 5. DOI: 10.12688/openreseurope.16734.1.

[80] M. B. Hocking, *J. Chem. Educ.* **1997**, *74 (9)*, 1055. DOI: 10.1021/ed074p1055.

[81] A. S. Ranadive, *J. Agric. Food Chem.* **1992**, *40 (10)*, 1922–1924. DOI: 10.1021/jf00022a039.

[82] UN Food and Agriculture Organization, *Vanilla production in 2017* **2017**.

[83] M. Fache, B. Boutevin, S. Caillol, *ACS Sustainable Chem. Eng.* **2016**, *4 (1)*, 35–46. DOI: 10.1021/acssuschemeng.5b01344.

[84] I. Marić, Y. Guo, M. J. L. J. Fürst, K. van Aelst, S. van den Bosch, M. de Simone, L. O. Martins, B. F. Sels, M. W. Fraaije, *Adv Synth Catal* **2023**, *365 (22)*, 3987–3995. DOI: 10.1002/adsc.202300868.

[85] M. Fache, B. Boutevin, S. Caillol, *European Polymer Journal* **2015**, *68*, 488–502. DOI: 10.1016/j.eurpolymj.2015.03.050.

[86] M. Fache, E. Darroman, V. Besse, R. Auvergne, S. Caillol, B. Boutevin, *Green Chem* **2014**, *16 (4)*, 1987–1998. DOI: 10.1039/C3GC42613K.

[87] Franziska Krause, *Dissertation,* University of Hamburg, Hamburg **2011**.

[88] W. Schlemmer, P. Nothdurft, A. Petzold, G. Riess, P. Frühwirt, M. Schmallegger, G. Gescheidt-Demner, R. Fischer, S. A. Freunberger, W. Kern, S. Spirk, *Angewandte Chemie (International ed. in English)* **2020**, *59 (51)*, 22943–22946. DOI: 10.1002/anie.202008253.

[89] K. Elbs, H. Lerch, *J. Prakt. Chem.* **1916**, *93 (1)*, 1–9. DOI: 10.1002/prac.19160930101.

[90] J. Gadamer, *Archiv der Pharmazie* **1897**, *235 (8-9)*, 570–577. DOI: 10.1002/ardp.18972350804.

[91] M. C. Glvez, C. G. Barroso, J. A. Prez-Bustamante, *Z Lebensm Unters Forch* **1994**, *199 (1)*, 29–31. DOI: 10.1007/BF01192948.

[92] M. Jawad, M. Ali, S. Qasim, A. Akbar, N. A. Khan, M. B. Sadiq, *BioMed research international* **2022**, *2022*, 7787958. DOI: 10.1155/2022/7787958.

[93] R. B. Sriprasanthi, M. N. Mohamad Ibrahim, S. Shamsudeen, F. Adam, S. A. Bhawani, *BioRes* **2012**, *7 (3)*, 4377–4399. DOI: 10.15376/biores.7.3.4377-4399.

[94] R.-R. Tian, Q.-H. Pan, J.-C. Zhan, J.-M. Li, S.-B. Wan, Q.-H. Zhang, W.-D. Huang, *Molecules (Basel, Switzerland)* **2009**, *14 (2)*, 827–838. DOI: 10.3390/molecules14020827.

[95] *RÖMPP Online: Syringaldehyd* (Ed: Thieme Gruppe) **2004**.

[96] J. Lee, Y. Li, J.-T. Cheng, I.-M. Liu, K.-C. Cheng, *Pharmaceuticals (Basel, Switzerland),* in press. DOI: 10.3390/ph17040538.

[97] A. Llevot, E. Grau, S. Carlotti, S. Grelier, H. Cramail, *Macromolecular rapid communications* **2016**, *37 (1)*, 9–28. DOI: 10.1002/marc.201500474.

[98] L. Weng, T.-H. Chen, Q. Zheng, W.-H. Weng, L. Huang, D. Lai, Y.-S. Fu, C.-F. Weng, *Biomedicine & pharmacotherapy = Biomedecine & pharmacotherapie* **2021**, *141*, 111865. DOI: 10.1016/j.biopha.2021.111865.

[99] J. Wu, Y.-S. Fu, K. Lin, X. Huang, Y.-J. Chen, D. Lai, N. Kang, L. Huang, C.-F. Weng, *Biomedicine & pharmacotherapy = Biomedecine & pharmacotherapie* **2022**, *153*, 113339. DOI: 10.1016/j.biopha.2022.113339.

[100] J. Zhou, H. Zhang, J. Deng, Y. Wu, *Macromol. Chem. Phys.* **2016**, *217 (21)*, 2402–2408. DOI: 10.1002/macp.201600305.

[101] D. E. Katsoulis, *Chemical reviews* **1998**, *98 (1)*, 359–388. DOI: 10.1021/cr960398a.

[102] X. López, J. J. Carbó, C. Bo, J. M. Poblet, *Chemical Society reviews* **2012**, *41 (22)*, 7537–7571. DOI: 10.1039/c2cs35168d.

[103] C. L. Hill, *Chemical reviews* **1998**, *98 (1)*, 1–2. DOI: 10.1021/cr960395y.

[104] J. F. KEGGIN, *Nature* **1933**, *132 (3331)*, 351. DOI: 10.1038/132351a0.

[105] J. J. Berzelius, *Annalen der Physik* **1826**, *82 (4)*, 369–392. DOI: 10.1002/andp.18260820402.

[106] M. T. Pope, A. Müller, *Angewandte Chemie* **1991**, *103 (1)*, 56–70. DOI: 10.1002/ange.19911030107.

[107] K.C. Dey, P. Kumari, *IJRST* **2017** *(7)*, 154–177.

[108] Marignac J., *Ann. chim. phys* **1860** *(60)*, 257–307.

[109] A. Rosenheim, O. Liebknecht, *Justus Liebigs Ann. Chem.* **1899**, *308 (1-2)*, 40–67. DOI: 10.1002/jlac.18993080104.

[110] H.-G. Jerschkewitz, E. Alsdorf, H. Fichtner, W. Hanke, K. Jancke, G. Öhlmann, *Zeitschrift anorg allge chemie* **1985**, *526 (7)*, 73–85. DOI: 10.1002/zaac.19855260711.

[111] M. T. Pope, M. T. Pope, *Heteropoly and isopoly oxometalates,* Inorganic chemistry concepts, Vol.8, Springer, Berlin, Heidelberg **1983**.

[112] M. Ammam, *J. Mater. Chem. A* **2013**, *1 (21)*, 6291. DOI: 10.1039/C3TA01663C.

[113] *Polyoxometalate Molecular Science* (Ed: J.J. Borrás-Almenar), NATO Science Series II, Vol.98, Springer, Dordrecht **2003**.

[114] Y. P. Jeannin, *Chemical reviews* **1998**, *98 (1)*, 51–76. DOI: 10.1021/cr960397i.

[115] H. Avcı Özbek, *Chem. Pap.* **2023**, *77 (10)*, 5663–5669. DOI: 10.1007/s11696-023-02918-w.

[116] N. I. Gumerova, A. Rompel, *Nat Rev Chem,* in press. DOI: 10.1038/s41570-018-0112.

[117] I. V. Kozhevnikov, K. I. Matveev, *Applied Catalysis* **1983**, *5 (2)*, 135–150. DOI: 10.1016/0166-9834(83)80128-6.

[118] L. Pettersson, I. Andersson, J. H. Grate, A. Selling, *Inorg. Chem.* **1994**, *33 (5)*, 982–993. DOI: 10.1021/ic00083a023.

[119] J. Cutright, S. Edwards, R. Jauregui, R. Mohseni, A. Vasiliev, *Silicon* **2023**, *15 (5)*, 2045–2053. DOI: 10.1007/s12633-022-02157-w.

[120] R. A. Robinson, R. G. Bates, *Anal. Chem.* **1971**, *43 (7)*, 969–970. DOI: 10.1021/ac60302a030.

[121] J.-C. Raabe, J. Albert, M. J. Poller, *Chemistry (Weinheim an der Bergstrasse, Germany)* **2022**, *28 (49)*, e202201084. DOI: 10.1002/chem.202201084.

[122] W. Deng, Q. Zhang, Y. Wang, *Dalton transactions (Cambridge, England 2003)* **2012**, *41 (33)*, 9817–9831. DOI: 10.1039/c2dt30637a.

[123] B. Huang, D.-H. Yang, B.-H. Han, *J. Mater. Chem. A* **2020**, *8 (9)*, 4593–4628. DOI: 10.1039/C9TA12679A.

[124] T. Ueda, *Analytical sciences the international journal of the Japan Society for Analytical Chemistry* **2021**, *37 (1)*, 107–118. DOI: 10.2116/analsci.20SAR17.

[125] M. Aureliano, *BioChem* **2022**, *2 (1)*, 8–26. DOI: 10.3390/biochem2010002.

[126] M. B. Čolović, M. Lacković, J. Lalatović, A. S. Mougharbel, U. Kortz, D. Z. Krstić, *Current medicinal chemistry* **2020**, *27 (3)*, 362–379. DOI: 10.2174/0929867326666190827153532.

[127] S. K. Ghosh, V. K. Perla, K. Mallick, T. Pal, *Nanoscale advances* **2020**, *2 (11)*, 5343–5351. DOI: 10.1039/d0na00481b.

[128] Y. Guo, C. Hu, *Journal of Molecular Catalysis A: Chemical* **2007**, *262 (1-2)*, 136–148. DOI: 10.1016/j.molcata.2006.08.039.

[129] K. Li, Y.-F. Liu, X.-L. Lin, G.-P. Yang, *Inorg. Chem.* **2022**, *61 (18)*, 6934–6942. DOI: 10.1021/acs.inorgchem.2c00287.

[130] A. Patel, N. Narkhede, S. Singh, S. Pathan, *Catalysis Reviews* **2016**, *58 (3)*, 337–370. DOI: 10.1080/01614940.2016.1171606.

[131] M. Samaniyan, M. Mirzaei, R. Khajavian, H. Eshtiagh-Hosseini, C. Streb, *ACS Catal.* **2019**, *9 (11)*, 10174–10191. DOI: 10.1021/acscatal.9b03439.

[132] Q. Wang, B. Xu, Y. Wang, H. Wang, X. Hu, P. Ma, J. Niu, J. Wang, *Inorg. Chem.* **2021**, *60 (11)*, 7753–7761. DOI: 10.1021/acs.inorgchem.1c00135.

[133] J.-J. Ye, C.-D. Wu, *Dalton transactions (Cambridge, England 2003)* **2016**, *45 (25)*, 10101–10112. DOI: 10.1039/C6DT01378C.

[134] S. Zhang, F. Ou, S. Ning, P. Cheng, *Inorg. Chem. Front.* **2021**, *8 (7)*, 1865–1899. DOI: 10.1039/D0QI01407A.

[135] N. Mizuno, M. Misono, *Chemical reviews* **1998**, *98 (1)*, 199–218. DOI: 10.1021/cr960401q.

[136] J. Zhong, J. Pérez-Ramírez, N. Yan, *Green Chem.* **2021**, *23 (1)*, 18–36. DOI: 10.1039/D0GC03190A.

[137] Z. Zhang, G. W. Huber, *Chemical Society reviews* **2018**, *47 (4)*, 1351–1390. DOI: 10.1039/C7CS00213K.

[138] R. Wölfel, N. Taccardi, A. Bösmann, P. Wasserscheid, *Green Chem* **2011**, *13 (10)*, 2759. DOI: 10.1039/c1gc15434f.

[139] J. Albert, D. Lüders, A. Bösmann, D. M. Guldi, P. Wasserscheid, *Green Chem* **2014**, *16 (1)*, 226–237. DOI: 10.1039/C3GC41320A.

[140] J. Albert, J. Mehler, J. Tucher, K. Kastner, C. Streb, *ChemistrySelect* **2016**, *1 (11)*, 2889–2894. DOI: 10.1002/slct.201600797.

[141] J. Albert, M. Mendt, M. Mozer, D. Voß, *Applied Catalysis A: General* **2019**, *570*, 262–270. DOI: 10.1016/j.apcata.2018.10.030.

[142] P. Preuster, J. Albert, *Energy Tech* **2018**, *6 (3)*, 501–509. DOI: 10.1002/ente.201700572.

[143] J.-C. Raabe, M. J. Poller, D. Voß, J. Albert, *ChemSusChem* **2023**, *16 (16)*, e202300072. DOI: 10.1002/cssc.202300072.

[144] S. D. Mürtz, J.-C. Raabe, M. J. Poller, R. Palkovits, J. Albert, N. Kurig, *ChemCatChem,* in press. DOI: 10.1002/cctc.202301632.

[145] J.-C. Raabe, T. Esser, F. Jameel, M. Stein, J. Albert, M. J. Poller, *Inorg. Chem. Front.* **2023**, *10 (16)*, 4854–4868. DOI: 10.1039/D3QI00937H.

[146] J.-C. Raabe, F. Jameel, M. Stein, J. Albert, M. J. Poller, *Dalton transactions (Cambridge, England 2003)* **2024**, *53 (2)*, 454–466. DOI: 10.1039/d3dt03883a.

[147] R. Goedecke, W. Hofen, R. Sass, H. Wendeler, G. Schembecker, G. Wozny, H. Hahn, W. Albert, *Verfahrensentwicklung: Grundlagen, Methodik, Technik, Praxis*, Wiley-VCH, Weinheim **2006**.

[148] A. Behr, H. Witte, M. Zagajewski, *Chemie Ingenieur Technik* **2012**, *84 (5)*, 694–703. DOI: 10.1002/cite.201100169.

[149] A. Behr, W. Ebbers, N. Wiese, *Chem.-Ing.-Tech.* **2000**, *72 (10)*, 1157–1166. DOI: 10.1002/1522-2640(200010)72:10<1157:AID-CITE1157>3.0.CO;2-O.

[150] B. Ahn, C. Park, J. J. Liu, Y. S. Ok, W. Won, *Renewable Energy* **2023**, *215*, 119004. DOI: 10.1016/j.renene.2023.119004.

[151] E. Müller-Erlwein, *Chemische Reaktionstechnik,* 3rd ed., Springer Fachmedien Wiesbaden, Wiesbaden **2015**.

[152] K. Sattler, *Thermische Trennverfahren: Grundlagen, Auslegung, Apparate,* 3rd ed., Wiley-VCH, Weinheim **2001**.

[153] A. Bokhary, M. Leitch, B. Q. Liao, *Journal of Water Process Engineering* **2021**, *40*, 101762. DOI: 10.1016/j.jwpe.2020.101762.

[154] J. Reichert, B. Brunner, A. Jess, P. Wasserscheid, J. Albert, *Energy Environ. Sci.* **2015**, *8 (10)*, 2985–2990. DOI: 10.1039/C5EE01706H.

[155] D. Voß, M. Kahl, J. Albert, *ACS Sustainable Chem. Eng.* **2020**, *8 (28)*, 10444–10453. DOI: 10.1021/acssuschemeng.0c02426.

[156] A. Asad, D. Sameoto, M. Sadrzadeh, in *Nanocomposite Membranes for Water and Gas Separation*, Elsevier **2020**.

[157] T. Melin, R. Rautenbach, *Membranverfahren: Grundlagen der Modul- und Anlagenauslegung,* 3rd ed., Chemische Technik/Verfahrenstechnik, Springer, Berlin, New York **2007**.

[158] M. H. Mulder, M. Mulder, *Basic principles of membrane technology,* 2nd ed., Kluwer Acad. Publ, Dordrecht **1996**.

[159] Camera-Roda, Loddo, Palmisano, Parrino, in press. DOI: 10.3303/CET1975001.

[160] T. Esser, M. Huber, D. Voß, J. Albert, *Chemical Engineering Research and Design* **2022**, *185*, 37–50. DOI: 10.1016/j.cherd.2022.06.045.

[161] I. F. Mota, P. R. Pinto, A. M. Ribeiro, J. M. Loureiro, A. E. Rodrigues, *Separation and Purification Technology* **2018**, *197*, 360–371. DOI: 10.1016/j.seppur.2018.01.001.

[162] A. J. Surman, P. J. Robbins, J. Ujma, Q. Zheng, P. E. Barran, L. Cronin, *J. Am. Chem. Soc.* **2016**, *138 (11)*, 3824–3830. DOI: 10.1021/jacs.6b00070.

[163] V. F. Odyakov, E. G. Zhizhina, *Russ. J. Inorg. Chem.* **2009**, *54 (3)*, 361–367. DOI: 10.1134/S003602360903005X.

[164] V. F. Odyakov, E. G. Zhizhina, R. I. Maksimovskaya, *Applied Catalysis A: General* **2008**, *342 (1-2)*, 126–130. DOI: 10.1016/j.apcata.2008.03.008.

[165] V. F. Odyakov, E. G. Zhizhina, *React Kinet Catal Lett* **2008**, *95 (1)*, 21–28. DOI: 10.1007/s11144-008-5374-7.

[166] E. G. Zhizhina, V. F. Odyakov, M. V. Simonova, *Kinet Catal* **2008**, *49 (6)*, 773–781. DOI: 10.1134/S0023158408060025.

[167] J.-C. Raabe, J. Aceituno Cruz, J. Albert, M. J. Poller, *Inorganics* **2023**, *11 (4)*, 138. DOI: 10.3390/inorganics11040138.

[168] H. Werhan, *Dissertation,* ETH Zurich **2013**.

[169] W. Yang, X. Du, W. Liu, Z. Wang, H. Dai, Y. Deng, *Direct Valorization of Lignocellulosic Biomass into Value-Added Chemicals by Polyoxometalate Catalyzed Oxidation under Mild Conditions*, Vol.58 **2019**.

[170] A. E. Plesu Popescu, J. Torralba, J. Bonet, J. Llorens, *Cleaner Engineering and Technology* **2021**, *4*, 100133. DOI: 10.1016/j.clet.2021.100133.

[171] W. Yang, X. Wang, S. Ni, X. Liu, R. Liu, C. Hu, H. Dai, *Separation and Purification Technology* **2021**, *267*, 118599. DOI: 10.1016/j.seppur.2021.118599.

[172] NREL, *Determination of Structural Carbohydrates and Lignin in Biomass: Laboratory Analytical Procedure (LAP) (Revised August 2012)* **2008**.

[173] J. Rumpf, X. T. Do, R. Burger, Y. B. Monakhova, M. Schulze, *Biomacromolecules* **2020**, *21 (5)*, 1929–1942. DOI: 10.1021/acs.biomac.0c00123.

[174] K. Siebertz, D. van Bebber, T. Hochkirchen, *Statistische Versuchsplanung: Design of Experiments (DoE),* 2nd ed., VDI-Buch, Springer Vieweg, Berlin, Heidelberg **2017**.

[175] B. Jones, D. C. Montgomery, *Design of experiment: A modern approach*, Wiley, Hoboken **2020**.

[176] J. Domínguez-Robles, T. Tamminen, T. Liitiä, M. S. Peresin, A. Rodríguez, A.-S. Jääskeläinen, *International journal of biological macromolecules* **2018**, *106*, 979–987. DOI: 10.1016/j.ijbiomac.2017.08.102.

[177] R. Gaspar, M. C. D. S. Muguet, P. Fardim, *Molecules (Basel, Switzerland)* **2023** *(28)*, 1–16. DOI: 10.3390/molecules28020687.

[178] N. Feng, S. She, F. Tang, X. Zhao, J. Chen, P. Wang, Q. Wu, O. J. Rojas, *Biomacromolecules* **2023**, *24 (6)*, 2541–2548. DOI: 10.1021/acs.biomac.3c00053.

[179] M. J. Suota, T. A. Da Silva, S. F. Zawadzki, G. L. Sassaki, F. A. Hansel, M. Paleologou, L. P. Ramos, *Industrial Crops and Products* **2021**, *173*, 114138. DOI: 10.1016/j.indcrop.2021.114138.

[180] J. M. Jardim, P. W. Hart, L. Lucia, H. Jameel, *Polymers* **2020** *(12)*, 1–25. DOI: 10.3390/polym12081795.

[181] P. Schlee, O. Hosseinaei, C. A. O' Keefe, M. J. Mostazo-López, D. Cazorla-Amorós, S. Herou, P. Tomani, C. P. Grey, M.-M. Titirici, *J. Mater. Chem. A* **2020**, *8 (44)*, 23543–23554. DOI: 10.1039/D0TA09093J.

[182] C. Guizani, D. Lachenal, *International journal of molecular sciences* **2017** *(18)*, 1–18. DOI: 10.3390/ijms18122520.

[183] S. Nisar, P. V. Barbará, B. Chachuat, J. P. Hallett, A. Brandt-Talbot, *Biomass and Bioenergy* **2025**, *201*, 108056. DOI: 10.1016/j.biombioe.2025.108056.

[184] J. J. Bozell, in *Plants and BioEnergy* (Eds: M. C. McCann, M. S. Buckeridge, N. C. Carpita), Springer New York, New York, NY **2014**.

[185] W. Deng, H. Zhang, X. Wu, R. Li, Q. Zhang, Y. Wang, *Green Chem* **2015**, *17 (11)*, 5009–5018. DOI: 10.1039/C5GC01473E.

[186] G. F. De Gregorio, R. Prado, C. Vriamont, X. Erdocia, J. Labidi, J. P. Hallett, T. Welton, *ACS Sustainable Chem. Eng.* **2016**, *4 (11)*, 6031–6036. DOI: 10.1021/acssuschemeng.6b01339.

[187] W. Partenheimer, *Adv Synth Catal* **2009**, *351 (3)*, 456–466. DOI: 10.1002/adsc.200800614.

[188] R. Prado, A. Brandt, X. Erdocia, J. Hallet, T. Welton, J. Labidi, *Green Chem* **2016**, *18 (3)*, 834–841. DOI: 10.1039/C5GC01950H.

[189] R. Prado, X. Erdocia, G. F. de Gregorio, J. Labidi, T. Welton, *ACS Sustainable Chem. Eng.* **2016**, *4 (10)*, 5277–5288. DOI: 10.1021/acssuschemeng.6b00642.

[190] Stärk, Taccardi, Bösmann, Wasserscheid, *ChemSusChem* **2010** *(3)*, 719–723. DOI: 10.1002/cssc.200900242.

[191] T. Voitl, *Dissertation,* ETH Zurich **2009**.

[192] T. Voitl, M. V. Nagel, P. R. von Rohr, *Holzforschung* **2010** *(64)*, 13–19. DOI: 10.1515/hf.2010.006.

[193] T. Voitl, P. R. von Rohr *WO 2008/106811 A1*.

[194] T. Voitl, P. R. von Rohr, *Ind. Eng. Chem. Res.* **2010**, *49 (2)*, 520–525. DOI: 10.1021/ie901293p.

[195] T. Voitl, P. R. von Rohr, N. Blank, I. Schober *WO 2010/106182 A1*.

[196] T. Voitl, P. Rudolf von Rohr, *ChemSusChem* **2008**, *1 (8-9)*, 763–769. DOI: 10.1002/cssc.200800050.

[197] H. Werhan, J. M. Mir, T. Voitl, P. Rudolf von Rohr, *Holzforschung* **2011**, *65 (5)*, 703–709. DOI: 10.1515/hf.2011.071.

[198] D. Voß, R. Dietrich, M. Stuckart, J. Albert, *ACS omega* **2020**, *5 (30)*, 19082–19091. DOI: 10.1021/acsomega.0c02430.

[199] F. Hu, S. Jung, A. Ragauskas, *Bioresource technology* **2012**, *117*, 7–12. DOI: 10.1016/j.biortech.2012.04.037.

[200] P. Sannigrahi, D. H. Kim, S. Jung, A. Ragauskas, *Energy Environ. Sci.* **2011**, *4 (4)*, 1306–1310. DOI: 10.1039/C0EE00378F.

[201] S. D. Shinde, X. Meng, R. Kumar, A. J. Ragauskas, *Green Chem* **2018**, *20 (10)*, 2192–2205. DOI: 10.1039/C8GC00353J.

[202] S. Maerten, C. Kumpidet, D. Voß, A. Bukowski, P. Wasserscheid, J. Albert, *Green Chem* **2020**, *22 (13)*, 4311–4320. DOI: 10.1039/d0gc01169j.

[203] X. Du, A. W. Tricker, W. Yang, R. Katahira, W. Liu, T. T. Kwok, P. Gogoi, Y. Deng, *Oxidative Catalytic Fractionation and Depolymerization of Lignin in a One-Pot Single-Catalyst System*, Vol.9 **2021**.

[204] W. Henry, *Phil. Trans. R. Soc.* **1803**, *93*, 29–274. DOI: 10.1098/rstl.1803.0004.

[205] V. I. Bruskov, L. V. Malakhova, Z. K. Masalimov, A. V. Chernikov, *Nucleic acids research* **2002**, *30 (6)*, 1354–1363. DOI: 10.1093/nar/30.6.1354.

[206] Y. Cui, E. P. Weeda, S. Omolabake, S. D. Karlen, C. M. Holland, S. S. Stahl, *ACS Sustainable Chem. Eng.* **2024**, *12 (26)*, 9795–9804. DOI: 10.1021/acssuschemeng.4c02120.

[207] K.-I. Matsumoto, M. Nyui, M. Kamibayashi, T. Ozawa, I. Nakanishi, K. Anzai, *Journal of clinical biochemistry and nutrition* **2012**, *50 (1)*, 40–46. DOI: 10.3164/jcbn.10-145.

[208] J. Reichert, J. Albert, *ACS Sustainable Chem. Eng.* **2017**, *5 (8)*, 7383–7392. DOI: 10.1021/acssuschemeng.7b01723.

[209] S. Dardelet, P. Froment, N. Lacoste, A. Robert, *Revue - A.T.I.P.* **1985** *(39)*, 267–274.

[210] José P. Araujo, *Dissertation,* University of Porto, Porto **2008**.

[211] F. M. Casimiro, C. A. E. Costa, C. M. Botelho, M. F. Barreiro, A. E. Rodrigues, *Ind. Eng. Chem. Res.* **2019**, *58 (36)*, 16442–16449. DOI: 10.1021/acs.iecr.9b02818.

[212] C. Fargues, Á. Mathias, A. Rodrigues, *Ind. Eng. Chem. Res.* **1996**, *35 (1)*, 28–36. DOI: 10.1021/ie950267k.

[213] C. Fargues, Á. Mathias, J. Silva, A. Rodrigues, *Chem Eng & Technol* **1996**, *19 (2)*, 127–136. DOI: 10.1002/ceat.270190206.

[214] R. Battino, T. R. Rettich, T. Tominaga, *Journal of Physical and Chemical Reference Data* **1983**, *12 (2)*, 163–178. DOI: 10.1063/1.555680.

[215] K. Fischer, M. Wilken, *The Journal of Chemical Thermodynamics* **2001**, *33 (10)*, 1285–1308. DOI: 10.1006/jcht.2001.0837.

[216] C. N. Murray, J. P. Riley, *Deep Sea Research and Oceanographic Abstracts* **1969**, *16 (3)*, 311–320. DOI: 10.1016/0011-7471(69)90021-7.

[217] R. Kondo, Y. Tsutsumi, H. Imamura, *Holzforschung* **1987**, *41 (2)*, 83–88. DOI: 10.1515/hfsg.1987.41.2.83.

[218] K. Gabov, R. J. A. Gosselink, A. I. Smeds, P. Fardim, *J. Agric. Food Chem.* **2014**, *62 (44)*, 10759–10767. DOI: 10.1021/jf5037728.

[219] O. Faix, *Holzforschung* **1991**, *45 (s1)*, 21–28. DOI: 10.1515/hfsg.1991.45.s1.21.

[220] L. Zhang, L. Yan, Z. Wang, D. D. Laskar, M. S. Swita, J. R. Cort, B. Yang, *Biotechnology for biofuels* **2015**, *8*, 203. DOI: 10.1186/s13068-015-0377-x.

[221] F. M. Antony, D. Pal, K. Wasewar, *Physical Sciences Reviews* **2021**, *6 (4)*, 1–24. DOI: 10.1515/psr-2018-0065.

[222] A. Pfennig*, E. Müller, R. Berger, E. Blass, D. Sluyts, in *Ullmann's Encyclopedia of Industrial Chemistry*, Wiley **2000**.

[223] P. Yin, D. Li, T. Liu, *Chemical Society reviews* **2012**, *41 (22)*, 7368–7383. DOI: 10.1039/C2CS35176E.

[224] G. Lagaly, *Dispersionen und Emulsionen: Eine Einführung in die Kolloidik feinverteilter Stoffe einschließlich der Tonminerale*, Steinkopff, Heidelberg **1997**.

[225] P. Sun, X.-M. Lin, M. K. Bera, B. Lin, D. Ying, T. Chang, W. Bu, M. L. Schlossman, *Proceedings of the National Academy of Sciences of the United States of America* **2024**, *121 (13)*, e2315584121. DOI: 10.1073/pnas.2315584121.

[226] N. R. Ronco, L. G. Gagliardi, C. B. Castells, in *Liquid-phase extraction* (Ed: C. F. Poole), Handbooks in separation science, Elsevier, Amsterdam, Netherlands, Kidlington, Oxford, Cambridge, MA **2020**.

[227] A. Siekierka, K. Smolińska-Kempisty, J. Wolska, *Membranes* **2021**, *11 (12)*, 1–16. DOI: 10.3390/membranes11120942.

[228] N. Nishiyama, T. Yokoyama, *JGR Solid Earth* **2017**, *122 (9)*, 6955–6971. DOI: 10.1002/2016JB013793.

[229] F. J. O'Brien, B. A. Harley, M. A. Waller, I. V. Yannas, L. J. Gibson, P. J. Prendergast, *Technology and health care official journal of the European Society for Engineering and Medicine* **2007**, *15 (1)*, 3–17.

[230] F. Xu, M. Wei, X. Zhang, Y. Song, W. Zhou, Y. Wang, *Research (Washington, D.C.)* **2019**, *2019*, 2581241. DOI: 10.34133/2019/2581241.

[231] F. P. Helmus, *Process plant design: Project management from inquiry to acceptance*, Wiley-VCH, Weinheim **2008**.

[232] A. Groysman, *Corrosion Problems and Solutions in Oil Refining and Petrochemical Industry*, Vol.32, Springer International Publishing, Cham **2017**.

[233] H. Kaesche, *Die Korrosion der Metalle*, Springer Berlin Heidelberg, Berlin, Heidelberg **2011**.

[234] F. Kong, S. Wang, J. T. Price, M. K. Konduri, P. Fatehi, *Green Chem* **2015**, *17 (8)*, 4355–4366. DOI: 10.1039/C5GC00228A.

[235] J. YANHUA, Q. WEIHONG, L. I. ZONGSHI, C. LUBAI, *Energy Sources* **2004**, *26 (4)*, 409–414. DOI: 10.1080/00908310490281528.

[236] R. M. Christie, *Colour chemistry,* 2nd ed., Royal Society of Chemistry, Cambridge **2015**.

[237] T. Dizhbite, G. Telysheva, V. Jurkjane, U. Viesturs, *Bioresource technology* **2004**, *95 (3)*, 309–317. DOI: 10.1016/j.biortech.2004.02.024.

[238] R. A. Rusdipoetra, H. Suwito, N. N. T. Puspaningsih, K. U. Haq, *RSC Adv.* **2024**, *14 (9)*, 6310–6323. DOI: 10.1039/D3RA08346B.

[239] F. Rosillo-Calle, A. Walter, *Energy for Sustainable Development* **2006**, *10 (1)*, 20–32. DOI: 10.1016/S0973-0826(08)60504-9.

[240] Lewis F. Moody, *Transactions of the A.S.M.E.* **1944**, 671–684.

B. Appendix

B.1 Utilized chemicals

Table B-1: Overview of utilized chemicals

Substance	Supplier info	GHS symbols	Hazard and precautionary statement
1-heptanol	Alfa Aesar 99 %		H: 319 P: 264; 280; 305+351+338; 337+313
Alkali lignin	Merck		H: 317; 319; 335 P: 261; 264; 272; 280; 302+352; 305+351+338; 321; 333+313; 363; 501
Argon	Heide Gas Grade 4.6		H: 280 P: 403
Deionized water	-	-	-
Dimethyl oxalate	Thermo scientific 99 %		H: 302; 314 P: 260; 270; 280;301+312; 303+361+353; 305+351+338
Dimethyl succinate	Thermo scientific 99 %		H: 319 P: 264; 280; 305+351+338; 337+313
Ethanol	VWR >99 %		H: 225; 319 P: 210; 233; 240; 241; 242; 305+351+338
Ethyl acetate	VWR >99.8 %		H: 225; 319; 336 P: 210; 233; 240; 305+351+338; 403+235
Helium	Linde AG Grade 4.6		H: 280 P: 403
Methanol	VWR HPLC-grade		H: 225; 301+311+331; 370 P: 210; 233; 280; 301+310; 303+361+353; 304+340+311

Methyl 4-hydroxybenzoate	Thermo scientific 99 %		H: 411 P: 273; 391; 501
Methyl acetate	Merck >99%		H: 225; 319; 336 P: 210; 305+351+338; 403+233
Methyl formate	Alfa Aesar 97 %		H: 224; 302+332; 319; 335 P: 210; 280; 301+312; 304+340; 305+351+338
Methyl syringate	Alfa Aesar 98 %		H: 319 P: 305+351+338
Methyl vanillate	Thermo scientific 99 %		H: 315; 319; 335 P: 261; 264; 271; 280; 302+352; 305+351+338
n-hexane	Merck >99 %	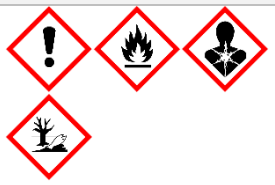	H: 225; 304; 361f; 373; 315; 336; 411 P: 210; 240; 273; 301+310; 331; 302+352; 403+235
Nickel (II) acetate	Merck >99 %	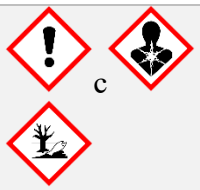	H: 302+332; 317; 334; 341; 350i; 360d; 372; 410 P: 202; 273; 280; 301+312; 302+352; 308+313
Nitrogen	Linde AG Grade 5.0		H: 280 P: 403
Octyl amine	Thermo scientific 99 %	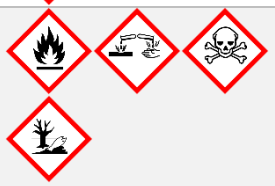	H: 226; 301+311; 314; 332; 335; 410 P: 210; 273; 280; 303+361+353; 304+340+310; 305+351+338
Oxygen	Westfalen AG Grade 5.0		H: 270; 280 P: 244; 220; 370+376; 403
Phosphomolybdic acid	Merck		H: 272; 314 P: 210; 220; 260; 280; 303+361+353; 305; 351; 338
Phosphoric acid	Grüssing 85 %		H: 290; 302; 314 P: 234; 270; 280; 301+312; 303+361+353; 305+351+338

Phosphotungstic acid	Merck		H: 302; 314; 411 P: P260; 264; 270; 273; 280; 301+312; 301+330+331; 303+361+353; 304+340; 305+351+338; 310; 321; 330; 363; 391; 405; 501
Potassium chloride	Thermo scientific 99 %	-	-
Silicotungstic acid	Merck		H: 314; 315; 319; 335; 412 P: 260; 261; 264; 271; 273; 280; 301+330+331; 302+352; 303+361+353; 304+340; 305+351+338; 310; 312; 321; 332+313; 337+313; 362; 363; 403+233; 405; 501
Syringaldehyde	Sigma Aldrich 98 %		H: 302; 315; 319; 335 P: 261; 305+351+338
Tetrahydrofurane	Sigma Aldrich >99.9 %		H: 225; 302; 319; 335; 351 P: 210; 280; 301+312+330; 305+351+338; 370+378; 403+235
Toluene	Thermo scientific 99.85 %		H: 225; 315; 361d; 336; 373; 304; 412 P: 202; 210; 273; 301+310; 303+361+353; 331
Vanillin	Sigma Aldrich 99 %		H: 319 P: 264; 280; 305+351+338; 337+313

B.2 Calibrations of GC-MS and GC-FID

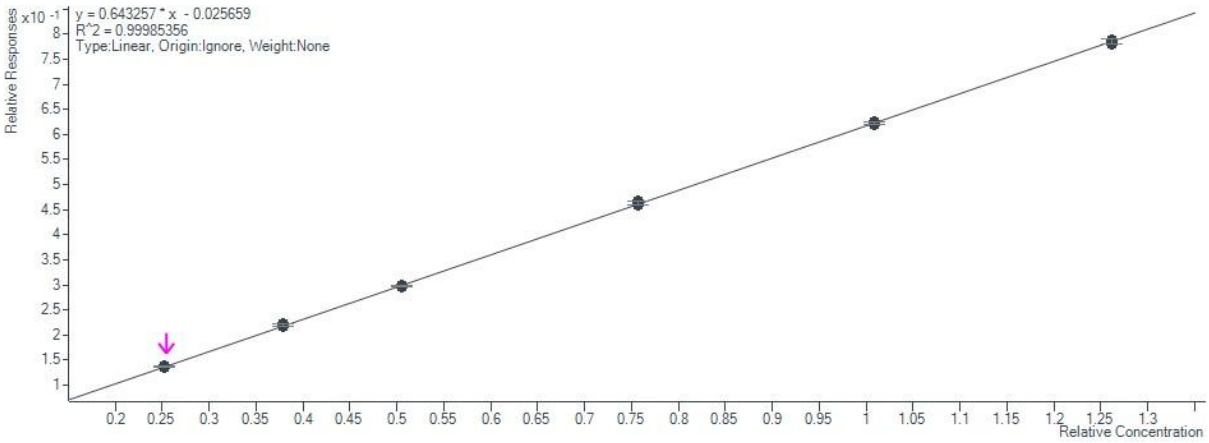

Figure B-1: Calibration of vanillin on GC-MS with an R² of 0.999.

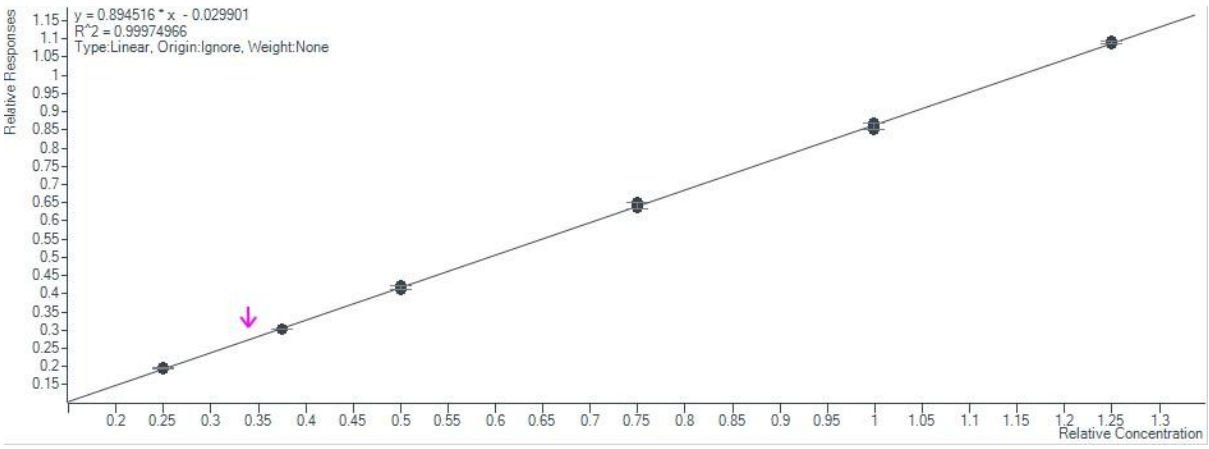

Figure B-2: Calibration of methyl vanillate on GC-MS with an R² of 0.999.

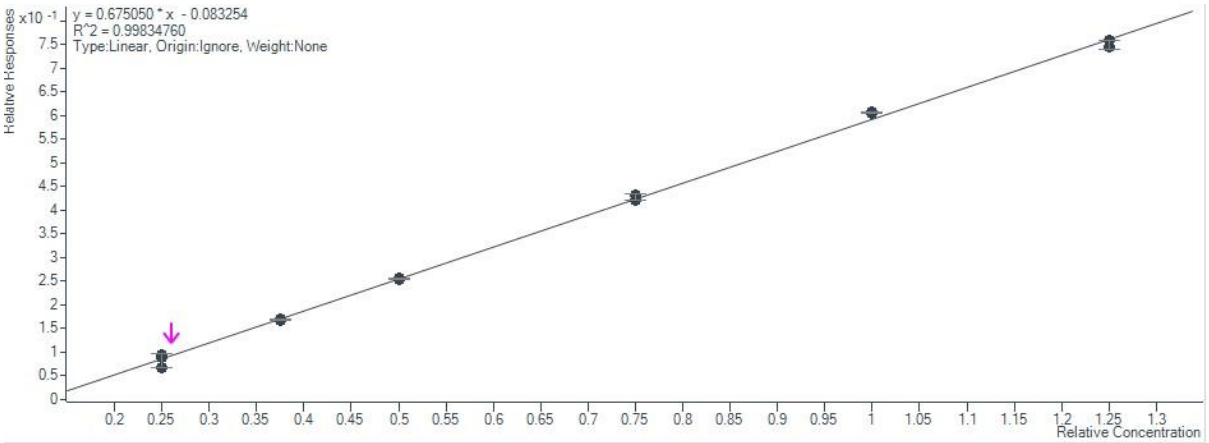

Figure B-3: Calibration of syringaldehyde on GC-MS with an R² of 0.998.

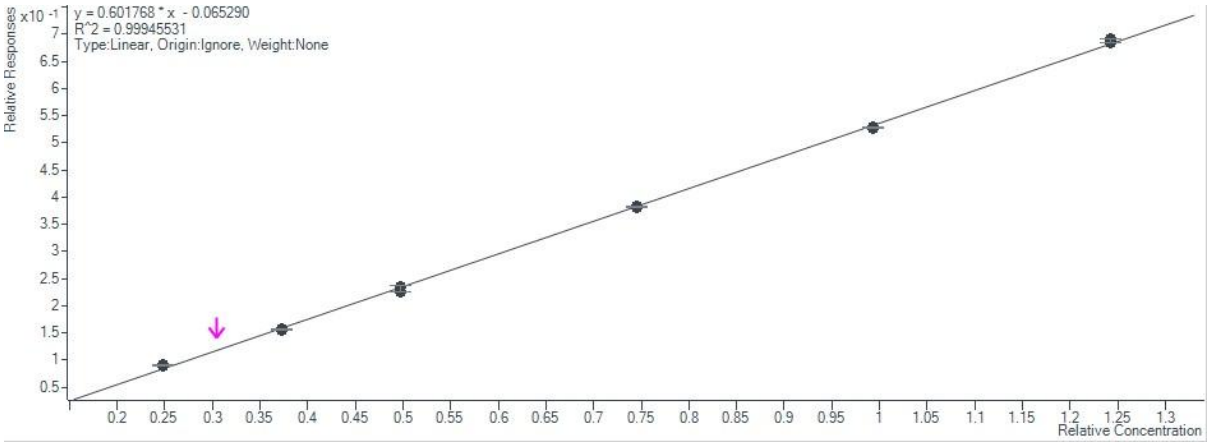

Figure B-4: Calibration of syringaldehyde on GC-MS with an R^2 of 0.999.

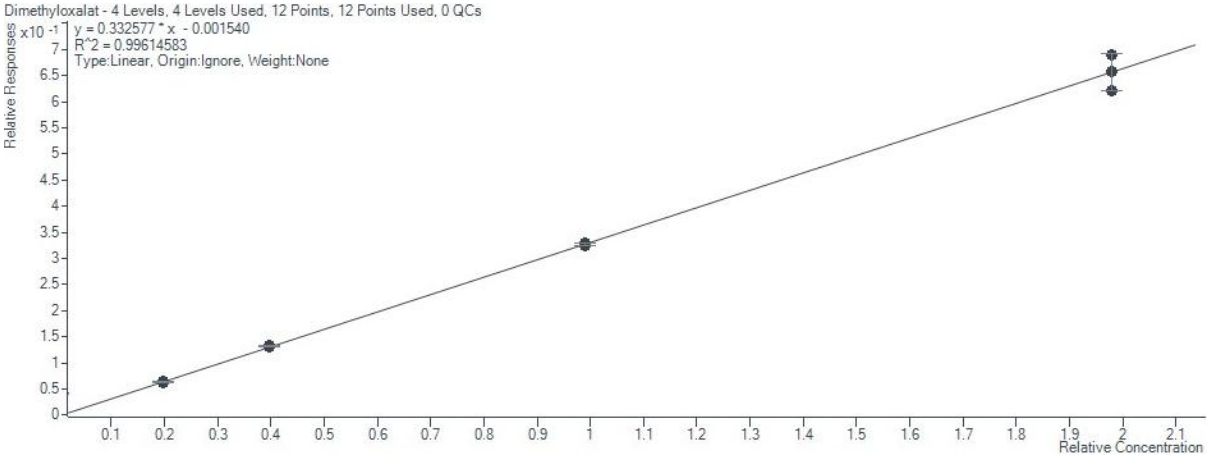

Figure B-5: Calibration of dimethyl oxalate on GC-MS with an R^2 of 0.996.

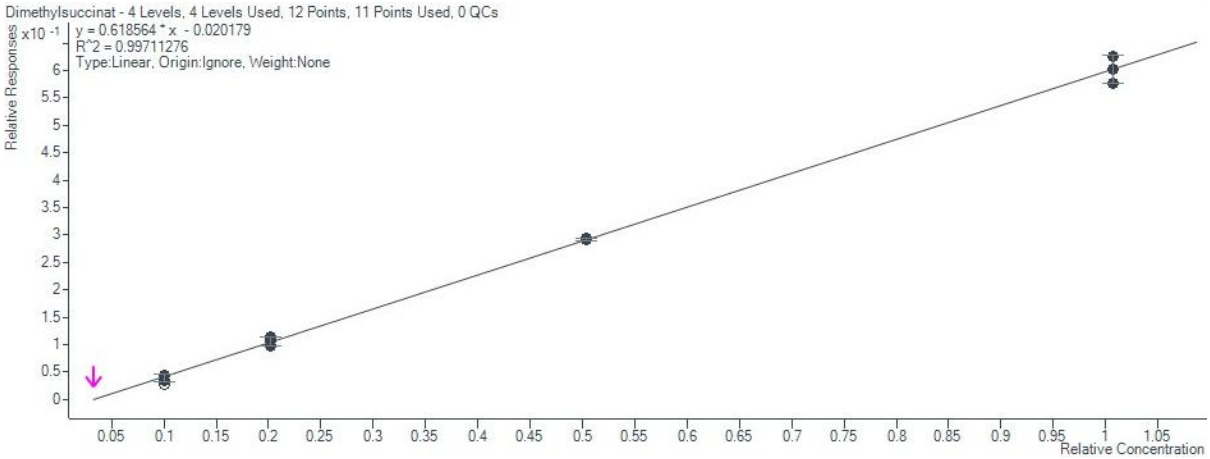

Figure B-6: Calibration of dimethyl succinate on GC-MS with an R^2 of 0.997.

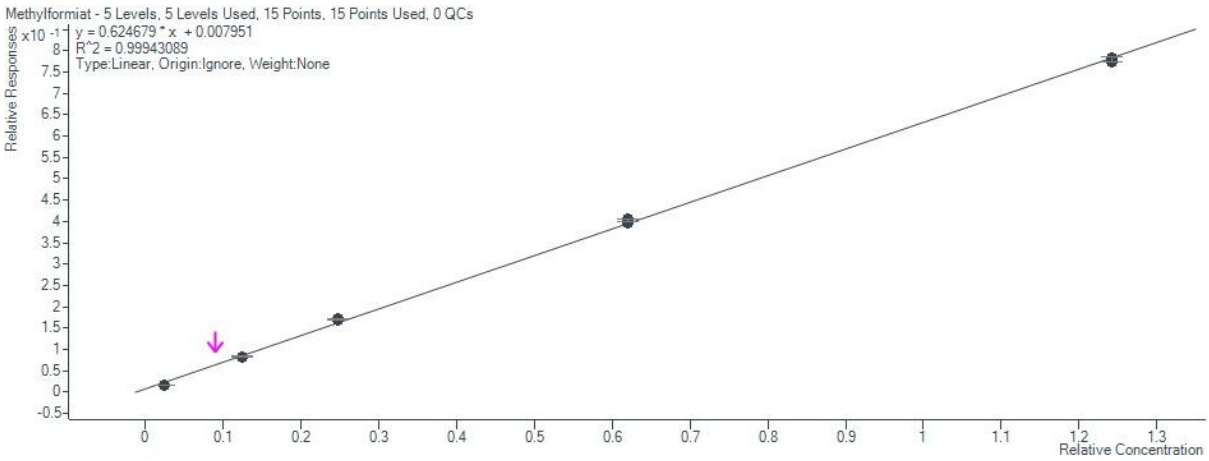

Figure B-7: Calibration of methyl formate on GC-MS with an R^2 of 0.999.

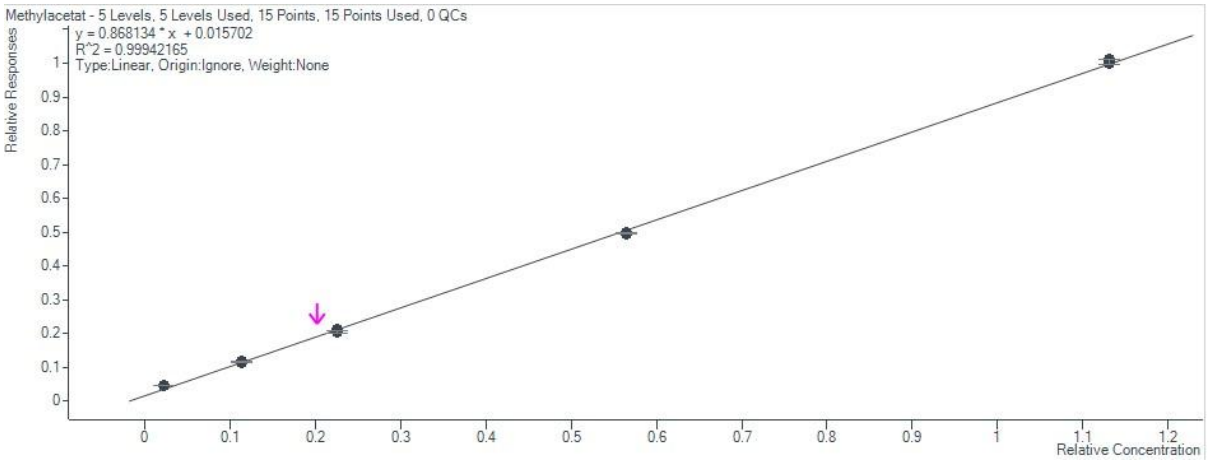

Figure B-8: Calibration of methyl acetate on GC-MS with an R^2 of 0.999.

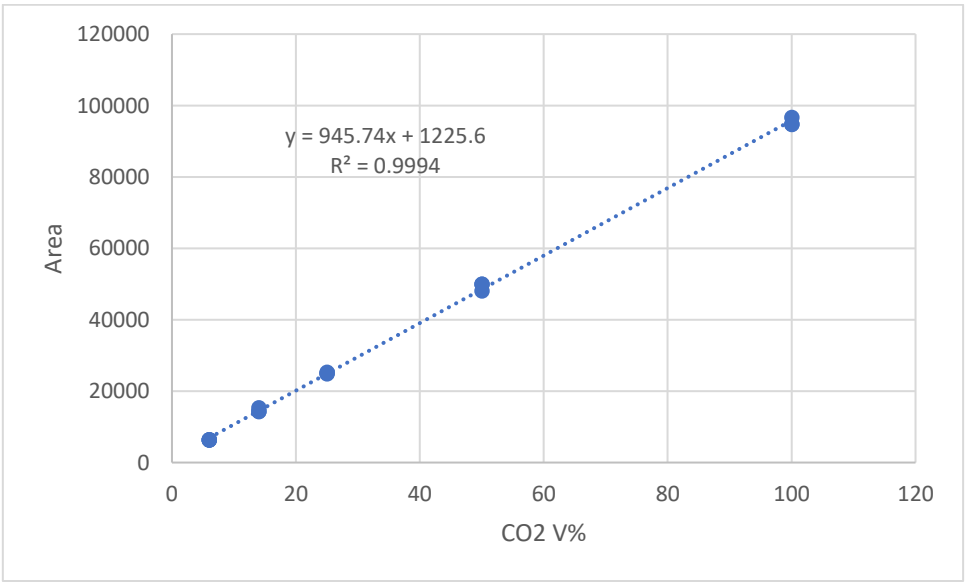

Figure B-9: Calibration of CO2 on GC-FID with an R^2 of 0.999.

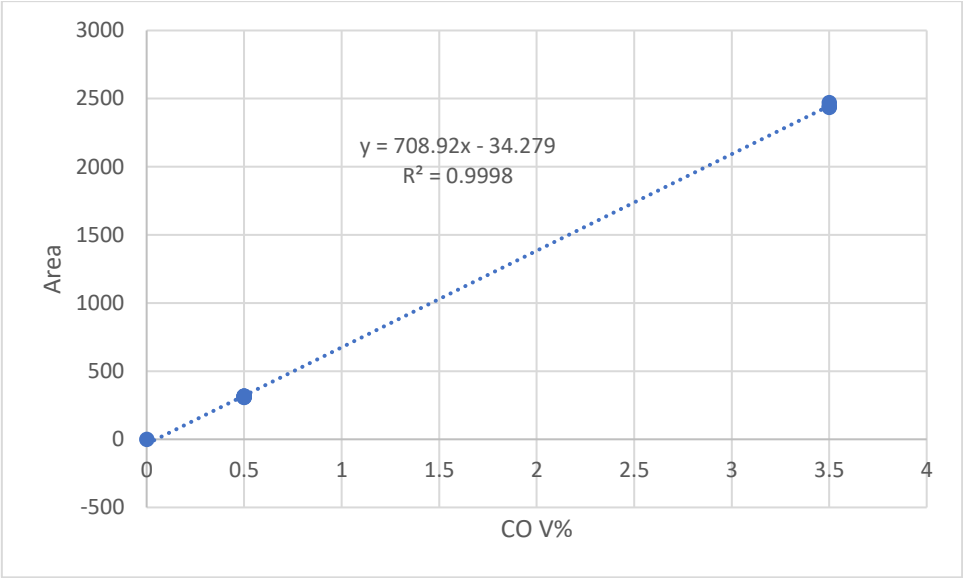

Figure B-10: Calibration of CO on GC-FID with an R^2 of 0.999.

B.3 SI on lignin characterization

Table B-2: Results of compositional analysis for substrates 1 to 13 showing the contents of lignin, cellulose, hemicellulose, ash and other, including moisture.

Substrate	Acid soluble lignin in wt.-%	Acid insoluble lignin in wt.-%	Water in wt.-%	Ash in wt.-%	Carbohydrates in wt.-%
1	89.5	1.0	3.6	0.5	5.3
2	73.4	2.0	8.2	0.4	16.0
3	59.8	5.4	7.0	0.3	27.5
4	91.5	2.1	3.4	0.1	2.9
5	93.4	2.0	8.0	0.5	0.0
6	93.4	1.3	5.7	0.5	0.0
7	0.6	66.1	14.4	0.0	18.8
8	97.0	1.3	7.3	0.5	0.0
9	88.0	1.4	3.0	0.5	7.0
10	74.8	5.7	7.3	0.4	11.8
11	63.8	1.3	3.4	0.4	31.1
12	70.6	1.9	4.3	0.4	22.8
13	83.7	3.1	3.4	0.5	9.3

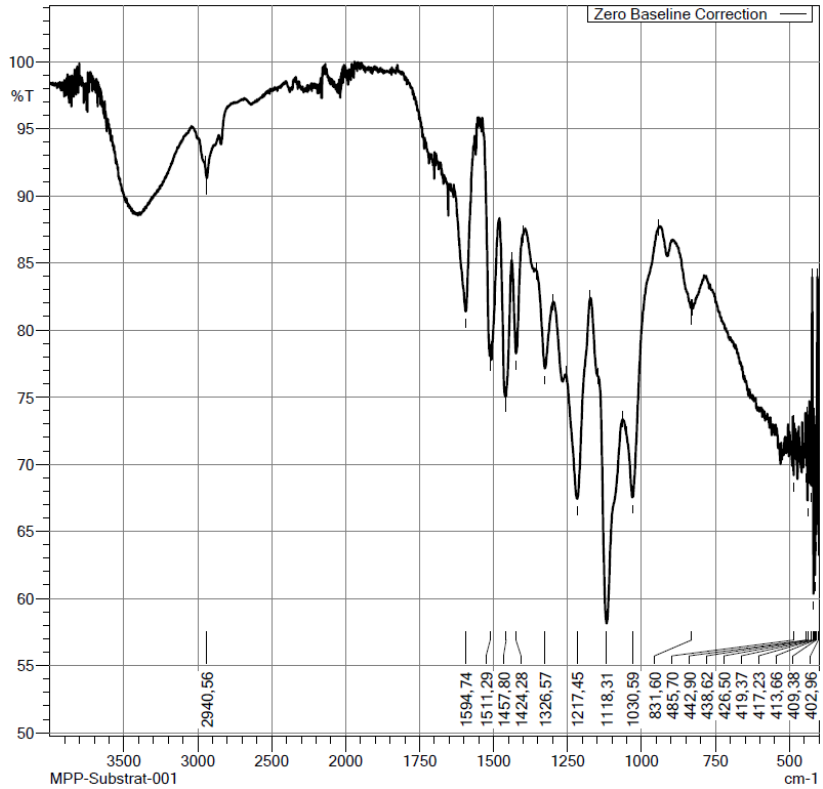

Figure B-11: FT-IR spectrum of substrate 1.

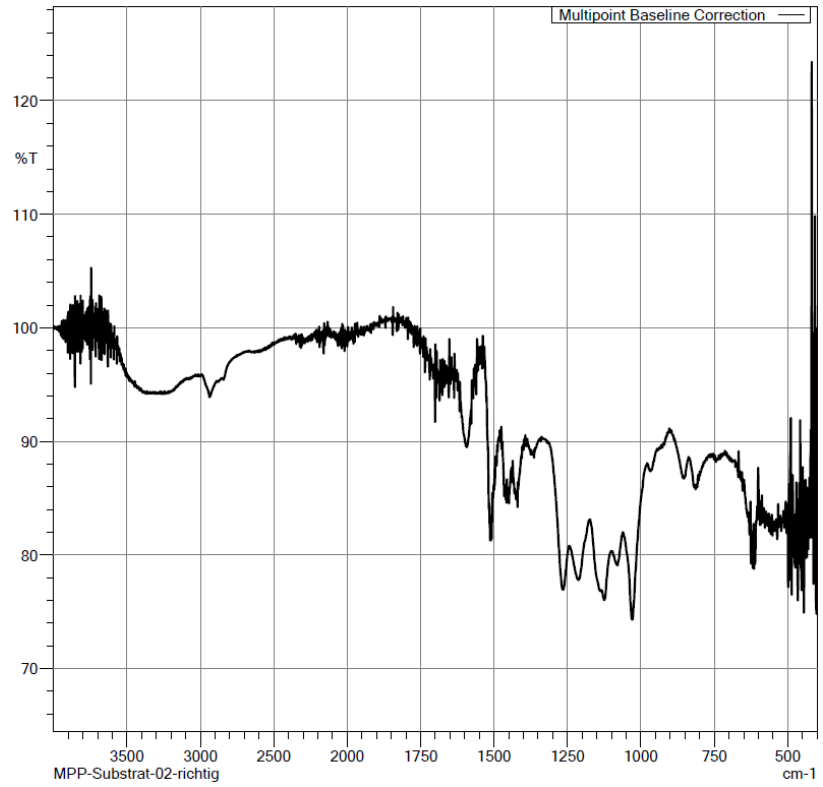

Figure B-12: FT-IR spectrum of substrate 2.

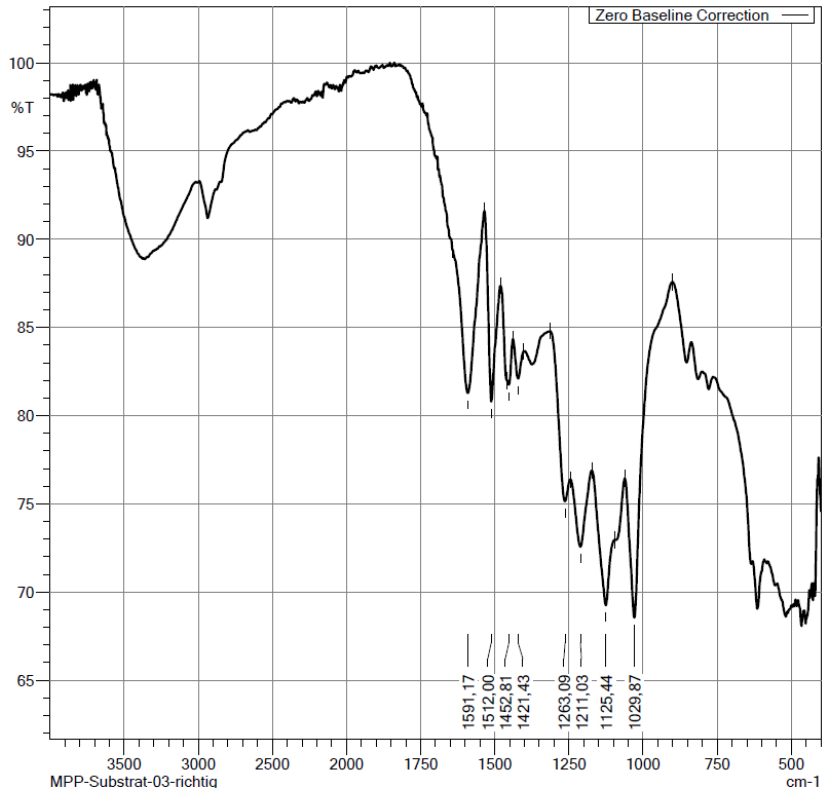

Figure B-13: FT-IR spectrum of substrate 3.

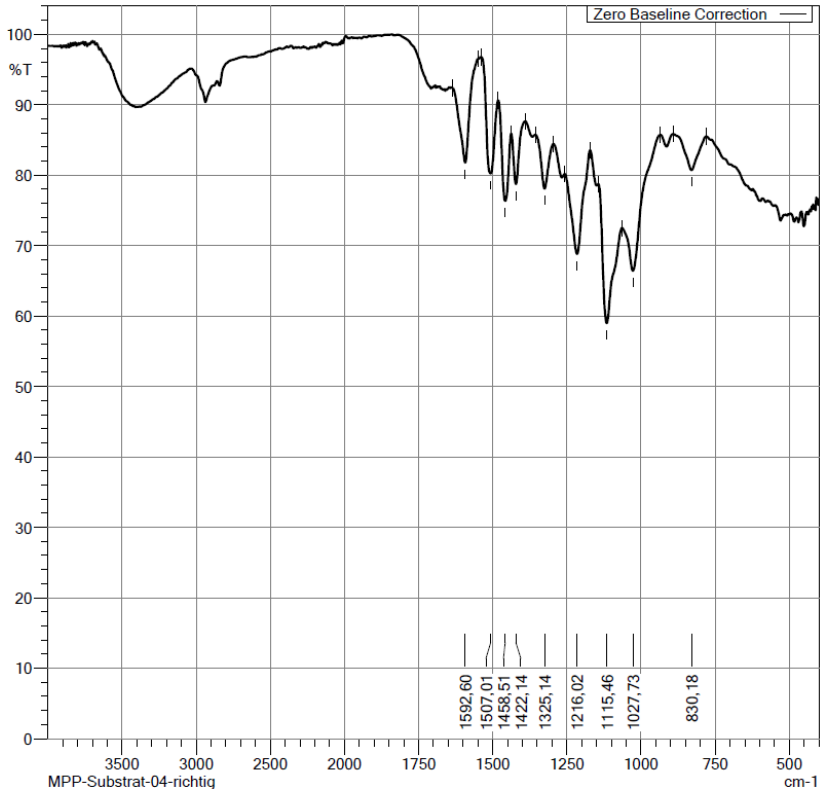

Figure B-14: FT-IR spectrum of substrate 4.

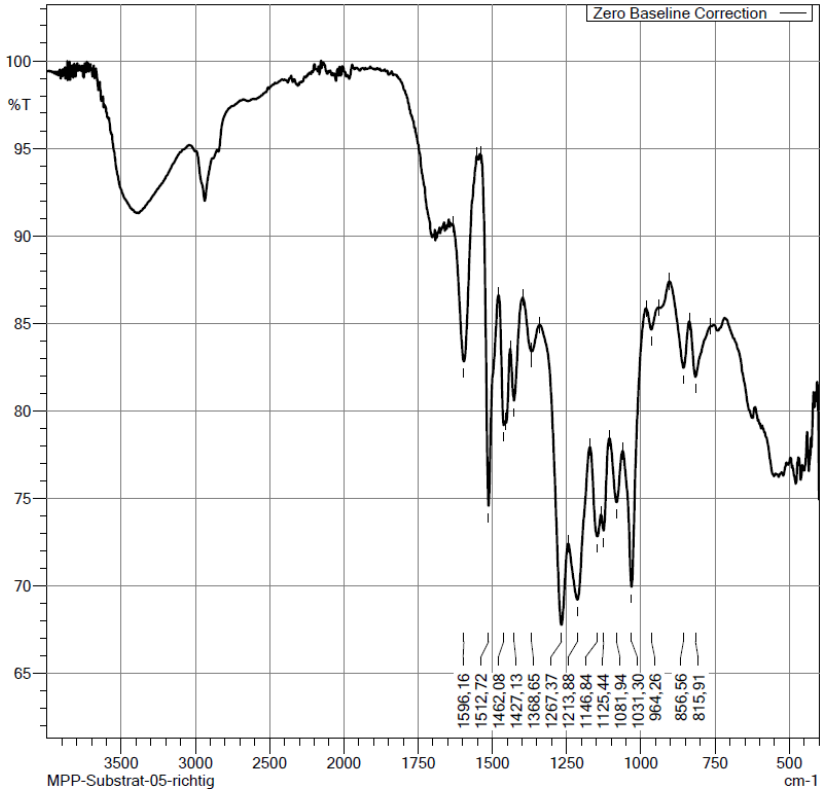

Figure B-15: FT-IR spectrum of substrate 5.

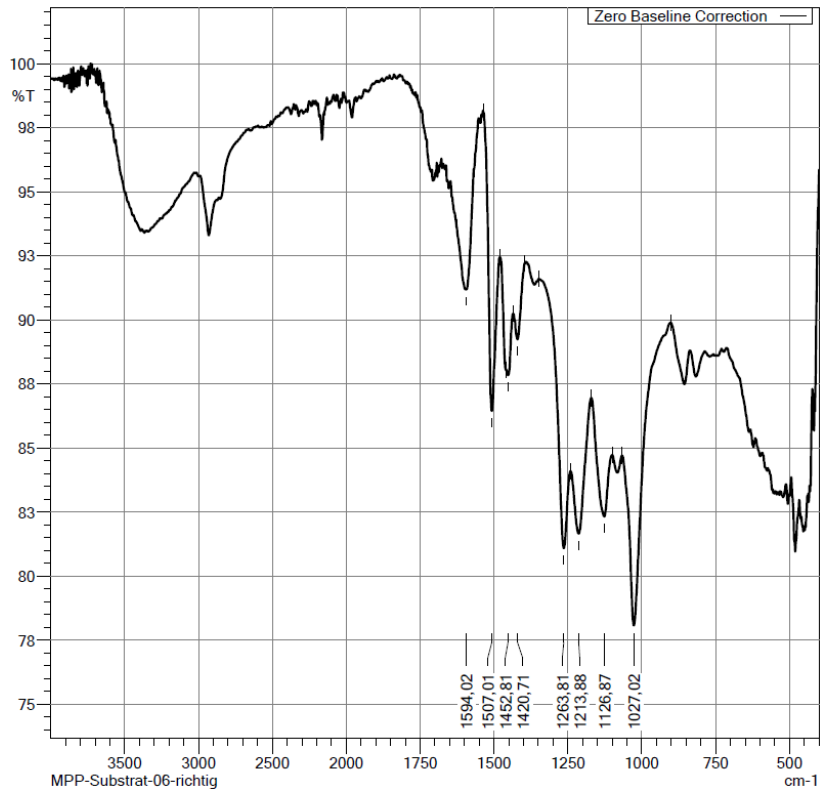

Figure B-16: FT-IR spectrum of substrate 6.

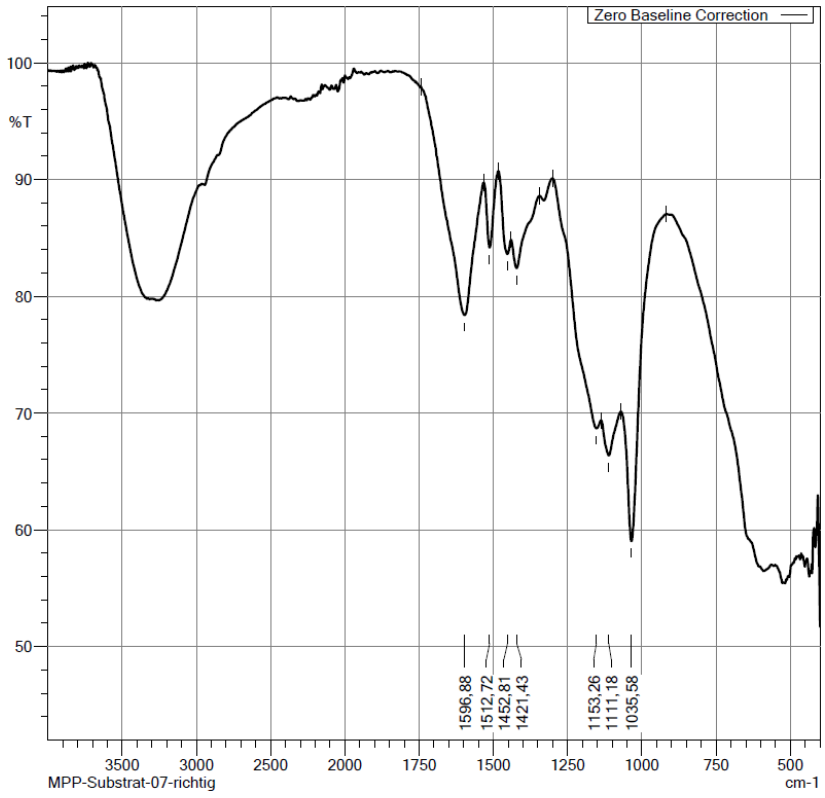

Figure B-17: FT-IR spectrum of substrate 7.

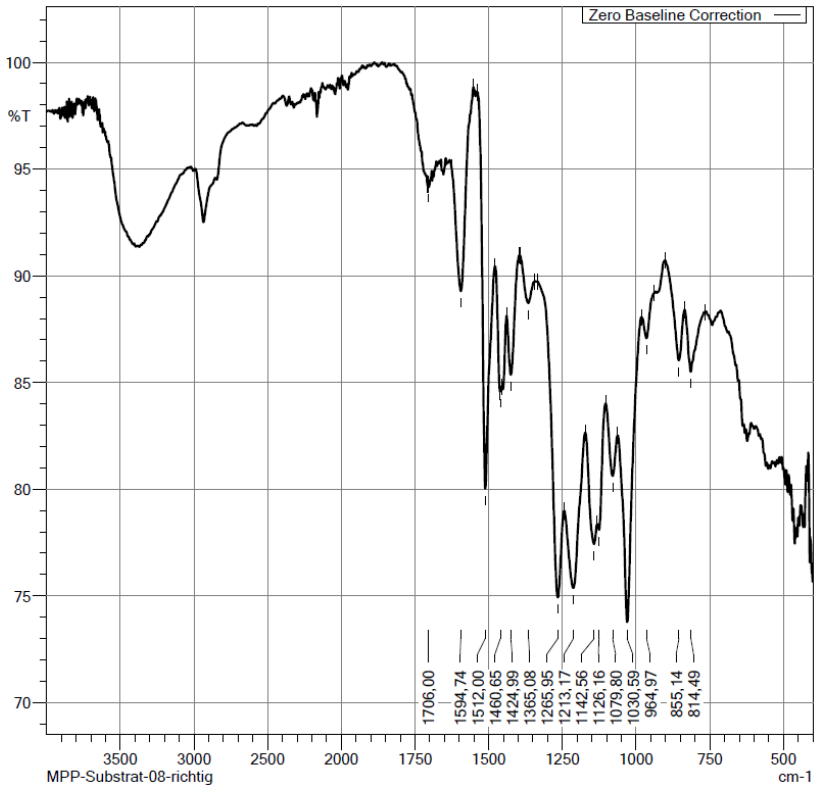

Figure B-18: FT-IR spectrum of substrate 8.

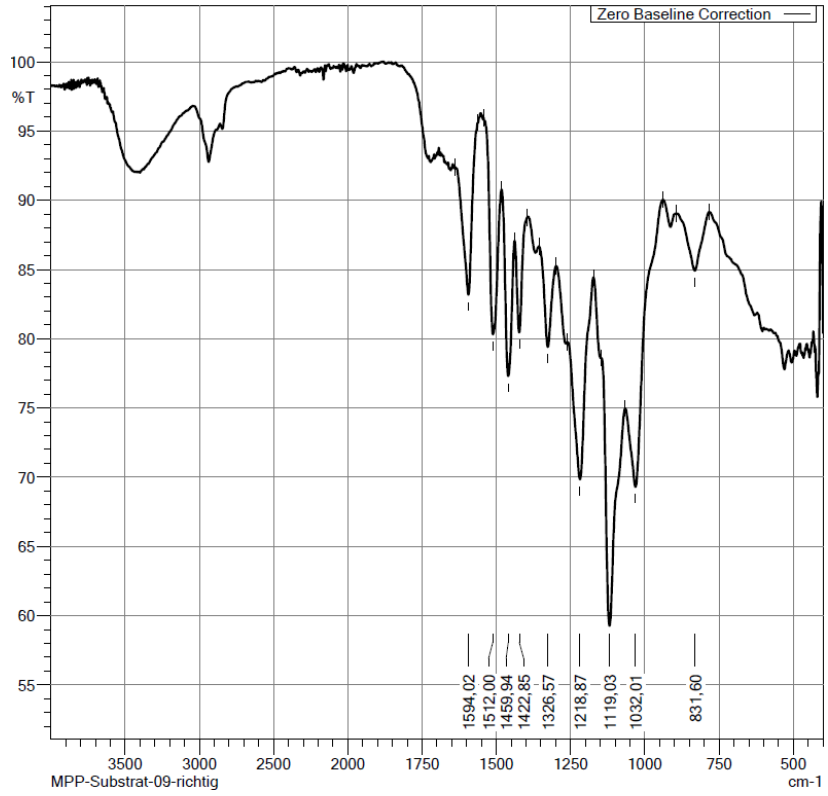

Figure B-19: FT-IR spectrum of substrate 9.

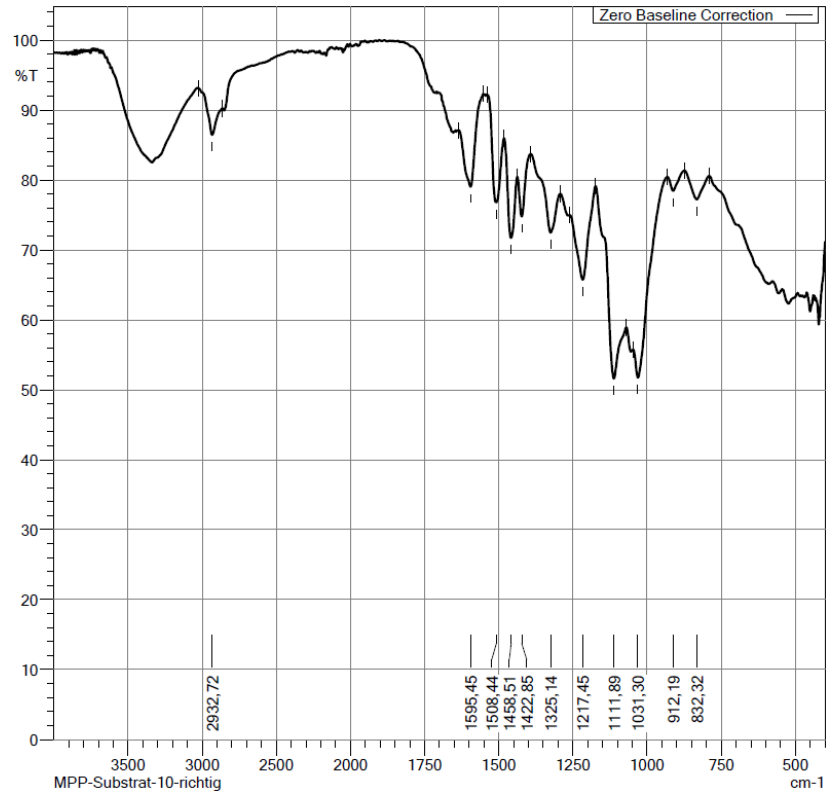

Figure B-20: FT-IR spectrum of substrate 10.

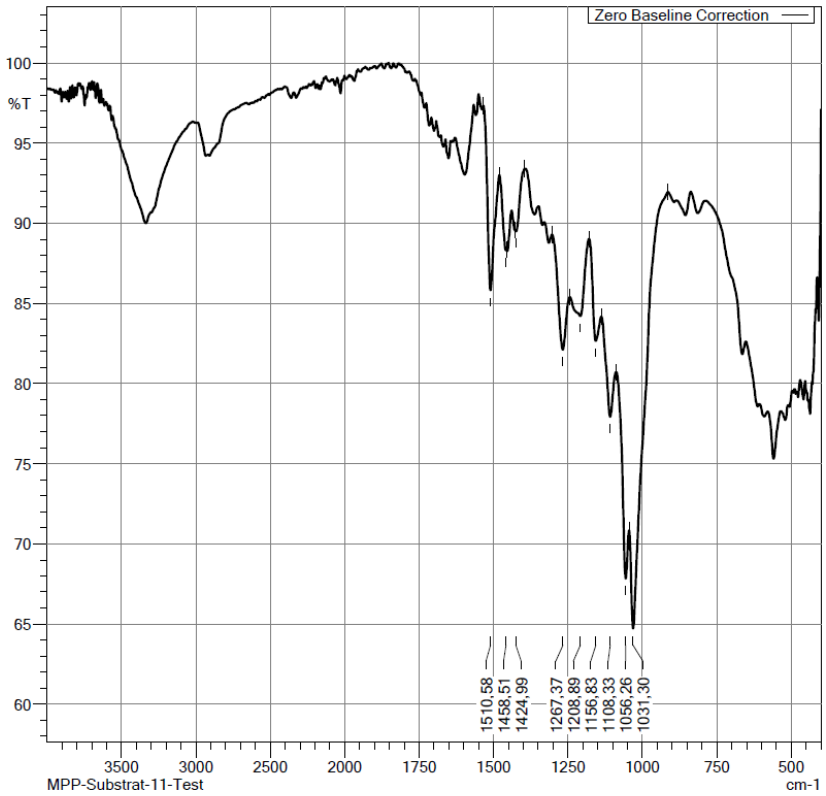

Figure B-21: FT-IR spectrum of substrate 11.

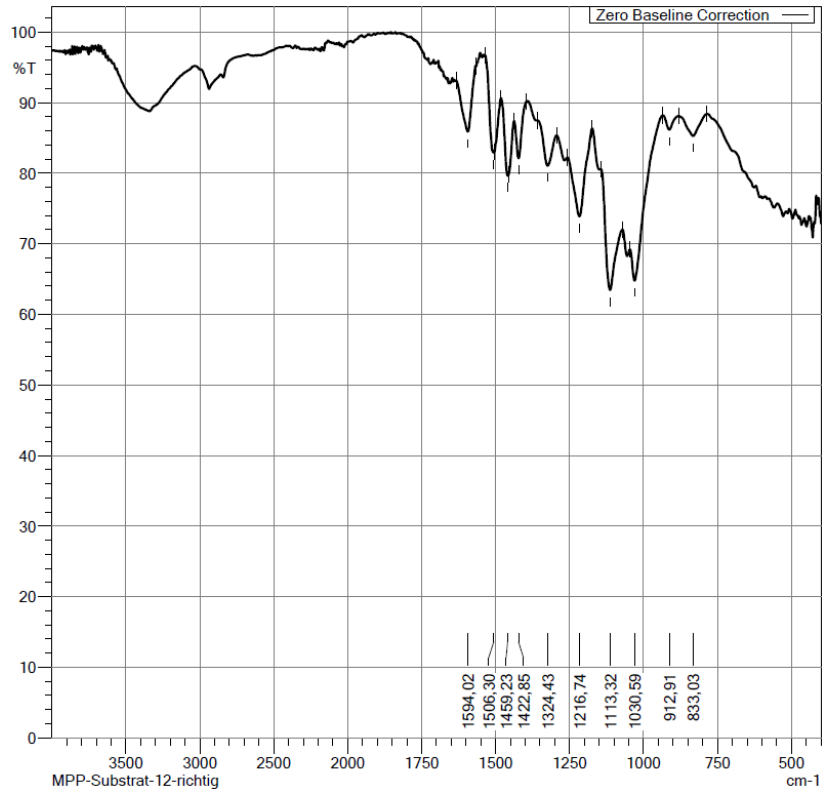

Figure B-22: FT-IR spectrum of substrate 12.

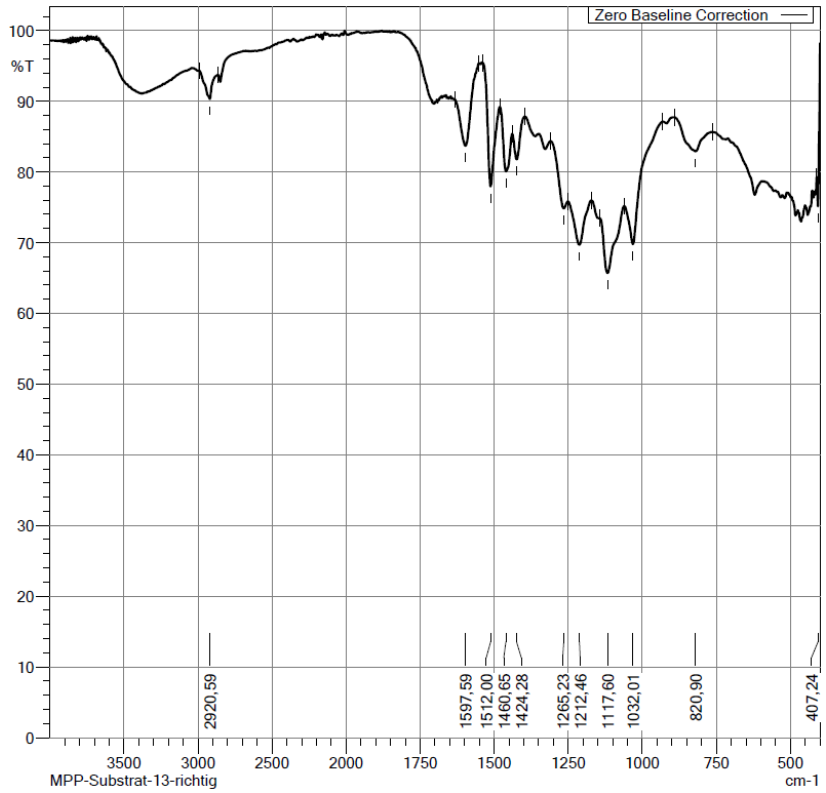

Figure B-23: FT-IR spectrum of substrate 13.

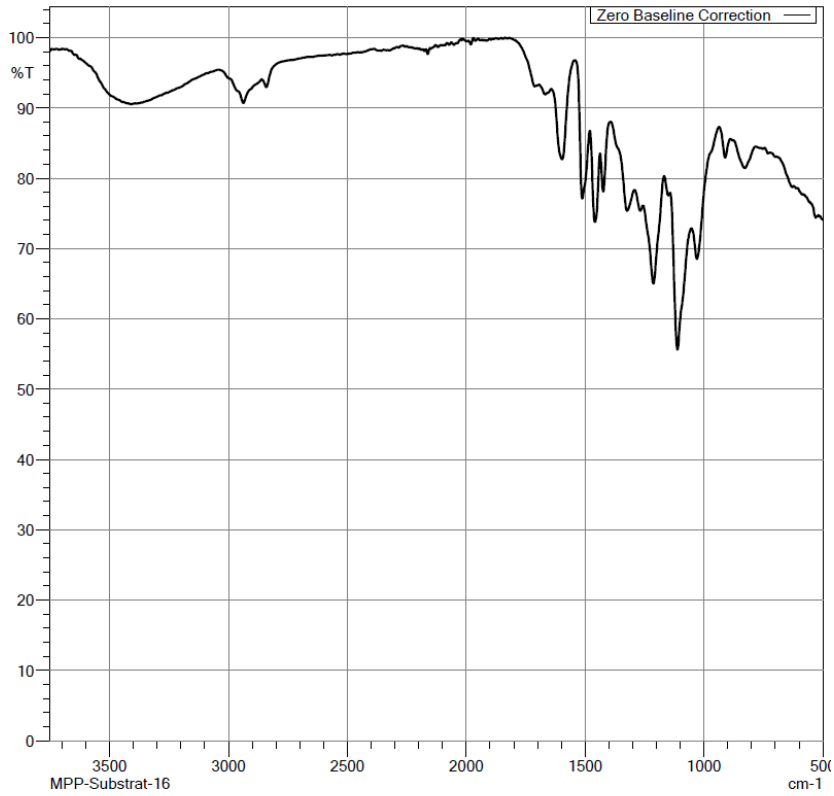

Figure B-24: FT-IR spectrum of substrate 16.

B.4 SI on solvent screening

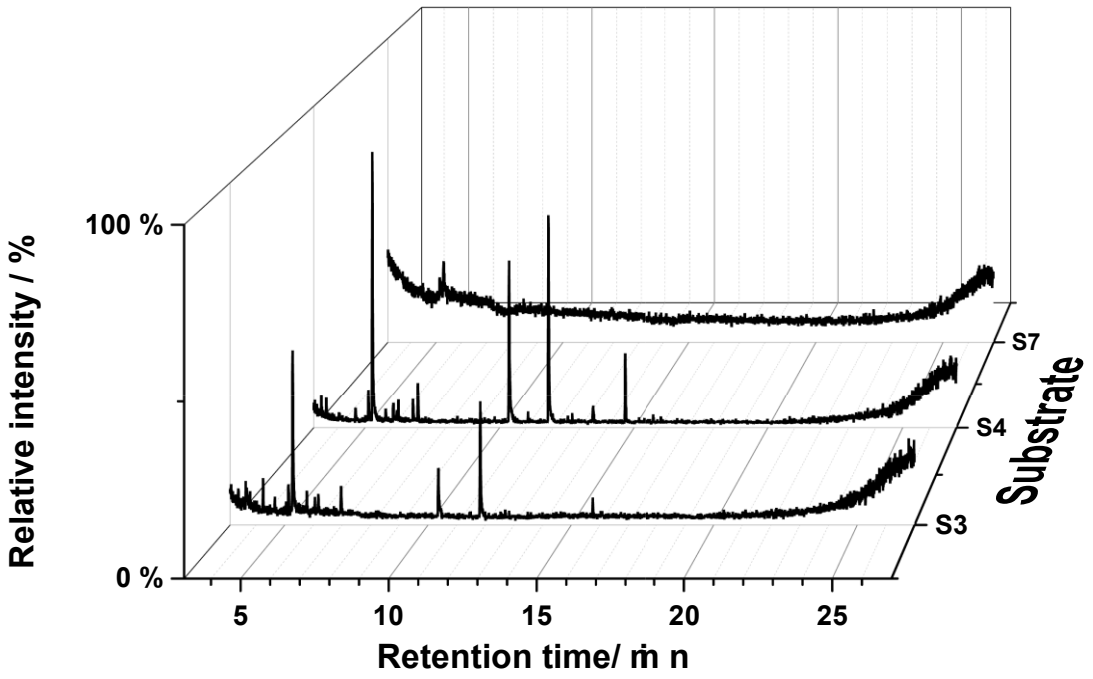

Figure B-25: Chromatograms by GC-MS for the liquid phases of the substrates kraft softwood lignin (S3), organosolv beech lignin (S4) and sulphite hardwood lignin (S7) in a methanol-water solvent system (1:1 v/v) carried out in Setup 1. Reaction conditions were 140 °C, 20 bar oxygen partial pressure, 24 h, 0 rpm, 10 mL solvent, 500 mg substrate (S3, S4, S7), 200 mg catalyst ($H_8PV_5Mo_7O_{40}$).

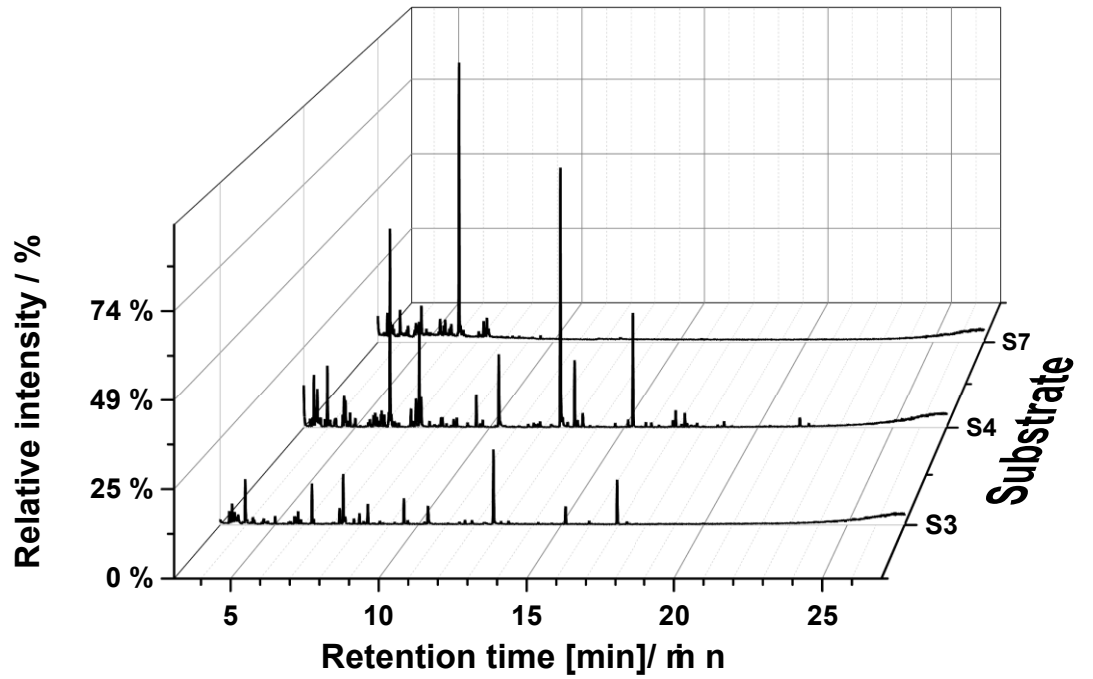

Figure B-26: Chromatograms by GC-MS for the liquid phases of the substrates kraft softwood lignin (S3), organosolv beech lignin (S4) and sulphite hardwood lignin (S7) in the pure ethanol solvent system carried out in Setup 1. Reaction conditions were 140 °C, 20 bar oxygen partial pressure, 24 h, 0 rpm, 10 mL solvent, 500 mg substrate (S3, S4, S7), 200 mg catalyst (HPMo-V_5).

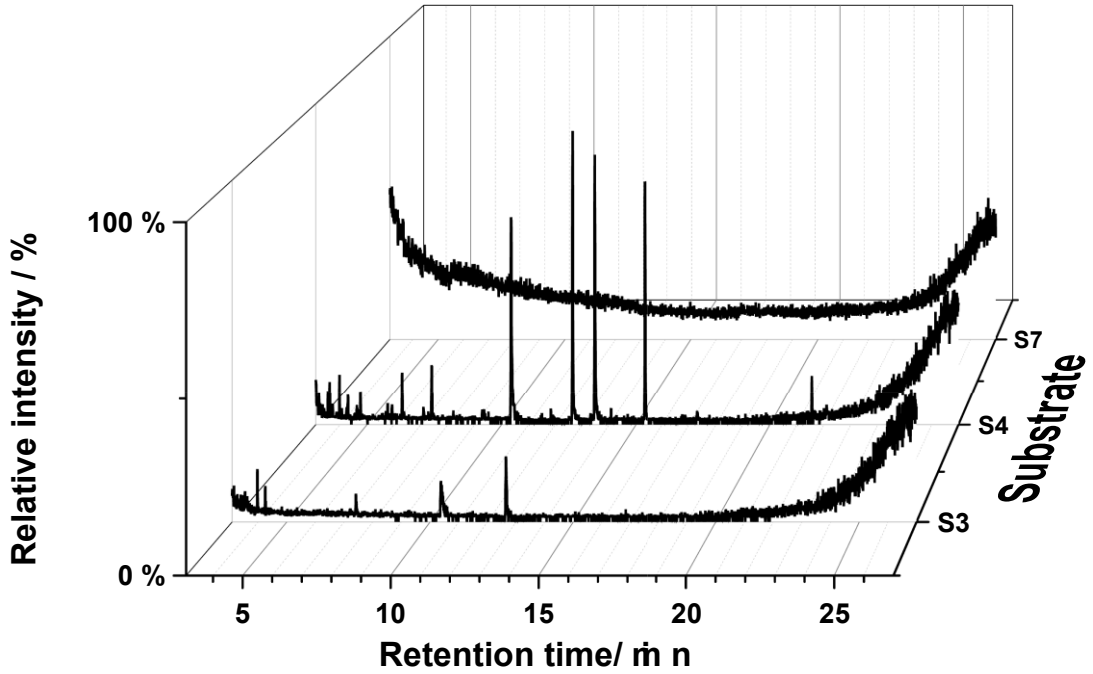

Figure B-27: Chromatograms by GC-MS for the liquid phases of the substrates kraft softwood lignin (S3), organosolv beech lignin (S4) and sulphite hardwood lignin (S7) in a ethanol-water solvent system (1:1 v/v) carried out in Setup 1. Reaction conditions were 140 °C, 20 bar oxygen partial pressure, 24 h, 0 rpm, 10 mL solvent, 500 mg substrate (S3, S4, S7), 200 mg catalyst (HPMo- V_5).

B.5 SI on final organosolv substrate selection

Table B-3: Overview of reaction parameters for the pre-selection of the new substrate for all remaining experimental studies investigated within this work. Experiments were conducted in Setup 1.

Reaction parameter	Parameter value	Details
Time	24 h	
Partial pressure	20 bar	Oxygen
Temperature	140 °C	
Substrate (mass)	500 mg	S1 – Organosolv softwood S4 – Organosolv beech (reference) S5 – Organosolv spruce S16 – Organosolv beech
Catalyst (mass)	200 mg	HPMo-Ni3
Solvent volume	10 mL	Methanol/Water (8:2 v/v)

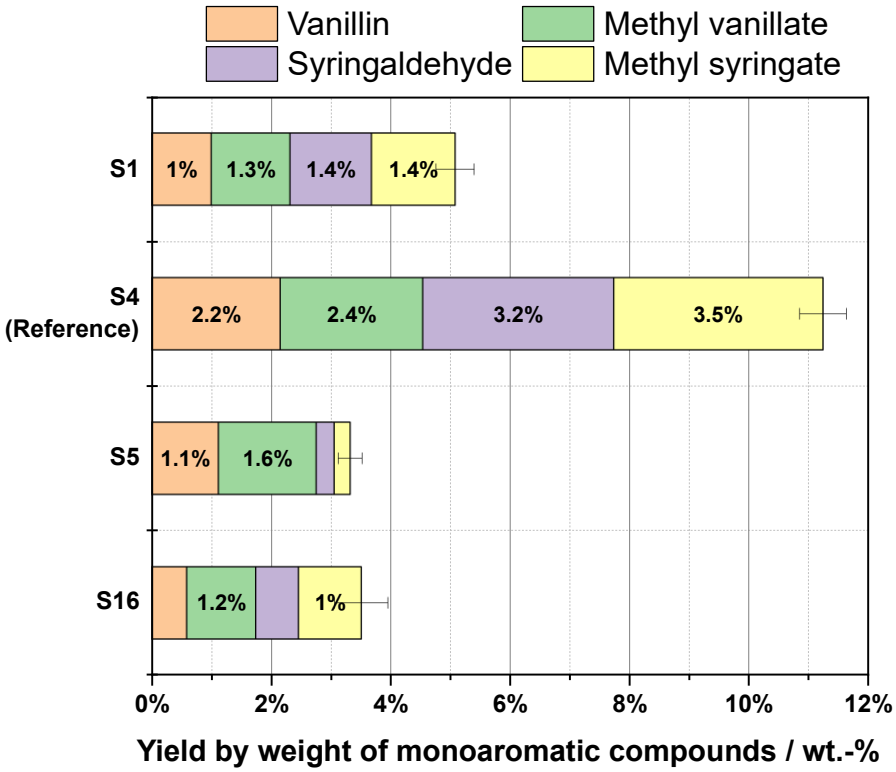

Figure B-28: Yield by weight of the desired monoaromatic compounds for the pre-selection of the new substrate for all remaining experimental investigations. Reaction conditions in Setup 1 were 140 °C, 20 bar oxygen partial pressure, 24 h, 0 rpm, 10 mL solvent, 500 mg substrate (S1: organosolv softwood, S4: organosolv beech wood, S5: organosolv spruce wood, S16: organosolv beech wood), 200 mg HPMo-Ni_3 catalyst.

B.6 SI on investigations of reaction time influence

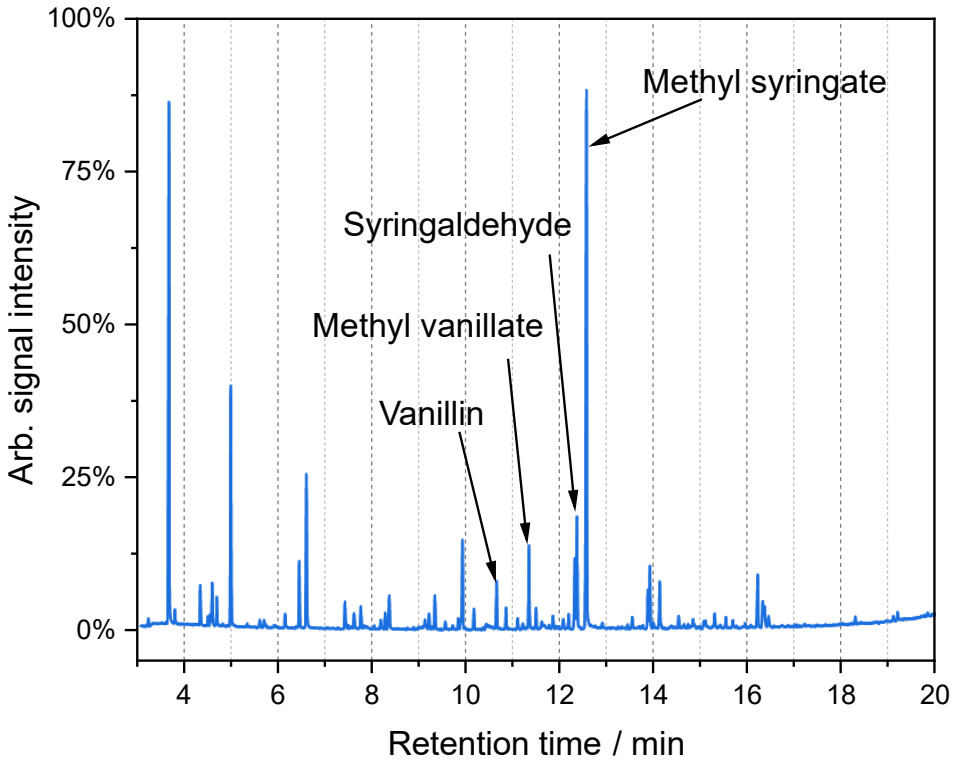

Figure B-29: Chromatogram measured by GC-MS for the reaction solutions obtained by using pure syringaldehyde as a substrate. Other reaction conditions were Setup 1, 140 °C, 20 bar oxygen partial pressure, 6 h reaction time, 10 mL of 95:5 v/v methanol-water-mixture, 510 mg syringaldehyde, 300 mg HPMo-V_5 catalyst.

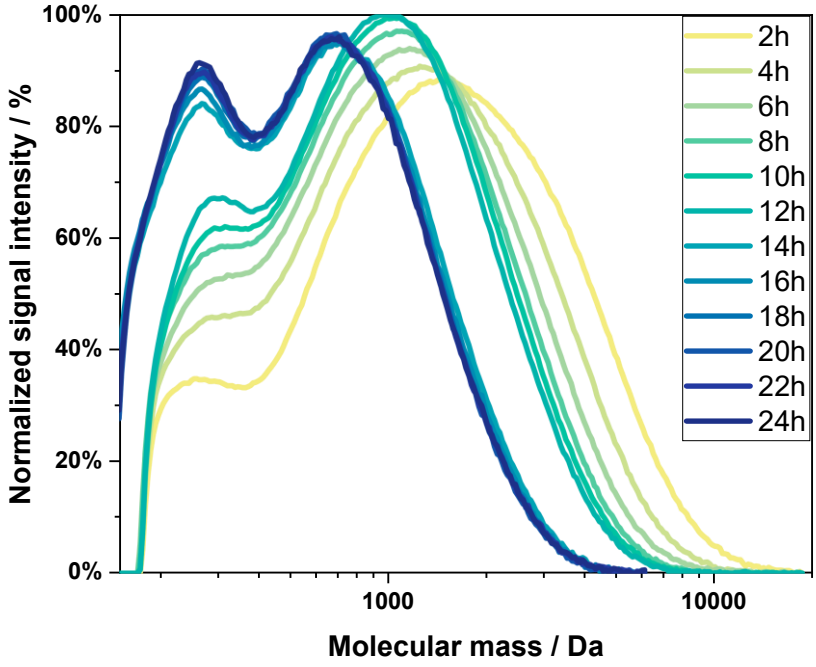

Figure B-30: Molecular mass distribution of reaction solutions obtained from the reaction time screening at following conditions: 140 °C, 20 bar oxygen partial pressure, 24 h, 0 rpm, 10 mL solvent, 500 mg substrate (S1: organosolv softwood, S4: organosolv beech wood, S5: organosolv spruce wood, S16: organosolv beech wood), 200 mg HPMo-Ni_3 catalyst.

B.7 SI on design of experiment investigations

Table B-4: Yield of desired monoaromatics, carbon yields of short-chained methyl esters (methyl formate, methyl acetate, dimethyl oxalate, dimethyl succinate) plus CO/CO_2, and carbon yield of solid residue acquired during Design-of-Experiment investigations at shown reaction conditions. Reactions were conducted in Setup 2 at 14 bar initial oxygen partial pressure, 16 hours reaction time, 30 mL solvent ($MeOH:H_2O$ in 8:2 v/v ratio), 1,500 g substrate (S1), $HPMo\text{-}Ni_3$ catalyst.

Run #	Temp. / °C	Stirrer / min^{-1}	Sub./Cat.-ratio	Yield Aromatics / wt.-%	Carbon yield Esters + CO + CO_2 / wt.-%	Carbon yield solid phase / wt.-%
1	120	0	2.5	8.43	15.3	21.9
2	120	500	1	3.24	8.5	15.5
3	120	500	4	3.66	9.1	10.6
4	120	1000	2.5	0.28	20.1	11.6
5	140	0	1	5.5	23.0	17.0
6	140	0	4	0.02	16.2	10.7
7	140	500	2.5	0	10.4	15.9
8	140	500	2.5	3.34	8.6	15.5
9	140	500	2.5	5.73	19.2	13.9
10	140	1000	1	6.4	17.9	14.5
11	140	1000	4	5.4	16.8	11.6
12	160	0	2.5	7.8	21.7	13.0
13	160	500	1	0	19.7	11.5
14	160	500	4	6.8	21.8	13.5
15	160	1000	2.5	6.0	21.2	17.5

Table B-5: ANOVA results for a quadratic model applied to the yield results shown in Table B-4.

Parameter	Sum of squares	df	Mean square	F-Value	p-Value
Model overall	117.86	9	13.10	18.41	0.0025
A-Temperature	10.35	1	10.35	14.55	0.0124
B-Stirrer	0.0761	1	0.0761	0.1069	0.7569
C-Catalyst Ratio	82.43	1	82.43	115.90	0.0001
AB	0.0042	1	0.0042	0.0059	0.9416
AC	4.95	1	4.95	6.96	0.0461
BC	1.29	1	1.29	1.81	0.2362
A^2	5.14	1	5.14	7.22	0.0434
B^2	0.1125	1	0.1125	0.1582	0.7072
C^2	14.84	1	14.84	20.86	0.0060
Residual	3.56	5	0.7113		
Lack of Fit	2.39	3	0.7973	1.37	0.4484
Pure Error	1.16	2	0.5822		
Cor Total	121.41	14			

B.8 SI on liquid-liquid-extraction

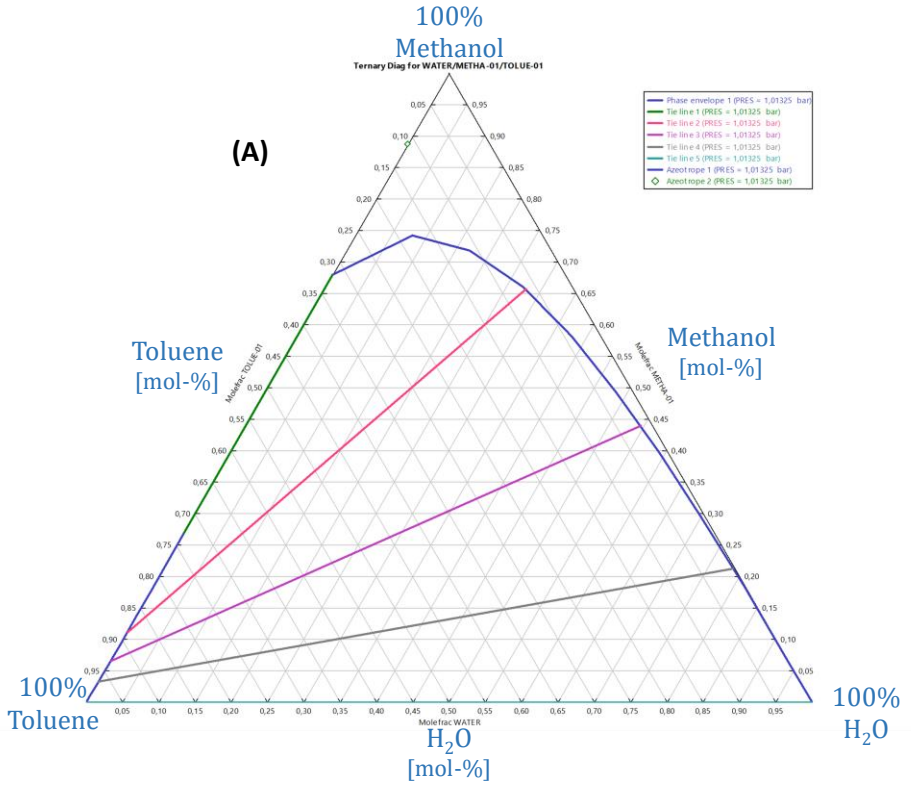

Figure B-31: Ternary diagram of methanol, water and toluene acquired from Aspen Plus.

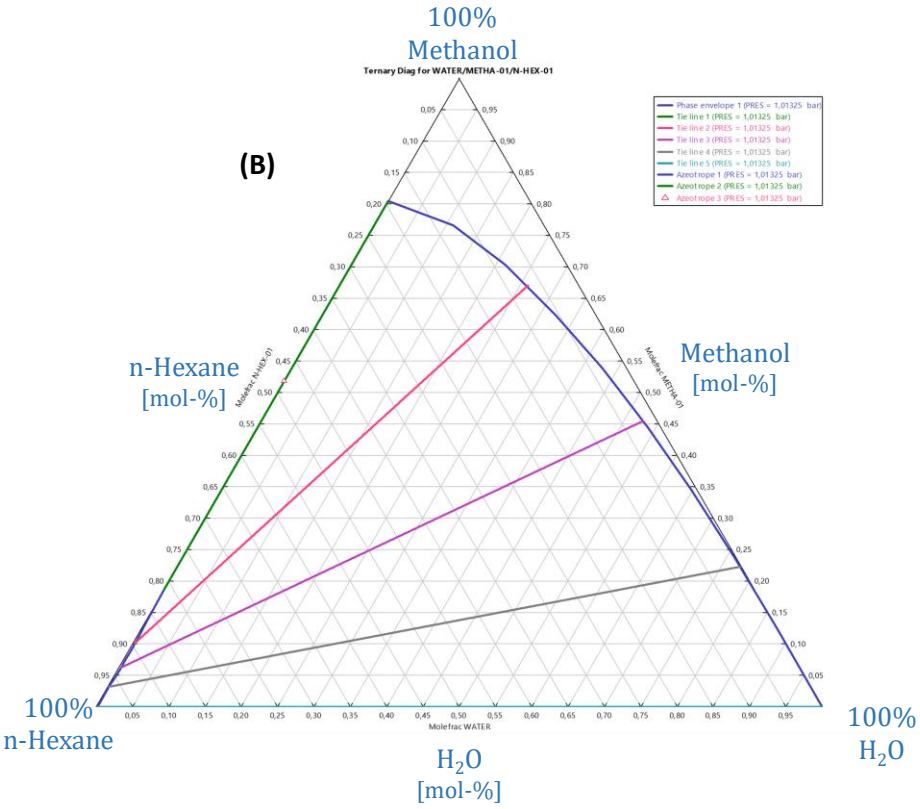

Figure B-32: Ternary diagram of methanol, water and n-hexane acquired from Aspen Plus.

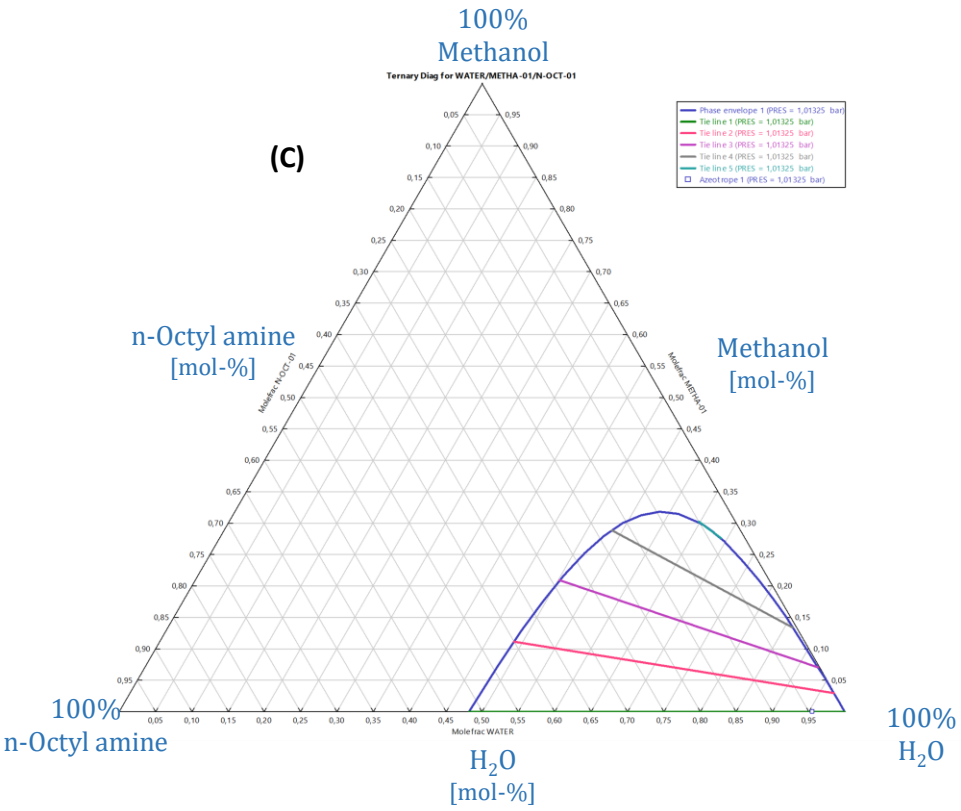

Figure B-33: Ternary diagram of methanol, water and n-octyl amine acquired from Aspen Plus.

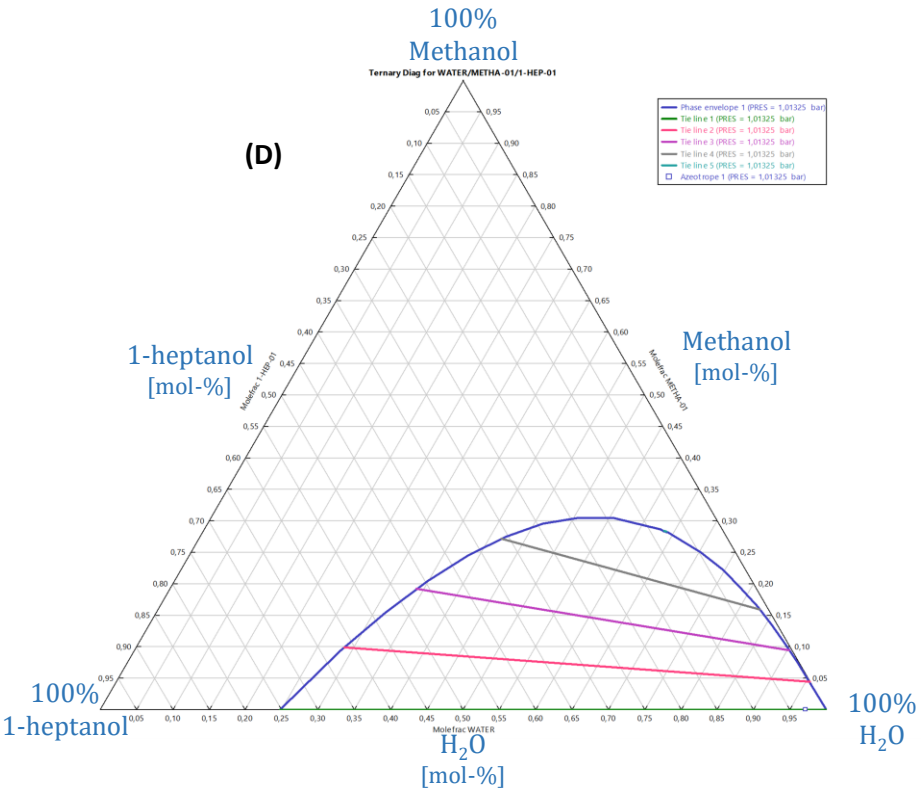

Figure B-34: Ternary diagram of methanol, water and 1-heptanol acquired from Aspen Plus.

B.9 SI for commissioning of continuous plant

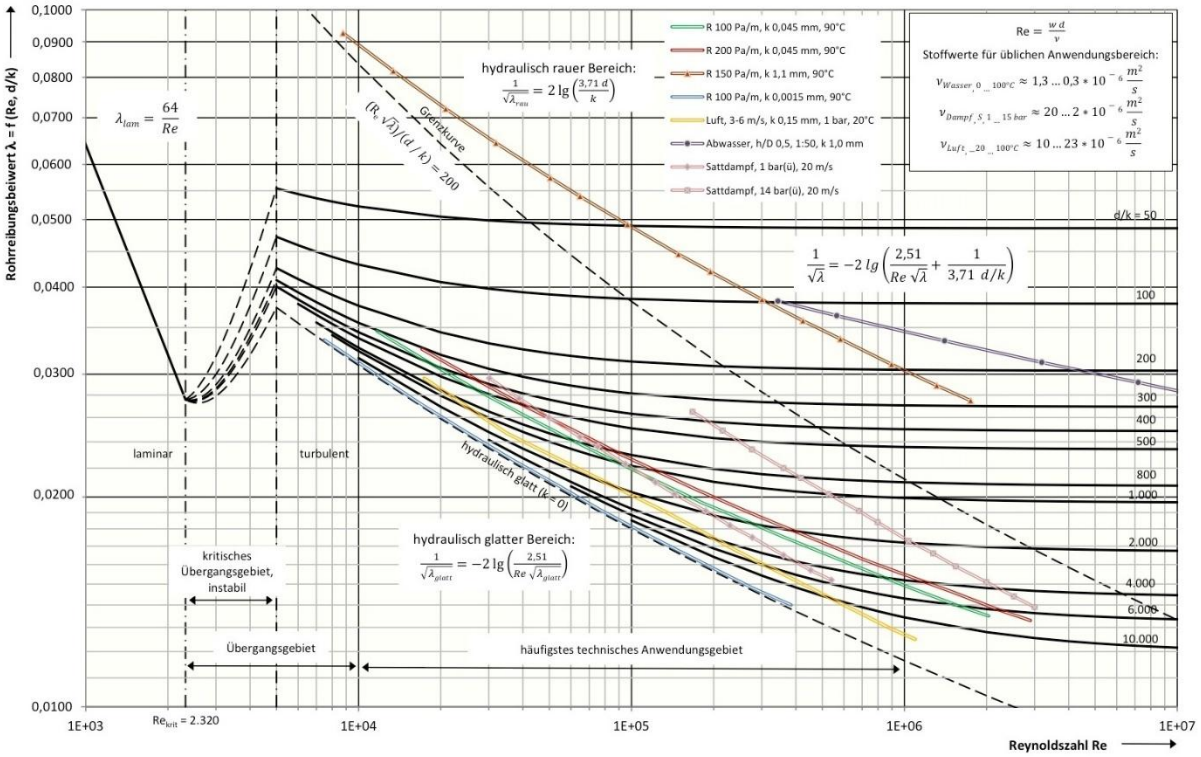

Figure B-35: Moody diagram for the identification of the Darcy friction factor formula depending on Reynolds number. [240]

Table B-6: Calculation of estimated pressure drop in continuous plant.

			Water	Methanol	Unit
$Re = \frac{v \cdot d}{\nu}$	v	Velocity	0.002652582	0.002652582	m/s
	d_i	Inner diameter	0.001	0.001	m
	A	Cross-sectional area	3.14159E-06	3.14159E-06	m²
	V.	Volume flow rate	8.33333E-09	8.33333E-09	m³/s
	ν	Kin. Viscosity	0.000001	0.00000055	m²/s
	Re	Reynolds number	2.652582385	4.822877063	
$\lambda_{lam} = \frac{64}{Re}$	f	Darcy friction factor	24.12743158	13.27008737	
	L	Length of pipe	2	2	m
$\Delta p = \lambda \cdot \frac{L}{D} \cdot \frac{\rho}{2} v^2 \cdot$	D	Inner diameter	0.001	0.001	m
	ρ	Density medium	1000	780	kg/m³
	v	Velocity	0.002652582	0.002652582	
	Δp	Pressure drop	169.7652726	72.82930196	pa
			0.001697653	0.000728293	bar

$$\dot{V} = c \cdot x + b \qquad \textbf{Eq. B-1}$$

Table B-7: Calibration factors and intercepts of pumps 1-4 for the continuous plant.

Pump	Calibration factor c	Unit of X	Intercept b / mL/min
P1	0.24765 mL/round	rpm	0.004675
P2	0.01924 mL/round	rpm	0
P3	0.977	mL/min	0.05
P4	0.2005 mL/round	rpm	0.0575

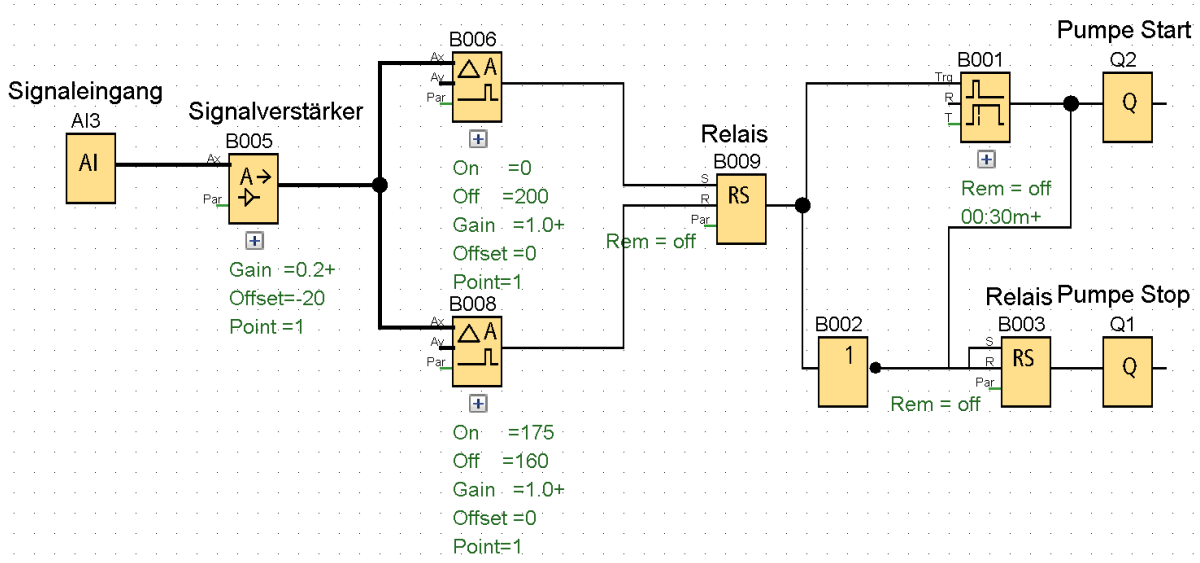

Figure B-36: Circuit diagram for the filling level controlling of Container 4 in the continuous plant (Setup 3). The control system was created with the Siemens software LOGO!.

C. Indexes

C.10 List of figures

C.11 List of tables

C.12 List of schemes

D. Acknowledgements (in German)

Wie der kleine Kolibri, der Tropfen für Tropfen gegen das Feuer kämpft, obwohl es aussichtslos scheint, so habe auch ich Schritt für Schritt, Zeile für Zeile an dieser Arbeit geschrieben – getragen von dem Gedanken:

„Ich tue, was ich kann."

Diese Dissertation ist das Ergebnis vieler kleiner Flüge zwischen Zweifel und Erkenntnis, zwischen Rückschlägen und Fortschritten. Sie ist nicht vollkommen, aber sie ist mein Beitrag – und mein Versuch, Verantwortung zu übernehmen, durch Beharrlichkeit, Neugier und Vertrauen in die eigene Wirkung. An dieser Stelle möchte ich ebenfalls all den Menschen danken, die mich auf diesem Weg begleitet und unterstützt haben.

Zunächst möchte ich selbstverständlich Prof. Dr.-Ing. habil. Jakob Albert für die Betreuung meiner Promotion und die Möglichkeit danken, dieses Projekt durchführen zu dürfen. Während meines Studiums hatte ich kaum Berührungspunkte mit holzbasierter Biomasse. Durch dieses Projekt entwickelte sich jedoch eine Leidenschaft für deren stoffliche Nutzung, die inzwischen auch meinen beruflichen Werdegang maßgeblich prägt.
In dem Zusammenhang möchte ich mich ebenfalls bei Jun.-Prof. Dr. rer. nat. Anna Katharina Beine für das kurzfristige Einspringen als Zweitgutachterin bedanken – das Engagement weiß ich wirklich zu schätzen!

Darüber hinaus danke ich Dr.-Ing. Dorothea Voß, Dr.-Ing. Anna Bukowski und Dr. Maximilian Poller, ohne deren Erfahrung, Expertise und Engagement dieses Projekt nicht möglich gewesen wäre. Doro hat es stets geschafft, den Überblick über alle laufenden Projekte zu behalten und war dennoch immer ansprechbar für ingenieurtechnische Fragen – ein verlässlicher Anker im Arbeitsalltag, der mir Sicherheit und Struktur gab. Anna ermöglichte mir eine reibungslose Einarbeitung in den Umgang mit und die Modifikation von Hochdruckreaktoren. Ihre humorvolle Art machte selbst technische Herausforderungen erträglich. Max unterstützte mich mit großer Ruhe und Pragmatismus bei zahlreichen Fragestellungen – insbesondere im chemischen Bereich – und war damit eine unschätzbare Hilfe im Alltag.
Mein besonderer Dank gilt auch allen weiteren Kolleg:innen der Arbeitsgruppe Albert für die jederzeit kollegiale und hilfsbereite Atmosphäre. Dieses Miteinander war gerade an herausfordernden Tagen ein großer Rückhalt. In besonderem Maße möchte ich dem Büro 126A danken: Stefanie Wesinger, Anne Wesner und Jan-Christian Raabe. Die Gespräche über –

wissenschaftlich eher irrelevante – Themen wie Friseurnamen, nordafrikanische Wüsten oder Trockenschränke haben nicht nur den Tag versüßt, sondern mich manchmal auch länger am Institut gehalten, als ursprünglich geplant. Jan danke ich zudem für seine akribische Arbeit bei der Katalysatorsynthese – ohne ihn wäre der Arbeitskreis vermutlich in ernsthafte Schwierigkeiten geraten. Anne danke ich für die enge Zusammenarbeit im HetPOM-Projekt, durch das ich meine Erfahrungen mit allen Bestandteilen der Lignocellulose vervollständigen konnte. Steffi danke ich für den Austausch im POMLig-Projekt. Der offene Dialog über unsere überschneidenden Themen hat mir oft einfache Lösungen für zunächst unlösbar scheinende Probleme eröffnet.
Auch den festangestellten Mitarbeiter:innen der Arbeitsgruppe möchte ich herzlich danken – insbesondere Michael Gröger, der mich bei zahlreichen analytischen Fragestellungen wie GC-MS-Messungen, Kalibrierungen und GPC-Analysen unterstützte und ebenso handwerklich beim Aufbau der kontinuierlichen Anlage zur Seite stand. Darüber hinaus sorgte er mit seinen Erzählungen aus dem Leben für so manchen heiteren Moment im Laboralltag.
Meinem Kollegen und engen Freund Philipp Kampe möchte ich außerdem herzlichst danken. Die Freundschaft, die wir in den letzten vier Jahren aufgebaut haben, weiß ich zu schätzen und ich hoffe, dass sie ein Leben lang hält.

Zuletzt und mir am wichtigsten gilt mein tiefster Dank meiner Familie und meiner Partnerin.

Mama, Papa, ich bin euch zutiefst dankbar für eure bedingungslose Unterstützung über all die Jahre, für euer Vertrauen und euer Verständnis. Ihr habt mich zu dem Menschen gemacht, der ich heute bin – ich hoffe, ich kann euch eines Tages ebenso viel zurückgeben.
Chiara, dir gebührt auch der allergrößte Dank. Du kamst in mein Leben, kurz bevor diese Reise begann, und hast mich vollständig dabei begleitet und ertragen. Danke für deine Geduld, deine Ermutigung und dafür, dass du an mich geglaubt hast – auch dann, wenn ich es selbst nicht tat. Ohne dich wäre dieser Weg ein anderer gewesen.

E. Declaration of oath

„I hereby declare under oath that I have written the present dissertation myself and have not used any sources or aids other than those indicated. Insofar as generative artificial intelligence (gAI)-based electronic tools were used in the preparation of this dissertation, I affirm that my own contribution was the primary focus and that a complete documentation of all tools used is provided in accordance with the principles of good scientific practice. I accept responsibility for any errors or distortions in content, incorrect references, violations of data protection or copyright law, or plagiarism that may have been caused by the use of gAI.“

Signature:

Max Papajewski

Date: October 19th, 2025

Eidesstattliche Erklärung

„Hiermit versichere ich an Eides statt, die vorliegende Dissertationsschrift selbst verfasst und keine anderen als die angegebenen Quellen und Hilfsmittel benutzt zu haben. Sofern im Zuge der Erstellung der vorliegenden Dissertationsschrift generative Künstliche Intelligenz (gKI) basierte elektronische Hilfsmittel verwendet wurden, versichere ich, dass meine eigene Leistung im Vordergrund stand und dass eine vollständige Dokumentation allerverwendeten Hilfsmittel gemäß der Guten wissenschaftlichen Praxis vorliegt. Ich trage die Verantwortung für eventuell durch die gKI generierte fehlerhafte oder verzerrte Inhalte, fehlerhafte Referenzen, Verstöße gegen das Datenschutz- und Urheberrecht oder Plagiate.“

Unterschrift:

Max Papajewski

Datum: 19. Oktober, 2025